THE TRANSMISSION OF LOAD THROUGH ANIMAL JOINTS

WITH PARTICULAR REFERENCE TO THE ROLE OF THE MENISCUS IN THE KNEE

by

N.G. SHRIVE

ST. EDMUND HALL

A thesis submitted for the degree
of Doctor of Philosophy.

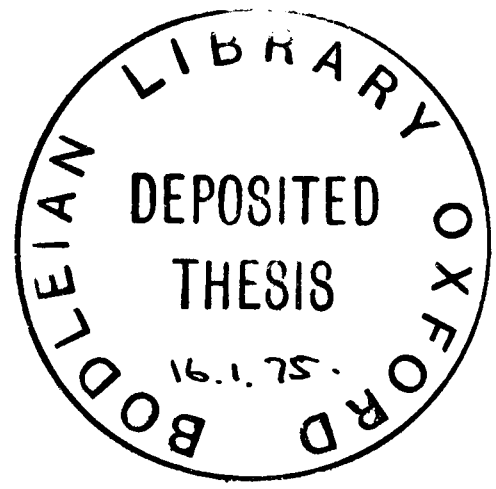

August 1974

University of Oxford.

ADDENDA

Page 4 last para, line 2: strength → tensile strength

5 line 9: motion becoming → motion by becoming

6 1.4 Para 2, line 2: The various → the majority of the various

39 line 22: circumferentially → circumferentially in a ground matrix

99 line 18: linearly increase → increase linearly

108 method 4. Para 2, line 4: radius of → radius required for

ABSTRACT

Load Transmission Through Animal Joints

A general description of synovial joints is given. The composition, function and degradation of the various materials and structures within synovial joints are discussed. Special consideration is given to the knee joint which is shown to be anomalous to other joints in certain aspects of the properties previously mentioned. If the meniscus cartilages of the knee, to which many functional roles have been attributed, may be shown to be weight-bearing, then observations concerning the knee would be in accordance with, rather than anomalous to other joints.

A simple model of the knee is analysed using simple stress-strain relationships and the validity of the results of the analysis are discussed. The analysis indicates that it is possible for the menisci to bear a large proportion of the load transmitted through the knee joint and shows how the function of weight-bearing may be performed.

Experiments were performed to determine whether or not the menisci carried load. The experimental apparatus and procedures are described and the results obtained are discussed. Various attempts are made to estimate the percentage of the total load through the joint carried by the menisci.

The conclusion drawn from the experimental results is that the menisci do carry a considerable proportion of the load between the femur and the tibia, and the significance of the result is discussed.

ACKNOWLEDGEMENTS

I should like to express my gratitude to all those who have helped me complete the work described in this thesis, especially Dr. J.J. O'Connor who supervised the project and was always willing to give help, advice and encouragement as necessary.

Also, Mr. J.W. Goodfellow, F.R.C.S., for his great enthusiasm and his aid on the medical aspects of the work.

Dr. C. Ruiz who acted as vice for John O'Connor for a year and gave much helpful advice in that period.

Prof. D.W. Holder for allowing me to carry out the work in the Department of Engineering Science - in spite of the occasional smells!

My wife for her patience, understanding and encouragement.

The S.R.C. and the A.R.C. for the financial support of myself and the project respectively.

Members of the staffs of Hedges' Abbatoir, Abingdon, the Radcliffe Infirmary, Oxford and Imperial College, London for the supply of specimens.

Mr. D. Hempstock for making the apparatus.

Mrs. Coleman and Mrs. Turner for the excellent typing.

The O.U. Computing Laboratory.

Mr. D. Duggan for advice on using PAFEC.

Mr. P. Flint and Mr. M. Lawrence for their aid with photography and the reproduction of the thesis.

To all those above and to the people not mentioned, but who gave aid in various ways - Many thanks.

NIGEL SHRIVE

August, 1974.

TABLE OF CONTENTS

CHAPTER 1

INTRODUCTION TO THE PROBLEM

1.1 Introduction

The work described in the thesis is a study of load transmission through one particular joint in the body - the knee. This chapter surveys current knowledge on the constitution, function and degradation of the materials within the joint; the specific framework and geometry of the joint and the dynamic and static loads to which the joint is subjected.

1.2 General description of Synovial Joints

When two or more bones of the skeletal system meet, the contact region is called a joint. There are three basic types of joint in the body, the differences reflected in the details of the articulations. In fibrous (e.g. flat bones of the skull) and cartilaginous (e.g. intervertebral disks) joints, little or no movement is allowed, whereas in the synovial type, the articulating bones move freely on one another.

There is considerable variety in the types of synovial joint which allow various ranges of movement, but all have the same basic structural pattern. The apposed ends of the bone are covered by thin layers of hyaline cartilage which on the articulating surfaces is more commonly known as articular cartilage. All the structures within the joint up to the edge of the hyaline cartilage are surrounded by a synovial membrane. Enclosed in this membrane is the lubricating synovial fluid and surrounding it and the bones is the fibrous connective tissue of the articular capsule. The joint usually has reinforcing ligaments to limit undesirable motion and sometimes contains pads of fibrocartilage and/or subsynovial collections of fat.

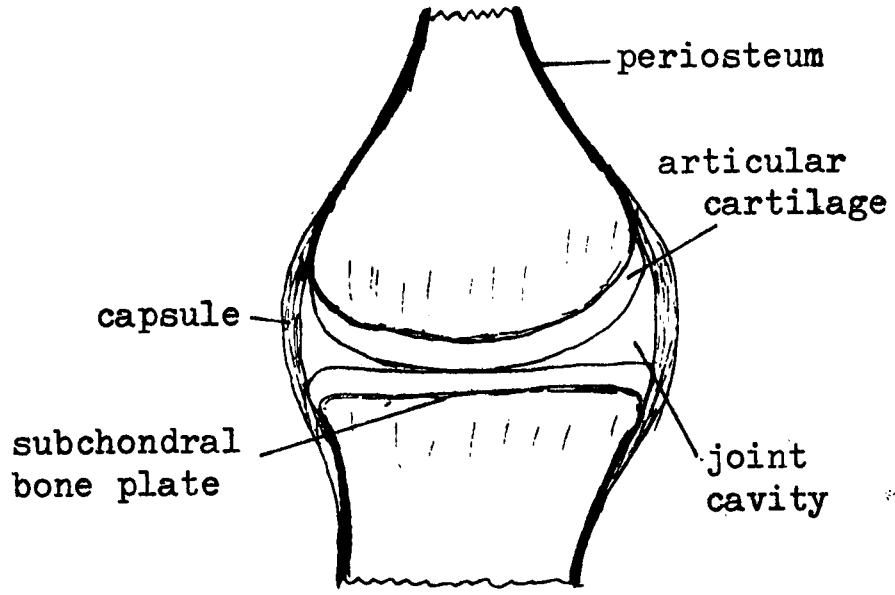

SYNOVIAL JOINT - SCHEMATIC

Diagram 1.1

The bone components of the joint have a thin surface layer of compact cortical bone and an internal zone of cancellous bone. This latter is arranged in a mesh of trabeculae, the pattern of

which arises as a response to functional demands. This was first noted by Wolff[1] and subsequent investigations, such as that by Toridis[2], indicate that the pattern of the trabeculae follows that of the principal stress trajectories in the bone. The articulating end of the bone is designated the subchrondral bone plate and it is this which is covered by the hyaline cartilage.

1.3 Articular cartilage

Articular cartilage is bluish white and slightly translucent in the early decades of life, becoming progressively more yellowish and opaque with age[3]. It is avascular and non-nervous containing 65-85% water and consisting of a network of collagen fibres embedded in a hydrated gel[4]. The fibres are made up of bundles of fibrils and their thickness varies with depth from the surface.

The gel incorporates proteoglycans and other proteins: the proteoglycans are chondroitin sulphate and to a lesser extent keratan sulphate, both covalently attached to proteins[4]. They are otherwise known as glycos-amino-glycans, a type of mucopolysaccharide.

The cartilage thickness varies from about 0.5 to 4 mm. in different joints in the body and also varies for specific joints with different animal species. The variation of average compressive stress from species to species varies within an order of magnitude, although there is no consistent relation-

ship between the stress and the thickness of the layer[5]. There is a relationship, however, between the deformation due to applied loads and the thickness and intrinsic elasticity of the cartilage[6].

The structure of the cartilage layer may be considered in zones. The extreme surface layer is a fine mesh of fibrils parallel to the surface with no particular orientation, whereas in the superficial layer immediately below this the fibres remain parallel to the surface but lie predominantly in a particular direction[7 - 12]. This direction may be easily determined by split line tests[9]. In the deep zone the fibres are perpendicular to the subchondral plate, and in the intermediate zone, as height from the subchrondral plate increases, turn obliquely, finally being parallel to the surface. The fibres tend to be randomly orientated other than in the plane described. They are anisotropic, like ropes, being stronger and stiffer along their length; the gel is weak, thus parallel to the surface the deep zone is very weak and the superficial zone relatively strong and stiff in the direction of fibre orientation[4, 13].

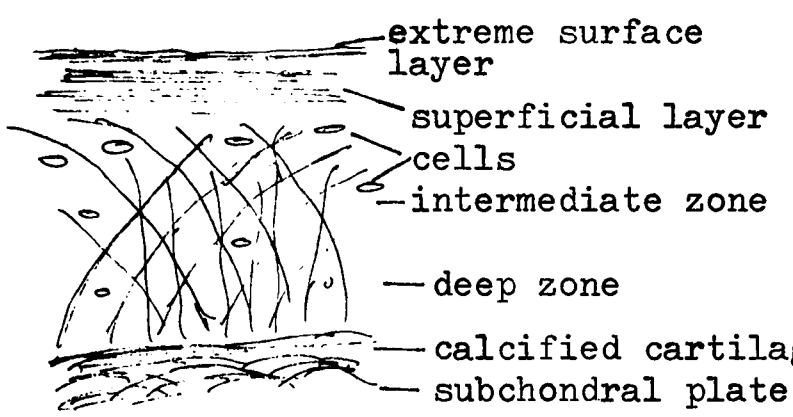

CROSS-SECTION VIEW OF ARTICULAR CARTILAGE

Diagram 1.2

The matrix and the cells appear to contribute very little to the strength of the cartilage. The cell density is at its highest just below the superficial layer and decreases with increasing depth from the surface[7]. In the young, the cells are fed by both synovial fluid and through the epiphysial

plate but in the mature, even though a pathway through the sub-chondral plate exists, synovial fluid is the major nutrient supplier[14,15].

In the superficial zone, the mucopolysaccharide content is low and it increases with depth creating an osmotic pressure which induces tension in the fibre mesh in the unloaded state[4]. On deformation there is some movement of the protein molecules causing electric polarization[16], but the mesh restricts this motion becoming subject to further tension[4].

In the loaded situation, the stress in the superficial layer may be tensile or compressive (see 2.3.2) and the fibre orientation appears to be along the lines of principal stress,[17] whereas from a less realistic analysis[17] it would appear that in the deeper zones, either a radial or oblique orientation would enable the matrix to resist tensile stresses without excessive deformation. Neither formation however, would be in complete accordance with the mechanical requirements throughout the whole range of motion of joints[17]. It is interesting to note that the fibre orientation is settled during embryonic growth suggesting that applied stresses do not cause its disposition.

As has been mentioned, in the mature the cells are fed by nutrients contained in the synovial fluid, and there are two mechanisms by which these may be circulated from the joint cavity to the cells. The cartilage is porous, the permeability being greater near the surface[19]; loading expresses fluid and unloading allows liquid to be soaked up, about 20 mins. being required for resaturation[8]. The second method is diffusion[8].

Cartilage therefore is a highly complex material in which

chemical and physical composition and mechanical properties are precisely and subtly interrelated. Its normal roles are to act as a highly deformable buffer between the bones and thus distribute the stresses applied thereto and, in conjunction with synovial fluid, to provide an extremely efficient joint lubrication system.

1.4 Lubrication

The surface of articular cartilage is 3 to 15 times rougher than normal engineering bearings[20], yet is smooth and slippery to touch. The coefficient of friction in synovial joints is low (circa 0.01)[19], being due to the lubricating synovial fluid acting in conjunction with the articular cartilage. Synovial fluid is a dialysate of blood plasma with the addition of hyaluronic acid, has non-Newtonian viscous properties, a distinct wear-protecting effect for cartilage[21] and is more than a mere lubricant since it supplies nutrients to the articular cartilage cells, as mentioned above.

The mode of lubrication is a point of much controversy. The various mechanisms proposed are of the fluid film type[22 - 32]. Two mechanisms particular to synovial joints have been proposed: Weeping lubrication[19, 25] involves the cartilage expressing liquid in order to maintain a fluid film between the surfaces, and boosted lubrication involves a change in the concentration of the hyaluronic acid[20, 26, 27].

In boosted lubrication, as the surfaces approach each other

the long chain molecules are unable to escape through the cartilage pores or parallel to the cartilage surface since they are too large. They become trapped. The small nutrient and water molecules escape either into the cartilage[20] or parallel to the surface[27]. The change in concentration of the acid increases the time for the reduction of the film thickness and thus prolongs the squeeze film mode. Also the acid chains are attracted and attach themselves to the cartilage surfaces so that a form of boundary lubrication exists when the squeeze film mode ceases.

Expulsion of liquid on loading is generally accepted, so a mode incorporating this feature seems most likely, but a different regime is probably employed in unloading when the cartilage absorbs liquid. The contact areas and hence the pressure distribution within the joint must play an important role in deciding the type of lubrication which occurs and this is recognized by Wiggins and Malkin[31]. Wiggins and Malkin and Greenwald and O'Connor[33] suggest that the pressure tends to a uniform value, the former for all joints from a study of the trabecula density of the cancellous bone near the subchondral plate; the latter for the hip from a study of a simple analytic model of that joint.

The maintenance of the excellent lubrication system within synovial joints, whatever it may be, depends critically on the perpetuation of the cartilage/fluid relationship as found in the healthy joint. The normal functions of lubrication and load transference are performed by the complete cartilage layer and the synovial fluid; if the integrity of one of these is lost there

is a resultant detrimental effect on the functional capabilities.

1.5 Joint degeneration and Incongruency

The two main degenerative diseases of synovial joints are rheumatoid and osteo-arthritis. The former begins with inflammation of the fibrous joint capsule and the synovial membrane, often accompanied by effusion into the joint. This affects the synovial fluid and the cartilage and degeneration of the cartilage slowly develops. Osteo-arthritis is a process in which the cartilage layer is gradually worn away. Unlike the rheumatoid form, in its critical stages there is no pain. The degenerative process, once begun, appears to be irreversible, attempts at repair by the cells within the cartilage tending to aggravate the already disordered function of the joint[34].

In the early stages, the appearance of the cartilage to the normal eye remains unchanged whilst there is a reduction in the mechanical stiffness accompanied by a decrease in the glycosaminoglycans content of the cartilage[35]. This is followed by the development of a matt irregular finish to the surface as erosion of the cartilage begins, with the cartilage being noticeably softer at this stage[34]. Fibrillation develops as a result of further loss in the surface material, revealing the fibres and presenting a filamentous appearance. Small fragments of cartilage become separated and lie free, usually at the edge of the joint cavity. Osteophytes develop, with, in the later stages of the disease, cyst and bone necrosis

also occurring.

The precise cause of the degenerative process is not yet known. However, the bone components of synovial joints are incongruent. This is obvious for the knee joint but not so clear for other joints[3, 36]. The reason for the incongruency may be to aid in supplying synovial fluid and thus the nutrients contained within to all areas of the joint by primary or secondary wetting[33, 37]; and in conjunction with the cartilage thickness distribution, to produce a state of uniform hydrostatic pressure in the joint under high loads[33]. An undoubted result of the incongruency is to produce areas of cartilage which habitually bear weight and other regions which only come into contact at high loads[33, 38]. As age increases greater congruency develops, changing the habitual contact areas[33].

The degeneration patterns of the cartilage in the hip are well established[34, 39, 40] and the areas in which degeneration is generally first observed are the areas of non-habitual contact for the young healthy joint[38, 39]. The relationship between the areas of non-habitual contact and the areas which first show degenerative changes was first noted by Harrison Shajowicz and Trueta[34] whose pressure areas, determined from studies of the trabecula system of the underlying bone, agree reasonably well with Greenwald's low load contact zones found by a dye technique[38]. Also, for the normal joint the areas of habitual contact are the areas with the stiffest cartilage as determined from indentation tests[41]. A similar connection between contact areas and degeneration patterns was observed

for the elbow and the patella-femoral joint.[42].

Habitual non-use of connective tissues in the body results in their undergoing atrophy and it has been proposed that a similar process occurs in the cartilage of the non-habitual contact areas[37]. As age increases and the joint surfaces become more congruent, the areas which were originally those of habitual non-contact become more and more those of regular contact. The cartilage cannot withstand the mechanical demands now made of it and hence begins to break down.

The degenerative process could also be caused by fatigue. Weightman et al[43] have shown that it is possible to develop fibrillation cracks in cartilage by repeated indentation tests in vitro. Radin et al[44, 45, 46], in a series of tests, produce clear evidence that repeated impact loading in vivo causes degeneration. Radin et al, however do not interpret this as a result of fatigue.

Osteo-arthritis shows that the maintenance of the precise relationship between cartilage structure and composition, synovial fluid and joint shape is necessary if failure of joint function is to be avoided. Since each individual treats his body differently and the metabolic rate also varies from person to person, it is not surprising that osteo-arthritis is not developed by everybody, although if life expectancy is increased, the disease could quite conceivably be inevitable in old age.

1.6 Magnitudes of loads transmitted by Joints

Throughout the previous three sections the magnitude of the loads transmitted by synovial joints has been mentioned. Much work has been done on the study of the loads transmitted, both statically and dynamically, through the joints of the lower limb, since these joints are the major weight bearing joints of the body.

Determination of the forces transmitted through joints in the dynamic situation involves the analysis of limb kinematics. Originally the main interest in gait analysis arose from the desire to simulate normal movement of the lower limbs with artificial legs; but knowledge of the weights and mass distributions of the segments of the body, and knowledge of the six components of load transmitted between the foot and the ground allows the calculation of the forces and moments at the joints needed to produce the observed motion.

The advent of the camera in the nineteenth century was an invaluable aid to locomotion study and progress in the study of human kinematics has been steady since that time. The introduction of force plates to measure the loads between the foot and the ground and studies of the activities of muscle groups increased the knowledge of the forces and moments applied to joints.

Paul[47] calculated values for the forces and moments applied to the hip which are closely resembled by the values determined by Rydell[48] from two special prosthetic devices. The latter's results are strictly only applicable to his prosthesis. Paul's work was extended to the knee joint by Morrison[49]

and he showed that in the normal walking cycle, a peak force of magnitude between two and four times body weight is transmitted through the knee joint. A more comprehensive study by Poulson[50] indicates similar peak loads in normal walking and up to seven or eight times body weight in walking down ramps or stairs. However, these solutions for loads transmitted through the knee, depend on the contact area assumed for the knee and the lines of action of the various ligaments and muscles. Both Morrison and Poulson's solutions for the knee joint conclude with the solution of two equations containing four unknowns. The use of different conditions for varying loading systems allows the number of unknowns to be reduced to two, and hence overall solution of the problem.

Furthermore, joint load analysis from cinematographic gait studies depends on the calculation of accelerations of limbs from sequential displacement measurements of markers on the moving human subject. This leads to a smoothing of the acceleration v. time graph. Direct measurements of the accelerations of the shank have been made[51] and hopefully accelerometry can be improved and used in conjunction with force plates and cinematography to give a more accurate estimate of the loads transmitted through joints in various activities.

1.7 The Knee - Anatomy

The knee joint is the articulation between the femur (thigh-bone) and the tibia, the larger of the two bones in the

shank[52, 53, 54]. The knee joint is functionally a hinge joint, but also allows a small amount of rotation of the leg especially in the flexed position. The joint is divisible into three articulations; the femeropatellar articulation and two tibio-femoral joints. The separation between the tibio-femoral joints is made by the intra-articular cruciate ligaments and the infra-patella synovial fold. The three cavities are separate but connected by restricted openings.

The articular surfaces of the femur are its medial and lateral condyles which have the form of rollers and diverge inferiorly and posteriorly, being separated by the inter-condylar fossa. The medial condyle is longer and more narrow than the lateral condyle. The contact surface for the patella is separate from the condylar surfaces but includes parts of both condyles, being derived mostly from the lateral condyle.

On the tibia there are two entirely separate cartilage covered areas. The surface of the medial condyle is oval, slightly concave and larger than the lateral condylar surface which is more circular and con-cave from side to side but con-cavo-convex anteriorly/posteriorl

The articular capsule is inseparable from the ligaments added to it. Posteriorly the

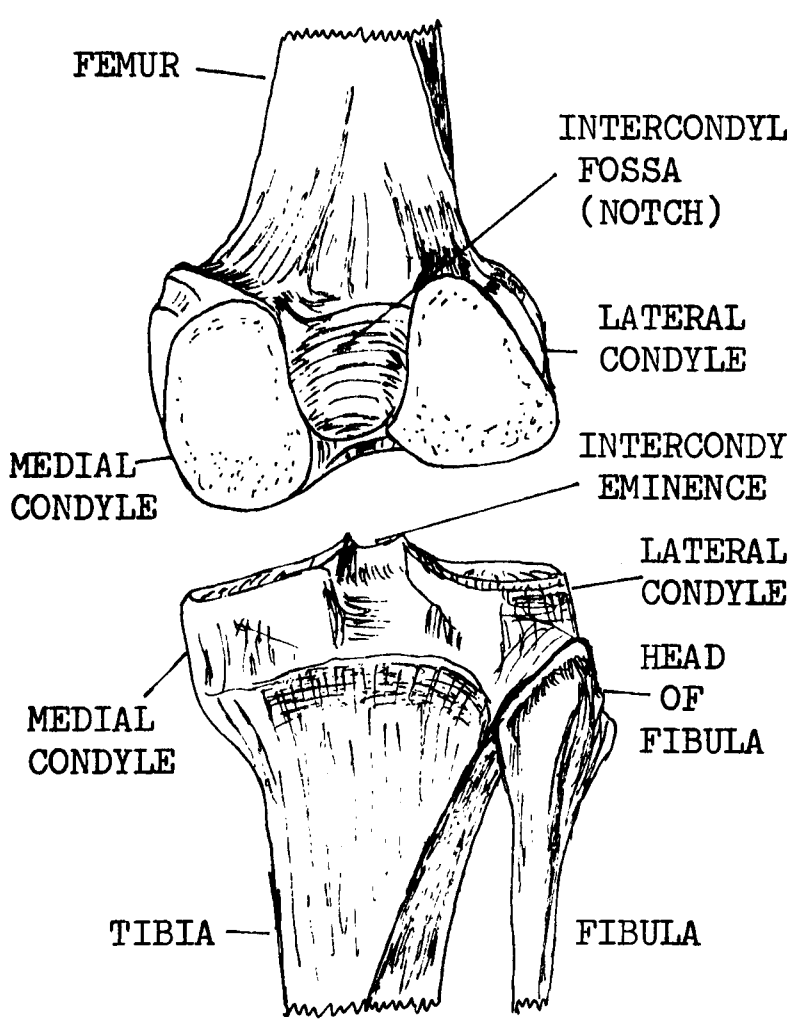

Posterior aspect of bones of knee

Diagram 1.3

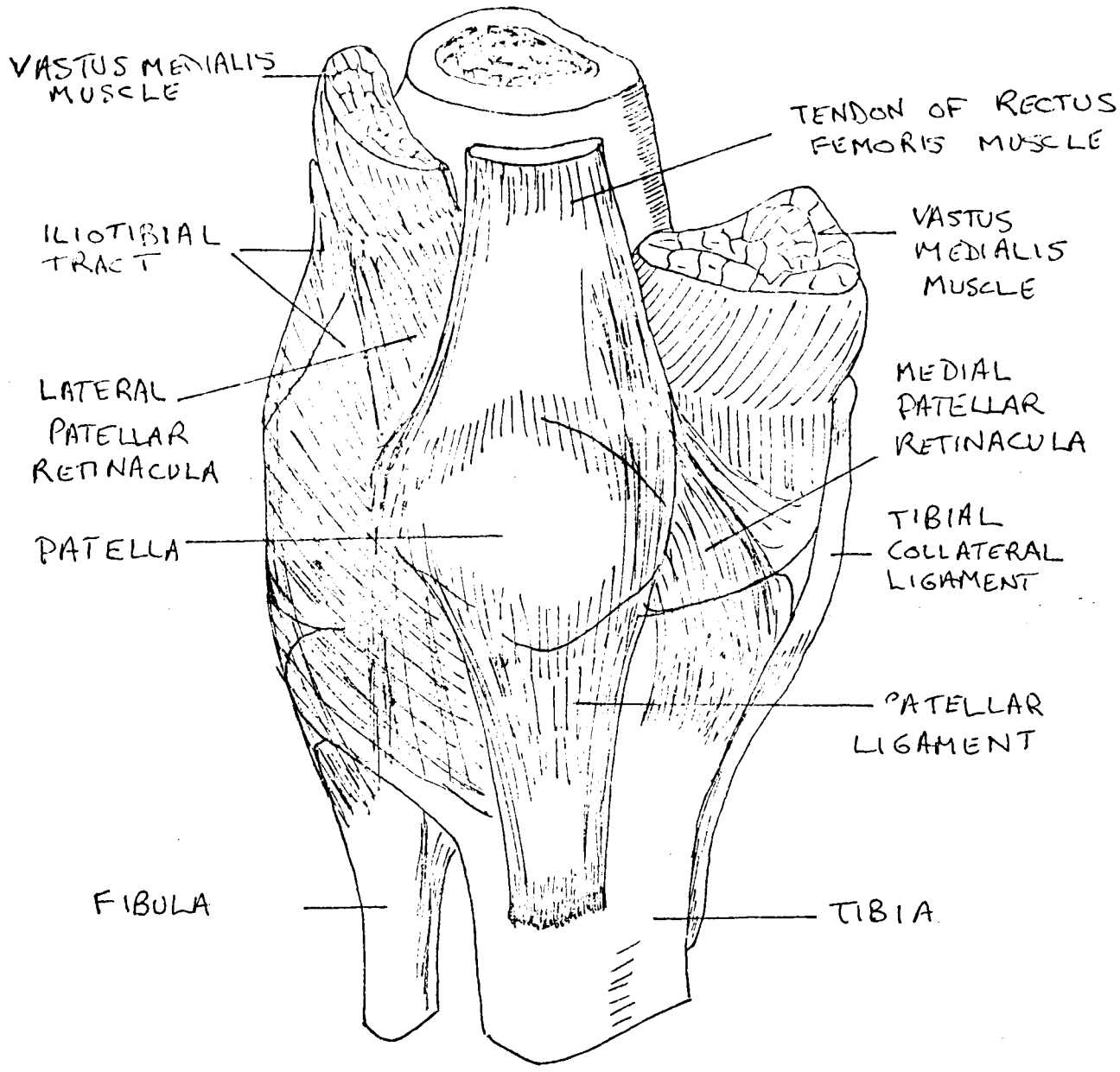

ANTERIOR VIEW OF KNEE AND LIGAMENTS

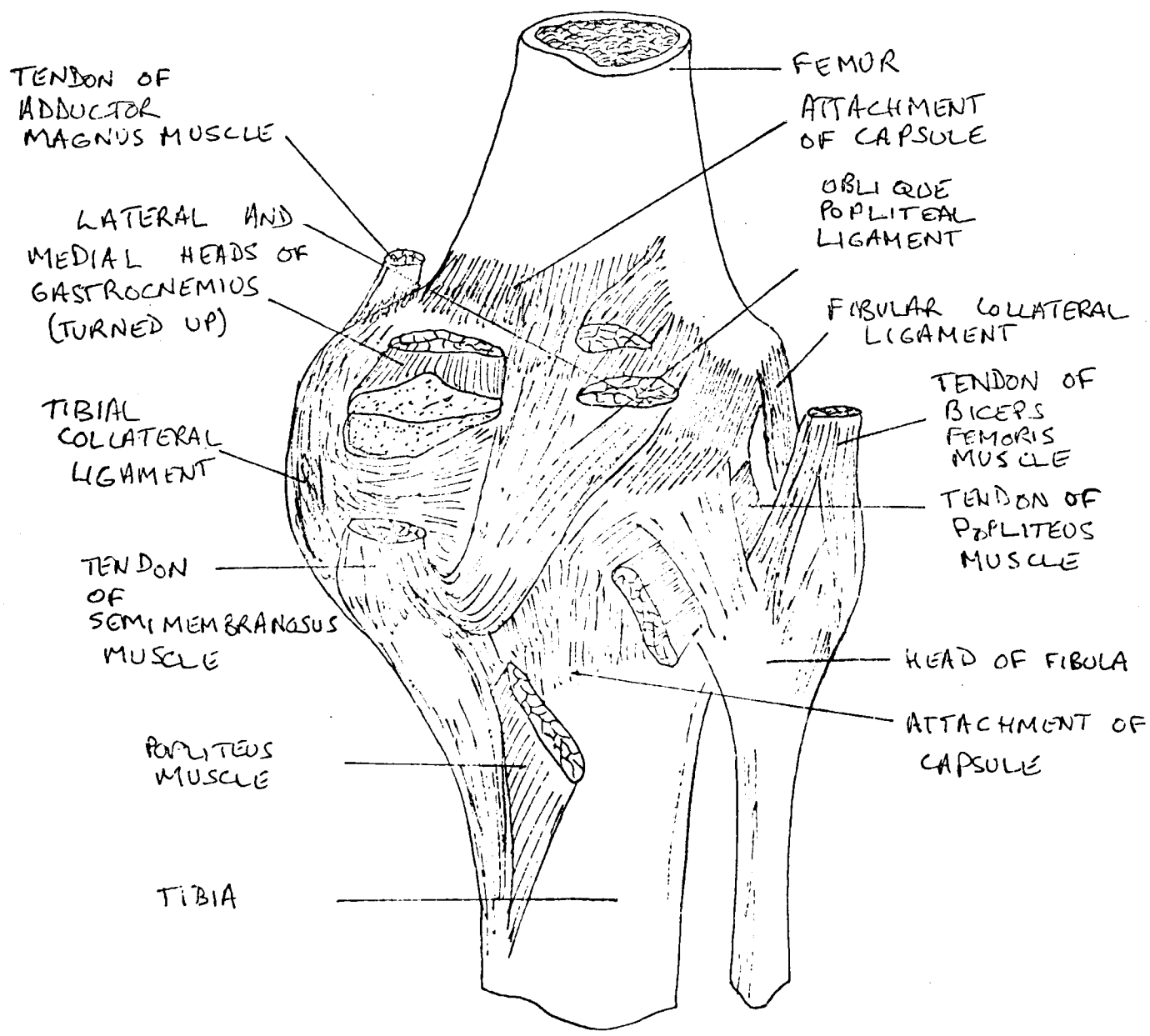

POSTERIOR VIEW OF CAPSULE OF KNEE

fibres of the capsule arise from the intercondylar fossa of the femur and attach below the tibial condyles and to the borders of the menisci. The external ligaments and tendons which reinforce the capsule are the fascia lata and ilio-tibial tract, the medial and lateral patellar retinacula, and the patellar,oblique popliteal and arcuate popliteal ligaments. These capsular ligaments are extensions of various muscle tendons.

The tendons of the muscles vastus medialis and vastus lateralis are attached to the medial and lateral margins of the patella and expand over the sides of the capsule as the medial and lateral patellar retinacula, inserting into the front of the tibial condyles round as far as the collateral ligaments. The fascia lata is superficial to the retinacula, covering the front and sides of the knee joint. On the lateral side of the fascia lata is the iliotibial tract which attaches to the oblique line of the lateral tibial condyle and to the head of the fibula.

The ligamentum patellae is an extremely strong flat band attached to the inferior border of the patella and is also continuous over the front of the patella with fibres of the quadriceps femoris muscle. The patellar ligament ends with attachment to the tibia. The oblique politeal ligament is a posterior reinforcement of the capsule provided by the tendon of the muscle semimem-branosus. The lower lateral part of the knee joint is strengthened by the arcuate popliteal ligament which

arises from the back of the head of the fibula and arcs upward and medially over the tendon of the popliteus muscle to spread out over the posterior surface of the joint.

The collateral ligaments are two strong bands on the sides of the knee and are not part of the capsule. The points of attachment of the collateral ligaments lie slightly behind the vertical axis of the bones. The tibial, or medial, collateral ligament extends from the medial condyle of the femur to the medial condyle and shaft of the tibia. Anteriorly it blends with the medial patellar retinaculum. The fibular, or lateral, collateral ligament is a rounded pencil-like cord attached to the lateral condyle of the femur and the lateral surface of the head of the fibula.

The intra-articular cruciate ligaments lie within the joint capsule but not the synovial membrane, and are strong cords which cross each other like an X. The anterior cruciate ligament arises from the rough nonarticular area in front of the eminence of the tibia and extends upward and backwards to the posterior part of the medial aspect of the lateral femoral condyle. The posterior cruciate ligament is directed upward and forward on the medial side of the anterior ligament and extends from the area behind the tibial eminence to the lateral

side of the medial femoral condyle.

The menisci are two crescent shaped wafers of fibrocartilage with triangular cross section. The menisci lie on the articular surfaces of the tibia and are loosely attached along their outer borders to the tibia, the lateral more weakly than the medial meniscus. At their ends, the horns, the menisci are firmly attached to the tibia in front of and behind the intercondylar eminence. The medial meniscus is broader posteriorly; anteriorly it is thin and pointed as it attaches to the tibia. The lateral meniscus is more nearly circular and close to its posterior attachment to the tibia there is frequently a bundle of fibres, the posterior meniscofemoral ligament, attaching it to the posterior cruciate ligament and the lateral side of the medial femoral condyle. Occasionally there is an anterior meniscofemoral ligament with a similar relationship with the anterior cruciate ligament. The transverse genicular ligament connects the two menisci across their anterior margins.

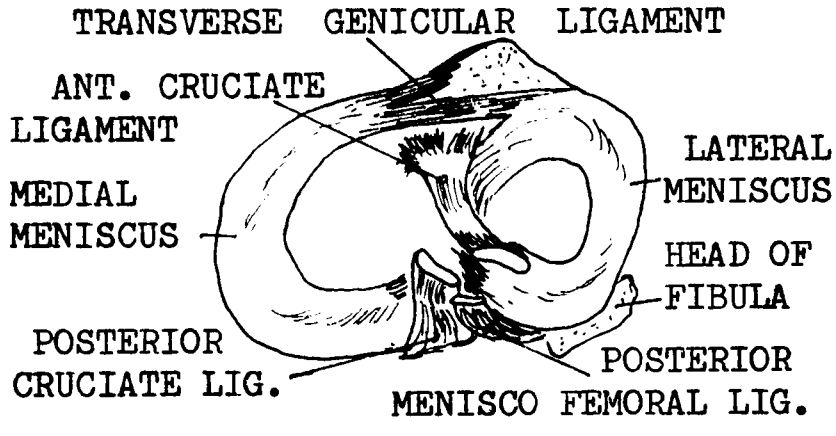

SUPERIOR ASPECT OF TIBIA
Diagram 1.6

Structural Roles of Components

A thorough study of the roles of the ligamentous structures and the menisci of the knee was carried out by Brantigan and Voshell[55]; other workers[56] tend to produce similar results. The roles of the ligaments are reasonably well defined, but the functions of the menisci are not (see later).

The anterior cruciate ligament limits backward sliding of the femur on the tibia, the posterior ligament limiting forward sliding. Abduction is limited by the medial collateral ligament and adduction by the lateral collateral ligament. Hyperextension is resisted by the cruciate ligaments and the posterior region of the capsule and its associated ligaments; hyperflexion is limited by the cruciate ligaments and the tissue surrounding the joint. In both these positions, some parts of the collateral ligaments are taut. Rotary motion is limited by the capsule, the collateral ligaments and the cruciate ligaments. Side motion of the femur on the tibia is limited by the capsule, the collateral ligaments, the cruciate ligaments and the tibial eminence. The patella increases the angle of the line of action of the quadriceps femoris muscle and applies a force posteriorly on the femur as the knee is flexed, thus controlling with the cruciate ligaments the relative positions of the two bones during flexion. The patella, with the infrapatella fat pad, also offers protection to the front of the joint. Finally, the screw-home mechanism, which is a medial rotation of the femur on the tibia in the final stages of extension, is caused by the cruciate ligaments.

Numerous roles are ascribed to the menisci. The menisci fill the gap between the femur and the tibia and deepen the surfaces of the tibia[52, 53, 54]; cushion hyperextension and hyperflexion[55]; protect the articular cartilage by absorbing shocks[57]; may act as shock absorbers in the dynamic situation, but do not significantly bear weight in the static situation[58]; act as Michell thrust pads to ensure excellent joint lubrication

but do not bear weight[59]; allow rotation to occur and spread synovial fluid[53]; facilitate complex movements, for example, the screw-home mechanism[60]; bear weight when the knee is fully extended, this function being an acquisition of recent evolutionary origin common only to human beings, and the possible structural instability of the menisci accounting for their frequent damage[60]. The majority of workers to whom reference has been made above usually consider the functions of the menisci to be combinations of the roles mentioned. Only two workers suggest that weight-bearing is a major functional role: Fairbank[61] from studies of the changes in the knee joint after meniscectomy; and Bullough et al[62] from the physical structure of the menisci. The menisci are found to be fibrous with the fibres running circumferentially. The greatest strength is along the line of the fibres and is similar to that for the surface layer of articular cartilage in the fibre direction[62].

Deane[58] performed two dye tests on knee joints with the menisci in situ. The joints were subjected to light load (4 Kgf) and it was found that no dye penetrated the areas of cartilage in contact with the menisci. The remaining contact studies were made with the menisci excised as were the contact studies of other researchers[63,64]. Deane and Kettelkamp and Jacobs are eventually non-committal as to the weight-bearing role of the menisci. Walker[65] clearly indicates that the menisci are considered to be non weight-bearing, as too does Morrison[49], by their assumed tibio-femoral contact areas.

1.8 The possibility of the menisci having a weight-bearing role

It is clear that there is uncertainty as to the functions of the menisci. There has been some speculation concerning a weight-bearing role and the purpose of this thesis is to investigate this further.

The geometry of the opposing bone surfaces of the hip and elbow joints are closely conforming but incongruent[3,36], and the geometry is closely linked to the various functions of the joints. The opposing bone surfaces of the ankle and should joints are also closely conforming but the opposing bone surfaces of the tibio-femoral joint are grossly incongruent. The apparent incongruity would not exist if the menisci have a weight-bearing role and furthermore:-

(a) A weight-bearing role of the menisci would produce larger contact areas than those previously determined for the tibio-femoral joint[58,63,64] with the advantages of a lower average pressure and smaller pressure gradients. Small pressure gradients should reduce the fluid loss from articular cartilage subjected to high pressure. It is likely that gross loss of fluid from high pressure zones will have a detrimental effect upon the articular cartilage and its ability to transmit loads. Greenwald and O'Connor[33] suggest that synovial joints transmit load by the development of uniform pressure distributions. The development of such a distribution in the knee only seems feasible if the menisci bear weight.

(b) In the tibio-femoral joint the areas of articular cartilage which first show signs of degeneration are those areas of the tibial condyles enclosed by the menisci. The cartilage elsewhere in the joint is usually in better condition[66]. If the menisci are non weight-bearing, the pattern of degenera-

tion found in the tibio-femoral joint is anomalous to the pattern observed in other joints (see 1.5).

(c) Removal of a meniscus increases the tendency for cartilage to degenerate in both dogs[57] and humans[67]. The cartilage degeneration is observed to occur on those areas of the tibial condyles previously enclosed by the menisci. The changes in the knee joint after meniscectomy[61] and the consistency with which degenerative changes develop[57,67] suggest that the phenomena are the result of a gross change in the load-bearing system of the joint.

If a weight-bearing role could be attributed to the menisci then not only are the above observations explicable, but also the concepts of 'cushioning hyperextension' and 'acting as shock absorbers' become more meaningful.

The question arises as to how the function may be performed. Fairbank[61] suggests that in full extension, when the femur approaches the tibia under load, the menisci are forced to expand centrifugally. The expansion is resisted by the development of circumferential tensile stresses which have a centripetal component. Bullough et al[62] have shown that the collagen fibre orientation in the menisci is predominantly circumferential and with such a structure the menisci can resist relatively large circumferential forces.

In full extension, the radius of curvature of the femoral condyles is at its largest, and hence the contact areas between the femoral and tibial condyles and the menisci, and the femoral and tibial condyles are also at their largest. As flexion occurs, the radius of curvature decreases and hence the contact between femoral condyles and menisci should be reduced. However, although it has not been previously

noticed in this context, the femoral condyles diverge posteriorly and could, therefore, push the menisci outwards medio-laterally to maintain full contact between the femoral condyles and menisci. Hence, if load-bearing occurs in full extension in the manner described above, load-bearing could also occur in all other joint positions. Thus load-bearing could quite possibly be a major functional role of the menisci.

1.9 Outline of Thesis

In Chapter 2, a very approximate theoretical study shows that the proposed method of load transmission, that is, the resistance of centrifugal forces by the development of circumferential tensile forces, is viable for a wide range of the various parameters involved, and that load bearing is likely to be a significant role of the menisci. However, because of the many approximations made there is a need for experimental evidence to support the theoretical predictions.

Chapter 3 discusses the experimental apparatus and methods. Compressive load/deflection tests were performed on both pig and human specimens and the radial expansion of the menisci was measured. In order to estimate the load carried by the menisci from the radial expansion measurements, it is necessary to determine the circumferential Young's modulus of the menisci. Hence tensile stress/strain data for small specimens of the menisci were obtained.

Chapter 4 discusses the results and conclusions drawn from the experiments described in Chapter 3. The results obtained from contact studies and the use of a pressure transducer are noted. It is concluded that the menisci do bear a significant proportion of the load transmitted through the intact healthy knee and Chapter 5 discusses the significance of this conclusion.

CHAPTER 2

A SIMPLE MODEL

2.1 Introduction

The analysis of the stress distributions in a real knee joint is obviously difficult. In this chapter a simple model is proposed and analysed using simple stress/strain relationships. The model is three dimensional and axi-symmetric.

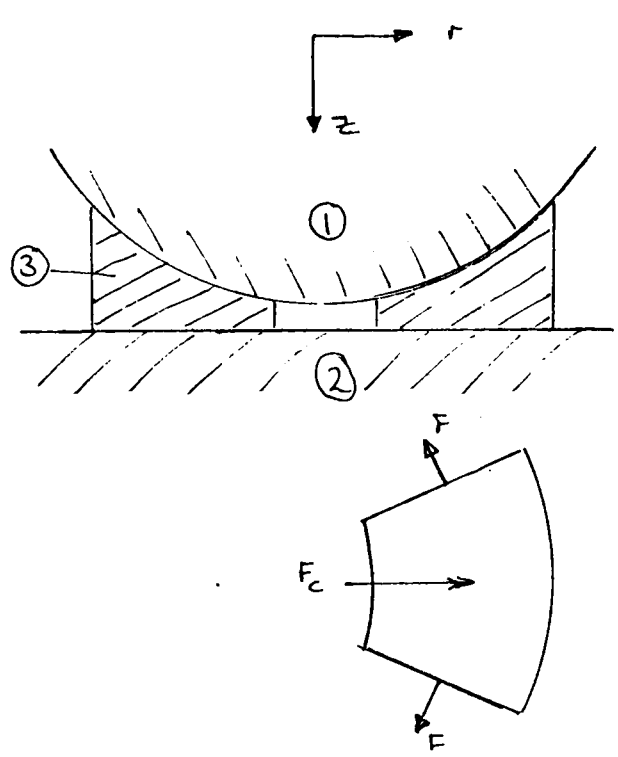

The proposed method of load transmission is that as the femur, (1), approaches the tibia, (2), the meniscus (3) is forced to expand radially because the summation of the pressure on the inclined femoral surface of the meniscus produces a centrifugal force, F_C. Radial equilibrium of the meniscus is maintained by the development of a circumferential tensile force, F, which has a centripetal component. The vertical components of the stresses on the femoral surface of the meniscus will sum to give the total vertical load carried by the meniscus. The order of magnitude of the vertical load will indicate whether weight-bearing can be a major or is merely a minor role of the meniscus.

2.2 Model Geometry

In the model analysed, the bone surfaces are covered with thin layers of articular cartilage (see diagram 2.1). The tibial surface is assumed to be flat although the condyles are slightly concave in the normal healthy joint. The femur is represented as an indentor with a flat central zone surrounded by an upturned dome of constant curvature. The radius of curvature of the flat zone corresponds to the inner radius of the meniscus and the radius of curvature of the dome corresponds to the radius of curvature of the femoral condyles in the coronal plane. The menisci are represented as a single annular ring, wedge-shaped in cross-section.

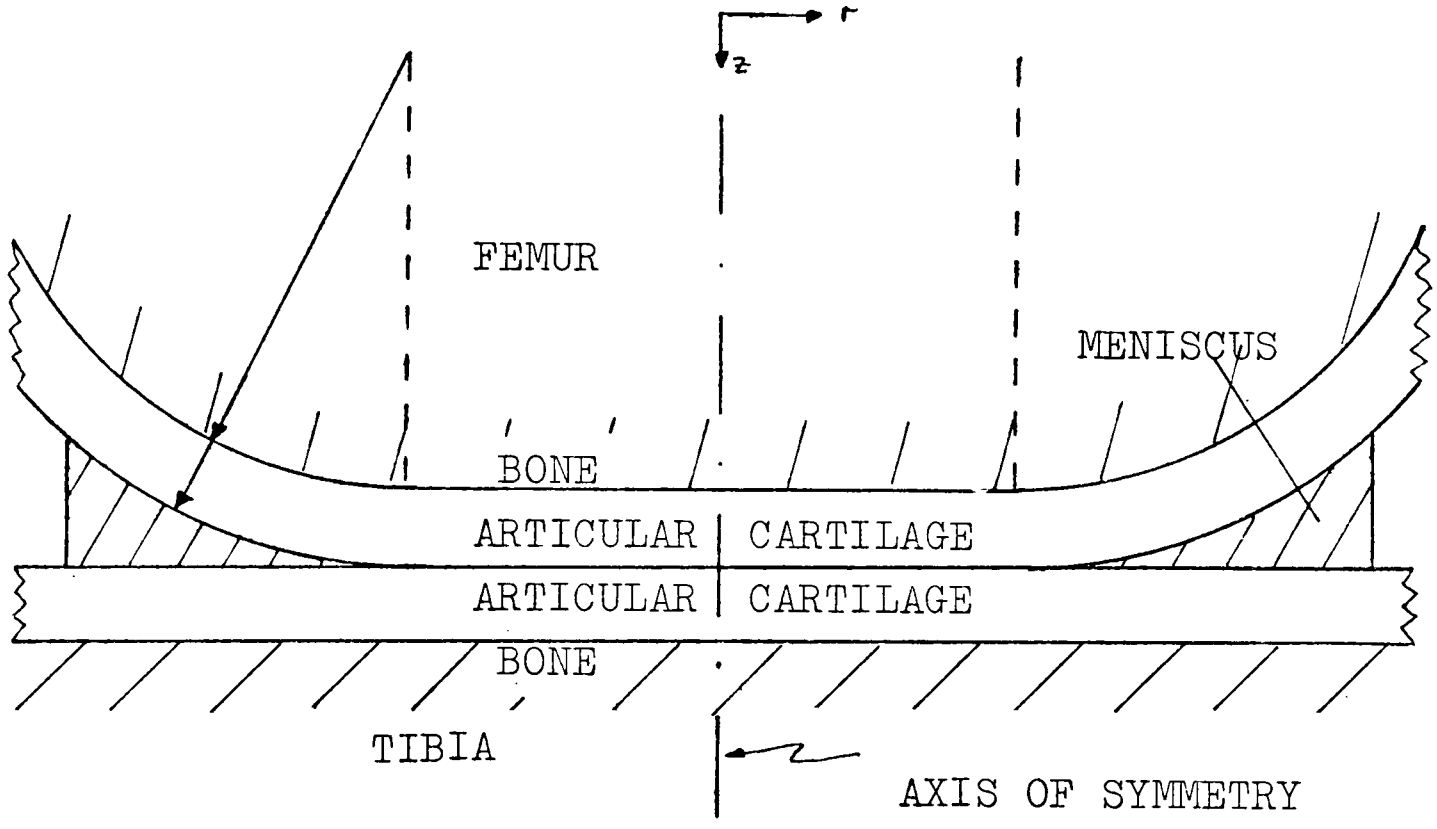

Diagram 2.1

It is considered that the geometry of the model is relevant to the actual joint because the notch and eminence contain the cruciate ligaments and there is no direct tibio-femoral contact or compressive load transference in this area. The exclusion of the notch and eminence therefore, leaves the geometry of the knee akin to that of the model. In the real knee, the radial expansion of the menisci is limited by their tibial attachments; clearly this feature is not reproduced by the model but this should not affect the proposed method of load transmission.

2.3 Analysis

2.3.1. Statement of the problem, boundary conditions, equilibrium conditions and necessary assumptions.

Diagram 2.2 represents the undeformed state of the model where:-

O_1 , O_2 = points in pole planes in femoral and tibial bone components:

r = radial distance of a point from the axis of symmetry:

r_m = inner radius of meniscus = outer radius of flat portion of femur:

c = width of meniscus:

R = Radius of femoral component:

t_1 , t_2 = cartilage thickness on femoral and tibial condyles respectively:

t = thickness of meniscus at radius, r

z_1, z_2 = axial distances from pole planes to femoral and tibial articular cartilage surfaces:

H = distance between pole planes:

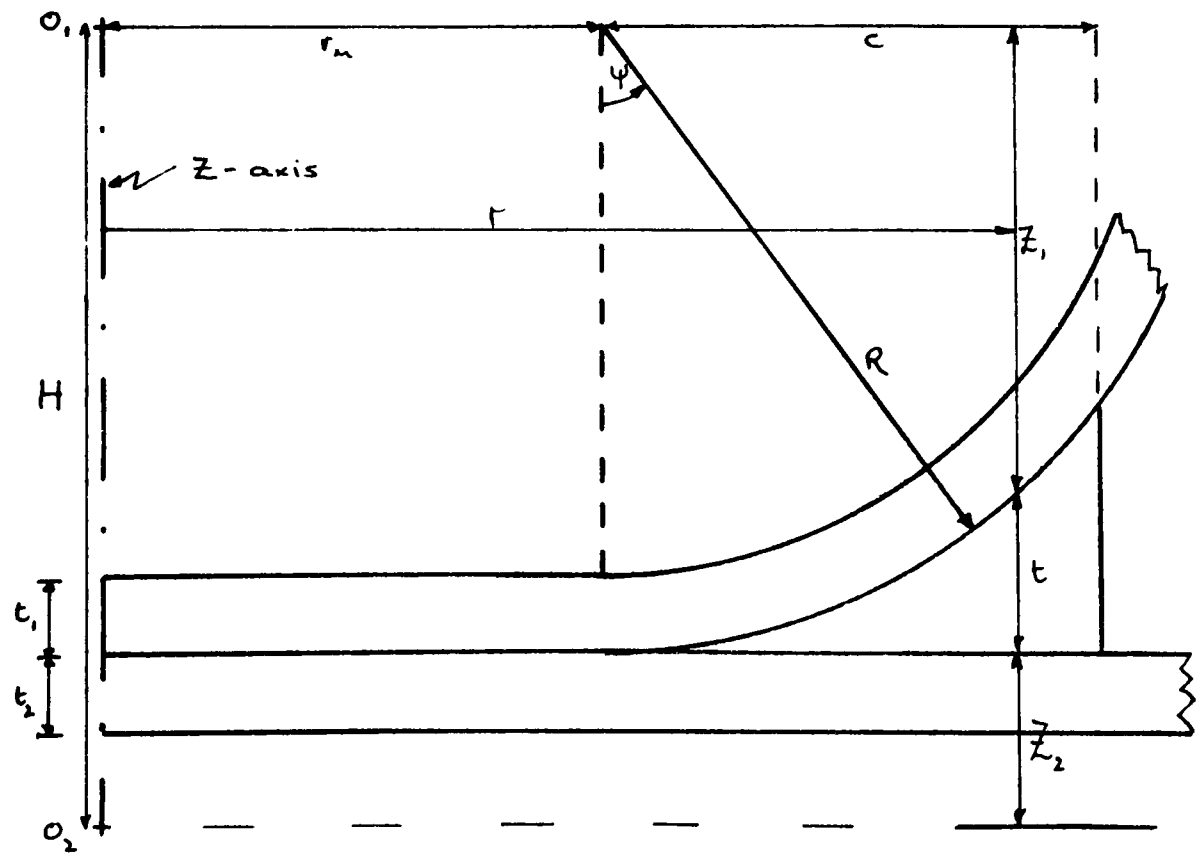

Diagram 2.2

UNDEFORMED STATE OF MODEL

The distance between the pole planes may be written as

$$H = Z_1 + Z_2 \qquad r \leq r_m$$

$$H = Z_1 + Z_2 + t \qquad r \geq r_m \qquad \text{.....2.1}$$

If the pole planes are made to approach each other by a distance, d (see diagram 2.3), then the meniscus will slide out a distance, a , and equations 2.1 become

$$H - d = Z_1' + Z_2' \qquad r \leq r_m + a$$

$$H - d = Z_1' + Z_2' + t' \qquad r \geq r_m + a \qquad \text{....2.2}$$

where Z_1' , Z_2' = new distances from pole planes to tibial and femoral articular surfaces

and t' = new thickness of meniscus at radius, r

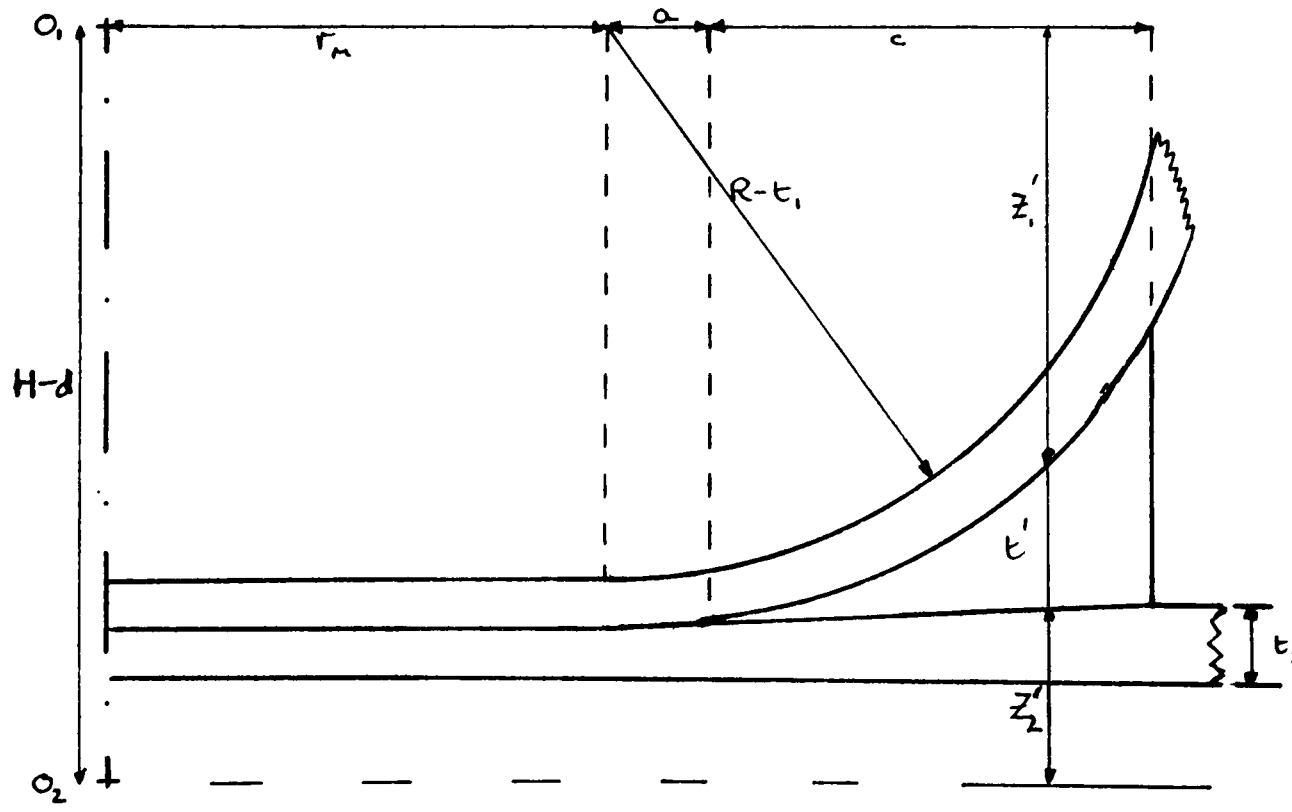

Diagram 2.3

DEFORMED STATE OF MODEL

Kempson et al[35] indicate that bone is very much stiffer than cartilage. It is reasonable to assume, therefore, that the bone layers are rigid in comparison to the cartilage layers, and that all deformation occurs in the cartilage layers.

Hence, subtracting equations 2.2 from equations 2.1, and noting that $(z - z')$ will be the deformation, ω, in the direction of the respective cartilage layers, gives:-

$$\begin{aligned} d &= \omega_1 + \omega_2 && r \leq r_m \\ d &= \omega_1 + \omega_2 + t && r_m \leq r \leq r_m + a \\ d &= \omega_1 + \omega_2 + t - t' && r_m + a \leq r \end{aligned} \quad \ldots\ldots 2.3$$

The displacement, ω, at radius, r, of the surface of a cartilage layer will be a function of the applied stresses on the total contact area, A:-

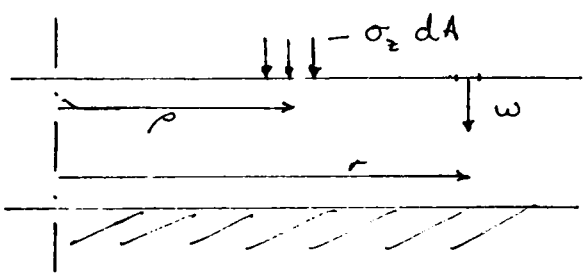

$$\omega_{(r)} = \int_A K_1(r,\rho)\ \sigma_z(\rho)\, dA \quad \ldots\ldots 2.4(a)$$

Although the function K_1 is known for simple indentation problems[76,79] for the elastic layer, explicit evaluation of the integral in 2.4(a) in terms of simple functions is not possible. Similarly for the meniscus,

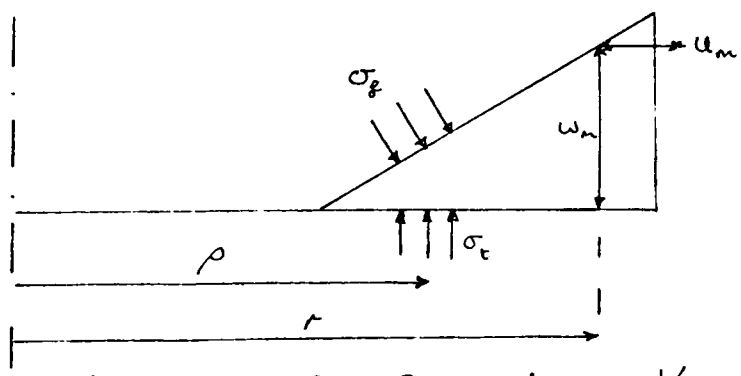

$$u_{m(r)} = \int K_2(r,\rho) f\left(\sigma_f(\rho), \sigma_t(\rho)\right) d\rho \quad \ldots\ldots 2.4(b)$$

and the relative approach of the meniscal surfaces

$$\omega_{m(r)} = \int K_3(r,\rho)\, g\left(\sigma_f(\rho), \sigma_t(\rho)\right) d\rho \quad \ldots\ldots 2.4(c)$$

In this case the functions K_2 and K_3 are not known. Continuation of an analysis based on equations 2.4 above would clearly be complex and hence a simpler method of analysis will be used. The aim of the analysis of the model is simply to estimate the order of magnitude of the proportion of the load carried by the meniscus.

Relationships between deformations and stresses for both layers and the meniscus are discussed below (§ 2.3.2.3). Once these are established it will be possible to determine the surface stress distributions from equations 2.3 above and then to determine the load, P necessary to give the relative approach, d, of the pole planes from

$$P = \int_0^{2\pi} \int_0^{\text{outer edge of miniscus}} \sigma_{zz}(r)\, r\, dr\, d\theta \qquad \text{.....2.5}$$

and the load carried by the meniscus will be

$$P_m = \int_0^{2\pi} \int_{\text{inner edge}}^{\text{outer edge of meniscus}} \sigma_{zz}(r)\, r\, dr\, d\theta$$

where the notation is conventional for cylindrical co-ordinates and will be used as necessary in all further equations.

Other conditions that may be used in the analysis are that radial and vertical equilibrium of the meniscus must be maintained and that the surface pressure is continuous at the inner radius of the meniscus. In the meniscal contact areas the stresses on the articular cartilage layers are assumed to be in equilibrium with the stresses on the surfaces of the meniscus. Also it is assumed that there are no surface shear stresses because the coefficient of friction in synovial joints is low (see 1.4). Hence the meniscus slides in and out frictionlessly and only normal stresses act on cartilage surfaces.

Furthermore, it is assumed that the cartilage layers and the meniscus are linearly elastic. Kempson[68] has shown that for loads in the physiological range, 90% of the deformation of cartilage is instantaneously recoverable on

load removal when the loading time is two seconds. In the walking cycle loading times are well within this value[49]. The assumption of linear elasticity is necessary for a simple solution of the problem but not justifiable considering the stress/strain behaviour of cartilage observed by Kempson et al[4] and this author (see Page A.65). To assume that the elastic modulus is constant throughout the cartilage structure is not strictly true since the cartilage layer is not uniform (see 1.3). However the reaction of the complete layer to an applied deformation is considered and the modulus therefore refers to the complete layer rather than the individual elements within the layer.

With the initial assumptions and boundary conditions stated, and the problem formulated, possible methods of solution are considered.

2.3.2. Method of Solution.

(1) Wedge Analyses:

It may be possible to obtain an estimate of the relative approach of the wedge surfaces using available solutions to various fixed-angle wedge problems[69]. It would be necessary to presuppose an applied stress distribution and to satisfy equilibrium on the articular cartilage-meniscus interfaces. Also the deformation of the meniscus would have to be compatible with that of the articular cartilage layers. The absence, indicated above of a solution for a finite width, wedge-shaped annulus carrying circumferential stress, together with the requirements above, suggest that

another method of solution would be more appropriate.

(2) Finite element Method of Stress analysis:

The finite element method of stress analysis has been applied to various biological structures[70, 71,72]. The analyses all involve idealizations of geometry and material properties as has been and will be done here. Allowance can be made for the different mechanical properties of the various materials present, and for these properties to be orthotropic. It would appear, therefore, that the method could be applied reasonably easily to the proposed model. There are, however, major differences between this model and the problems already solved.

In the latter, at material interfaces, the nodes on the surface of one material are also nodes on the surface of the adjacent material; no surface slip is allowed so that when load is applied, the two material surfaces maintain their relative positions and the surface nodes remain nodes for both materials. In the proposed model the meniscus slides radially outwards as load is applied. This means that the articular-cartilage-meniscus interface nodes can not be treated as nodes with elements of different stiffnesses on either side. They must be made separate, though initially at the same position, and then allowed to move in relation to one another when load is exterted. On the inner edge of the meniscus, nodes on the articular surfaces which were originally in contact with meniscal nodes would be displaced relative to each other. A node on one surface would have to become coincident with a node on the other surface, offset not being allowed. On the outer edge of the meniscus, more articular cartilage nodes would be

displaced as the contact area grew.

A second difficulty raised by the meniscal expansion is that it is quite possible for the outer femoral surface of the meniscus to separate from the opposing articular cartilage. The results of the analysis performed in the following sections shows that this does occur under certain conditions; and personal observation during experiments indicated that under high loads, separation of this type is not uncommon. Certain problems involving slip and separation have been solved by the finite element method[73, 74, 75] but the slip amplitude in those cases is small compared to the node spacing.

A final complication is that if the radial expansion is large compared to the original inner radius of the meniscus, then the circumferential strains will be large. As will be seen in the analysis below and in Chapter 4, circumferential strains of 25% or more often occur. Stress analysis based on the theory of infinitesimal strains is doubtful under these conditions.

The consequence of these complications is that the problem is more intricate than those already solved and hence the associated programming would be much more involved. To solve the problem by this method would probably be very gratifying, but would take a considerable amount of time. The end results would be more accurate for small strains than those eventually obtained below, but would give the same basic information - an order of magnitude of the percentage of the total load carried by the menisci. It was decided to use the simpler, cruder and less time consuming method described below.

(3) The Thin Layer Approximation:

The thin layer approximation is a stress/strain relationship in which the normal displacement at any point on a surface is considered to be proportional to the normal stress at that point. For the thin layer approximation, Tu and Gazis[76] show

$$\sigma = k\epsilon = k\frac{\omega}{t} \qquad \ldots.2.6$$

where σ is the stress normal to the surface, ϵ is the strain normal to the surface defined by the deformation, ω, normal to the surface divided by the original thickness, t, of the layer and

$$k = \frac{E}{2(1-\nu^2)} \qquad \ldots2.7$$

where E is the Young's Modulus and ν is the Poisson's ratio of the material.

Tu and Gazis consider the problem of a plate pressed between two spheres and show that the important factor as regards the validity of the thin layer approximation is the area-aspect ratio, b/t, where b is the total width of the contact area; and indicate the thin layer approximation to be valid for the range $2 < b/t < \infty$.

O'Connor[77], considering a small torsional couple applied to a plate between two identical spheres indicates the range to be $10 < b/t < \infty$, with experimental evidence showing reasonable agreement. Furthermore, O'Connor[78] has derived the exact solution for a thin elastic layer covering a rigid flat surface and subject to a specified stress distribution on its upper surface, and indicates the thin layer approximation to be valid for $4 < \frac{b}{t} < \infty$. It is interesting to note that with the applied compressive stress normal to the surface, the stress parallel to the surface

in the layer immediately below the surface, is compressive within the contact area but, depending on the area-aspect ratio, may become tensile beyond the contact area. Also if the applied stress is parallel to the surface, then the surface layer is always subject to tension, in direction of applied stress.

A numerical solution, based on exact equations, has been derived for the problems of rigid indentors pressing into thin layers on rigid flat surfaces[79]. The problems for the two indentors considered may be solved using the thin layer approximation (see Appendix 2a) and the results compared with the numerical solution. There appears to be a difference of a factor of 3-35 between the two solutions.

The various problems considered, therefore, indicate that the thin layer approximation will be reasonably accurate for the articular cartilage layers if the area-aspect ratio is high. The geometry assumed in the eventual numerical solution of the problem gives a ratio of approximately 10.

The major sources of error of the analysis lie in the solution of the stresses and strains in the meniscus. A stress/strain relationship similar to the thin layer approximation is assumed to exist in the meniscus, which is effectively considered to be made up of series of interconnected springs in the θ and z-directions. The springs in one direction, when deformed, have no effect on the springs in theother, Poisson's ratio being set to zero. There are no radial springs as σ_{rr} is also set to zero. The radial width of the meniscus, therefore remains constant, and deformations in specified directions may be directly related to the stresses in those directions. The errors introduced to the analysis by such simple relation

ships are discussed in Appendix 2(b).

2.3.3. Determination of strain and stress in z- direction in meniscus.

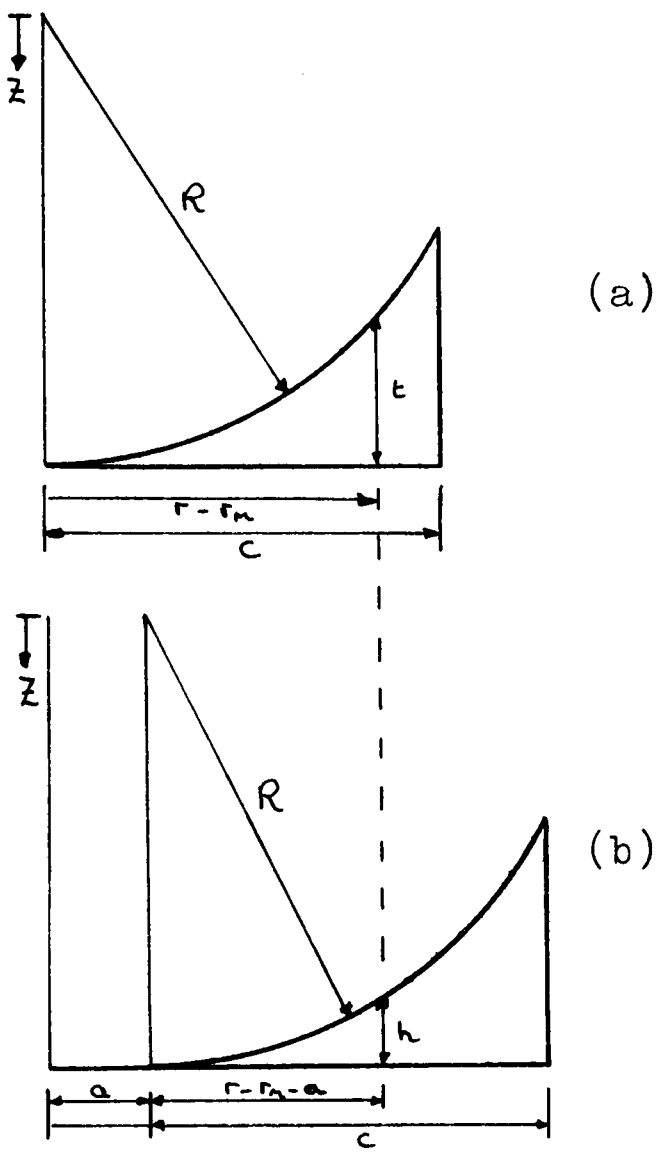

The thickness of the meniscus at radius, r in the undeformed state is t (see diagrams 2.2. and 2.4.a). The femoral surface is the arc of a circle radius R, hence

$$t = R\left[1 - \left(1 - \left(\frac{r - r_m}{R}\right)^2\right)^{\frac{1}{2}}\right] \quad \ldots 2.8$$

If the meniscus slides out an amount, a, and remains undeformed then the height at radius, r, will be h where,

$$h = R\left[1 - \left(1 - \left(\frac{r - r_m - a}{R}\right)^2\right)^{\frac{1}{2}}\right] \quad \ldots 2.9$$

Diagram 2.4

(a) meniscus undeformed

(b) undeformed (in z- direction) but expanded to radius a.

However, a deformation, ω_m occurs so that the final height at radius, r, is t' $(= h - \omega_m)$ and the strain in the z- direction is

$$\epsilon_{zz} = \frac{\omega_m}{h} \quad \ldots 2.10$$

If k_1 is the coefficient relating stress to strain in the z- direction of the meniscus and k_2 is the Tu and Gazis modulus relating stress to strain in the z- direction in the articular

cartilage layer then

$$\sigma_{zz}(r) = k_1 \frac{\omega_m}{h} = k_2 \frac{(\omega_1 + \omega_2)}{t_o} \qquad \ldots 2.11$$

where t_o is the total thickness of the articular cartilage in the z - direction (see Appendix 2.c).

The third of equations 2.3 gives, when using $t' = h - \omega_m$

$$d - (t - h) = \omega_1 + \omega_2 + \omega_m \qquad 2.12$$

and using 2.11, 2.12 becomes

$$d - (t - h) = \sigma_{zz}(r)\left(\frac{h}{k_1} + \frac{t_o}{k_2}\right) \qquad 2.13$$

giving

$$\sigma_{zz}(r) = k_1 \frac{d - R\left[\left(1 - \left(\frac{r - r_m - a}{R}\right)^2\right)^{\frac{1}{2}} - \left(1 - \left(\frac{r - r_m}{R}\right)^2\right)^{\frac{1}{2}}\right]}{\left(R\left[1 - \left(1 - \left(\frac{r - r_m - a}{R}\right)^2\right)^{\frac{1}{2}}\right] + t_o \frac{k_1}{k_2}\right)} \qquad \ldots 2.14$$

this being valid for $r_m + a \geq r \geq r_m + a + c$

2.3.4. Determination of stress in direct articular cartilage contact area.

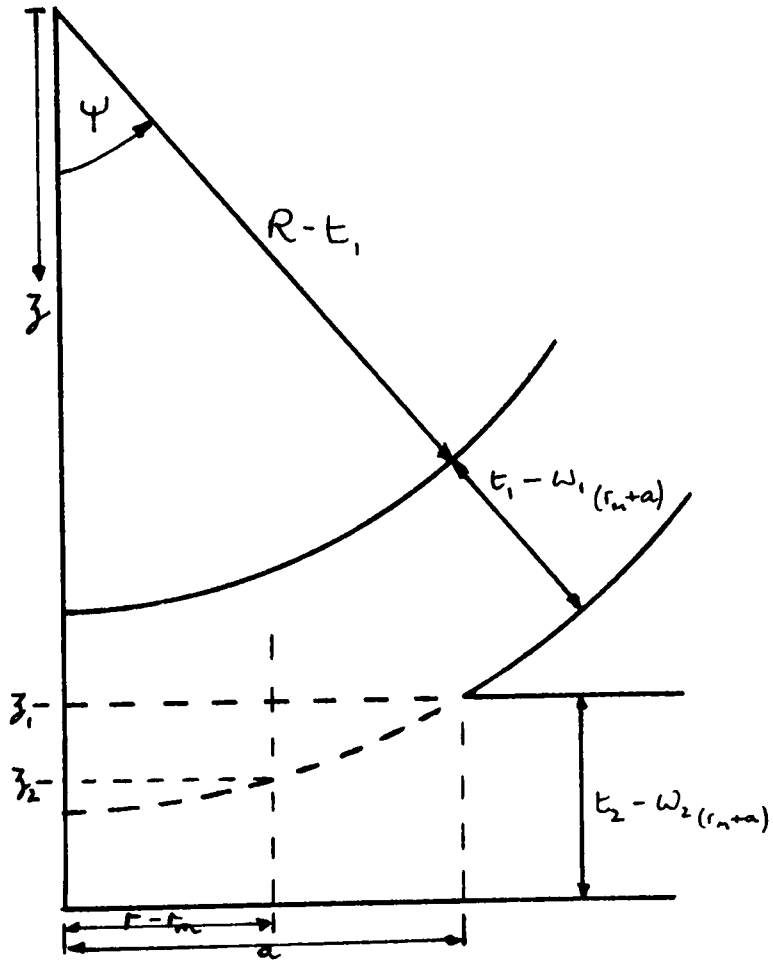

Diagram 2.5

Increase in Direct Articular Cartilage Contact Area

Now consider the articular cartilage layers. The total thickness of cartilage in the undeformed state in the z - direction is

$$t_o = t_2 + t_1 / \cos\psi \qquad 2.15$$

In order for there to be no surface discontinuities in the cartilage layers within the contact zone, the normal stress is assumed to be a continuous function of radius.

From equation 2.14

$$\sigma_{zz}(r_m+a) = k_2 \frac{d - R\left[1 - (1 - \frac{a^2}{R^2})^{\frac{1}{2}}\right]}{t_o} \qquad \ldots 2.16$$

hence

$$(\omega_1+\omega_2)_{(r_m+a)} = d - R\left[1 - (1 - \frac{a^2}{R^2})^{\frac{1}{2}}\right]$$

From diagram 2.5 it can be seen that for $r < r_m + a$

$$(\omega_1+\omega_2)_r = (\omega_1+\omega_2)_{(r_m+a)} + z_2 - z_1$$

hence

$$(\omega_1+\omega_2)_r = d - R\left[1 - (1 - \frac{a^2}{R^2})^{\frac{1}{2}}\right] + \left(R^2 - (r-r_m)^2\right)^{\frac{1}{2}} - \left(R^2 - a^2\right)^{\frac{1}{2}}$$

$$= d - R\left[1 - (1 - \frac{(r-r_m)^2}{R^2})^{\frac{1}{2}}\right] \qquad \ldots 2.17$$

It may be seen from 2.17 that when $r = r_m$, $\omega_1 + \omega_2 = d$.

d is the distance of approach of the two pole points, and must be the cartilage deformation in the flat central zone. The overall stress distribution for the model is thus:-

$$\sigma_{zz}(r) = k_2 \frac{d}{t_o} \qquad (\psi = 0),\ r \leq r_m$$

$$\sigma_{zz}(r) = k_2 \frac{1}{t_o}\left(d - R\left[1 - (1 - \frac{(r-r_m)^2}{R^2})^{\frac{1}{2}}\right]\right) \qquad r_m \leq r \leq r_m + a \qquad \ldots 2.18$$

$$\sigma_{zz}(r) = k_1 \frac{\left(d - R\left[\left(1 - (\frac{r-r_m-a}{R})^2\right)^{\frac{1}{2}} - \left(1 - (\frac{r-r_m}{R})^2\right)^{\frac{1}{2}}\right]\right)}{\left[R\left(1 - (1 - (\frac{r-r_m-a}{R})^2)^{\frac{1}{2}}\right) + t_o \frac{k_1}{k_2}\right]} \qquad r_m+a \leq r \leq r_m+a+c$$

2.3.5. Derivation of relationship between expansion and deflection.

Before equations 2.18 may be appropriately substituted into equation 2.4, it is necessary to find the relationship between the relative approach of the pole planes, d and the expansion, a, of the meniscus. These two parameters must be interrelated, only one a existing for a specified d and the value of a depending on the geometric constants and the stress/strain modular ratios. The relationship may be found from a study of the meniscus. On an element at radius, r,

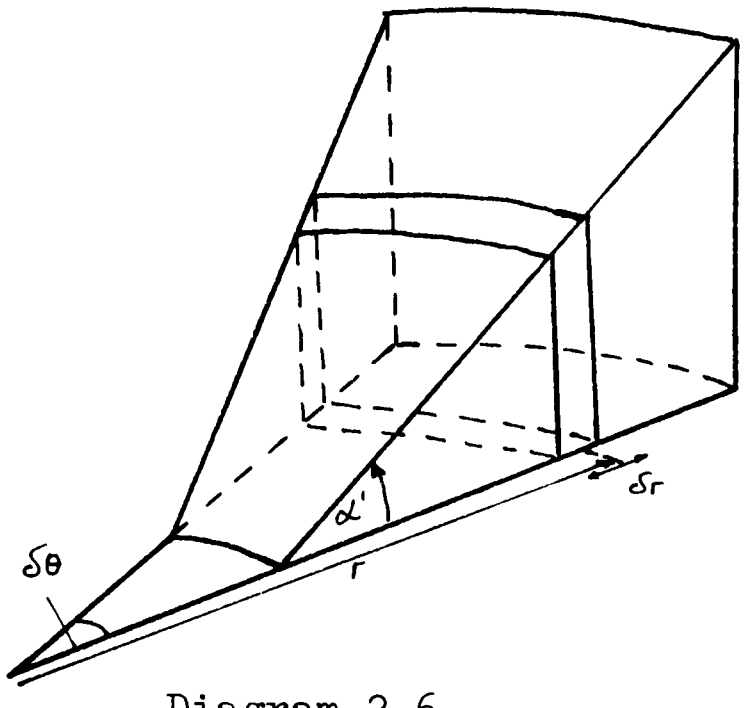

Diagram 2.6

(see diagram 2.6), the vertical force on the tibial surface is $\sigma_{zz}(r)\, r\, \delta r\, \delta\theta$ As there is no shear stress in the z- direction, this force must be balanced by the vertical component of the force acting on the femoral surface. This force acts normally to the femoral surface and must be therefore $\sigma_{zz}(r)\, r\, \delta r\, \delta\theta\, \sec\alpha'$ ....2.19(a)

and the radial component of this force is centrifugal in direction and is $\sigma_{zz}(r)\, r\, \delta r\, \delta\theta\, \tan\alpha'$ ....2.19(b)

The sum of these forces over the femoral surface of the meniscus is balanced by hoop stresses developing as the meniscus expands, which sum to a force, F, which has a centripetal component $F\delta\theta$ (see diagram 2.7). Hence,

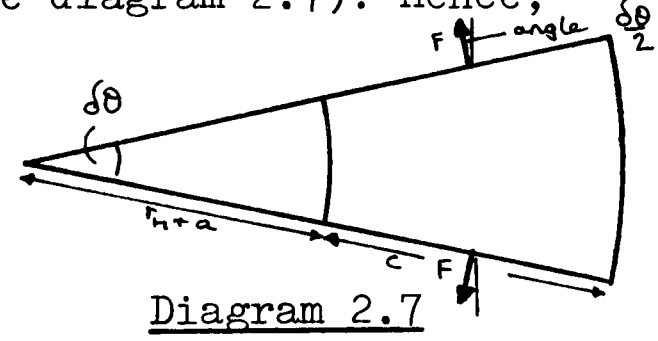

Diagram 2.7

$$F\delta\theta = \left(\int_{r_m+a}^{r_m+a+c} \sigma_{zz}(r)\, r \tan\alpha'\, \delta r \right) \delta\theta \quad \ldots.2.20$$

(Centripetal component of F's is $2F\sin\frac{\delta\theta}{2} = F\delta\theta$ for small $\delta\theta$)

The hoop force, F, may also be obtained from consideration of the hoop strain developed in the meniscus as it expands. If the meniscus slides out a distance, a, the fibre which is at radius r was unstrained at radius $(r-a)$. Its length, therefore, has increased from $2\pi(r-a)$ to $2\pi r$, and hence the strain induced is $\frac{a}{r-a}$. If k_3 is the coefficient relating stress to strain in the circumferential direction of the

meniscus then

$$\sigma_{\theta\theta} = k_3 \frac{a}{r-a} \qquad \ldots 2.21$$

The area this stress acts upon is $t' \delta r$, t' being the height of the deformed meniscus at radius, r. Hence

$$F = \int_{r_m+a}^{r_m+a+c} k_3 \frac{a}{r-a} t' \, dr = \int_{r_m+a}^{r_m+a+c} \sigma_{zz}(r) \; r \tan \alpha' \, dr \qquad \ldots 2.22$$

The only unknown in the equation is tan α' which is the slope of the femoral surface of the deformed meniscus and is defined as $\frac{\partial t'}{\partial r}$.

When equation 2.22 is considered in detail (see Appendix 2c) it is apparent that the highest power of d present in the equation is the square. If d is treated as a constant for a specified value of a, and then extracted from equation 2.22, a quadratic equation in d is obtained in the form

$$X d^2 + Y d + Z = 0 \qquad \ldots 2.23$$

where X, Y and Z are integrals between the limits specified in equation 2.22, and functions of the geometric constants, the moduli of elasticity and a. Solution of the constants X, Y and Z will allow a value of d to be calculated for a specified value of a and the whole problem may be solved to determine P by back substitution of equations 2.18 into equation 2.4.

2.3.6. Incremental Procedure.

If the strains are large, as occurs if the meniscus expands a distance of the same order as the unde formed inner radius, then strains should be calculated on an incremental

basis:-

$$\epsilon_{z\,(r,a_o)} = \int_0^{a_o} \frac{\Delta \omega_{m(r)}}{t'_{(r)}}$$

that is, the strain in the z-direction at radius, r, for a given value of the expansion, a_o, is the sum of all the increments of true strain as expansion moves from zero to a_o. A similar expression would be used for $\epsilon_{\theta\,(r,a_o)}$

If there is an increase in deflection Δd, with a corresponding increase in expansion Δa and load ΔP, then assuming these increases to be very small, and following the same procedure as above, equation 2.22 becomes

$$\Delta d \int_{r_m+a}^{r_m+a+c} \frac{1}{\left(\frac{t_o}{k_2} + \frac{h}{k_1}\right)} \frac{\partial t'}{\partial r}\, r\, dr = \Delta a \left[\int_{r_m+a}^{r_m+a+c} \frac{k_3}{r-a}\, t'\, dr + \int_{r_m+a}^{r_m+a+c} \frac{r-r_m-a}{R\left(\frac{t_o}{k_2} + \frac{h}{k_1}\right)} \frac{\partial t'}{\partial r}\, r\, dr \right] \quad ..2.24$$

where

$$t' = h\left(1 - \frac{\sigma_{zz}(r)}{k_1}\right)$$

and $\sigma_{zz}(r)$ is defined by an equation similar to 2.14(3)

In order to determine $\sigma_{zz}(r)$ as in equation 2.14(3) it is necessary to sum all the increments of $\Delta\sigma_{zz}(r)$ which are

$$\Delta\sigma_{zz}(r) = \frac{\Delta d - \frac{r-r_m-a}{R}\Delta a}{\left(\frac{h}{k_1} + \frac{t_o}{k_2}\right)} \quad ...2.25$$

Therefore in order to solve 2.24 it is necessary to do a summation on equation 2.25 but equation 2.25 cannot be solved until the relationship between Δd and Δa is known, and this relationship is determined by equation 2.24.

A similar situation arises if $\nu \neq 0$ and $\sigma_{rr} \neq 0$; the width of the meniscus would not remain constant and hence the limits of integration would become functions of the integrand.

2.3.7. Determination of Geometric constants and Modular ratios.

In order to solve the contact problem it is necessary to have values of R, r_m, C, t_1, t_2, $\frac{k_1}{k_2}$ and $\frac{k_1}{k_3}$. Values of these parameters were selected in the following manner, and were called the 'standard case parameters'. The effect of varying the parameters from their standard values is discussed.

A knee joint was dissected and the values of R, r_m and C were estimated. R was measured by the use of a three-legged gauge[38]. The menisci lie on the tibial condyles and have the shape of semi-lunar arcs; r_m was taken as the distance to the inner edge of the meniscus from where the centre of the semi-lunar arc was taken to be, and the average for both menisci was used. The width, C, of the menisci is variable so the widths were measured with vernier calipers at various points around the arcs of both menisci and the values obtained, averaged. The bones were sectioned and t_1 and t_2 measured.

The modular ratio $E_1 \left(= \frac{k_1}{k_2}\right)$ is the value of the stress/strain coefficent in the Z-direction in the meniscus divided by the Tu and Gazis' modulus in the Z-direction of the articular cartilage layers. The meniscus is a fibrous material with the fibres running circumferentially[62]; the compressive stiffness perpendicular to the fibres will not be high and should be less than the stiffness in the Z-direction in the articular cartilage layers, the structure of which has been described in 1.2.

$E_2 \left(= \frac{k_1}{k_3}\right)$ is the ratio of the stress/strain coefficients in the Z- and θ- directions for the meniscus. The tensile stiffness

parallel to the fibre direction is very much higher than perpendicular to it.[4] However it is in the compressive stiffness perpendicular to the fibre direction which is of interest, and it would seem reasonable to expect the compressive stiffness perpendicular to the fibre direction to be greater than the tensile stiffness in the same direction. A simple analogy to the material is a reinforced concrete bar which has very little resistance to tensile stresses perpendicular to the direction of reinforcing steel, but a much greater resistance to compressive stresses. The compressive modulus of elasticity of the cartilage layer normal to its surface has been estimated to be up to 25 N/mm^2 [19,80]. The tensile modulus of elasticity in the fibre direction for the menisci is estimated to be at least 150 N/mm^2 (see 4.4). Therefore a value of 0.1 for E_2 is considered a reasonable estimate.

2.4 Results

The numerical solution of the contact problem (see Appendix 2.e) shows that unlike the Hertz problem[76,79,80], the relationship between the deflection, d, and the increase in contact radius, a, is almost linear (see Figure 2.f.1).

The relationship between the load, P, and the deflection, d, (figure 2.f.2) shows that, although the materials have been considered to be linearly elastic, as load and deflection increase so too does the overall joint stiffness. This is to be expected:-

Consider two bars of the same material and length but of different cross-sectional areas A_1 and A_2 where $A_1 > A_2$. If the same force, P, is applied to both bars, the respective deformations will be $\delta_1 = \frac{PL}{A_1 E}$ and $\delta_2 = \frac{PL}{A_2 E}$ and $\delta_1 < \delta_2$.

In terms of load/deflection, bar one is stiffer than bar two. In the model and in the joints, as load is applied and the meniscus expands radially, the contact area increases. On the basis of the above, the load/deflection stiffness may be expected to increase with load.

The value of the load ratio, P_m / P where P_m is the load carried by the meniscus and P is the total load, is one of the important results of the analysis. The variation of P_m/P with the parameters involved in the calculation is shown in figures 2f. 3, 4 and 5. The physical dimensions of the meniscus are important; the narrower the width, c, and the larger the inner radius, r_m , of the meniscus the less the value of P_m. The modular ratios are also significant but even if the meniscus is relatively flexible ($E_L = 1.0$) the load ratio P_m/P remains in the middle to high percentage range. Indeed, with reasonable ranges of the physiological values the analysis indicates that P_m is invariably a significant proportion of the total load, P.

Increasing the flexibility of the meniscus increases the deflection of the joint for a given load (figure 2.f.6). Total removal of the meniscus should, therefore, have a significant effect on the load/deflection curve of the joint. The effect of meniscectomy is shown in figure 2.f.7. Hence, comparison of load/deflection tests on a real joint before and after meniscectomy should indicate whether weight-bearing is a significant role of the real menisci.

As has been mentioned, as load is applied to the model, the meniscus expands radially. Figure 2.f.8 shows that the meniscus expands steadily with load: measurement of the radial expansion of the real menisci in situ should, therefore, give some indication as to the weight-bearing role of the menisci.

The stiffer the meniscus circumferentially, the less the

expansion and the greater the load carried. Measurements of the radial expansion of real menisci and attempts to estimate the load carried by them were made (see Chapters 3 and 4).

In the model, when the meniscus has been removed, the initial contact radius is reduced from $r_m + c$ to r_m. The joint is, therefore, initially more flexible than when the meniscus is present but the increase in contact radius is more rapid and the joint stiffening more noticeable (see figures 2.f. 7 and 8).

The stress distributions with and without the meniscus for a load of $P/\pi k_2 = 20$ are shown in figure 2.f.9. Clearly there are a lower average stress and lower stress gradients when the meniscus is present. The change in stress in the centre of the joint after meniscectomy is significant and attempts were made to measure the change in real joints.

In figure 2.f.9., when the meniscus is present, $\sigma_{zz}(r)$ remains compressive at the outer edge of the meniscus. The thin layer approximation indicates that there will be a discontinuity in the surface deformation at that point. This is not always the case. If the meniscus is made wider or more flexible, the calculation shows that $\sigma_{zz}(r)$ becomes tensile on the outer edge of the meniscus. This can not occur in practice since the cartilage surfaces (meniscal-femoral, meniscal-tibial) are not attached to each other to allow the transmission of tension. The surfaces would separate. The physical explanation of this is that as the radius, r, increases, the gap between the articular cartilage surfaces increases. The meniscus has an original outer height, t_{max} and if the distance the meniscus slides out is large, then the gap between the two articular cartilage surfaces may be greater than $t_{max} + d$ (the distance of approach of the two

bones). Hence the meniscus is unable to touch both surfaces unless it is subject to tension. This can not occur, hence the surfaces separate.

2.5 Conclusions

The analysis of the model shows that the load carried by the meniscus, P_m, is affected mainly by the values chosen for the modular ratios E_1 and E_2, the meniscal width, c, and inner radius, r_m. The dependance on the variables R, t_1 and t_2 is less significant. For all values of the variables within a reasonable range of the measured or expected physiological values, the load carried by the meniscus is a significant proportion of the total load through the joint, and is about 60% for the most reasonable values.

The model does not accurately represent a real tibio-femoral joint in its geometry and the assumed mechanical properties of the constituent materials. The method of analysing the model is approximate. It is therefore necessary to support the results of the analysis with experimental evidence. Such evidence may be obtained from comparing compressive load/deflection curves of joints with and without the menisci, measuring the radial expansion of the menisci and measuring the change in pressure distribution after meniscectomy. Attempts were made at all three types of experiment, but, for reasons explained in 4.1.1. centred mainly on the first two. Knowledge of the circumferential Young's modulus of the menisci is required to estimate the load, P_m, from the radial expansion measurements. Hence small circumferential sections of the menisci were tested in tension. The apparatus for both the compression and tension tests is described in the next chapter.

CHAPTER 3

EXPERIMENTAL APPARATUS AND METHOD

3.1 Introduction

This chapter will describe the reasons for performing the experiments, the apparatus and its function, and the procedures adopted to obtain the results presented in the following chapter.

3.2 Experimental Objectives

The analysis in Chapter 2 suggests that the menisci can carry a significant proportion of the load transmitted through the joint. If they do, there will be a marked increase in the deflection for a given load after the menisci have been excised. Tests were performed to ascertain if this was so in practice.

When the initial tests vindicated the premise that the menisci bear a substantial fraction of the load through the joint, the aim became to estimate the value of this fraction. Load/deflection tests were performed on 17 human and 45 pig specimens and estimates of the load fraction were made for each specimen. However, these estimates were not precise and therefore it was necessary to try to confirm these estimates by other means.

An attempt was made to measure the pressure distribution across the cartilage surfaces by use of a pressure transducer, but the attempt was unsuccessful.

In the initial tests, it was noticed that the menisci expanded radially with increasing load. For the final 11 human and 19 pig specimens, the dependence of radial expansion on load was measured during the load/deflection tests. As will be shown in Chapter 4, knowledge of the circumferential tensile Young's modulus is required to calculate the meniscal load from the measured expansions, and consequently tension tests were performed on small circumferential specimens of the menisci in order to determine the modulus.

In the course of the compressive load/deflection tests it was possible to show that if circumferential tensile forces can not be developed by the menisci, then the menisci can not transmit load. A simple radial cut through a meniscus will not allow the development of circumferential tensile forces, and was shown to be equivalent to total excision in load-bearing terms.

It was necessary to remove various structures from the joint during a compressive test series on a joint and the effect of these excisions was noted.

Qualitative evidence with regard to the load-bearing role of the menisci should be obtainable from the load relaxation response of the joint. With the menisci present and load-bearing, the overall contact area would be larger than when the menisci are absent, and hence the

average pressure and the pressure gradients should be lower. If the load relaxation response depends on fluid flow away from the high pressure areas, then the load relaxation responses should be different with and without the menisci. Hence, the responses were determined.

In order to perform the compressive load/deflection tests on complete joints and the tension tests on small specimens from the menisci, it was necessary to have a compression/tension testing machine with facilities to measure both load and deflection. A standard testing machine was used with adaptations to allow joints to be tested in anatomical positions in a physiological environment.

3.3 Apparatus

3.3.1 The Instron Universal Testing Machine

The basic unit used in all experiments was an Instron Table Model 1112, Low Speed, with a Tension-Compression Cell 2511-312, of 500 Kgf capacity. The 1112 model is the more recent version of the 1102 Model. The low speed system gives cross-head speeds one-tenth of those of the standard type.

In addition to the standard accessories, the instrument had load-cycling controls, extension cycling controls and automatic and duplex chart control, which enabled the machine to be run between two fixed loads, two fixed positions or, as was found most useful, a fixed position and a fixed load. The automatic chart control could be

set to cause the movement of the recorder chart to follow the motion of the cross-head automatically and synchronously. Cyclic load-deflection plots were thus obtained in the form of closed-loop hysteresis diagrams. Load was measured by the load cell and the deflection scale determined from the relative speeds of the cross-head and the recorder chart.

3.3.2 Instron Adaptations

3.3.2.1 Compression Tests

For the compression tests on complete joints, it was necessary to hold the joints in different anatomical positions in a physiological environment, and to allow for variation in joint preparation. Therefore, a number of adaptations were made to the Instron.

With reference to Diagram 3.1, the sliding plate combination and the Hydraclamp allow for variation in joint preparation and for varying joint positions. Joints were attached to two mounting cups (see Diagram 3.3) which were screwed onto the upper and lower joint mounting plates. The joint could then be enclosed in the polythene tubing through which a fluid at the appropriate body temperature was circulated. The physiological environment was thus created. The photograph opposite Diagram 3.1 shows a pig joint in position.

With further reference to Diagram 3.1, considering the adaptations in more detail, and beginning at the cross-head, the cross-head had a protruding stud onto which the cross-head adaptor was screwed. The upper

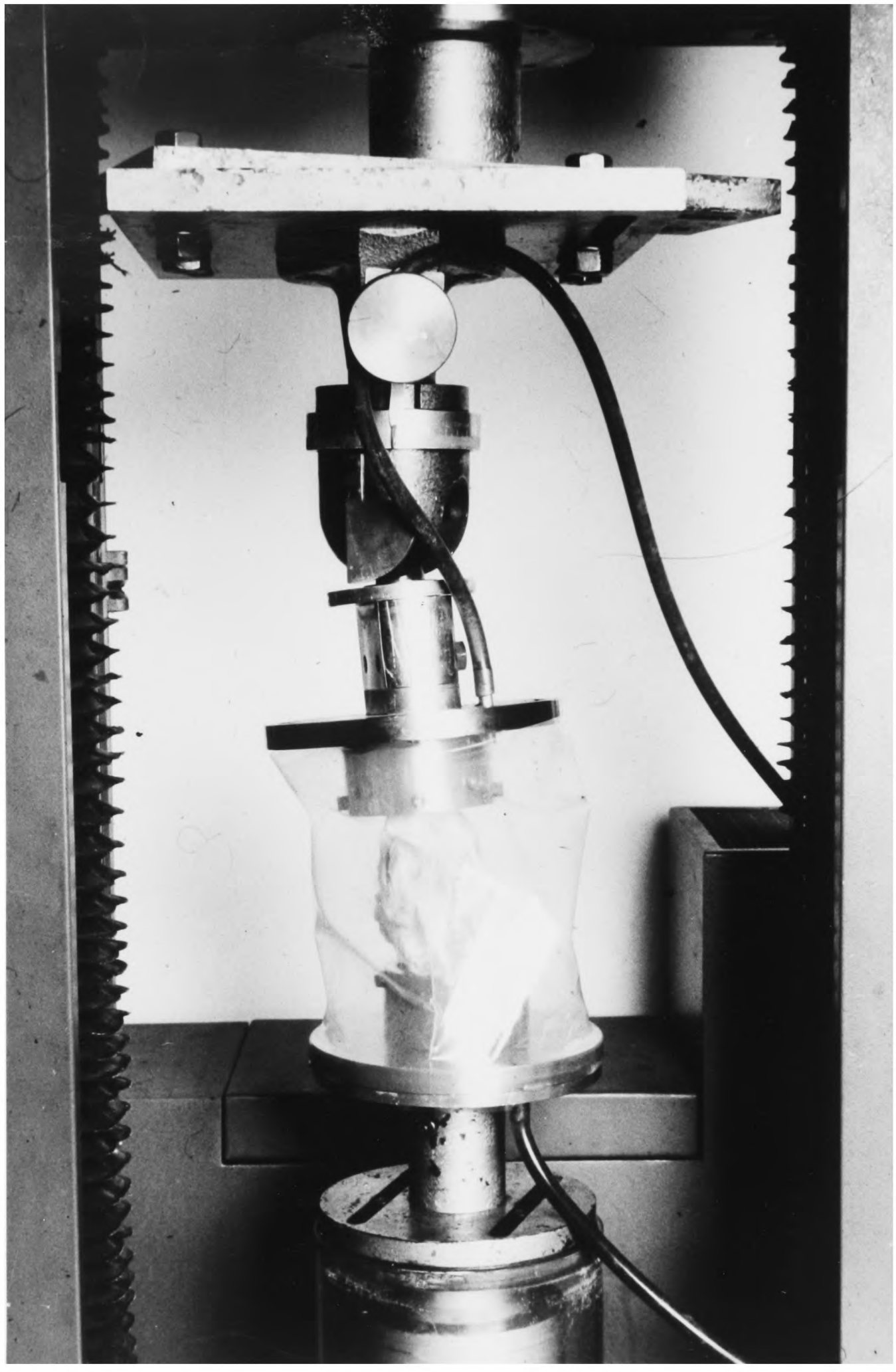

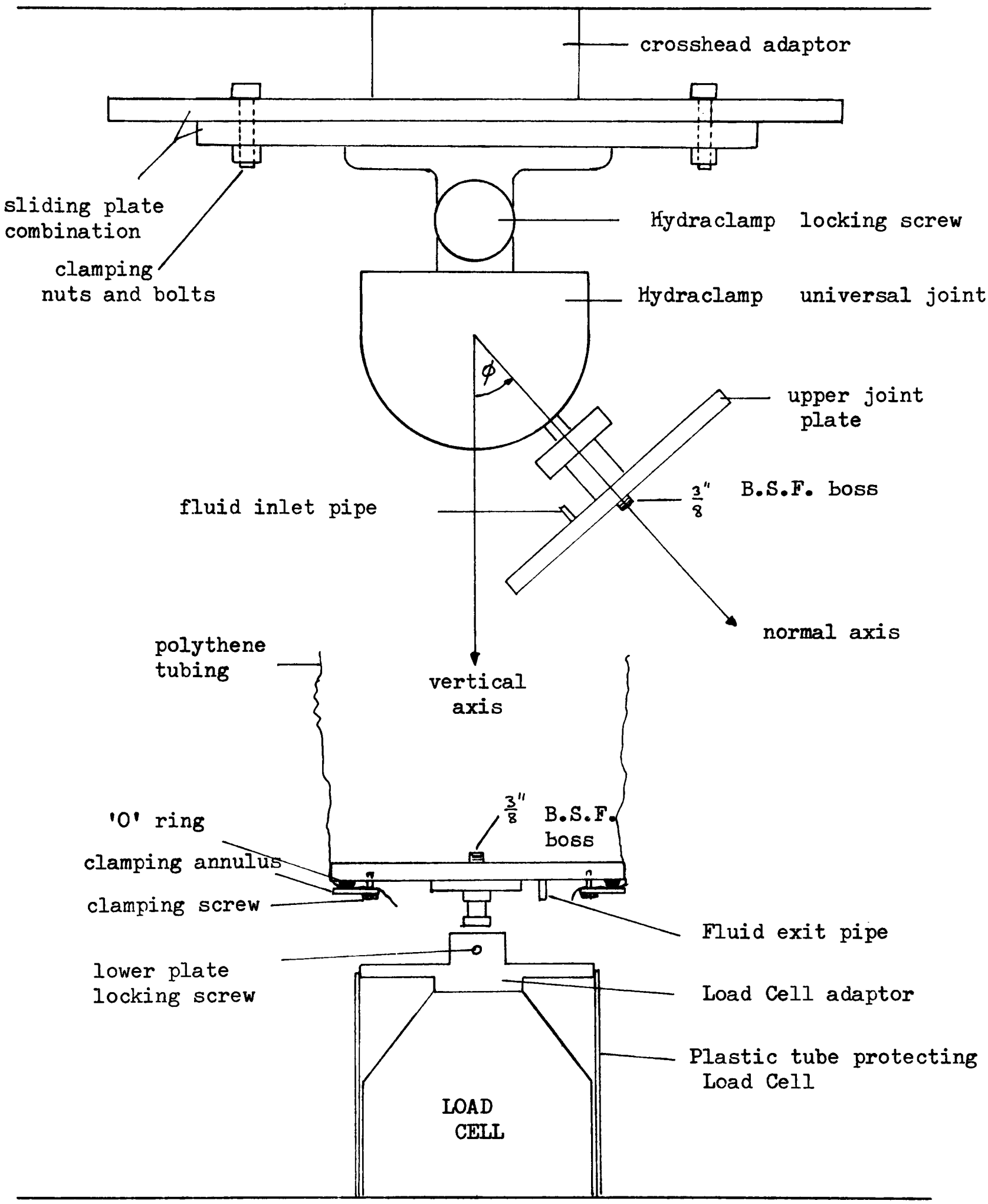

not to scale

Diagram 3.1

Instron adaptation

sliding plate was bolted onto the adaptor, parallel to the cross-head. The sliding plate combination allowed the lower plate to be moved both perpendicular (for anterior/posterior movement) and parallel (for lateral movement) to the upper plate (see Diagram 3.2).

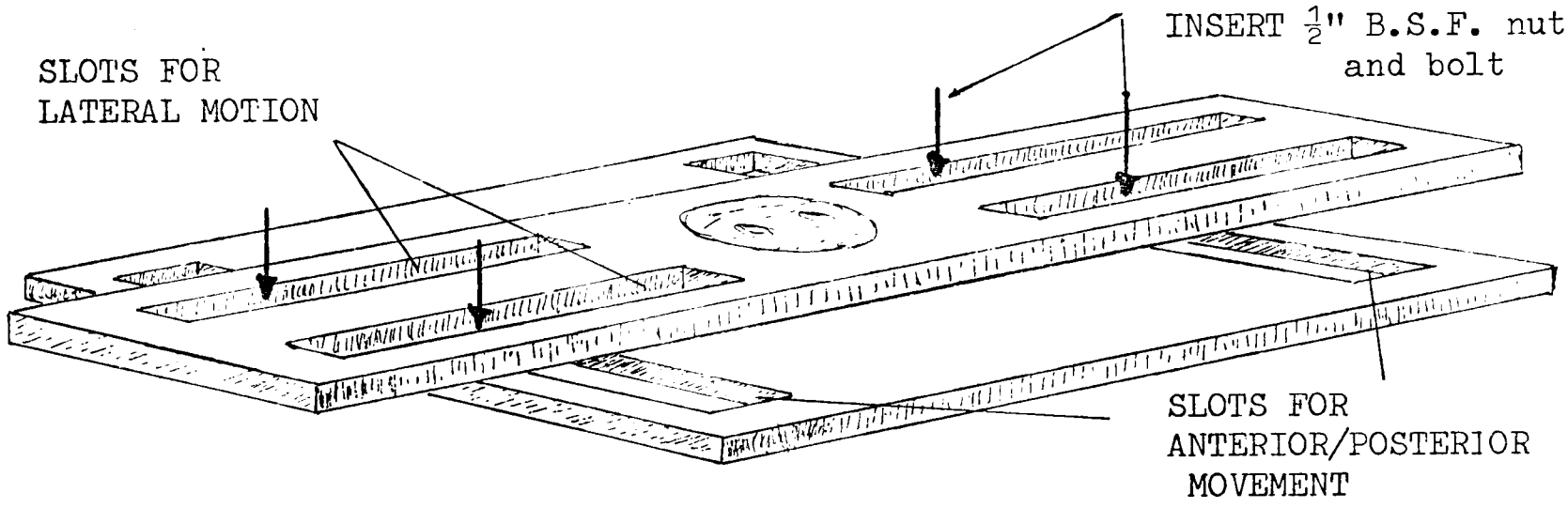

not to scale

Diagram 3.2

Sliding plate combination

Within the limits of travel allowed by the slots, the lower plate could be clamp in any position by means of four ½" B.S.F. bolts.

Attached to the lower sliding plate was a Hydraclamp universal joint which allowed 2π rotation about the vertical axis, 2π rotation about the normal axis and the angle ϕ to vary from zero to $\pi/2$ (see Diagram 3.1). The Hydraclamp could be locked in any position within this range.

The joints were attached to the machine by means of circular mounting cups (see Diagram 3.3) which were screwed onto bosses protruding from the upper and lower

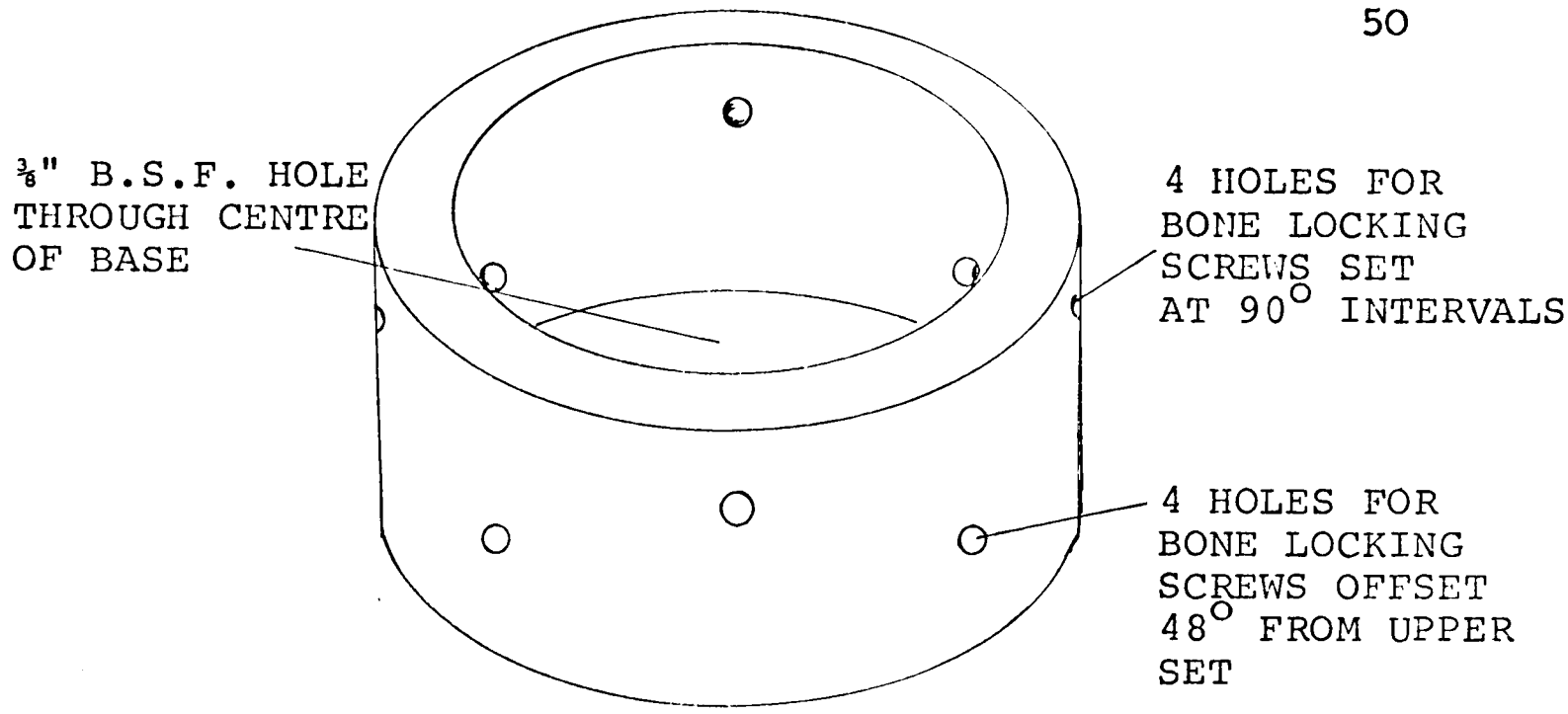

DIAGRAM 3.3

JOINT MOUNTING CUP

joint mounting plates. The method of attaching the joints to the mounting cups is described later.

The two circular joint plates were of the same design so that the polythene tubing which formed the sides of the fluid bath could be fixed at both ends. For reasons explained later the option of fixation to the upper plate was never used. The polythene tubing was attached to a joint plate in the following manner:- Consider the lower plate (see Diagram 3.1): on its underside there was a groove containing a rubber "O" -ring. On a smaller radius eight holes were drilled and tapped to half the depth of the plate. The tube was pulled down over the outer radius of the plate and the excess was folded over the "O"-ring. An annulus was then screwed down onto the plate squashing the polythene against the "O"-ring and thus creating a liquid-tight seal between plate and tube.

The fluid used to form the fluid bath was Ringer's solution, a salt solution resembling blood serum containing various quantities of Na Cl, Ca Cl_2 and K Cl.

The solution was maintained at the body temperature appropriate for the joint being tested and was circulated from a thermostatically controlled reservoir which contained a small circulating pump (Gallenkamp WF 360 and 366 respectively).

A push-fitted stud was attached to the lower joint plate. This stud produced a ⅜" B.S.F. boss on the upper surface and a 1" diameter boss with a circumferential groove on the under surface. The lower boss fitted into a 1" diameter hole in the load cell adaptor. When the boss was in place in the hole, a locking screw could be locked into the groove on the boss. If left unlocked, the lower plate assembly was free to rotate about the vertical axis (see Diagram 3.1). A plastic tube was push-fitted onto the load cell adaptor to protect the load-cell in case of accidents with the fluid bath.

3.3.2.2 Tension Tests

For the tension tests on small circumferential sections of menisci, standard Instron apparatus (in this case, screw-action jaws with 25 mm. wide serrated jaw-faces) was found unsuitable. The specimens were nominally square in cross-section and necessarily short in length (see 3.4.2.2.(c)). The short length meant that only a very small section could be clamped in the jaws. The jaws were free to rotate through a few degrees about axes perpendicular to the direction of tightening. Thus the jaws tilted when contact was made with a specimen and the jaws came into contact at the ends opposite to those holding the specimen (see Diagram 3.4). Some tilt

remained no matter how tight the jaws were made.

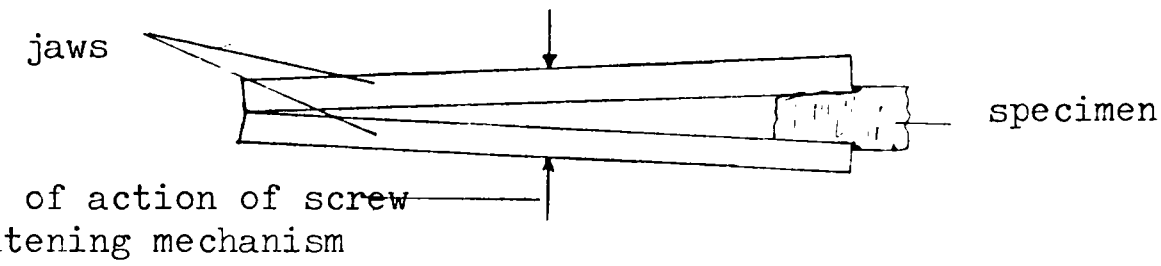

Result of Clamping Specimen in Large Jaws Diagram 3.4

The specimens, therefore, regularly slipped out of the jaws. Also the serrations on the jaw faces tended to cause the specimens to split along their length and many specimens failed to remain square-on to the jaws on clamping due to deformations caused by shear.

Two smaller clamps were designed to fit into the standard jaws; they had a more suitable mechanism for clamping specimens.

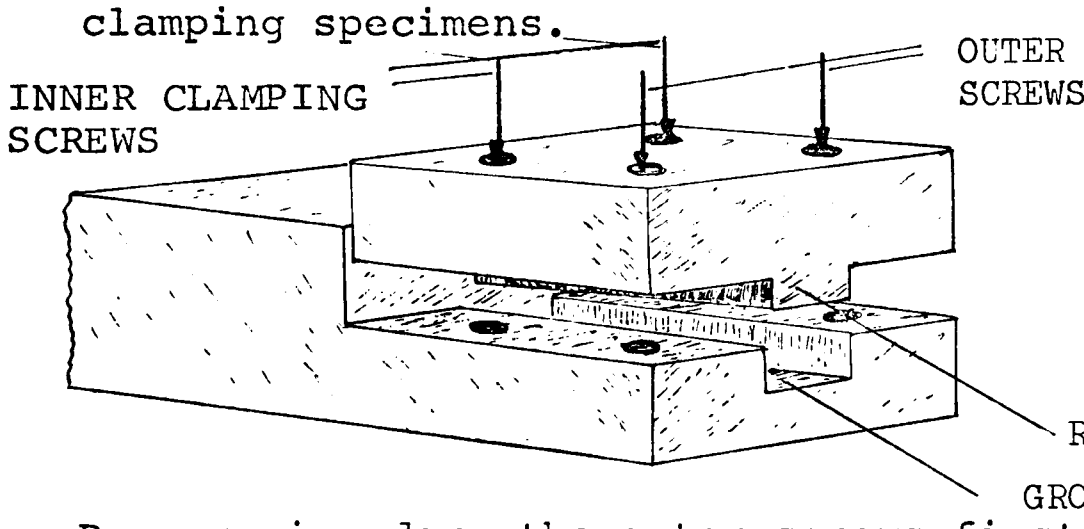

Diagram 3.5.

Tension Specimen Clamp.

By screwing down the outer screws first (see Diagram 3.5) the major problem of the large clamps was removed. By placing specimens in the groove the problem of shear distortion was removed. The complete combination is shown in Diagram 3.6.

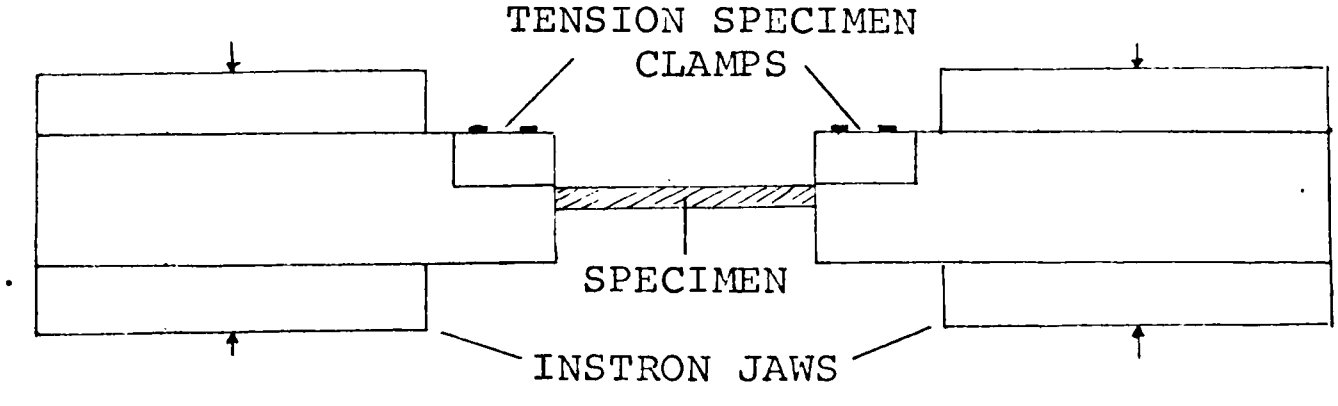

DIAGRAM 3.6

TENSION SPECIMEN IN POSITION

3.3.3 Pressure Transducer

The pressure transducer used was a Kulite LQL-080-100 with a sensitivity of 1mv/psi and working range 0-300 psi. Obviously when placed in a joint the pressure reading obtained would not be the pressure which normally existed at that point under the particular load, because the presence of the transducer would cause extra deformation of the cartilage. The use made of the transducer is explained in section 3.4.3.

3.4 Method

3.4.1 Compression Tests

3.4.1.1 Preparation and Mounting of Joints

Human joints were obtained at post-morten and stored at $-20^{o}C$. Pig joints were obtained within twelve hours of death and similarly stored. Storage at this temperature over a period of time has no effect on the mechanical properties of the materials[68].

After thawing, excess soft tissue was removed. The fibula was cut away near its junction with the tibia and the ends of the femur and tibia were cut at angles to the shaft axes, according to the desired loading position (see Diagram 3.7).

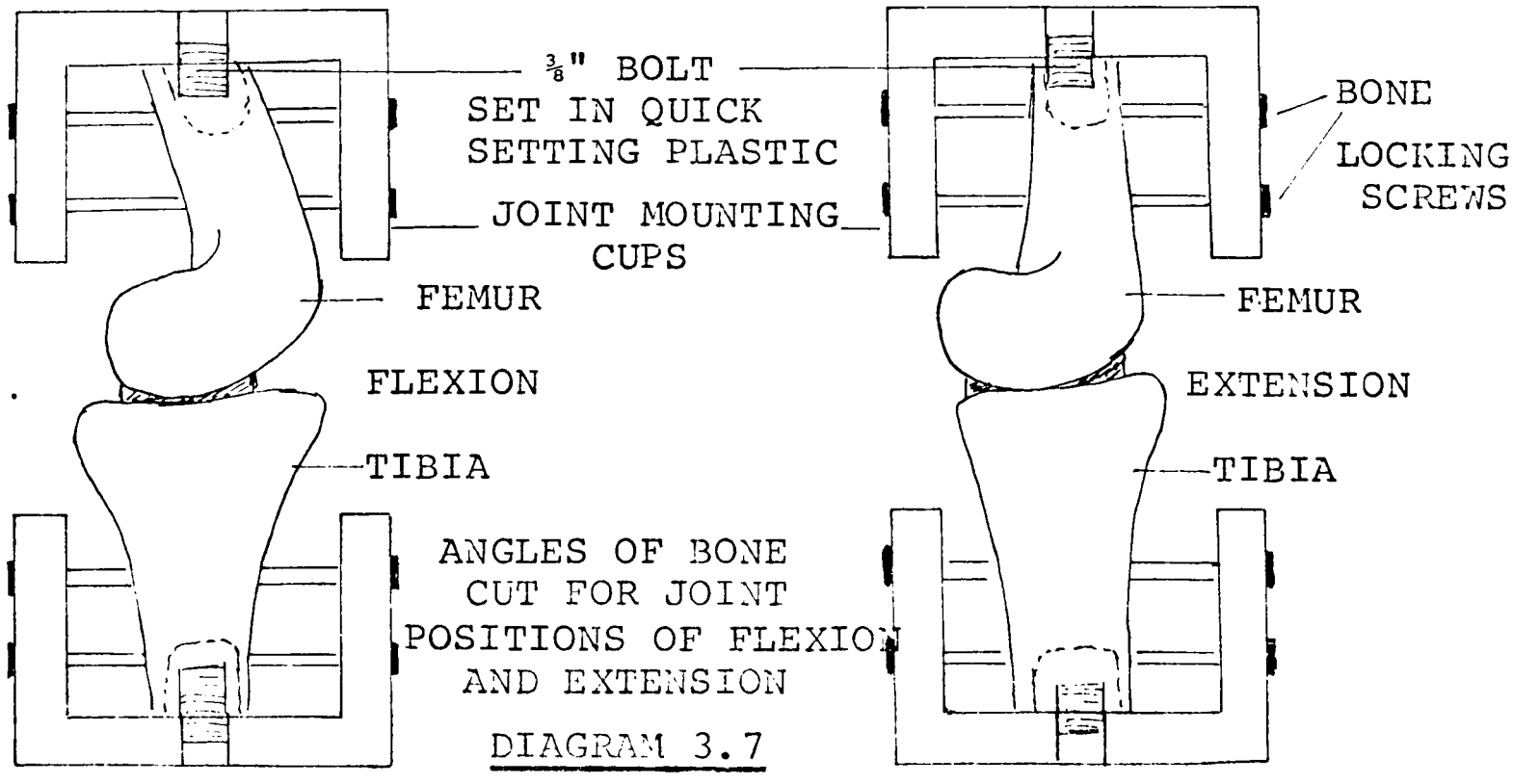

DIAGRAM 3.7

The bone marrow was removed from the shafts of the bones to a depth suitable for the next part of the preparation, which was to insert and set ⅜" B.S.F. bolts into the shafts of the bones. The bolts were fixed in position with a quick-setting mounting plastic (North Hill Plastics Ltd., Powder, N.H.P. 2031.19, and Liquid, N.H.P. 1844). Approximately ¼" of the bolts were left protruding out of the ends of the bones, normal to the place of the end cut. When the plastic had set, mounting cups (Diagram 3.3) were screwed onto the exposed ends of the bolts such that the shafts were in the cups.

If the joint had been prepared accurately the ends of the bones would be square against the base of the cup. Finally, eight screws were screwed through the walls of the cup onto the bone and this procedure produced total rigid attachment of cup to bone.

The joint could now be mounted in the machine. The lower joint plate with attached polythene tubing was screwed onto the tibial mounting cup. The joint was then screwed via the femoral mounting cup onto the upper joint plate. The joint and its attachments were thus left hanging from the Hydraclamp. The Hydraclamp was adjusted until the joint was in the desired position of flexion or extension, with the boss on the underside of the lower joint plate vertical. The Hydraclamp was locked in this position and the sliding plates adjusted until the boss was directly above the hole in the load-cell adaptor. The sliding plates were clamped together and the cross-head lowered until the boss fitted fully inside the

hole. The locking screw was tightened to achieve total fixation of the joint in the machine.

3.4.1.2 Procedure, Compression Tests

The final procedure developed over a period of time and a brief description of this procedure is given.

When the joint had been mounted in the machine, polythene pipes were attached to the inlet and outlet pipes on the joint plates. Through these pipes Ringer's solution was circulated to maintain the fluid bath (see 3.3.2.1). After mounting, the joint was left until the desired body temperature had been attained.

It was found most convenient not to attach the polythene tubing which formed the sides of the fluid bath to the upper joint mounting plate because of the necessity to expose repeatedly the joint for 'surgery'. Adequate depths of fluid for immersing joints could be maintained without the attachment.

The zero position for the joint was determined: it was considered to be the point at which, after cyclic loading, the specimen was subject to neither tension nor compression. When the joint was allowed to relax in this zero position, the load cell recorded slight compression. The cross-head speed was kept constant for all the tests on any one specimen, and eventually, for all specimens. The rate used and the reasons for its use are discussed in 4.2.7.

The zero position, once determined, was the position to which the cross-head returned after each cycle. The other limit of the cycle was a maximum load of 200 Kgf. This load

was about twice the body weight of the pigs (weight at death between 100 and 110 Kg) and at least twice the body weight of the human specimens.

Initially the joint would be intact with the capsule and ligaments in position and cyclic loading was continued until a limit cycle was obtained (see 4.2.4). Loading would be stopped, the fluid supply closed off and the fluid bath allowed to drain away to the reservoir. The polythene tubing which formed the sides of the bath would be squashed down towards the lower joint plate and a piece of 'surgery' performed. The tubing would then be straightened, the fluid bath returned and cyclic loading begun and continued until another limit cycle had been obtained. Limit cycles were thus obtained for each joint in the following sequence:-

(a) complete;

(b) patella and patellar tendon removed;

(c) collateral ligaments and soft tissue at posterior of joint removed;

(d) one meniscus cut radially;

(e) the second meniscus cut radially;

(f) both menisci fully excised;

(g) the cruciate ligaments cut.

The loading curves of the limit cycles for each of these seven conditions are compared in Chapter 4.

In the first few experiments, the menisci were observed to be loose initially and then to expand and become taut when load was applied. A technique was deve-

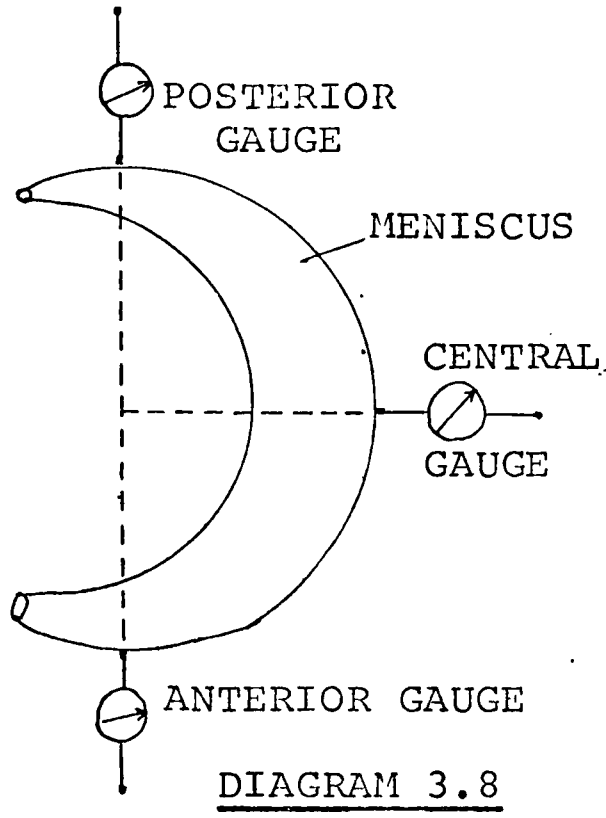

DIAGRAM 3.8

DIAL GAUGE POSITIONS

loped for measuring the radial expansion, using three Mercer dial gauges (0.01 mm.division, 25 mm travel), positioned as shown in diagram 3.8. The dial gauges were supported from a bar held between two retort stands. The movements detected by the dial gauges include the effects of gross movement of the menisci about their tibial attachments added to the effects of circumferential strain. The analysis of these movements is given in Chapter 4. Expansion was measured as a function of load in the final 11 human and 19 pig specimens only. Because the Instron is a displacement machine, there is no creep if the cross-head is stopped when a certain load is achieved, but load relaxation does occur. The expansion of the menisci at a given load could be determined by noting the initial position of the menisci and their position when the cross-head was stopped at the given load. After each reading the cross-head was returned to the zero position and a few minutes recovery were allowed before the next reading was taken. The radial expansion measurements were made after the limit cycle for (c) above had been obtained.

After the radial expansion measurements had been made and after (f) above, load relaxation tests were performed. They were preceded by a one hour relaxation period. The

joints were loaded to 200 Kgf and the cross-head stopped. With the recorder chart moving at a known speed a load/time plot could thus be obtained.

3.4.2 Tension Tests

3.4.2.1 Preparation and mounting of specimens

As has been mentioned, in order to estimate the load carried by the menisci from the radial expansion measurements, it was found necessary to determine the circumferential Young's modulus of the menisci. It was decided to test small sections of the menisci because the menisci are crescent-shaped with a varying wedge-shaped cross-section and varying width (see section 1.7). Kempson's method for producing specimens for tension tests from articular cartilage[4] can not suitably be applied to the menisci.

To prepare the specimens, a handle was manufactured to hold two scalpel blades with their cutting edges parallel. A cut was then made around the meniscus near its outer edge. The inherent inaccuracy of cutting fibrocartilage by eye is discussed in 4.4.3. The section thus made was then cut parallel to its tibial surface. Specimens therefore came from approximately the same area from each meniscus (see Diagram 3.9). Occasionally one of the blades would bend at the beginning of a cut and having bent, remain so for the rest of the cut. Specimens were nominally square in cross-section but did vary in size.

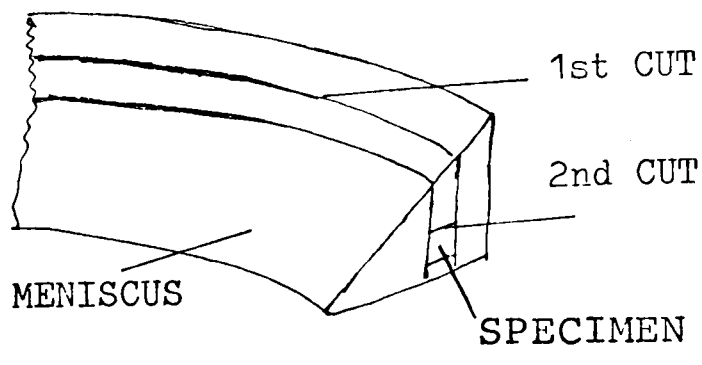

Diagram 3.9

The cross-section of the specimen was measured with Vernier calipers immediately after its production.

The problem of longitudinal splitting of specimens was mentioned in 3.3.2.2. The problem was cured by tying the ends of the specimen with cotton, which also increased the friction coefficient between clamp and specimen thus reducing the number of specimens which slipped out of the clamps.

Placing the specimen in the clamps as shown in Diagram 3.6 involved straightening the specimen and imposing a residual stress system upon it.

3.4.2.2. Procedure, Tension Tests

(a) Initial Tests

The specimens were not immersed in a physiological solution so the effect of drying was determined. A specimen was prepared, mounted and cyclically loaded between a fixed position and 5 Kgf. The specimen was left for one hour at room temperature (21^{o}C) and the loading was repeated. The initial shapes of the curves were very different but the final slopes were the same within the limits of accuracy of measurement. As regards an estimate of the elastic modulus from the final slope of the graph, therefore, the effects of drying could be ignored. Nevertheless, during all further experiments, the specimens were regularly wetted with Ringer's solution.

The effect of strain rate also needed to be considered. If the cross-head speed was the same for specimens of different lengths, different strain rates would occur. A specimen was tested at various strain rates of the order 10^{-2} sec^{-1}, and it was found that the slope of the graph in the higher load range was unaffected.

(b) Methods for determining strain

Standard strain measuring apparatus could not be used. The physical constitution of the menisci made attachment of electric strain gauges to the specimen difficult. It was found that extensometers cut straight through the specimens because the surface coefficient of friction is very low and hence a relatively high normal force is required to fix a knife-edge to the material.

An optical method was attempted: two marks were made on the specimen with Indian Ink. The specimen was filmed whilst being loaded; the load-time plot of the chart recorder could be synchronised to the film by means of the light indicators on the control console of the test frame. The console was viewed via a mirror placed near the specimen.

To determine the strain/time diagram the film was projected and the gauge length marked as a function of time. However, the difference between the gauge lengths was of the order of the thickness of the two pencil lines, and taking the difference of two large numbers to find a small number is a notoriously inaccurate method. The strain/time diagrams were totally unreliable, repetition of the analysis of the film for a given specimen producing entirely different sets of results.

(c) Method used

A procedure of extrapolation was finally adopted. The cross-head movement was measured on the recorder chart and thus a strain for the complete inter-clamp length could be

deduced. The inter-clamp length was measured by use of a travelling microscope attached to the cross-head of the machine. Knowledge of the load and the cross-sectional area allowed the determination of an effective modulus 'E' for a given inter-clamp length, ℓ. The effects of the stress and strain concentrations at the clamps were considered to be the same for various inter-clamp lengths. Thus by calculating 'E' at various inter-clamp lengths for a given specimen and plotting 'E' v. $\frac{1}{\ell}$, extrapolation to $\frac{1}{\ell} = 0$ should give an estimate of the Young's modulus (see Diagram 3.10.) Because an intercept at $\frac{1}{\ell} = 0$ was required, rectilinear extrapolation was used, the estimate so obtained being either over or under the true value as shown. However if a sufficiently large number of specimens are tested at various lengths, a plot similar to the predicted one should be obtained, allowing for variation in modulus from specimen to specimen.

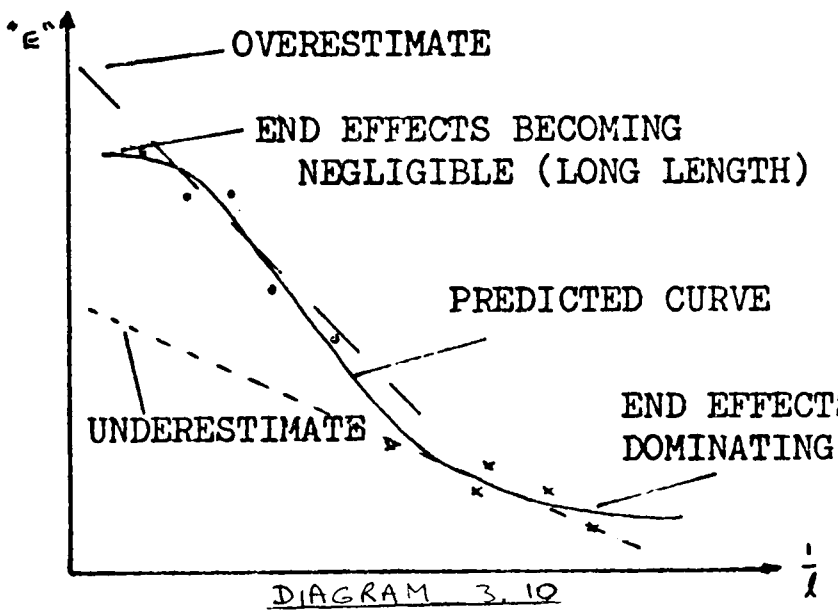

Expected Plot of Effective Young's Modulus "E" $(= \frac{PL}{Ag})$ v $\frac{1}{L}$.

The restrictions placed upon the method are ones of length. The minimal inter-clamp length should be at least three times the largest cross-sectional dimension, so that some part of the specimen is not influenced by the end effects. The physical size of the meniscus restricts the maximum length.

Tests were performed on the longest length first and the length was progressively reduced. Generally three lengths

were used for each specimen and each length was tested at two cross-head speeds to give two estimates of the slope and to confirm that the strain-rate did not affect the slope. The second cross-head speed was one fifth that of the first (see Page A65).

3.4.3. Supplementary Experiments

3.4.3.1 Pressure Transducer Tests

The intended use of the transducer was to measure the pressure distribution across the joint with and without the menisci. The transducer used (see 3.3.3) had a diameter of 3.25 mm and a depth of 0.75 mm. It was recognised that the insertion of a transducer of this size into the joint would increase the deformation of the cartilage in the vicinity of the transducer, leading to an overestimate of the pressure.

It was found that whenever the transducer was placed under a meniscus, the application of load caused the ejection of the transducer. However, it was possible to keep the transducer in a fixed position within the area enclosed by the meniscus. The load to cause a given transducer reading was measured both with and without the menisci.

3.4.3.2 Dye Tests

Deane[58] developed a method of using dyes of different colours to produce a sequence of contact studies for the knee as the knee was flexed. A similar technique was used to determine the contact areas at 200 Kgf with and without the menisci for some specimens and to determine the contact areas at various loads when the menisci were absent for other specimens. A hypodermic syringe was used to inject dye on to the relevant areas.

CHAPTER 4

EXPERIMENTAL RESULTS

4.1 Introduction

This chapter gives a description, analysis and interpretation of the results obtained from the compressive load/deflection tests on complete joints, the load relaxation tests, the radial expansion measurements, the dye tests, the pressure transducer tests and the tension tests on small specimens from the menisci.

4.1.1. General Description of Results

The load/deflection curves are considered in section 4.2. The curves compared are the loading curves of the limit cycles (see 4.2.4 and page A 42) of the seven tests as described in 3.4.1.2. A typical result (see next page) indicates that under light loads the joint is flexible but a rapid stiffening occurs as load is increased, followed by a steady increase in stiffness with load. The analysis of the model in Chapter 2 predicts increasing stiffness with load because of increasing contact areas. Reasons for the initial flexibility are discussed in §4.2.3. A typical set of load/deflection curves (see next page) shows that the removal of the patella, the patellar tendon, the collateral ligaments and the soft tissue at the rear of the joint have little effect on the overall load/deflection curve. However,

Specimen 7 M/79yrs./63.5 kg./169 cms. 20° flexion

(a)complete
(b)patella removed
(c)collaterals cut
soft tissue removed
(d)medial cut
(e)lateral cut
(f)both excised
(g)cruciates cut

Chart Speed: 100cms./min.
X-head Speed: 2.5cms./min.

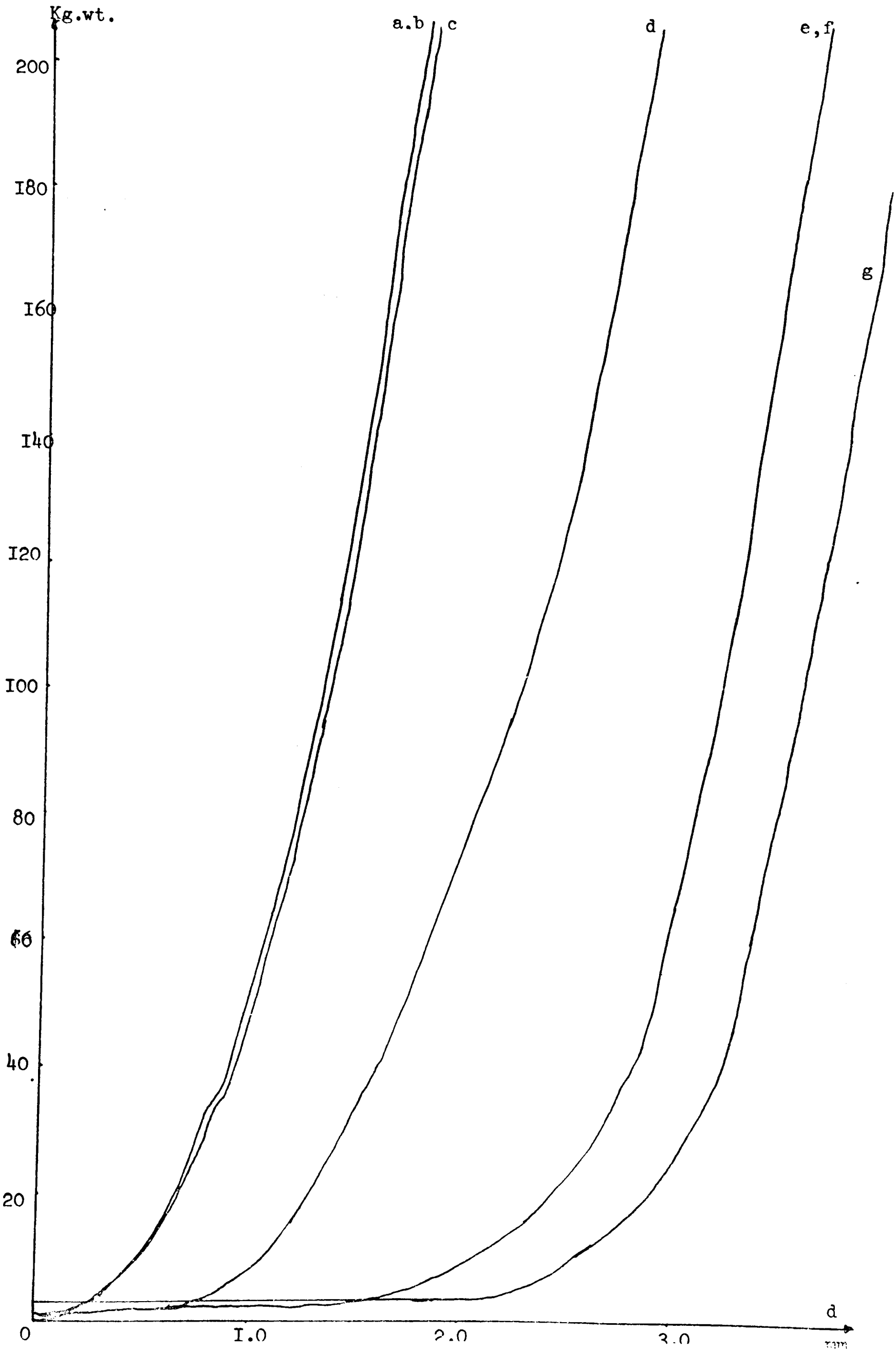

there is invariably a significant increase in the deflection for a given load after a meniscus has been cut radially. The analysis of the model in Chapter 2 showed that such an increase could be expected if the menisci carried a significant proportion of the load through the joint. There is invariably a second increase in the deflection for a given load after the second meniscus has been cut radially, and total excision of the menisci after both have been cut radially has little or no further effect on the load/deflection curve. There is another change, however, when the cruciate ligaments are cut. Clearly there is variation from specimen to specimen in the size of the changes in the curves but the general pattern was apparent in all 62 specimens tested. The load/deflection curves are considered in detail in section 4.2 beginning with a description of the condition of the specimens used in 4.2.1 and finishing with estimates of P_M/P in an analysis of the results in 4.2.6 and a consideration of the accuracy of the analysis in 4.2.7.

Typical results from the load relaxation tests are shown on pages A58-A60 and the difference in the curves with and without the menisci is not great. Section 4.3 discusses these results.

Typical radial expansion measurements are shown on pages A61-A63. Although in contact with both femur and tibia the meniscus is loose and flexible at low loads. On the application of a small load (between 10 and 40 Kgf) the menisci became taut and stiff. The rate of expansion with load is considerably reduced but expansion continues to increase with load. In 4.4.1 the expansion measurements are analysed.

The tension tests on small specimens of the menisci produced data which could be analysed in different ways. The data are presented on pages 95 to 9 and show that although there is considerable spread in the results, part of the expected curve is obtained. The analysis of the data is discussed in 4.4.2.

The knowledge obtained from the expansion measurements and the tension tests is used to make a number of estimates of the load, P_m, carried by the menisci. Four different methods are used to estimate P_m but all produce unrealistic values ($P_m > P$ where P is the total load through the joint). The calculations and the reasons for the overestimations are considered in 4.4.3.

The dye tests showed that both femoral and tibial condyles became completely stained when no load was being transmitted through the joint and the menisci were not present. The result implies that under these conditions, there was no inter-condylar contact. When load was applied and inter-condylar contact made, the contact area increased with load. When the menisci were present, no dye penetrated the meniscal contact areas. When the joint was unloaded, it was sometimes possible to inject dye via the femoral notch onto the area on the tibial condyles enclosed by the menisci, giving further evidence that there was a gap between the femoral and tibial condyles.

The transducer tests showed that with the transducer on the area enclosed by the menisci, the load to cause the same transducer reading after the menisci had been removed was only 0.5 to 0.6 the load required when the menisci were present.

There was, therefore, a significant increase in stress with the removal of the menisci. Unfortunately after a few tests the transducer was irreparably damaged and was not replaced for financial reasons.

The conclusions drawn from the results of the various experiments are discussed in §4.5. It is recognised that in most normal activity joint surfaces are not static in relation to one another, but the compression tests remain relevant to the dynamic case because tests were performed with specimens in a variety of positions and the results from all positions are similar. In Chapter 5 there is a discussion of the implications and the general significance of the results with regard to present knowledge of the knee.

4.2 Load/deflection Tests

4.2.1 Specimens

Experiments were performed on both pig and human knees. The geometric structure of pigs' knees is similar but smaller than that of humans, that is, the three bone components, tibia, femur and patella exist with connecting ligaments in similar positions with similar functions. The tibial surfaces of the pigs' knees are more convex and the menisci are thus proportionately larger than their human counterparts, 'filling' a larger gap and covering a greater proportion of the tibial plateau. The analysis indicates that pigs' menisci may be expected to transmit a higher percentage of the total load than human ones: using a value of $r_m = 4.0$ and meniscal width, $c = 13.5$, the meniscus in the analysis carries 90% of the load.

The pig specimens were all taken from young adult animals weighing between 100 and 110 Kg. The first twenty-five specimens were sectioned and all had epiphyseal plates indicating that full maturity had not been attained. In all specimens the hyaline cartilage had a bluish-white translucent appearance showing that it was in excellent condition. These joints may be expected to have functioned normally under load.

The human specimens were in an age range from 37 years to 79 years, with average age 63.3 years. The physical state of the specimens varied. The majority had visible signs of degeneration on the tibial plateau, a few contained lesions of the menisci and some menisci were extremely thin. The articular cartilage in all joints was yellowish in colour. Generally the cartilage in contact with the menisci was in much better condition than that elsewhere in the joint. These findings were in agreement with the observations of Bennett, Waire and Bauer[66].

The latter in their study of the degeneration patterns of the knee showed that for their specimens, degeneration on the tibial plateau was observed in all cases over the age of 15 years, and degeneration of the menisci could be observed in the third decade of life. Age dependent bone changes consisted of the femoral condyles becoming flatter and the tibial condyles more concave[66]. Such changes tend to make the joint surfaces more congruent, as do age dependent bone changes in other joints[3,37]. The slow erosion of the menisci in the narrowing gap between the femoral and tibial condyles involved shredding of the inner edge and thinning of the menisci[66]. The analysis in Chapter 2 indicates that the

thinner the menisci, the less the load carried by them.

It is unfortunate, yet unavoidable, that all the specimens used were well over the age of 15 years. The results however should show the same trends as the results from the pig specimens, though not as clearly. The estimates of load carried by the menisci for the human specimens will be less than may be expected for young healthy joints.

4.2.2 Successful Experiments

A total of 17 human and 45 pig knees were tested. Of these 16 human and 42 pig were considered to be successful. In the unsuccessful human experiment, the femur dislocated posteriorly on the tibia on loading after the lateral meniscus had been cut. Pig specimen 20 (see page A43) dislocated arteriorly on loading after the medial meniscus had been cut. In some of the later pig tests, performed in various degrees of flexion, dislocation on loading occurred after the cruciate ligaments had been cut. These experiments were considered successful because the effect of meniscectomy had been noted previously.

Pig Specimen 1 was not restricted from rotating at the junction of the lower joint plate to the load cell adaptor and when load was applied after the menisci had been removed, an irrecoverable rotation occurred. The rotation does show that the menisci have a rotational stabilising role, but does not allow an estimate of the meniscal load to be made. Pig Specimen 2 (Pages A43, A47) was loaded to a maximum of 100 Kgf, and the zero position was not chosen as for later experiments, but was taken to be the position for which there was no load relaxation when the joint was initially mounted

in the Instron. Cyclic loading put the joint into tension at the zero position so chosen (page A47).

The overall success rate was considered quite acceptable.

4.2.3 Joint Positions

The tests were performed with the joints in a variety of positions ranging from hyperextension to 30° flexion, the majority of tests being performed at or near the former position. Hyperextension was chosen as the position for the initial tests because it is the only anatomical position in which the patella and its associated tendons and ligaments are loose. This fact is easily demonstrated on oneself by locking the knee in extension whilst standing and relaxing the leg muscles. The knee cap may be moved medially and laterally on the patellar surface between the condyles. In all other joint positions, not only is the patella tendon taut but other tendons also. Hence, for cadaveric specimens, only in hyperextension where no stabilising muscle forces are required, will the femur and tibia assume their correct anatomical relationship. The reason why joints tended to dislocate in the tests in flexion after meniscectomy and all the ligaments had been cut, may well be that a true anatomical position had not been achieved when the joint was mounted in the testing machine.

However, hyperextension is the position in which it is thought that load-bearing may occur[60.61] and hence demonstration of the load bearing function of the menisci in other positions was considered necessary. A list of the positions in which joints were tested is given on page A43. The results from tests in all positions showed the same trends.

4.2.4 Limit Cycle

The typical achieval of a limit cycle is shown on page A42. The cause of the phenomenon is thought to be as follows:-

As described on page 5, articular cartilage is porous and normally contains water and synovial fluid. On compression liquid is expelled from the cartilage. During the tests the joints were immersed in Ringer's solution and hence the cartilage was soaked with this after the capsule had been cut. On the first application of load in any test the cartilage would be reasonably replete with fluid and if full relaxation had been allowed the cartilage would be saturated. Some of the fluid would be expressed and when unloading occurred the cartilage would soak up fluid. If the load was not reapplied the cartilage would have time to recover all the lost fluid. This was not allowed and hence prior to reloading, the amount of liquid absorbed was not as great as that expelled. Consequently there was a progressive reduction of the fluid in the cartilage until the situation occurred in which the volume of liquid expelled on loading equalled that absorbed on unloading. When this situation had occurred, the load/deflection curves of consecutive cycles became coincident. The curve so obtained was designated the limit cycle. The loading paths of the limit cycles are compared for the seven tests on each specimen as previously described.

The power absorbed in the hysteresis loop varied in the range 10 to 30 milliwatts. The tensile straining curve of a meniscus section shown on page A65 indicates that the meniscus

specimen absorbs very little power (approx. 0.04 milliwatts). Hence a role of shock absorber for the menisci seems doubtful. The menisci transmit substantial load between the femur and tibia, but do not absorb much energy in doing so.

4.2.5 Interpretation of Curves from a Test Series

The loading curves of the limit cycles of eight of the sixty-two joints tested are presented on pages A44-A51. The curves are typical of the results except for Pig Specimen 2 (page A47) for which a different zero position was used (§4.2.2). The typical curves show that the joints stiffen with load and that shifts in the loading curves occur at certain points in the tests on each joint. The most noticeable shifts occur after the cutting of each meniscus and after the cruciate ligaments were cut. The changing stiffness with load and the shifts in the curves will be used to make two estimates of the load carried by the meniscus.

All curves indicate that the joint is initially quite flexible, but that as load increases there is a dramatic stiffening followed by a further steady increase in stiffness. This is thought to be due to two factors:-

(a) There is a gap between the femoral and tibial condyles in the no-load position of the limit cycle (see below). Any tensile forces in the ligaments will be balanced by compressive stresses on the contact areas between the menisci and the femoral and tibial condyles. When the femur approaches the tibia, the lengths of the ligaments will reduce with a corresponding reduction in the tension in the ligaments. The necessary balancing force is also reduced, but the menisci, originally loose, expand and become taut, the rate of expansion being rapidly reduced. The menisci have a non-linear

stress/strain relationship as shown on Page A65. The initial gross movement of the menisci can thus be easily accommodated at low loads.

The initial part of the load/deflection curve, therefore, is a function of the reduction in tension in the ligaments of the joint and an increase in the compressive stresses on the contact areas as the menisci expand. When the femoral and tibial condyles come into direct contact a situation similar to that of the model has developed and hence an increase in stiffness is expected because of the increasing contact areas (§2.4).

(b) Compression of articular cartilage causes expulsion of fluid and compression of the basic cartilage matrix[8]. As fluid is expelled, further fluid available for expulsion is decreased. The increase in the contact area will reduce the rate of flow of fluid away from the centre of the contact area and hence fluid will become trapped between the cartilage surfaces[29]. Compression of the trapped fluid will cause an increase in the cartilage stiffness which will be apparent in the overall load/deflection curve.

Thus each individual curve shows increasing joint stiffness with increasing load. There is also a general pattern to the curves from a test series on a joint, as previously mentioned, involving a series of shifts in the loading curves. The sizes of the shifts vary from joint to joint but the overall pattern is maintained in all of the sixty-two specimens tested.

The effect of the removal of the patella on the load/deflection curve for the complete, intact joint was usually negligible. After the collateral

ligaments were cut and the posterior region of the capsule removed, however, there was often a change in the load at the zero position, and an increase in the deflection for a given load. Both these effects were usually small, but noticeable. If the ligaments or capsule were in tension when the joint was mounted, due to any slight ab- or adduction, medial or lateral rotation, or because of the position of flexion or extension, then cutting them will result in a loss of upwards force on the load cell and hence an apparent increase in compression. Thus the zero load was changed. If the bone components moved further apart or underwent a slight reorientation (see Diagram 4.1) due to the removal of the constraint applied by the ligaments, the precise mode of contact between them would not be maintained and an alteration in the load/deflection curve would correspondingly occur.

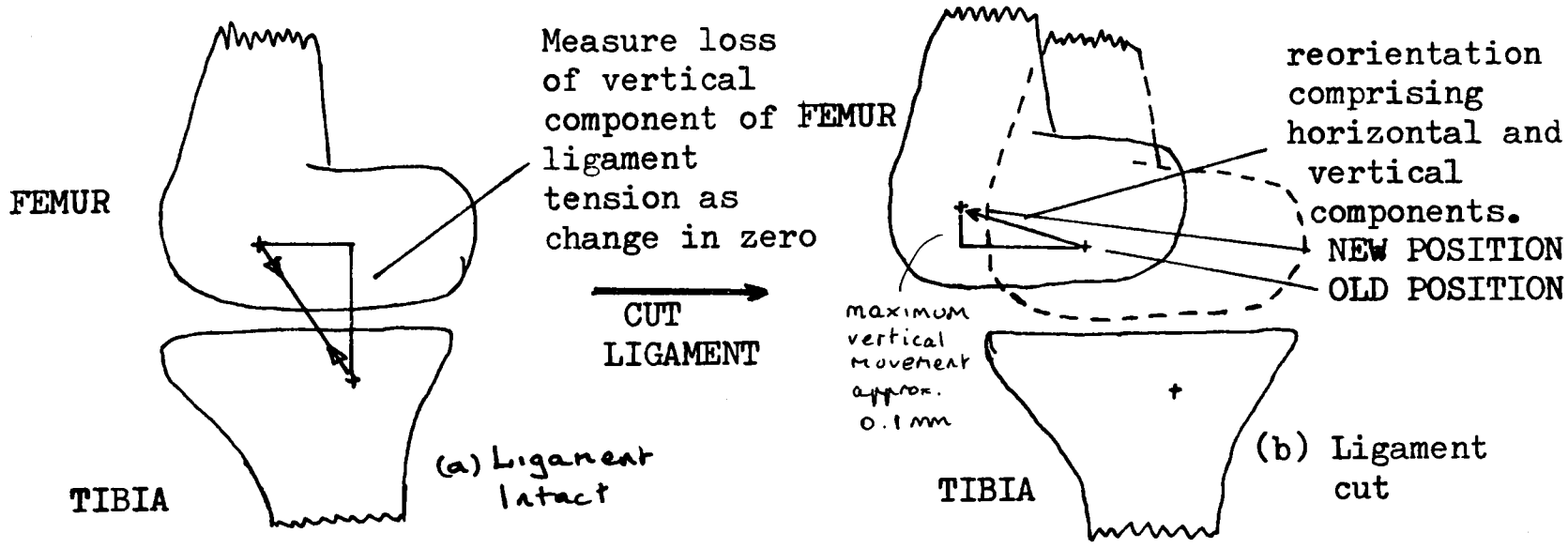

Diagram 4.1

After the first meniscus had been cut there was invariably a definite increase in the deflection for a given load. This may have been caused by a further change in the relative bone positions similar to that above, and by the fact that if the meniscus was load bearing, then to achieve the same load after meniscectomy would require a greater deformation of the articular

cartilage, as demonstrated by the model.

There was a further increase in the deflection for a given load when the second meniscus was cut. Total excision usually did not produce a further change, indicating that the method of load transmission proposed is correct since cutting a meniscus is equivalent to its excision in load bearing terms.

In the final test, a change in the zero load similar to that caused by cutting the collateral ligaments often occurred. The change was usually more pronounced than the latter suggesting that the cruciate ligaments were subject to greater tensile loads in the positions adopted than the collateral ligaments. The effect was most noticeable in the tests performed in hyper-extension indicating that the cruciate ligaments play a large role in limiting this position. In flexion, dislocation often occurred in this final test showing that the cruciate ligaments are also important in limiting the anterior-posterior movement of the femur on the tibia. On the curve there was an initial flat zone when the crosshead first moved, giving an indication of the size of the gap between the condyles at this stage of the test series, since there was then nothing joining the bones together. This was not necessarily the gap at the beginning of the series, for reasons mentioned previously.

The size of the gap between the femoral and tibial condyles as indicated by the curve of the final test is of the same order of magnitude as the overall joint deformations. Bone stiffness is of the order of 5×10^3 N/mm^2 [81]. Hence if the bone lengths are say 200 mm total, with average cross-sectional area of 100 mm^2 and the gap is 2.0mm, a tensile load of 5kN is

required for the condyles to touch. The tension in the ligaments varies but has a maximum of approximately 20 Kgf(200 N) Re-orientation of the bones may cause an increase in the gap between the condyles but is unlikely to create the gap.

Secondly, crosshead movements of 3mm. or more are not uncommon on the load/deflection curves. If the cartilage on the direct tibio-femoral contact areas has a total thickness of 4.5mm (as measured for the model analysis), then if no gap between the condyles exists, the strain in the cartilage of the tibio-femoral contact areas will obviously be large. For these two reasons a gap between the femoral and tibial condyles must exist when the joint is complete, and no load is applied.

4.2.6 Load estimations.

There are two sources of information that can be used to obtain estimates of the load carried by the menisci from the load/deflection curves. These sources are the slopes of the curves and the differences in load between the curves at a given deflection.

If the menisci and the articular-articular contact areas are considered to act as separate springs (see Diagram 4.2(a)) then the estimated proportion of the load carried by the menisci will be the same from both sources.

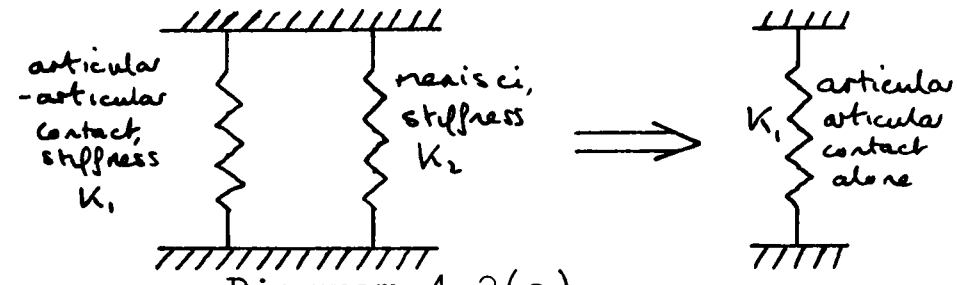

Diagram 4.2(a)

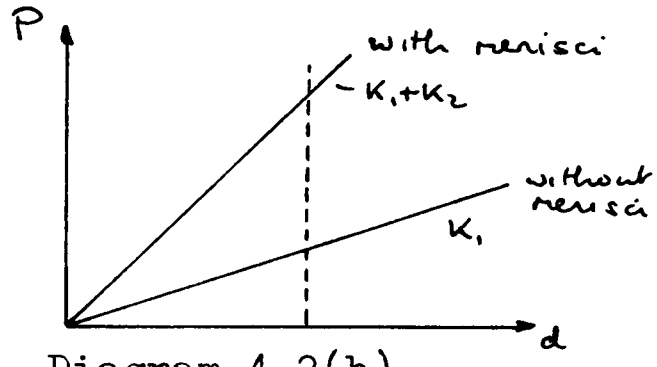

Diagram 4.2(b)

Diagram 4.2(b) shows the load/deflection characteristics for this spring model. The load carried by the menisci at a

deflection, d, is $K_2 d$. At this deflection the difference in load between the two lines is $K_2 d$ and the proportion of the load carried by the menisci is $\frac{K_2}{K_1 + K_2}$ Consider the slopes: $\left(\frac{\Delta P}{\Delta d}\right)_1 = K_1 + K_2$ and $\left(\frac{\Delta P}{\Delta d}\right)_2 = K_1$, hence the fraction of load carried by the menisci is $1 - \frac{\left(\frac{\Delta P}{\Delta d}\right)_2}{\left(\frac{\Delta P}{\Delta d}\right)_1} = \frac{K_2}{K_1 + K_2}$

The real situation is more complicated than that suggested above. Let the spring system shown in Diagram 4.2(c) represent the knee. K_1 again represents the tibio-femoral direct contact, but only acts after the condyles meet at a deflection, d_o. K_2 depicts the menisci and the articular cartilage with which they are in contact, and K_3 is the machine stiffness.

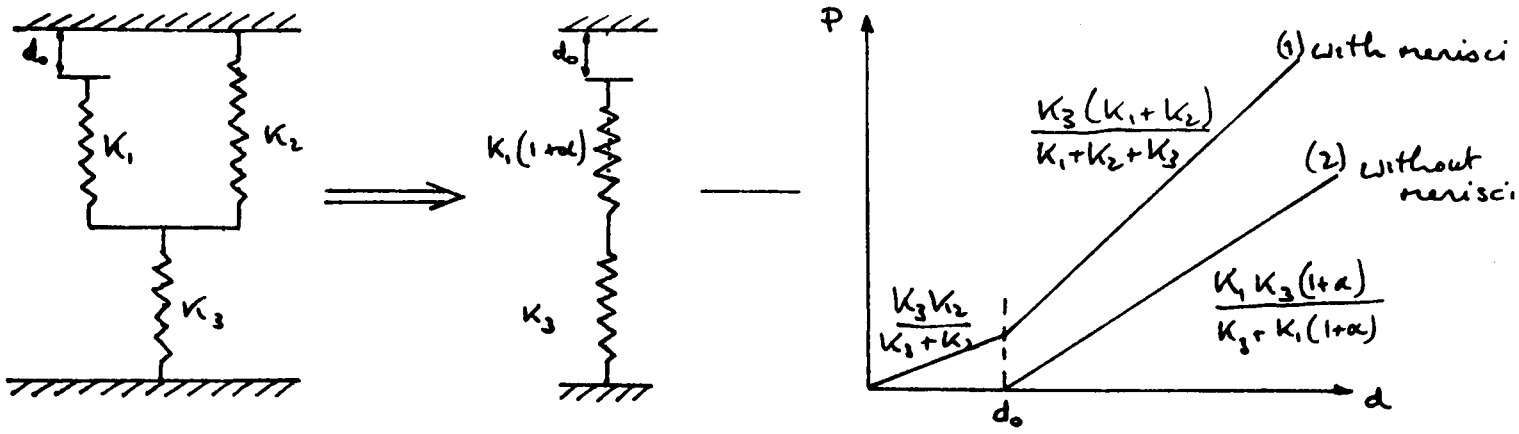

Diagram 4.2(c) Diagram 4.2(d)

When the menisci are removed, contact still only occurs after the bones have approached each other by d_o. Looking at the model analysis results (fig. 2.f.8), it is clear that for a given load the direct articular contact area is much larger without the menisci than with. The spring constant K_1 is increased by a factor αK_1, to allow for this change in stiffness. The load/deflection characteristic is as in 4.2(d). At a given deflection, d $(> d_o)$,

$$P_1 = \frac{K_3 K_2}{K_2 + K_3} d_o + \frac{K_3 (K_1 + K_2)}{K_1 + K_2 + K_3} (d - d_o)$$

$$P_2 = \frac{K_1 K_3 (1 + \alpha)}{K_3 + K_1 (1 + \alpha)} (d - d_o)$$

If the difference between the two curves is considered to be the load carried by the meniscus,

$$P_1 - P_2 = \frac{K_3^2 (K_2 - \alpha K_1) d}{(K_1 + K_2 + K_3)(K_3 + (1+\alpha)K_1)} + \frac{K_3\left[(1+\alpha)(K_1^2K_2 + K_2^2K_1 + K_1K_3^2 + 2K_1K_2K_3) - K_1K_3^2\right]}{(K_3 + K_2)(K_1 + K_2 + K_3)(K_3 + (1+\alpha)K_1)} d_o$$

The load carried by the menisci, however

$$P_{menisci} = \frac{K_3 K_2}{K_1 + K_2 + K_3} d + \frac{K_1 K_2 K_3}{(K_1 + K_2 + K_3)(K_3 + K_2)} d_o \quad (\text{for } d \geq d_o)$$

and

$$P_{menisci} = \frac{K_3 K_2}{K_3 + K_2} d \quad (\text{for } d \leq d_o)$$

hence if $d \leq d_o$ the estimation $P_1 = P_{menisci}$ is correct, but if $d \geq d_o$ then an underestimate is obtained - this result is more easily seen by considering $K_3 >> K_1$ and K_2.

$$P_1 - P_2 = K_2 d - \alpha K_1 (d - d_o) \quad \text{with } P_{menisci} = K_2 d$$

However if the cutting of the menisci allows the gap between the condyles to increase to d_ω then using $K_3 \gg K_1$ and K_2 again,

$$P_1 - P_2 = K_2 d - \alpha K_1 (d - d_\omega) + K_1 (d_\omega - d_o)$$

This means that in the region $d_o \leq d \leq d_\omega$ the value obtained will be an overestimate, but that as d increases, the tendency will be towards an underestimate.

If the slope method is used,

$$1 - \frac{\left(\frac{\Delta P}{\Delta d}\right)_2}{\left(\frac{\Delta P}{\Delta d}\right)_1} = \frac{K_3 (K_2 - \alpha K_1)}{(K_1 + K_2)(K_3 + (1+\alpha) K_1)}$$

So long as $\alpha > 0$, the proportion of the load carried by the menisci calculated by this method will always be less than the actual value (approximately $\frac{K_2}{K_1 + K_2}$)

$\propto$ will increase with load because the articular-articular contact area is proportional to $(r_m + a)^2$ and initially increases more rapidly when the meniscus is absent (ref. fig.2.f.8). The estimates obtained using both methods should become progressively more inaccurate as the load increases.

For the model, both methods may be used to calculate P menisci/P and the values so obtained compared to the actual value (see Table 4.1). As forecast, both estimates are low and the deflection method clearly gives the better estimate.

$\frac{P}{\pi k_2}$	actual value	slope method	deflec^n method
5	63.75%	42.5%	55%
10	63.33%	36%	51%
20	62.5%	19%	45%

Table 4.1

For the model, the ratio joint stiffness with meniscus ÷ joint stiffness without meniscus may be plotted as a function of load (see Diagram 4.3.a). The ratio rapidly decreases with increasing load and dips below unity at $P/\pi k_2 = 120$. Hence $\propto K_1 > K_2$ above this load. The overall contact area when the meniscus is present is larger than when the meniscus is absent (at $P/\pi k_2 = 250$, $(r_m + a + g)_{with} = 26$, $(r_m + a)_{without} = 22$). However, the implication is that for the latter case, an increase in load, ΔP, causes an increase in deflection, Δd, which is less than for the former case. Hence as load increases further the deflections for a given load will tend to be the same value.

Diagram 4.4 shows the stress distributions for a given deflection for the joint with and without the meniscus as determined in the analysis in Chapter 2. The total load transmitted through the joint is $P = \int_0^{2\pi} \int_0^{\text{outer edge of meniscus}} \sigma_{zz}(r)\, r\, dr\, d\theta$,

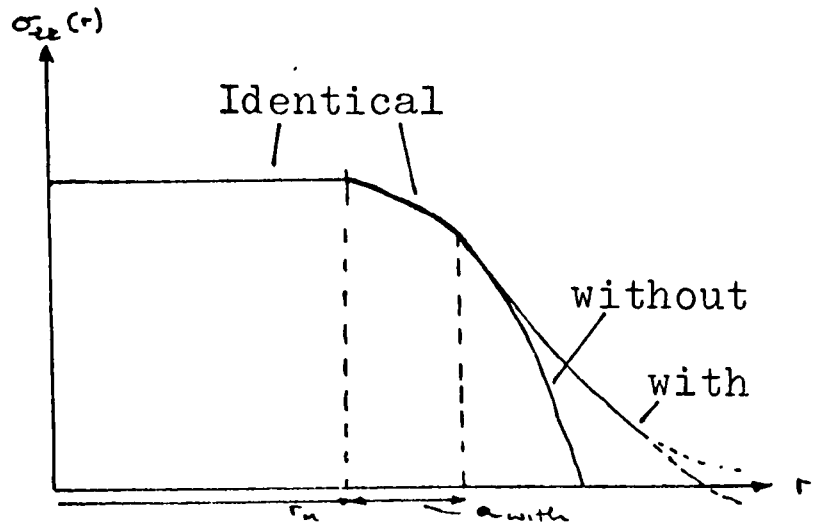

STRESS DISTRIBUTIONS FOR SAME OVER-ALL JOINT DEFLECTION WITH & WITH OUT MENISCUS

Diagram 4.4

and clearly the load will always be greater when the meniscus is present. Hence for any given load, d without meniscus $>$ d with and thus the slope ratio will tend to unity at high loads as $d_{without}$ tends to the same value as d_{with}.

Experimental values of the same ratio are plotted for the human and pig specimen groups in Diagram 4.3.b. The values obtained showed some scatter and hence the curves shown are the means for the groups with the standard deviation added and subtracted. If the load was expressed in fractions of body-weight there was no significant reduction in the scatter of the values of stiffness ratio.

The 16 successful human experiments were considered for the human group, and the 42 successful pig experiments for the pig group. For both groups the cartilage stiffening mentioned in 4.2.5 will cause a more rapid increase in the joint stiffness when the menisci are absent, but the reduction in stiffness ratio should be similar to that predicted by the model.

It will be noticed that for the 'human' group the slope ratio drops below unity and thus negative estimates for $P_{menisci}$ will occur when the slope method is used. The load estimates from both methods for each group are shown in histogram form in diagrams 4.5. The number of specimens at a particular percentage, A, is taken to be the number within the range A $\mp$ 2.5% and is plotted every 5%. The wider spread of results at the lower loads reflects the larger standard

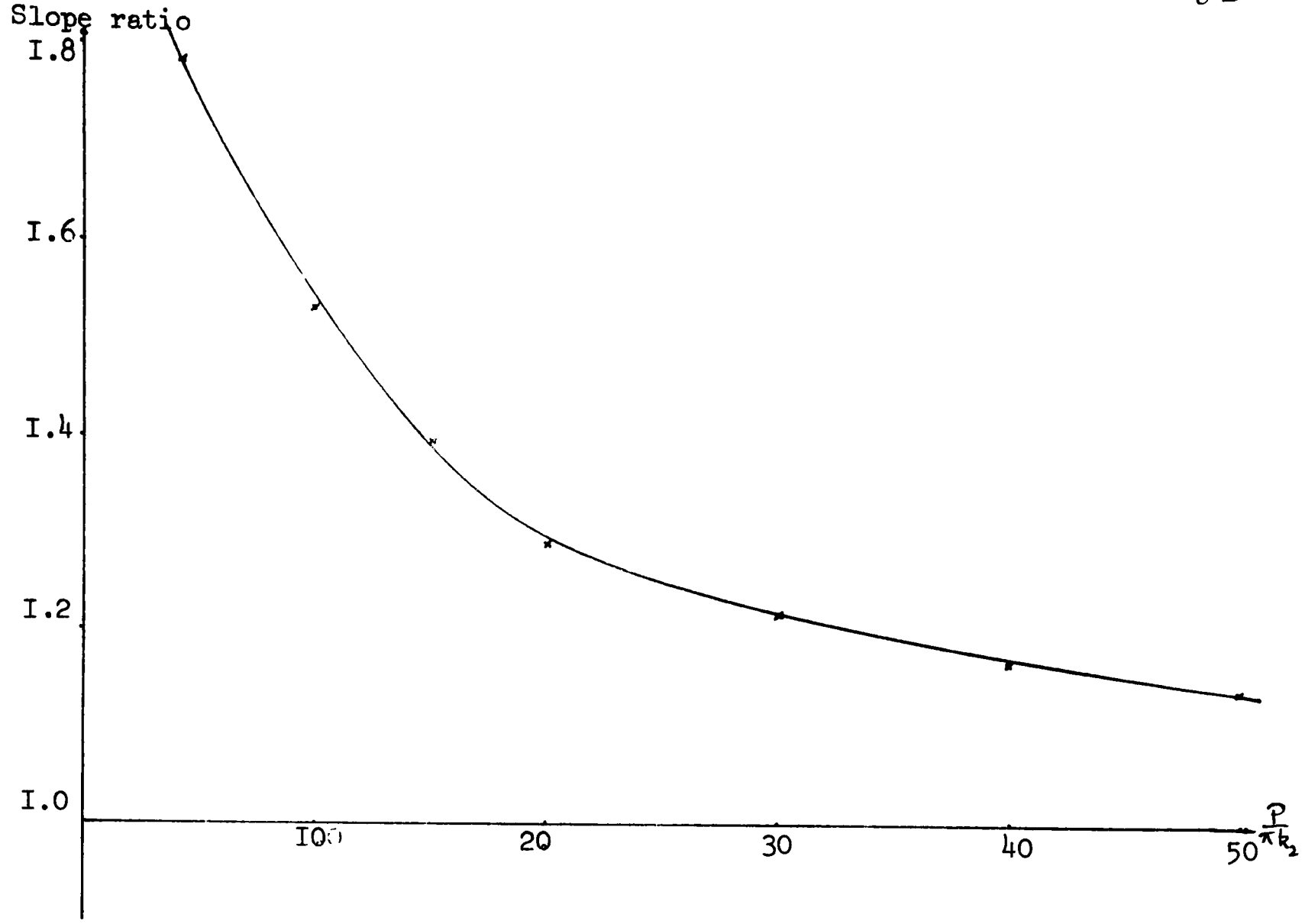

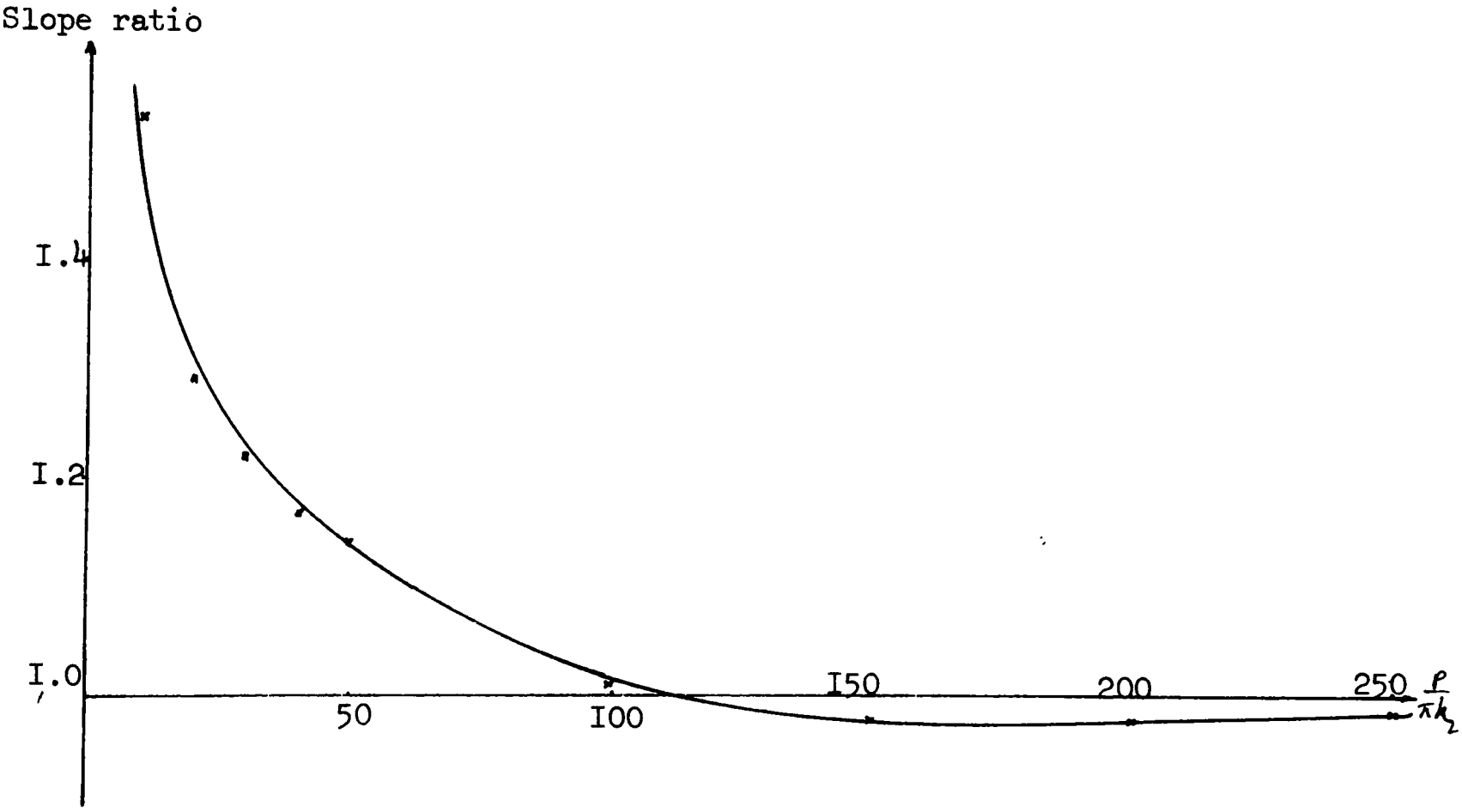

Slope ratio : $\frac{\text{Stiffness with meniscus}}{\text{Stiffness without meniscus}}$ v. Load

MODEL ANALYSIS : STANDARD CASE

Diagram 4.3.a

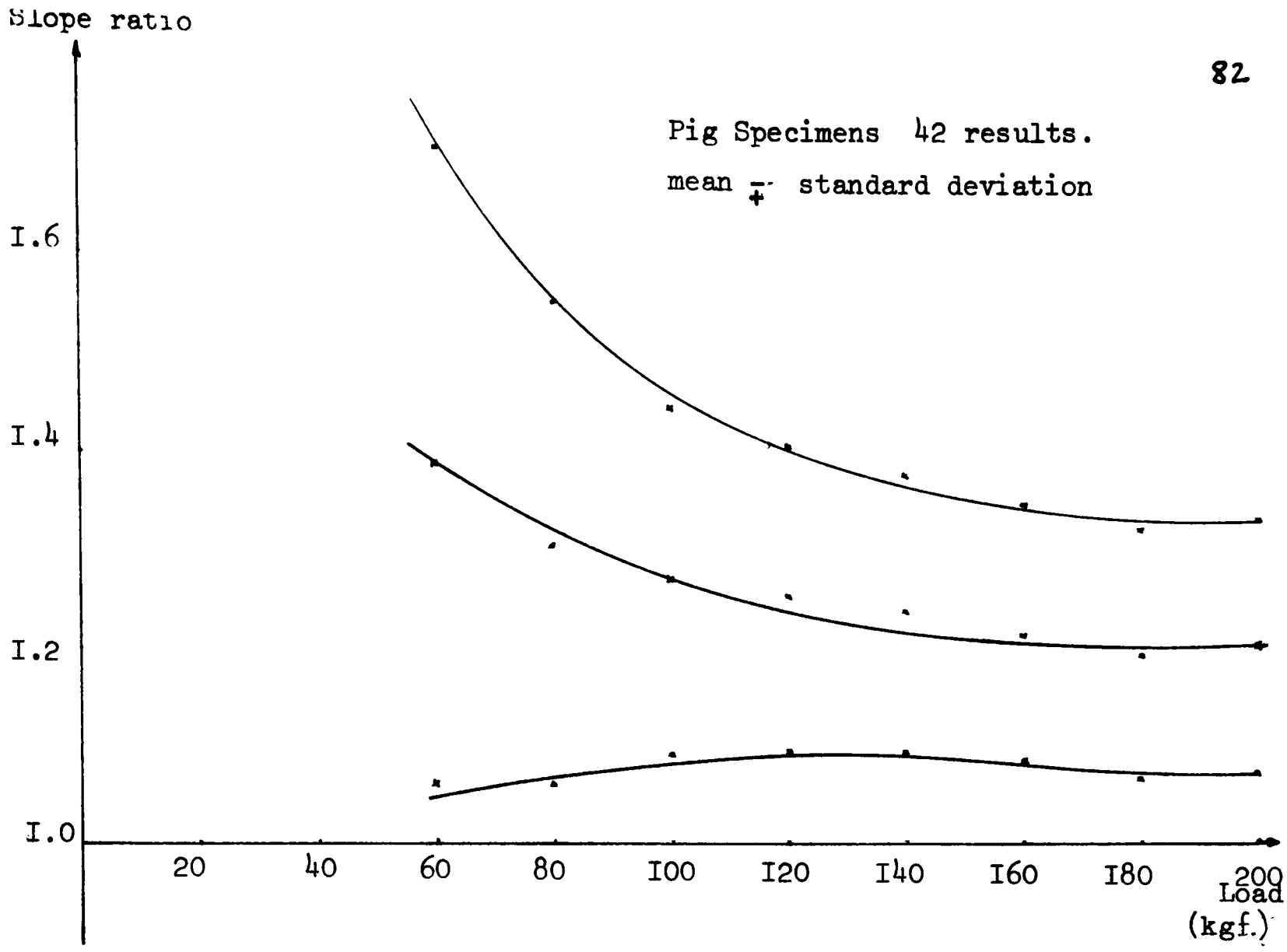

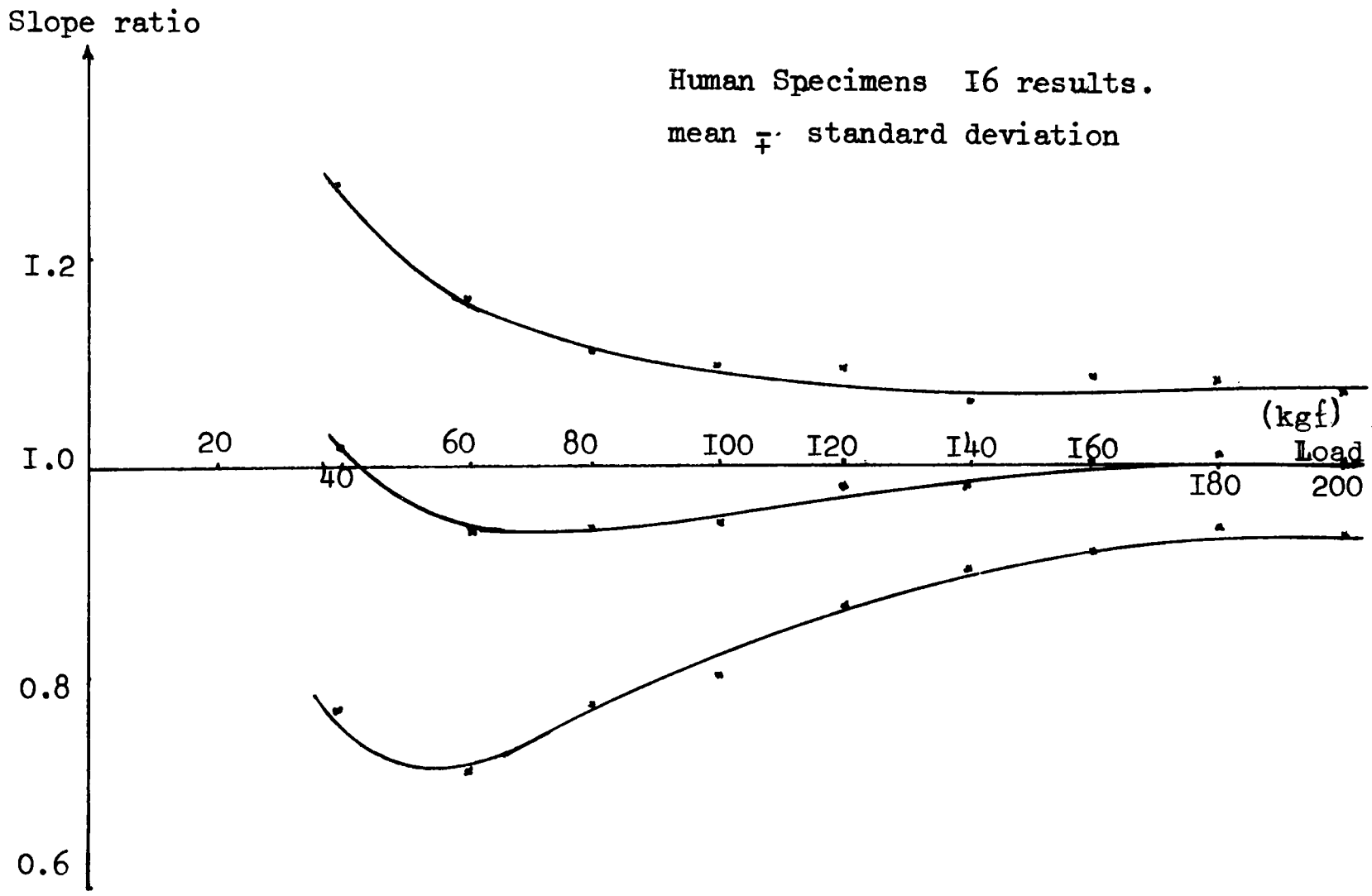

Slope ratio v. Load for experimental results.

42 pig specimens and I6 human specimens loaded between 0 and 200 Kgf.

Diagram 4.3.b

deviations at these loads and the greater errors there (see next section).

In summary, therefore, the load/deflection curves may be used to make two estimates of the meniscal load, $P_{menisci}$. Because of the difference in initial contact areas and the different rates of increase in contact area with load with and without the menisci, underestimates of $P_{menisci}$ are obtained from both methods. The formulation of the slope method is such that negative estimates of $P_{menisci}$ may occur. The deflection method, therefore, gives the more reasonable estimate.

Use of the deflection method indicates that the meniscal load is at least 35% of the total load at 200 Kgf and at least 45% at 100 Kgf for old human specimens. The percentages are expected to be higher in young healthy joints. For pig specimens the percentages are 75 and 85% at the respective loads. It is therefore quite clear that the menisci transmit a significant proportion of the load between the femur and the tibia.

4.2.7 Errors

There are a number of errors which may be introduced to the calculations of load carried by the menisci from the load deflection curves. The first is from the accuracy of the recording system on the Instron.

The quoted value of this (see Appendix 3) is $\mp \frac{1}{2}\%$ dynamic accuracy for the pen to deflect full scale in 3 seconds. If the chart speed is 100 cms/min. this means 5 cms. chart travel for the full scale deflection. Typical loading in vivo is rapid and the maximum cross-head speed that gave steepest slopes of about 5 cms. for full scale deflection was 2.5 cms/min.

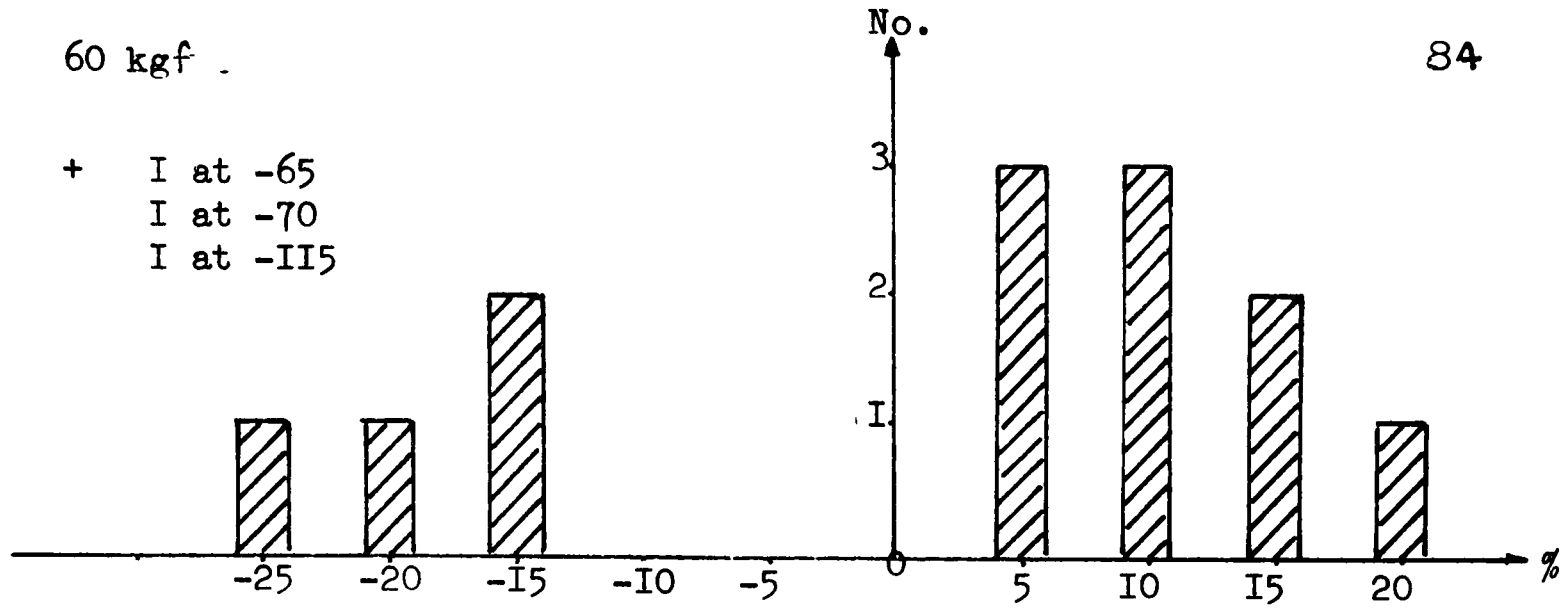

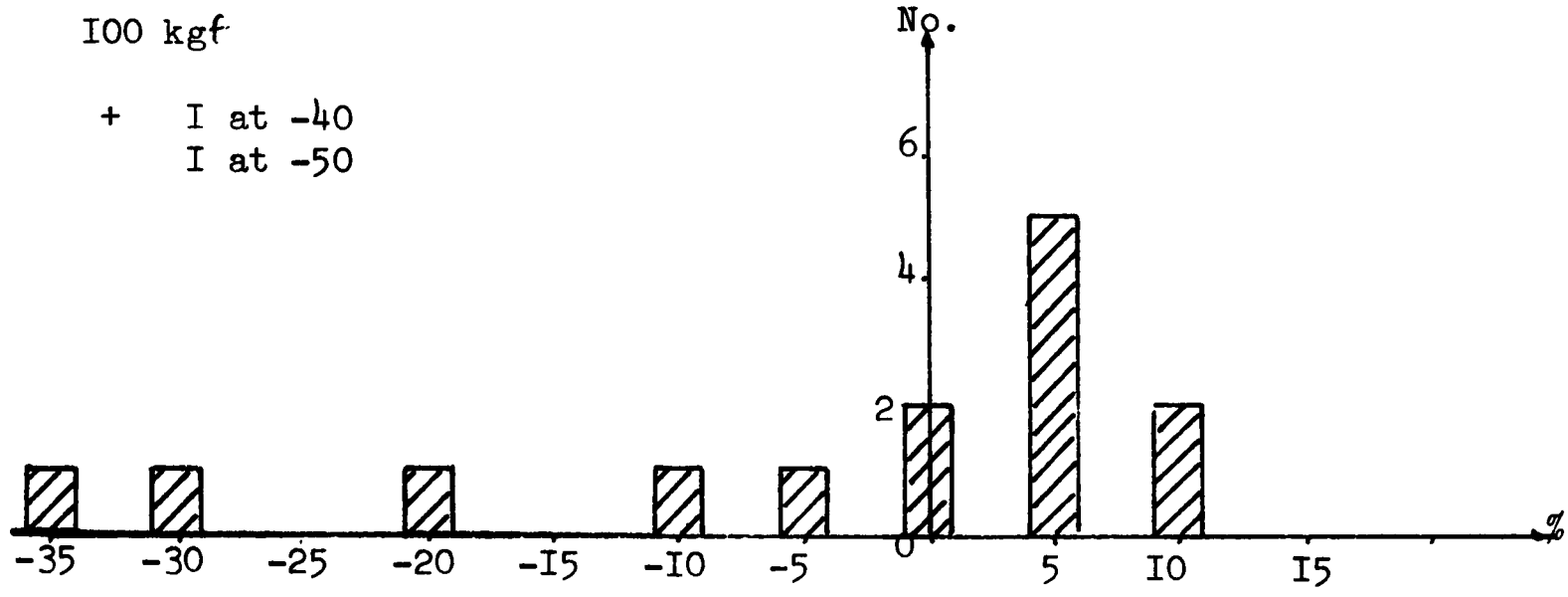

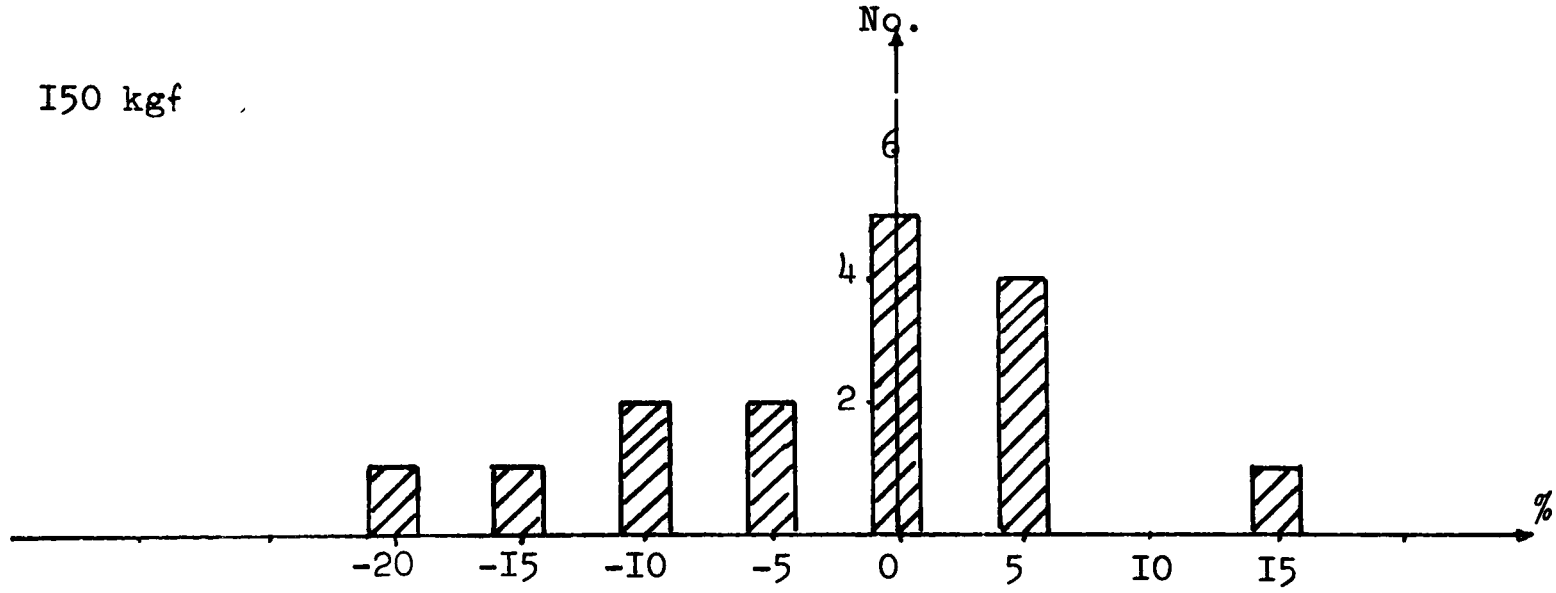

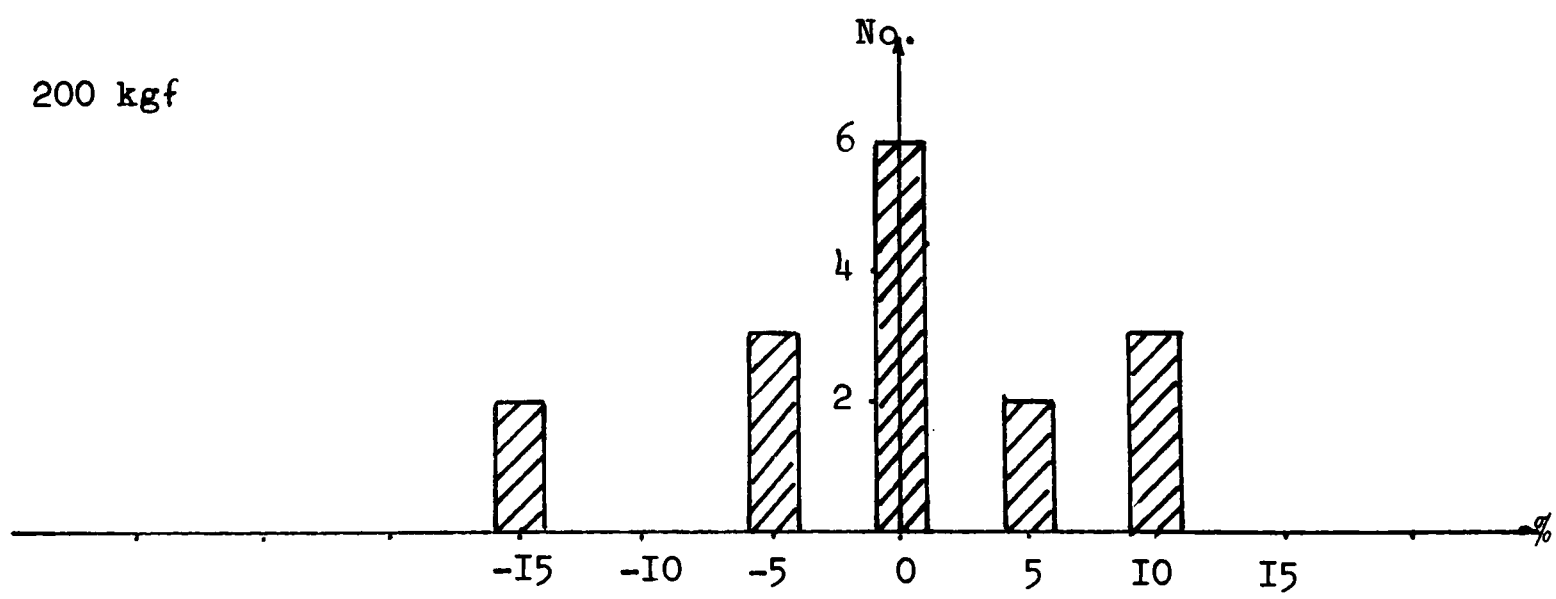

Histograms of % load carried by menisci determined by slope method.
Human Specimens I6 out of I7 specimens at all loads.

Diagram 4.5.a

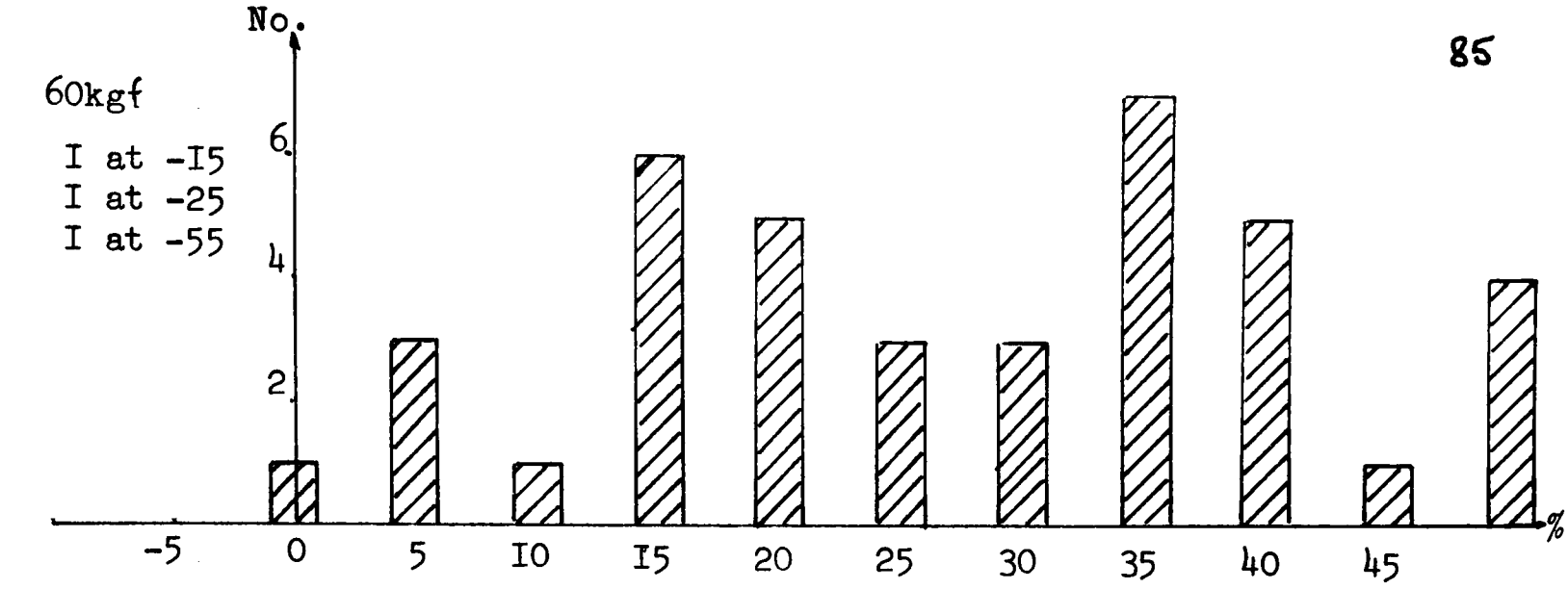

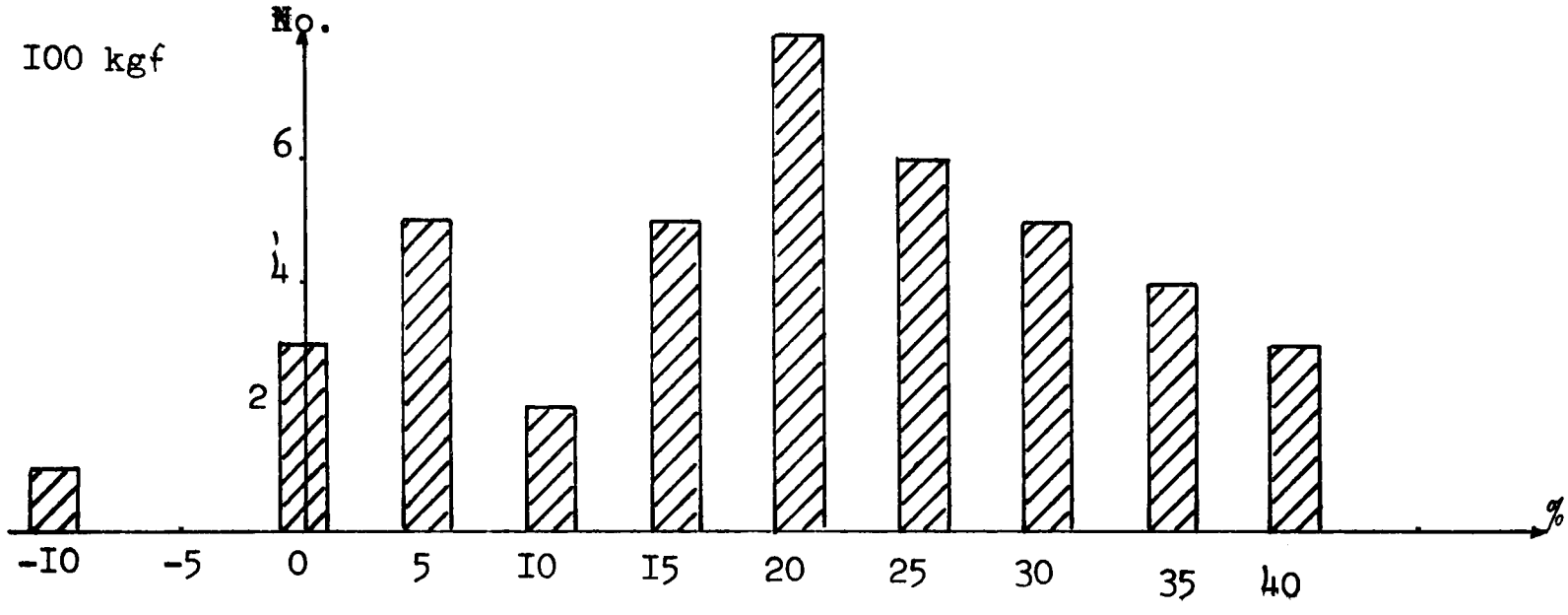

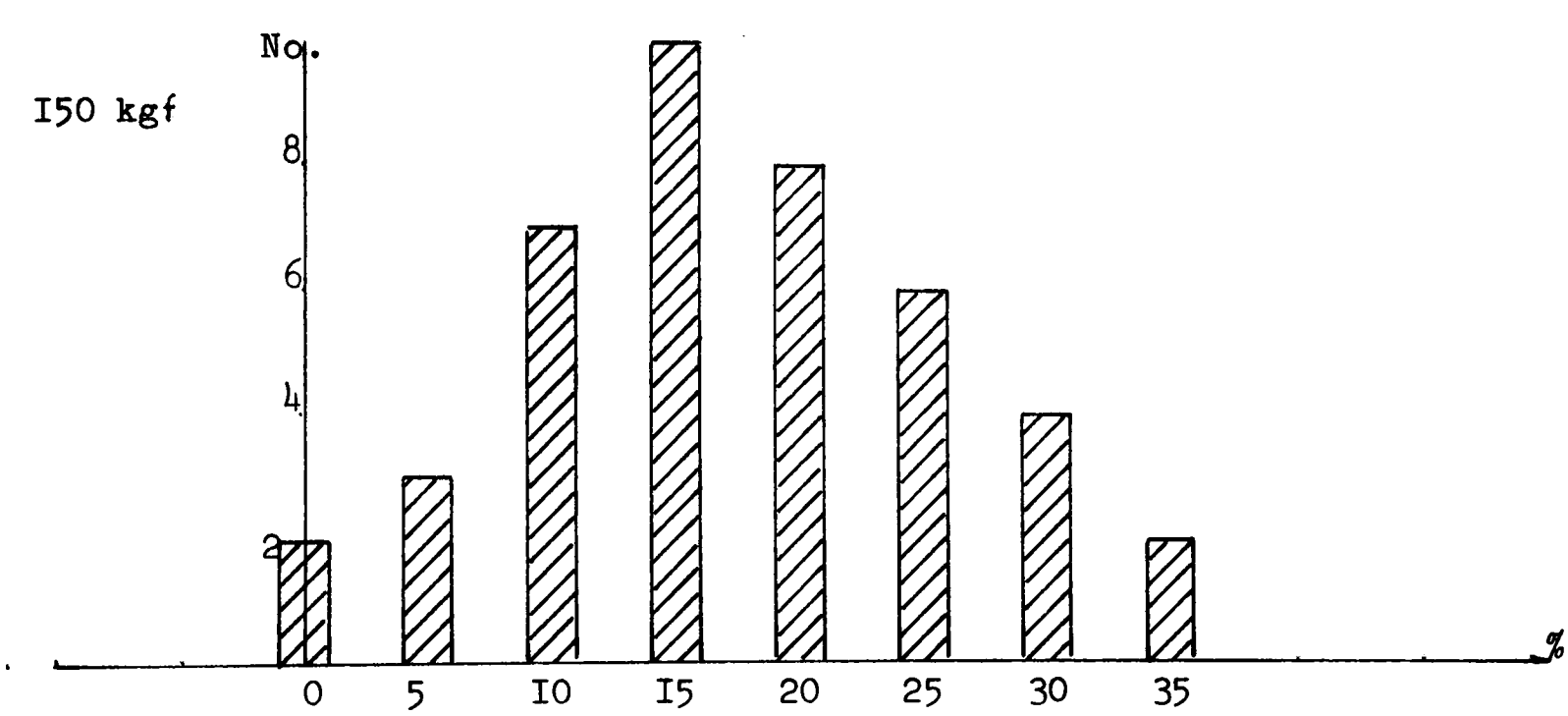

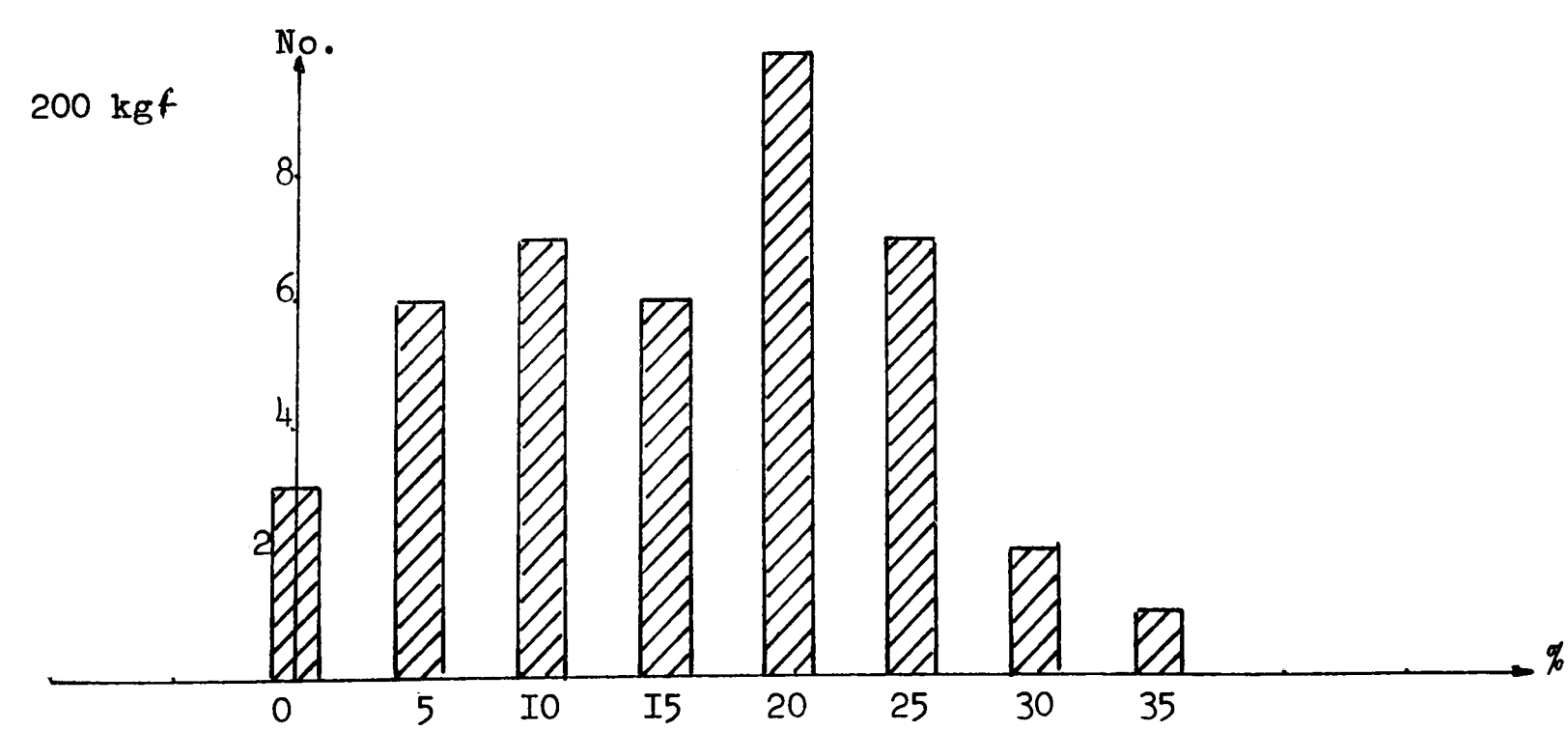

Histograms of % load carried by menisci determined by slope method.
Pig Specimens 42 out of 45 specimens.

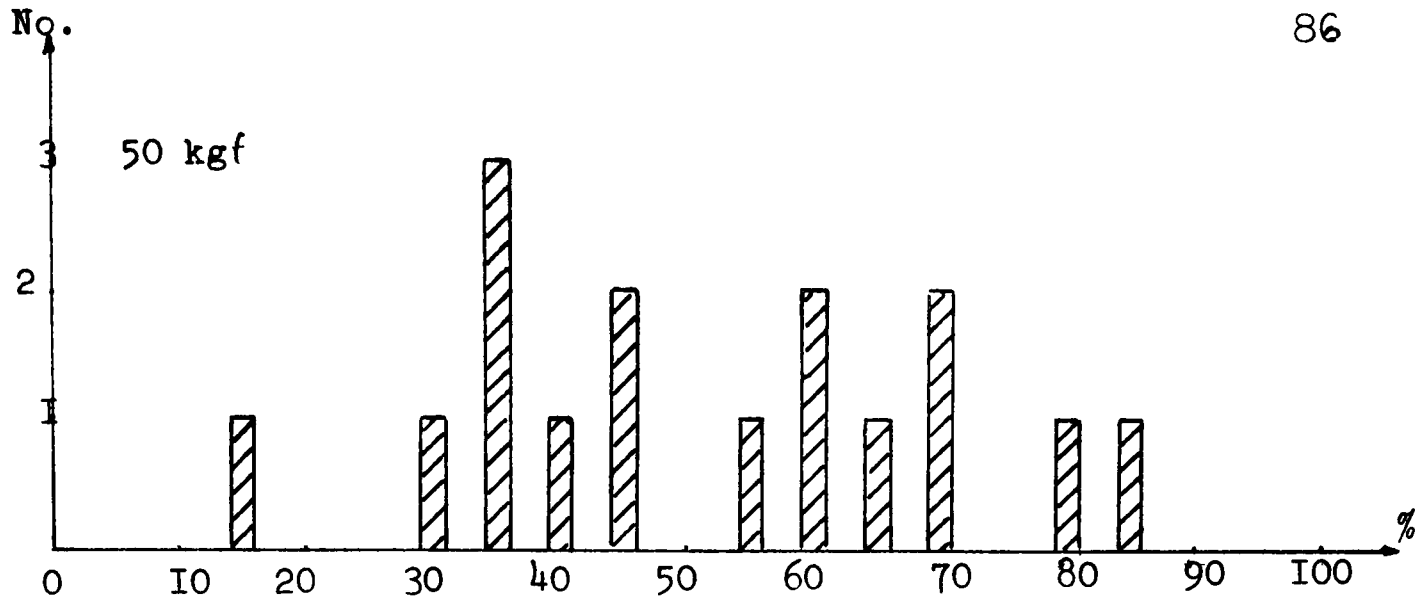

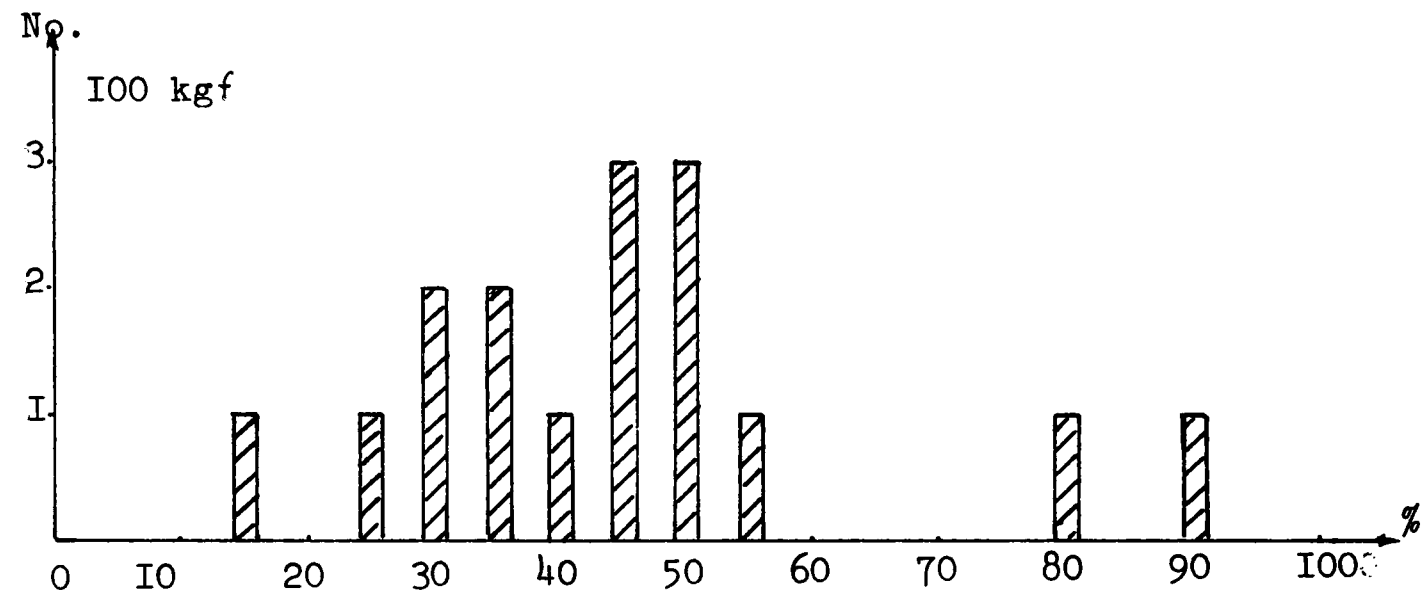

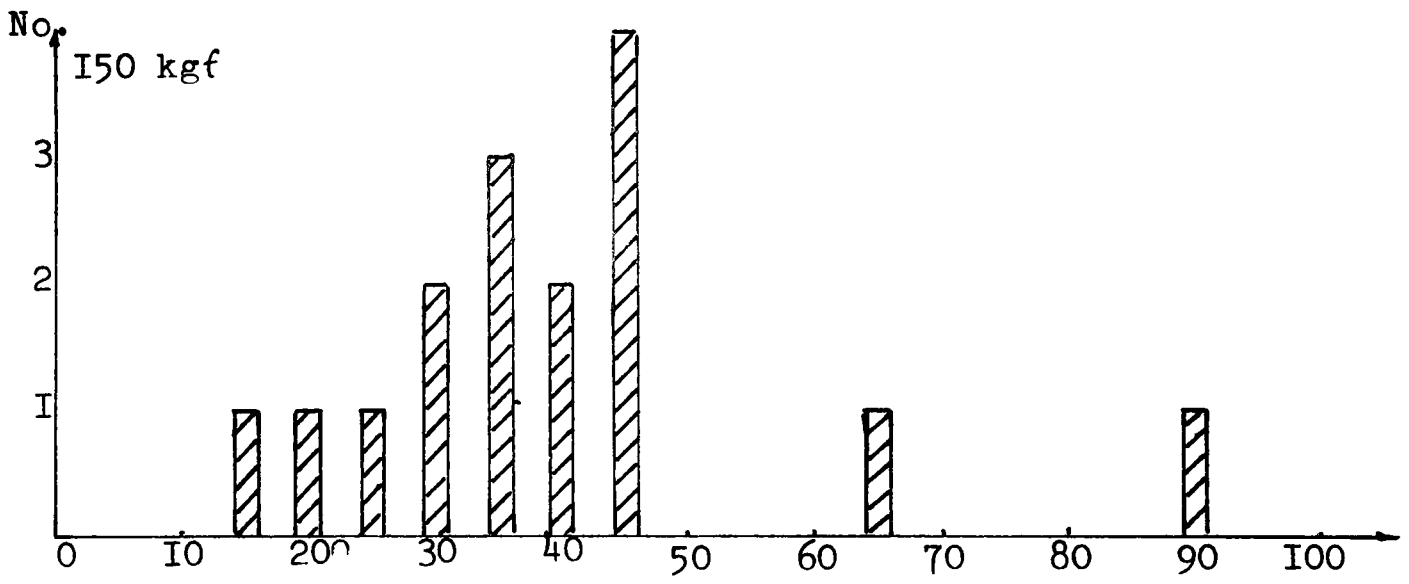

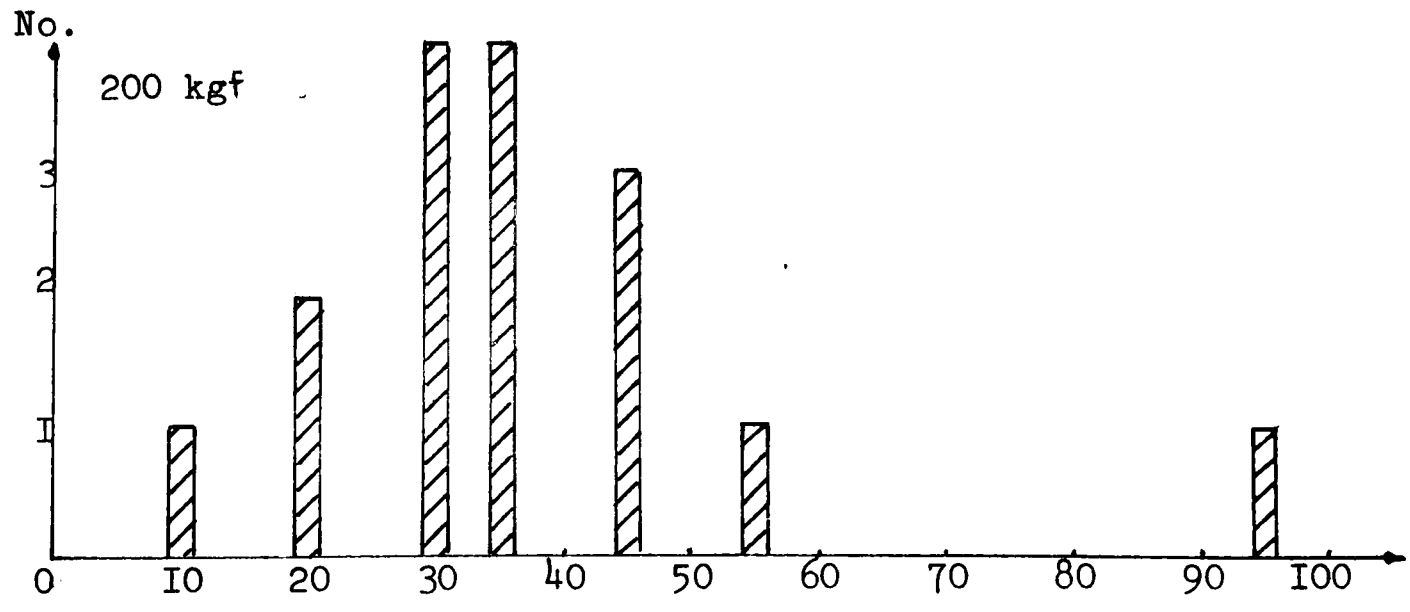

Histograms of % load carried by menisci determined by deflection method. Human Specimens I6 out of I7 specimens.

Diagram 4.5.c

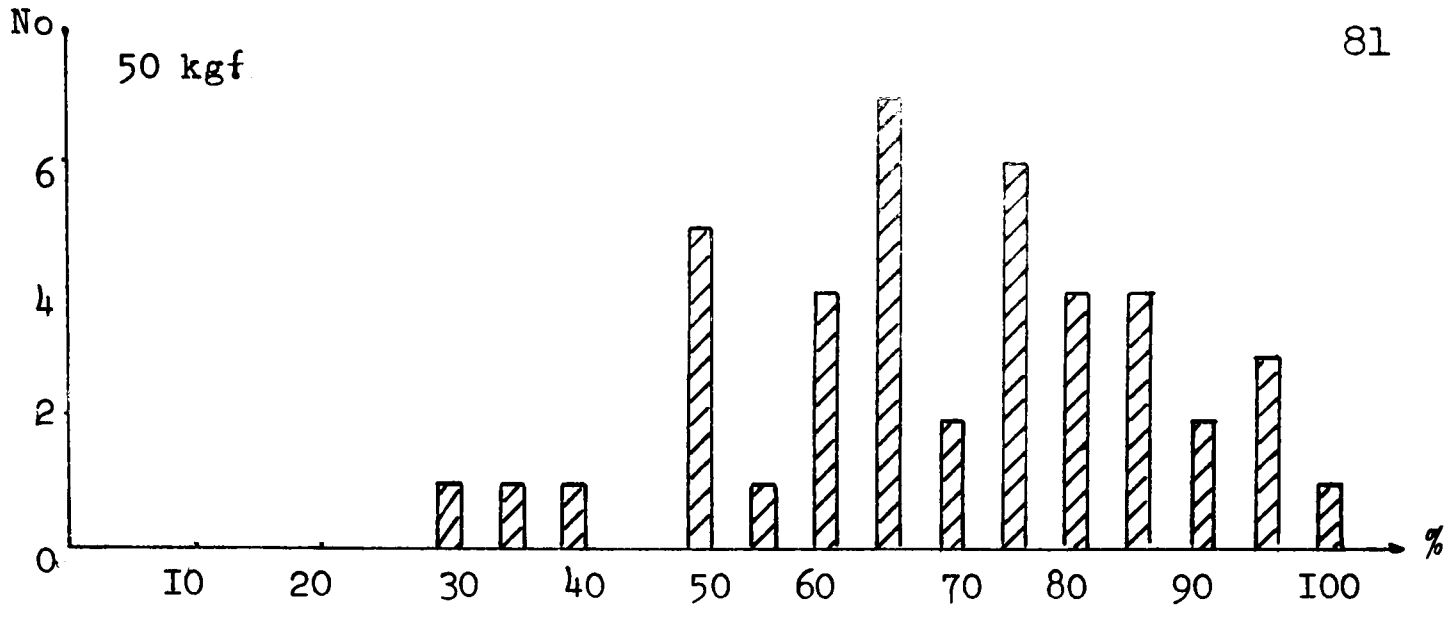

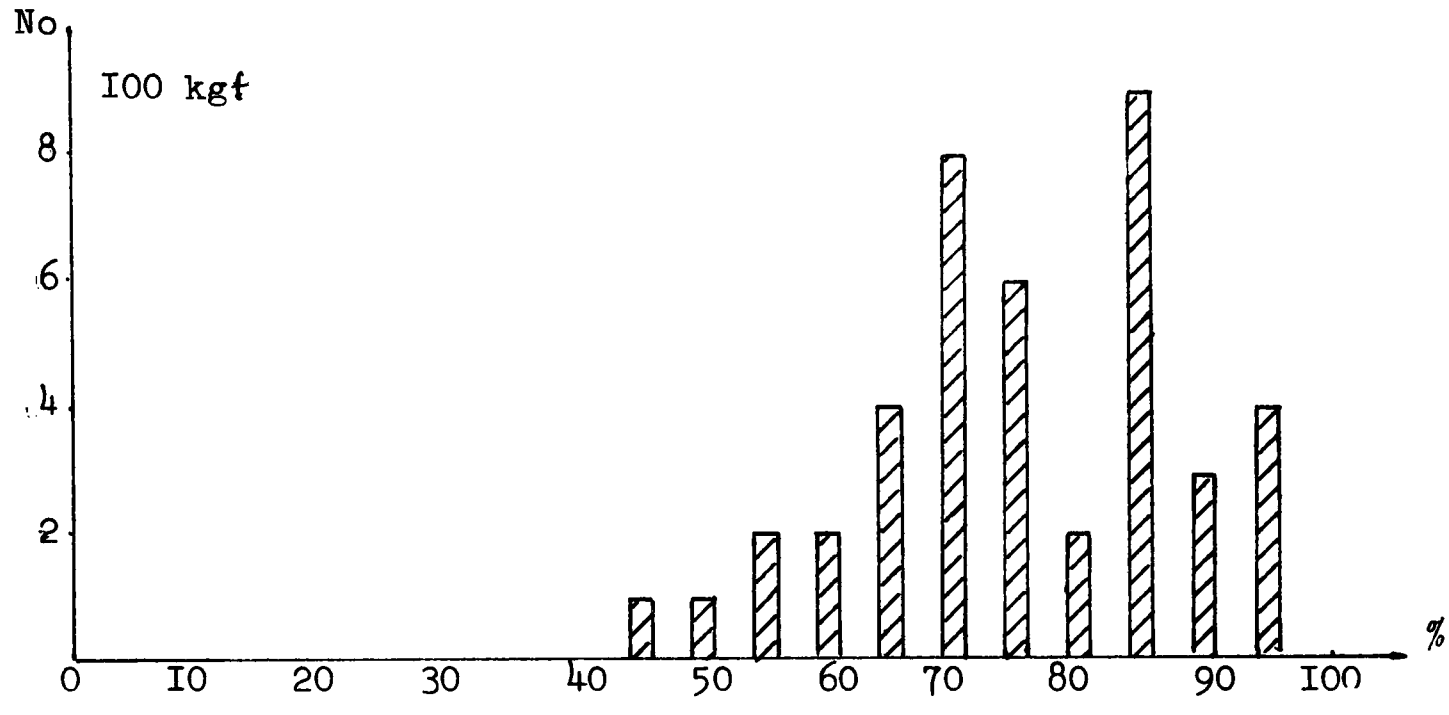

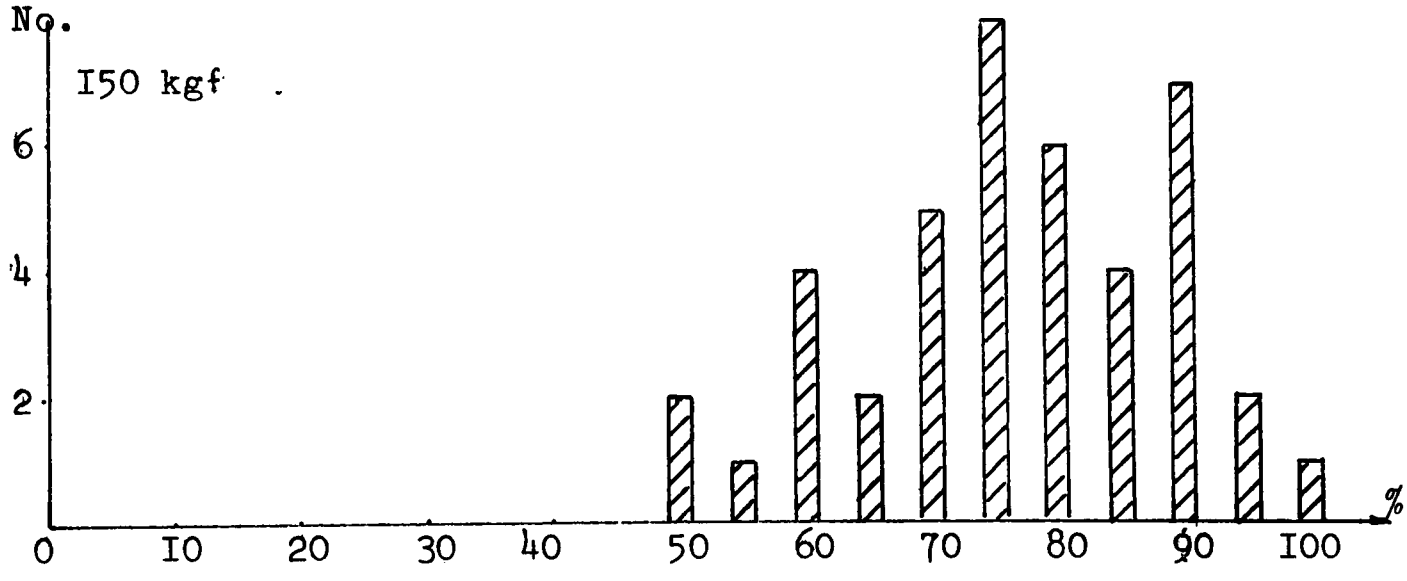

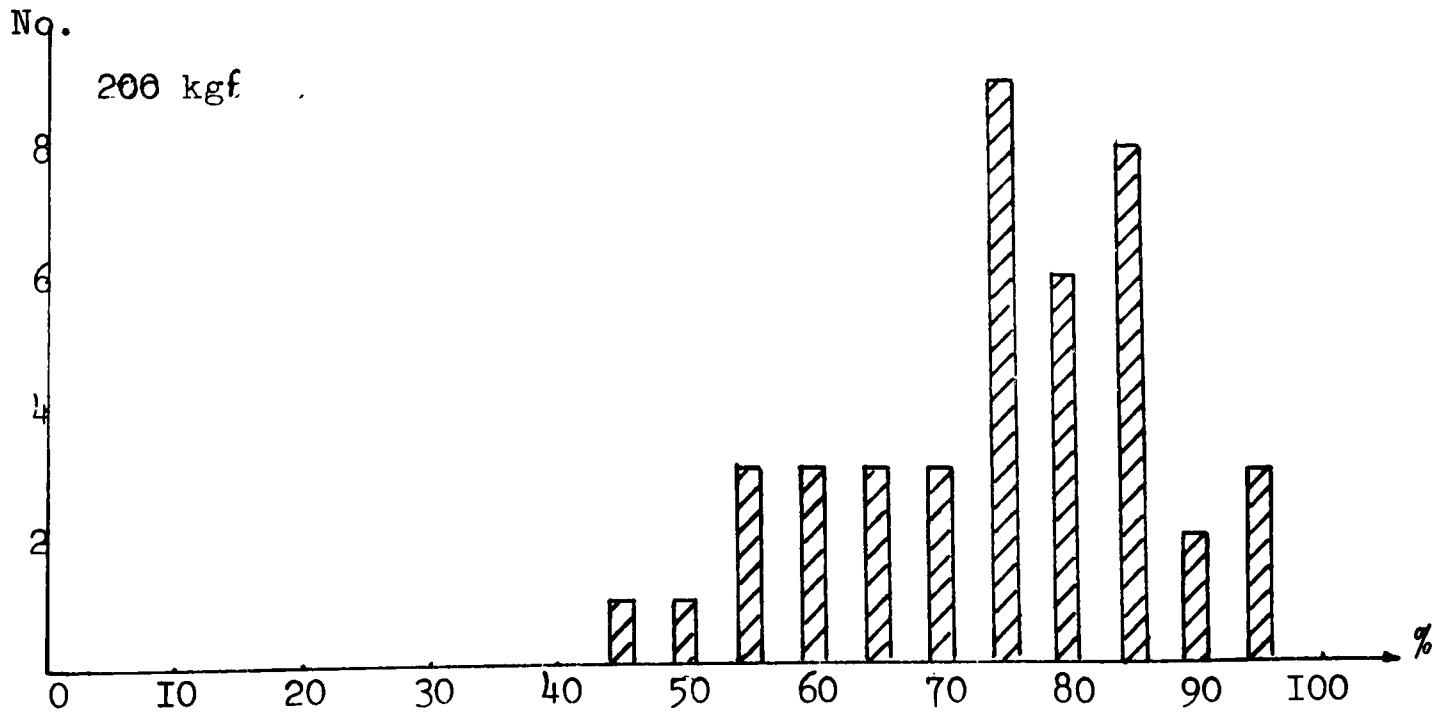

Histograms of % load carried by menisci determined by deflection method.
Pig Specimens 42 out of 45 specimens.

This speed was usually used. If both chart and cross-head speeds are reduced by a factor of five, then curves are reproducible up to a slope of approximately 3 cms. for full scale deflection. The slopes of the results are well within this limit and thus the quoted accuracy. However, they are subject to three other errors.

The first of these is simply their measurement which is made directly from the Instron recordings. The second is the stiffness of the machine and the adaptions. This was measured to be 0.12 mm. for 200 Kgf with the Hydraclamp in the 'vertical' position, but will be higher when the Hydraclamp is angled away from the vertical due to the bending moment applied to it. In the load estimate from the slope ratios, if $K_3 \gg K_1$ and K_2 then terms containing K_3 tend to cancel. Since K_3 is variable and larger than K_1 and K_2, no allowance was made for it in the load estimates. The final error is made up of two components: the slopes measured can be a function of the reduction in tension in the ligaments and compression of the cartilages. Any displacement of the zero position on the load scale due to the cutting of the collateral ligaments will mean that the comparison of slopes may not necessarily be for the same compression of the joint. The errors due to these will be larger at low loads than higher ones. The spread in the results is much greater at the low loads.

The deflections are also subject to error. The chart drive clutch tended to slip at the low load end as the direction of motion was altered. Therefore, the start point of the load deflection cycle was prone to a slow progression along the chart

paper. This was not always the case and adjustment of the clutch had no effect. The result was that the limit cycle was reached slightly more rapidly than if there was no slip. Extra cycles were allowed when slip occurred.

A second error occurs in the copying of the limit cycles to produce the results presented. If the zero points of the curves are not exactly superimposed an error will be introduced, which will appear in the estimation of load. If the slope is 200 Kgf for 5 cms. chart travel, then a 2.5 mm. difference in the zero positions of two curves will result in an error of 10 Kgf in the load at a specific deflection. Hence, for small load differences, and estimations at low loads, the error will be much larger than for high loads and load differences. Alterations in the load at the zero position will also affect the estimations, again introducing a much larger error at low loads.

The spread in estimates at the low loads reflects this larger error. If there is a 10 Kgf error due to both the effects mentioned, giving a total of 20 Kgf , then this will give 20% error in an estimate of 50% at 200 Kgf , but 100% error in an estimate of 40% at 50 Kgf. The best estimate of the percentage should come from both methods at low loads but the errors obviously spread the estimates too widely to give a conclusive value. The high load estimates are more accurate but must be accepted as being low.

4.3 Load relaxation

If the menisci are load bearing then their removal will cause a change in the contact areas and hence the stress distribution in the joint. The load relaxation characteristics of the two situations should be different.

If in the complete joint the areas of contact are considered to be two circles of the same radius with the same stress distribution on each, and the radius of the circles is reduced when the menisci are removed; and if the stress distribution is taken to be parabolic with a maximum of σ_m at the centre of the circles dropping to zero on the outer edge, then $P = \pi \sigma_m R^2$ where P is the total applied load and R is the radius of the circles.

Let the cartilage be a material which may be represented by a Maxwell element (see Diagram 4.6)

The equation relating ϵ and σ is

$$\eta \dot{\epsilon} = \frac{\eta}{E} \dot{\sigma} + \sigma$$

For stress relaxation $\dot{\epsilon} = 0$ and $\epsilon = \epsilon_0$ at $t = 0$

$$\therefore \quad \sigma = E \epsilon_0 e^{-\frac{t}{\tau}} \quad \text{where } \tau = \frac{\eta}{E}$$

$$= \sigma_0 e^{-\frac{t}{\tau}}$$

for a given load P

(1) with the menisci present

$$P_1 = \pi R_1^2 (\sigma_{m0})_1 e^{-\frac{t}{\tau_1}}$$

$[(\sigma_{m0})_1$ means σ max at $t = 0$ for case (1)$]$

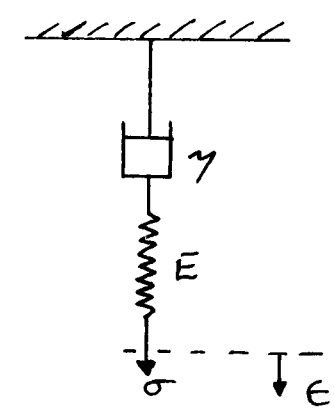

Diagram 4.6

Maxwell element

(2) without the menisci

$$P_2 = \pi R_2^2 (\sigma_{no})_2 e^{-\frac{t}{\tau_2}}$$

at $t = 0$ $P_1 = P_2$

$$\therefore \frac{(\sigma_{no})_1}{(\sigma_{no})_2} = \left(\frac{R_2}{R_1}\right)^2$$

as $R_2 < R_1$ if the menisci are load bearing, then $(\sigma_{no})_2 > (\sigma_{no})_1$

Now suppose that η is inversely dependent on the rate of loss of fluid from the cartilage, and thus the stress gradient; the greater the gradient the smaller η and hence τ

In this case, therefore $\tau_1 > \tau_2$

and hence at a given time $P_1 > P_2$

Typical results are presented on pages A 58-60. The effect of meniscectomy is not as marked as had been hoped. Human Specimen 11 is typical of the 10 human specimens tested and pig specimen 45 is typical of 17 out of the 20 pig specimens tested. Pig specimen 33 is typical of the other three pig specimens. The results indicate that fluid flow away from high pressure zones is not as rapid as expected. To make quantitative estimates of the meniscal load from the results would require knowledge of the contact areas and stress distributions. The stress distribution was not determined and hence no estimates were made.

4.4 Radial expansion and circumferential moduli tests

4.4.1 Radial expansion tests

The results are shown in Appendix 4.7. The menisci were usually loose and easily moved at the zero position and as the femur approaches the tibia the menisci were pushed outwards and became taut. Once taut expansion increased slowly and steadily with load. The readings were taken simultaneously

from three dial gauges supported from a bar held between two retort stands. The gauges were kept stationary relative to the joint.

Errors would be introduced to the readings if there was any rigid body motion or if the dial gauge arms were not directed along a radius. The anterior and posterior readings were taken in line with each other to eliminate rigid body movement, but were subject to error if the direction was not radial (see Diagrams 4.7).

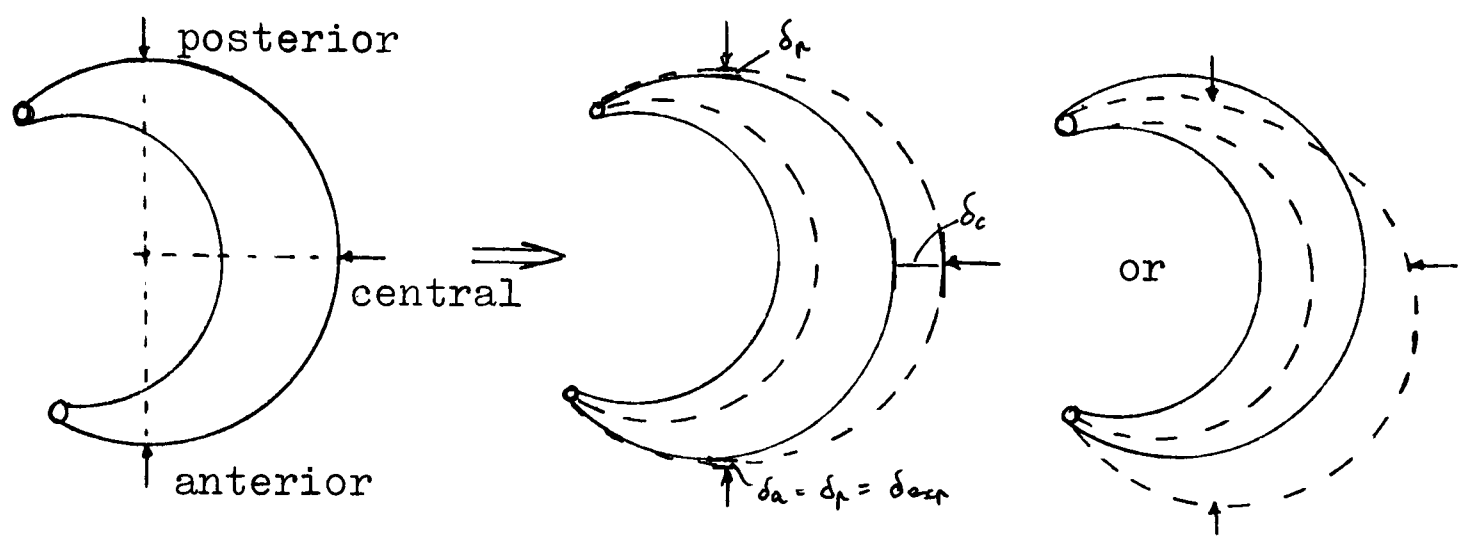

(a) (b) (c)

diagram (a) shows the undeformed state and (b) indicates the expansion that would be measured if there was no rigid body motion as shown in (c). In the case of (c)

$$\delta_{p.} = -\delta_{\text{rigid body}} + \delta_{exp.}$$

and $$\delta_{a.} = \delta_{\text{rigid body}} + \delta_{exp.}$$

hence $$\delta_{exp.} = (\delta_{p.} + \delta_{a.}) / 2$$

However if the gauges were not lined on radii then they would not measure $\delta_{exp.}$ correctly nor would correct measurement be made if the trio of gauges was rotated such that one of the anterior/posterior gauges was nearer the appropriate adjacent

horn than the other. The reading from the central gauge would be incorrect if there was any rigid body motion at all. Depending on where the gauge was initially placed there would be either an increase or a decrease due to this motion. The anterior/posterior average is likely to give a better estimate of the expansion at that point, than the central reading at the crown.

4.4.2 Determination of circumferential modulus.

It is shown in the analysis that the load carried by the menisci depends critically on the circumferential modulus of elasticity. To determine this, tests were performed as described in 3.4.2.2. The specimens were cyclically loaded between a fixed position and 5 Kgf(50N) load and the limit cycle was quickly obtained. Stress relaxation tests showed that compared to the joints, the material is relatively elastic, only 1/5 of the load being lost after 20 mins.

The shape of the loading curves was similar to that obtained by Kempson in his tests on the surface layer of articular cartilage in the fibre direction; that is, initially quite flexible followed by a stiffening to a very near linear load/deflection relationship.

The proposed extrapolation was attempted, but there was a large spread about the least squares straight line fitted to the data. The estimation of cross-sectional area was considered to be the main cause of the deviation. The area was determined by the use of vernier calipers but contact with the material was difficult to detect because of the material's great flexibility in the transfibre directions. Measurements

of the area at a particular point on the length often differed by 10% and sometimes 20%. Some variation along the length was expected, but lay within the limits mentioned above.

The Instron plotted the load, P, against the increase in separation of the clamps, δ. Hence, including end effects, for two particular tests of the same specimen at different lengths ℓ_1 and ℓ_2

$$\delta_1 = \frac{P\ell_1}{A E_1} \quad \text{and} \quad \delta_2 = \frac{P\ell_2}{A E_2}$$

where E_1 and E_2 are the apparent moduli at the respective lengths. (P/δ_1) and (P/δ_2) were measured for the near linear part of the two curves. ℓ_1 and ℓ_2 were the distances between the clamps at the zero position and were measured with a travelling microscope mounted on the machine cross-head. Eliminating A from the equations above:-

$$\frac{E_1}{E_2} = \frac{(P/\delta_1)}{(P/\delta_2)} \frac{\ell_2}{\ell_1}$$

Hence if E_1/E_2 is plotted v. $\frac{\ell_2}{\ell_1}$ with ℓ_2 always the shorter of the two lengths, the effect of the cross-sectional area measurement is removed from the data. Diagrams 4.8 are plots of $\frac{E_1}{E_2}$ v. $\frac{\ell_2}{\ell_1}$ and show that the data has a reasonably narrow bandwidth. The curves are more of the type $y = \frac{1}{x}$ than the straight line fitted, but as the former has no intercept on the $x = 0$ line, the latter was used. As $\ell_1 \to \infty$ for a fixed value of ℓ_2 then the correct value of E_1 and thus E should be obtained from E_2. The straight lines fitted show that the actual value of E is at least 2.5 times that obtained from the shorter lengths. This short-length value (using the measured cross-sectional areas) lies between 60 and 80 N/mm^2 for the

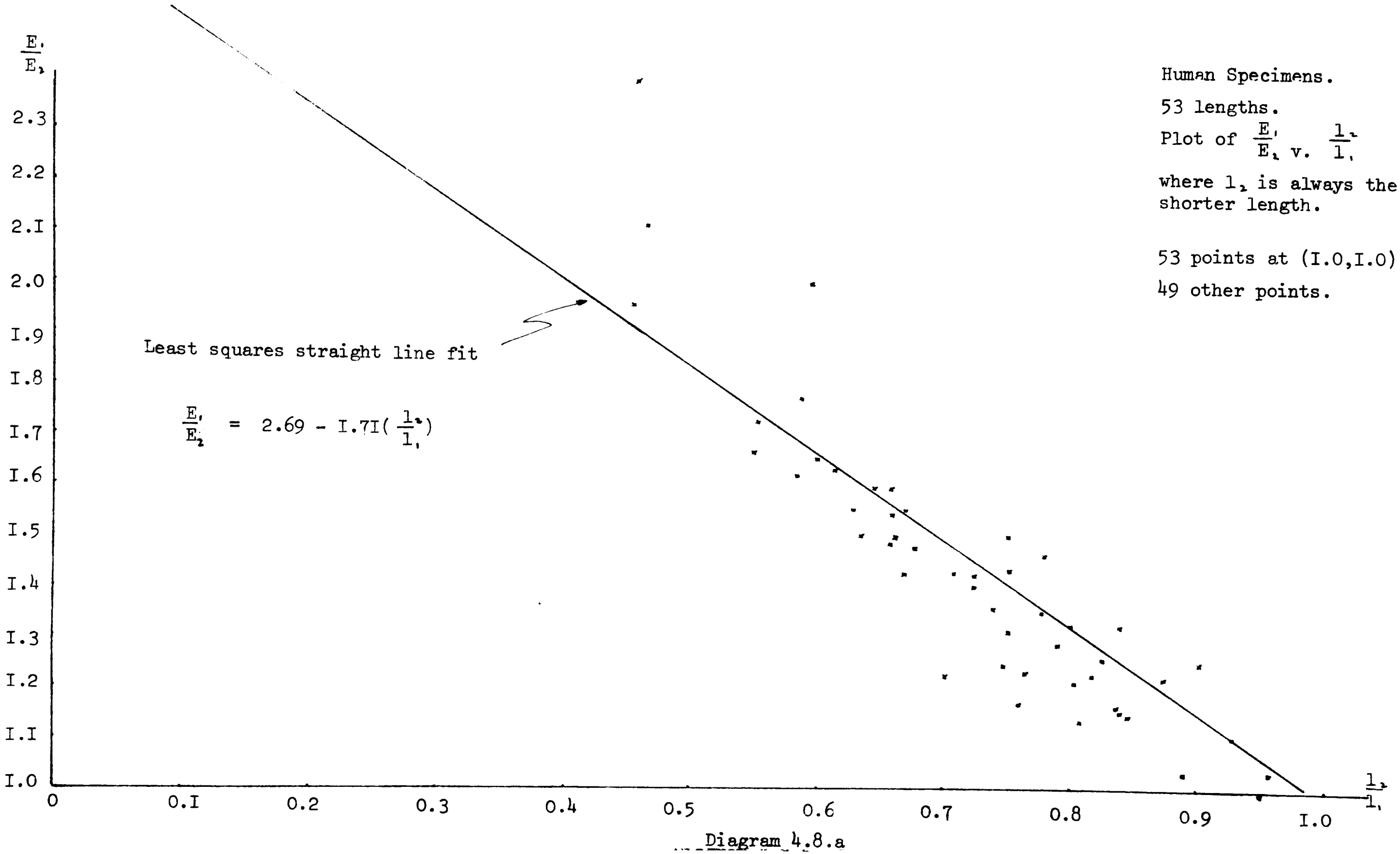

Human Specimens.

53 lengths.

Plot of $\frac{E_1}{E_2}$ v. $\frac{l_2}{l_1}$

where l_2 is always the shorter length.

53 points at (I.0,I.0)

49 other points.

Diagram 4.8.a

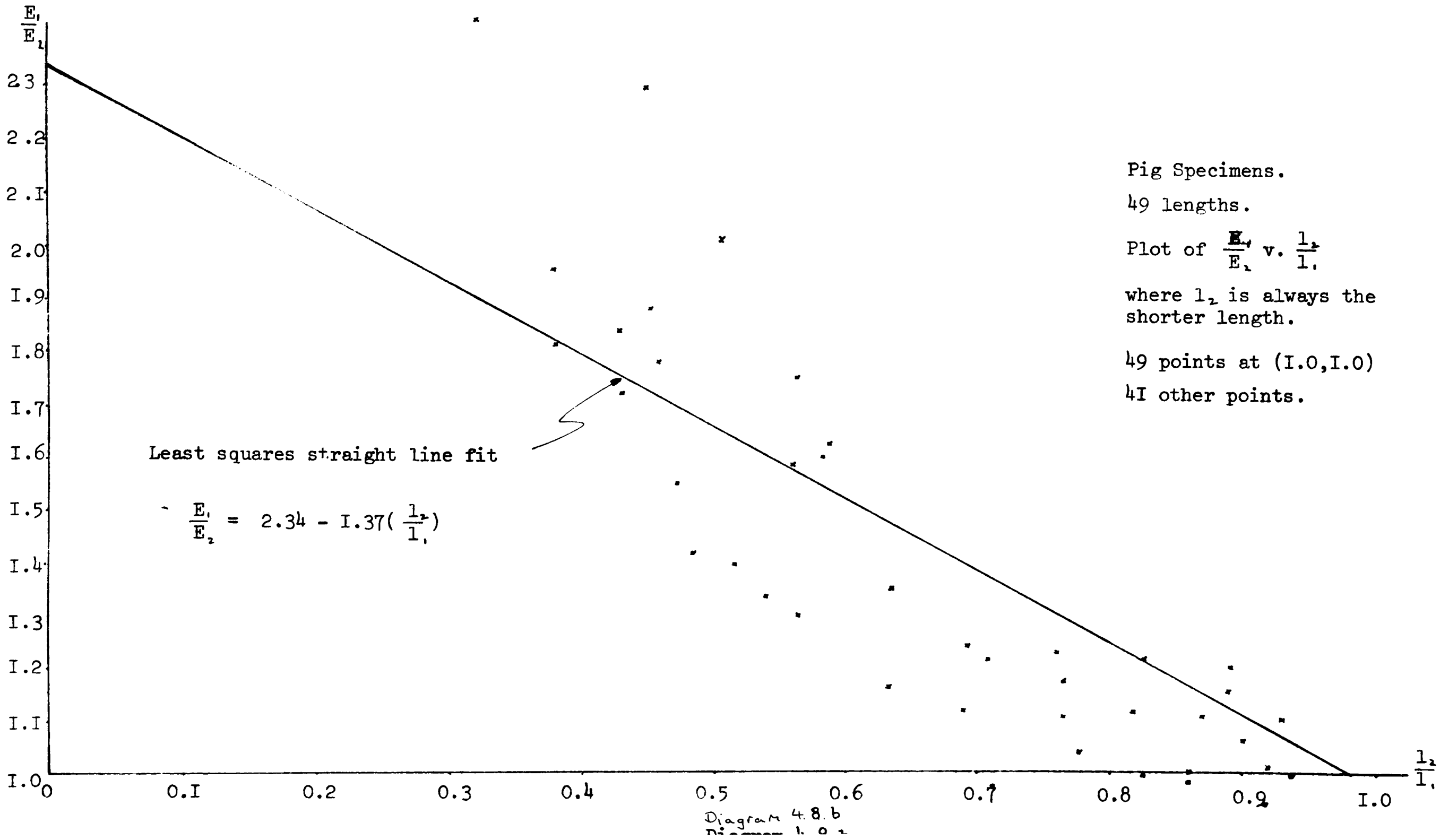

Pig Specimens.

49 lengths.

Plot of $\frac{E_1}{E_2}$ v. $\frac{l_2}{l_1}$

where l_2 is always the shorter length.

49 points at (1.0,1.0)

41 other points.

Diagram 4.8.b

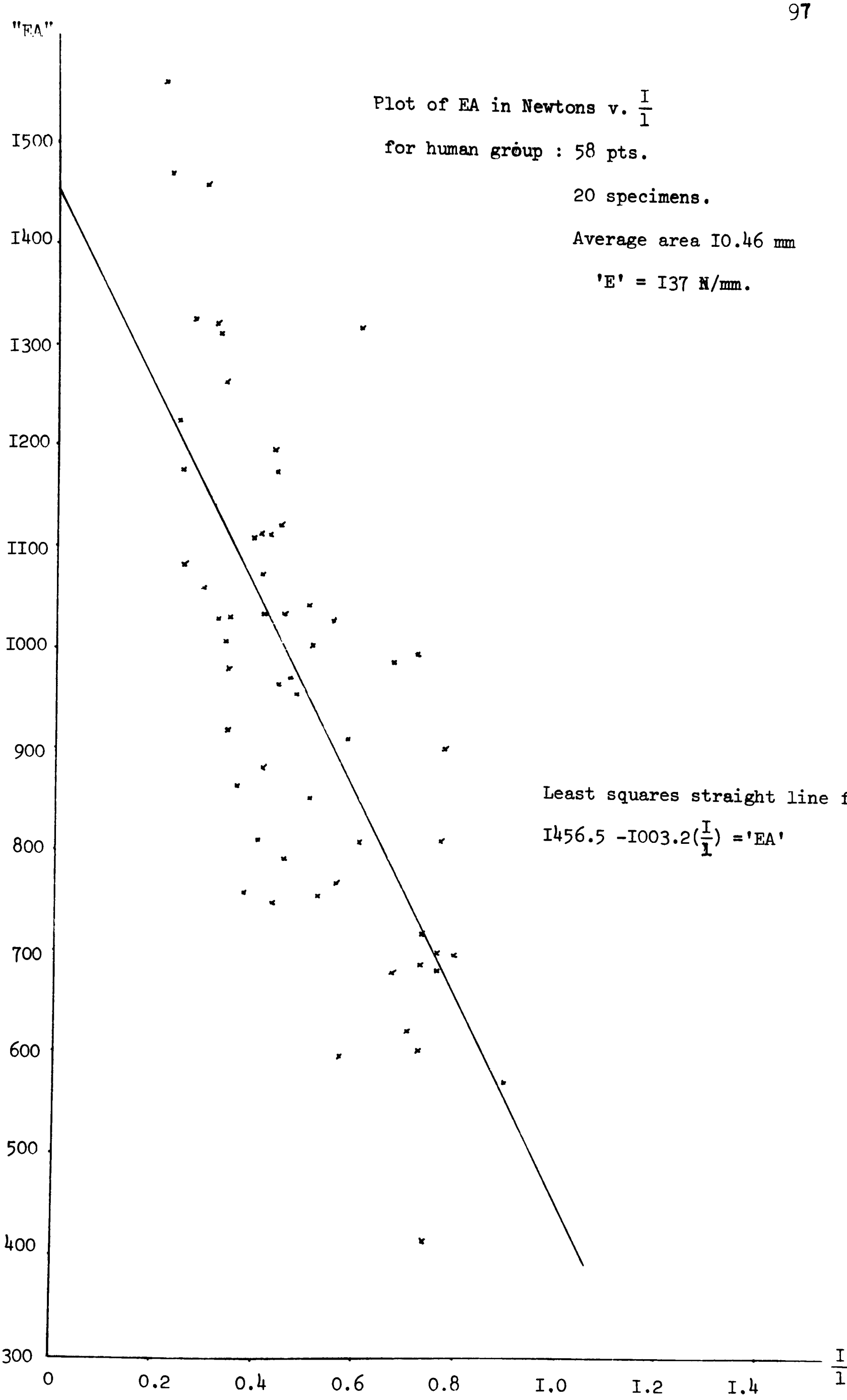

Plot of EA in Newtons v. $\frac{I}{l}$

for human group : 58 pts.

20 specimens.

Average area I0.46 mm

'E' = I37 N/mm.

Least squares straight line fit

I456.5 -I003.2($\frac{I}{l}$) ='EA'

Diagram 4.0 8

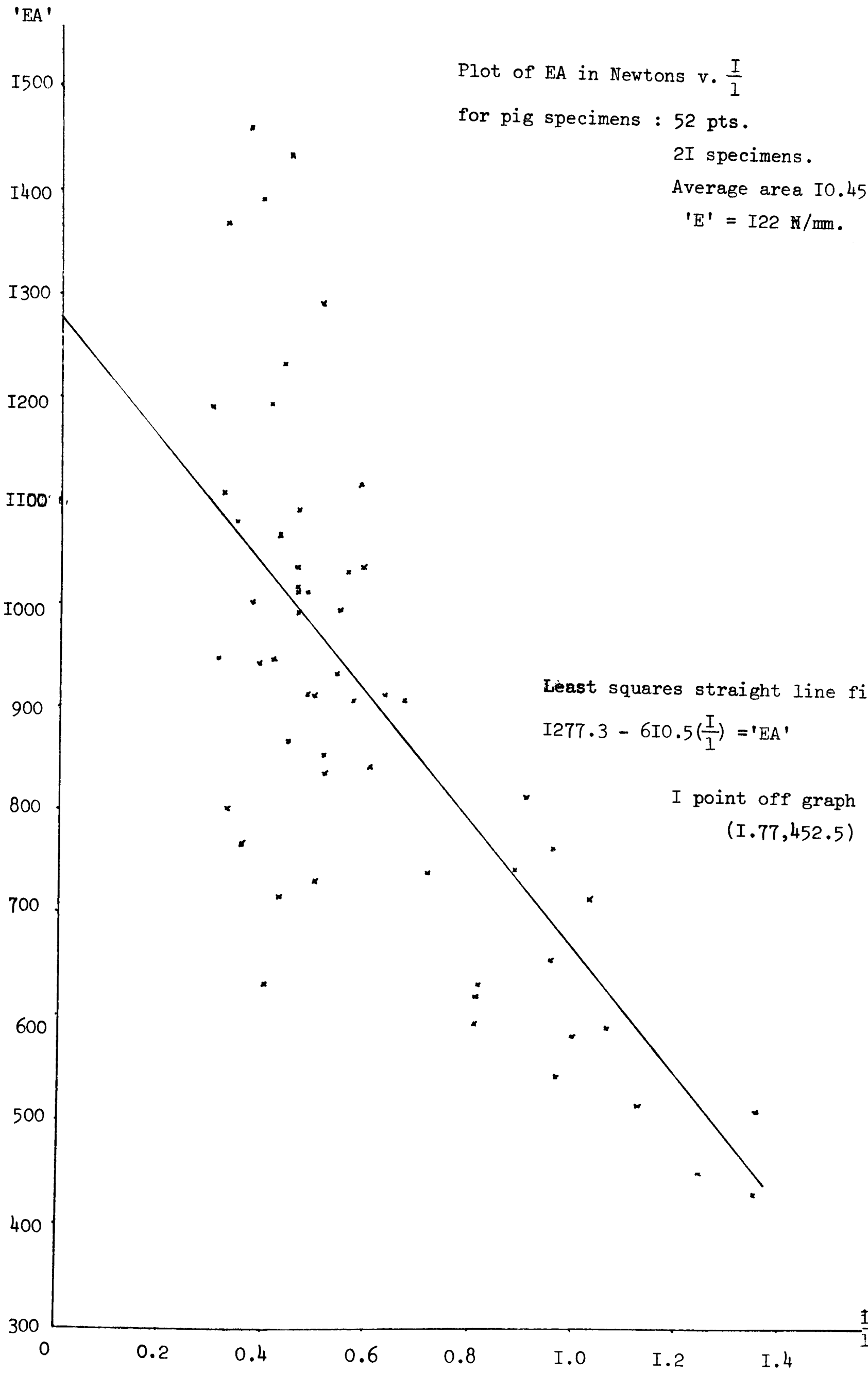

Plot of EA in Newtons v. $\frac{I}{l}$

for pig specimens : 52 pts.

2I specimens.

Average area I0.45 mm.

'E' = I22 N/mm.

Least squares straight line fit

$I277.3 - 6I0.5(\frac{I}{l}) = \text{'EA'}$

I point off graph

(I.77,452.5)

Diagram 4.9.b.

pigs. Hence the actual value of the Young's modulus may be expected to be at least 150 N/mm^2.

Another way of presenting the data is to plot $EA\,(=\frac{Pl}{\delta})$ v. $\frac{1}{l}$ These plots are shown in diagrams 4.9. Again a curve of the type $y=\frac{1}{x}$ is suggested as the best fit, but as before an intercept was required. Using the average areas of the specimens gave values of E of 140 and 120 N/mm^2.

From the type of curve expected (3.4.2.2.), the data suggest that the value of E obtained is low, since the lengths used put the data in the large $\frac{1}{l}$ range. The value of E may be expected to be low also because the stiffness is greatest along the line of the fibres and the method used for cutting would not follow the fibre direction exactly. Kempson's results show that the stiffness decreases rapidly as the angle of cut increases away from the fibre direction. The pig menisci are smaller and thus it is more difficult to cut around a circumference; the value obtained for the pigs is not unexpectedly lower than that for the humans.

4.4.3. Load Estimates.

Knowing the radial expansion, the circumferential modulus of elasticity and the physical dimensions of the menisci, it should be possible to estimate the load carried by the menisci. The values of c, the width, r_m, the inner radius, h_o the outer height and α, the arc angle were estimated for each specimen: c and h_o vary around the arc and were taken to be the 'average' values: r_m and α depend on where the centre of the arc was deemed to be and were thus prone to about 10% error, the values of c and h_o probably being more accurate.

There are a number of ways in which the load may be estimated:

Method 1:

Assume the meniscus to be part of a triangular wedge-shaped annulus of dimensions mentioned above and wedge angle β (see Diagram 4.10).

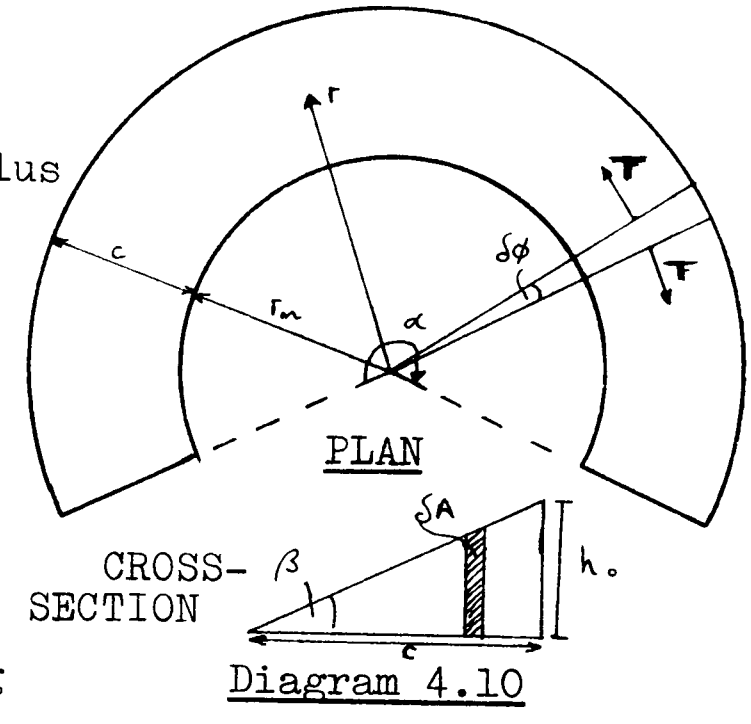

Diagram 4.10

When loaded, let the meniscus be strained uniformly at a given radius, r, the inner raduis increasing from r_m to $r_m + a$, and the width remaining constant. As for the analysis in Chapter 2, assume that only two stress components exist, σ_{zz} and $\sigma_{\theta\theta}$; no shear is allowed and σ_{rr} only has a value on the upper surface of the wedge and then immediately falls to zero.

If the stress $\sigma_{zz}(r)$ is assumed to be zero on the outer edge and to linearly increase to σ_i at the inner edge, then the circumferential tension, T, may be determined from compatability and equilibrium considerations.

(a) Compatibility:

$$\varepsilon_{\theta\theta}(r) = \frac{a}{r-a} = \frac{1}{E_\theta}\sigma_{\theta\theta} + \frac{\nu\,\sigma_{zz}(r)}{E_z}$$

Hence $$T_{compatibility} = \int_{r_m+a}^{r_m+a+c} \sigma_{\theta\theta}(r)\,\delta A = \int_{r_m+a}^{r_m+a+c} \left(\frac{E_\theta\, a}{r-a} - \nu \frac{E_\theta}{E_z}\sigma_{zz}(r) \right) \delta A$$

(b) Equilibrium:

$$T_{equilibrium} = \int_{r_m+a}^{r_m+a+c} \sigma_{zz}(r)\,\tan\beta\; r\,\delta r$$

Equating these determines the value of σ_i and hence

the total vertical force, P, may be found

$$P = \int_0^{\alpha} \int_{r_m+a}^{r_m+a+c} \sigma_{zz}(r)\, r\, \delta r\, \delta\phi$$

$$= \alpha a E_\theta \left(c - r_m \log \frac{r_m+a}{r_m}\right)\left(\frac{c + 3(r_m+a)}{3(r_m+a) + c\left(1 + \frac{E_\theta}{E_z}\nu\right)}\right) \qquad \ldots.4.1$$

If the stress distribution $\sigma_{zz}(r)$ is assumed to be uniform instead of linearly increasing as above,

$$P = \alpha a E_\theta \left(c - r_m \log \frac{r_m+a}{r_m}\right)\left(\frac{c + 2(r_m+a)}{2(r_m+a) + c\left(1 + \frac{E_\theta}{E_z}\nu\right)}\right) \qquad \ldots.4.2$$

The value of P calculated by 4.2 is greater than 0.9 times the value calculated by 4.1 for the cases considered, so the stress distribution is not significantly important in determining the order of magnitude of the load.

Estimates using this method are given in Table 4.2 as are the estimates for the next three methods. Poisson's ratio is assumed to be 0.4[79].

Method 2:

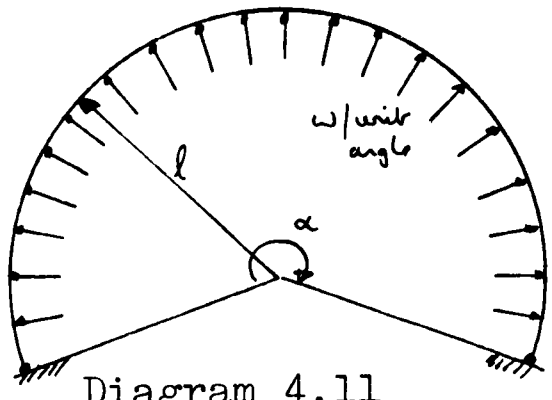

Diagram 4.11

Consider the meniscus to be a circular two pin arch of radius, ℓ, and angle α subject to a uniform internal load, ω per unit angle (see Diagram 4.11). The problem is symmetric and may be separated as in Diagram 4.12a.

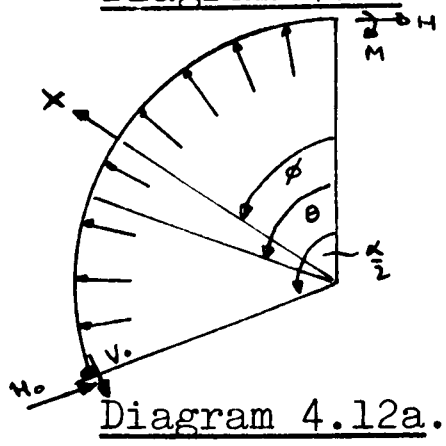

Diagram 4.12a.

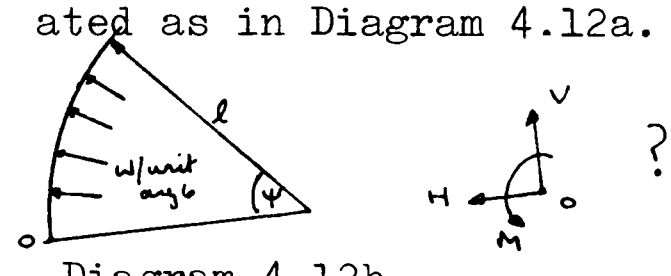

Diagram 4.12b.

The reason for introducing the force, X, will be seen later. In order to solve the problem it is necessary to know the equivalence shown in 4.12b. and the equivalence can be shown to be

$$M = \omega l \ (1 - \cos\varphi)$$

$$H = \omega \sin\varphi$$

$$V = \omega (1 - \cos\varphi)$$

The main structure (4.12a.) is one degree redundant. It may be solved using Castigliano's Theorem of minimum strain energy in conjunction with resolutions in two perpendicular directions and a moment equation. These latter are:-

resolving horizontally: $H - X\sin\phi - \omega\left(1 - \cos\frac{\alpha}{2}\right) + H_o \sin\frac{\alpha}{2} - V_o \cos\frac{\alpha}{2} = 0$

resolving vertically: $V_o \sin\frac{\alpha}{2} - X\cos\phi - \omega \sin\frac{\alpha}{2} + H_o \cos\frac{\alpha}{2} = 0$

moments about pin: $M - \omega l \left(1 - \cos\frac{\alpha}{2}\right) + Hl\left(1 - \cos\frac{\alpha}{2}\right) - Xl\sin\left(\frac{\alpha}{2} - \phi\right) = 0$

U, the total strain energy is

$$U = \int_0^{\frac{\alpha}{2}} \frac{M_\theta^2}{2EI} l \, d\theta + \int_0^{\frac{\alpha}{2}} \frac{S_\theta^2}{2AE} l \, d\theta$$

where M_θ is the moment at angle θ and S_θ is the axial force at angle θ. Both terms are included because large circumferential forces will develop, similar to a thin tube under internal pressure, and the magnitude of the bending term is unknown, though expected to be small.

Only one of the four conditions available for Castigliano's Theorem need be used. The conditions are:-

$$\frac{\partial U}{\partial H} = \frac{\partial U}{\partial M} = \frac{\partial U}{\partial H_o} = \frac{\partial U}{\partial V_o} = 0$$

The solution obtained was checked by using another of the conditions and found to give

$$H = a_1 \omega + a_2 X$$

where ,

$$a_1 = \frac{\frac{\ell^3}{EI}\left(\frac{\alpha}{2}\cos^2\frac{\alpha}{2} - \frac{3}{4}\sin\alpha - \frac{\alpha}{4}\right) + \frac{\ell}{AE}\left(\frac{\alpha}{4} + \frac{1}{4}\sin\alpha - \sin\frac{\alpha}{2}\right)}{\frac{\ell^3}{EI}\left(\frac{\alpha}{2}\cos^2\frac{\alpha}{2} - \frac{3}{4}\sin\alpha - \frac{\alpha}{4}\right) + \frac{\ell}{AE}\left(\frac{\alpha}{4} + \frac{1}{4}\sin\alpha\right)}$$

and

$$a_2 = \frac{\left[\frac{\ell^3}{EI}\left(\cos\frac{\alpha}{2} - \frac{1}{4}\cos\phi + \frac{\alpha}{4}\left(\sin\phi - \sin(\alpha-\phi)\right) - \frac{3}{4}\cos(\alpha-\phi) + \left(\frac{\alpha}{4} - \frac{\phi}{2}\right)\sin\phi\right) + \frac{\ell}{AE}\left(\frac{1}{4}\cos(\alpha-\phi) + \left(\frac{\alpha}{4} - \frac{\phi}{2}\right)\sin\phi - \frac{1}{4}\cos\phi\right)\right]}{\frac{\ell^3}{EI}\left(\frac{\alpha}{2}\cos^2\frac{\alpha}{2} - \frac{3}{4}\sin\alpha - \frac{\alpha}{4}\right) + \frac{\ell}{AE}\left(\frac{\alpha}{4} + \frac{1}{4}\sin\alpha\right)}$$

All the other reactions may be determined by use of the three equilibrium equations mentioned above, and the result for M_θ and S_θ is:-

$$M_\theta = \omega\ell\left(1 - a_1\right)\left(\cos\theta - \cos\tfrac{\alpha}{2}\right) + X\ell\left(\sin\left(\tfrac{\alpha}{2} - \phi\right) - a_2\left(\cos\theta - \cos\tfrac{\alpha}{2}\right) - \left[\sin(\theta-\phi)\right]\right)$$

and

$$S_\theta = \omega - \omega\left(1 - a_1\right)\cos\theta + X\left(a_2\cos\theta + \left[\sin(\theta-\phi)\right]\right)$$

where the $[\ ]$ brackets indicate that the term should only be included if $\theta > \phi$.

The deflection curve for the arch may now be determined by using Castigliano's deflection Theorem, which in this problem becomes $\left(\frac{\partial U}{\partial X}\right)_{X=0} = \delta_x = \delta_\phi$ $\left\{\begin{array}{l}\text{radial deflection at } \phi \\ \text{as } \phi \text{ is varied}\end{array}\right\}$

where δ_x is the deflection in the direction of the force X and the condition X = 0 is applied since the deflection is required for the case of the internal load, ω, alone. The deflection theorem gives:-

$$\delta_\phi = \frac{\omega\ell^3}{EI}\left(1 - a_1\right)\left(-\frac{3}{4}\cos(\alpha-\phi) - a_2\left(\frac{\alpha}{2}\cos^2\frac{\alpha}{2} + \frac{\alpha}{4} - \frac{3}{4}\sin\alpha\right) + \left(\frac{\alpha}{4} - \frac{\phi}{2}\right)\sin\phi - \frac{1}{4}\cos\phi + \cos\frac{\alpha}{2} - \frac{\alpha}{4}\sin(\alpha-\phi) + \frac{\alpha}{4}\sin\phi\right)$$

$$+ \frac{\omega\ell}{EA}\left(\left(1 - a_1\right)\left(\frac{1}{4}\cos(\alpha-\phi) + \left(\frac{\alpha}{4} - \frac{\phi}{2}\right)\sin\phi - \frac{1}{4}\cos\phi - a_2\left(\frac{\alpha}{4} + \frac{1}{4}\sin\alpha\right)\right) + 1 + a_2\sin\frac{\alpha}{2} - \cos\left(\frac{\alpha}{2} - \phi\right)\right)$$

$$\delta_\phi = \frac{\omega l^3}{EI}(F_m) + \frac{\omega l}{EA}(F_A)$$ where F_m and F_A are the moment and axial load factors as defined in the previous statement.

In order to relate the arch to the meniscus, the latter was assumed to be a triangular wedge as in Diagram 4.13, and

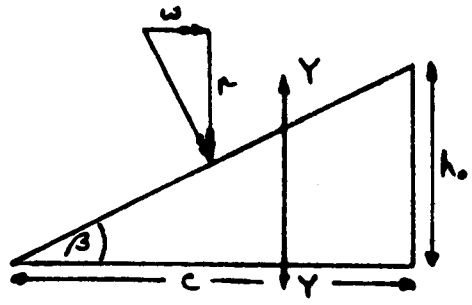

Diagram 4.13

$$l = r_m + \tfrac{2}{3}c$$

for the triangle

$$I_{YY} = \frac{c^3 h_0}{36}$$

$$A = \frac{c\,h_0}{2}$$

hence $\omega = \dfrac{\delta_\phi E}{\frac{l^3}{I}F_m + \frac{l}{A}F_A}$ and $p = \dfrac{\omega}{\tan\beta}$

hence the total vertical load $P = \alpha p = \dfrac{\alpha\,\delta_\phi E}{\left(\frac{36\,l^3 F_m}{c^4} + \frac{2\,l F_A}{c^2}\right)}$

Method 3:

Instead of assuming that the meniscus may be treated as a thin arch as in Method 2, let it now be considered as a thick arch. Separated along the line of symmetry it may be considered as in 4.14.

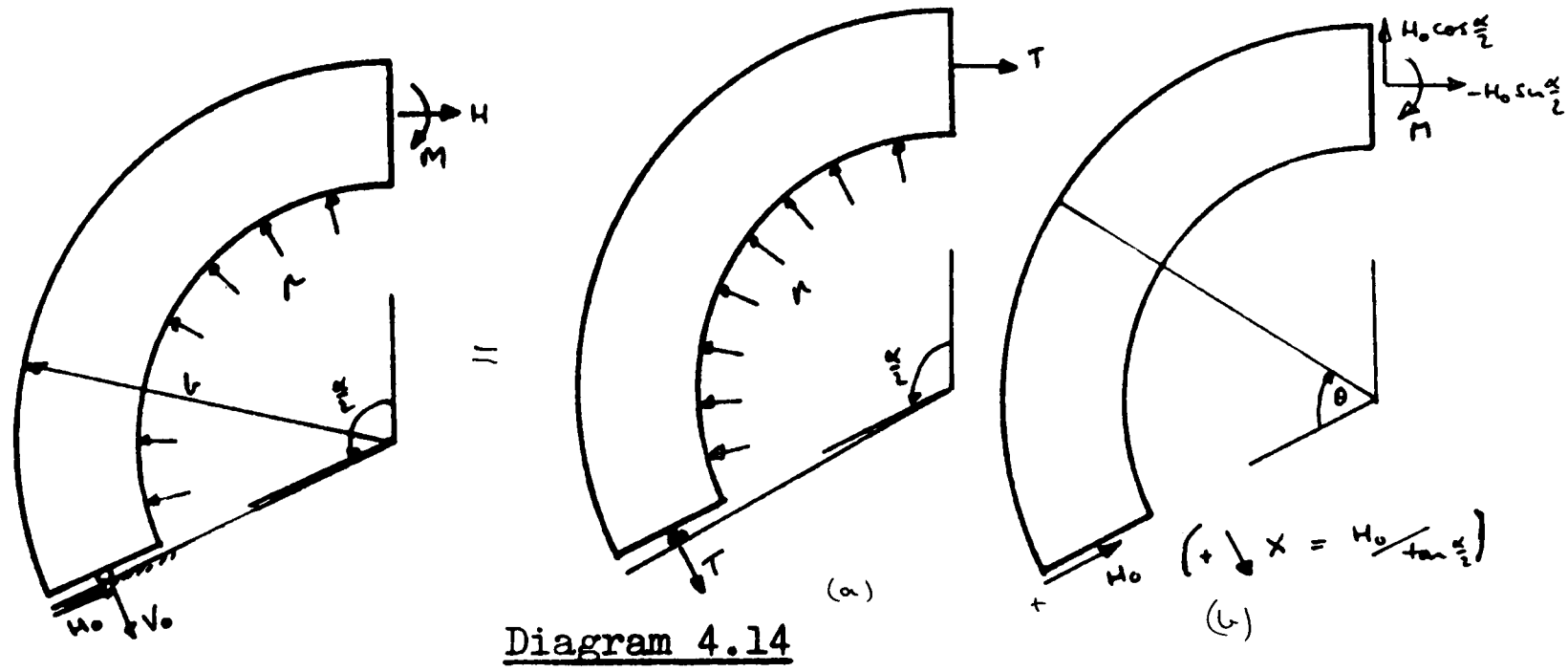

Diagram 4.14

Let the arch have a rectangular section of depth h_0 and be subjected to a uniform internal pressure, p.

(a) in Diagram 4.14 is simply a thick cylinder under uniform

internal pressure and (b) is a thick curved bar with an end shear force H_o. So that there will be no resultant shear force on the crown face, there should be an axial force X as shown on the diagram. However if θ_2 is near $\pi/2$ then X will be small compared to H_o and as $\frac{H_o}{h_o}$ is approximately 0.1 p, (shown later) it is neglected.

The two problems (a) and (b) ((b) without force X) have standard solutions[69]. If b is defined as r_m + "width of meniscus" (discussed later) then the stresses are:-

for (a)
$$\sigma_{rr} = \frac{r_m^2 p}{b^2 - r_m^2}\left(1 - \frac{b^2}{r^2}\right)$$

$$\sigma_{\theta\theta} = \frac{r_m^2 p}{b^2 - r_m^2}\left(1 + \frac{b^2}{r^2}\right)$$

for (b)
$$\sigma_{rr} = \left(2Ar - \frac{2B}{r^3} + \frac{D}{r}\right)\sin\theta$$

$$\sigma_{\theta\theta} = \left(6Ar + \frac{2B}{r^3} + \frac{D}{r}\right)\sin\theta$$

$$\tau_{r\theta} = -\left(2Ar - \frac{2B}{r^3} + \frac{D}{r}\right)\cos\theta$$

where $A = \frac{H_o}{2Nh_o}$, $B = -\frac{H_o r_m^2 b^2}{2Nh_o}$, $D = -\frac{H_o}{Nh_o}(r_m^2 + b^2)$

with $N = r_m^2 - b^2 + (r_m^2 + b^2)\log\frac{b}{r_m}$

These solutions are exact for all the arch if the stresses are distributed over the end $\theta = 0$ in the manner described. If this is not the case then Saint-Venant's principle allows the solution to be valid at large distances from this end, but not at it.

If the assumptions are made that the solution is correct for all θ and that the material is homogeneous and isotropic

with a Young's modulus E and Poisson's ratio ν, then the above stresses may be converted to strains and thence to displacements. Although the stress distributions are exact, the displacements thus calculated are not because the boundary conditions can not be satisfied at all radii.

Prior to the use of boundary conditions, it may be shown for (a)

$$u = \frac{A r_m^2}{E(b^2 - r_m^2)} \left[(1-\nu) r + \frac{b^2}{r} (1+\nu) \right] ; \quad v = 0$$

where u is the radial displacement and v the tangential; and for (b)

$$u = \frac{-2D}{E} \theta \cos\theta + \frac{\sin\theta}{E} \left[D(1-\nu) \log r + A(1-3\nu) r^2 + \frac{B(1+\nu)}{r^2} \right] + C_2 \sin\theta + C_3 \cos\theta$$

$$v = \frac{2D\theta \sin\theta}{E} - \frac{\cos\theta}{E} \left[A(5+\nu) r^2 + \frac{B(1+\nu)}{r^2} - D(1-\nu) \log r \right] + \frac{D(1+\nu)}{E} \cos\theta + C_1 r + C_2 \cos\theta - C_3 \sin\theta$$

where A, B & D are defined above and C_1, C_2 and C_3 are arbitrary constants of integration to be determined by the boundary conditions, which are:-

$$u = 0 , \quad v = 0 \quad \text{at} \quad \theta = 0$$

$$\frac{\partial u}{\partial \theta} = 0 , \quad v = 0 \quad \text{at} \quad \theta = \frac{\alpha}{2}$$

u and v have been calculated for (a) and hence the constants of (b) must be used to adjust u and v to satisfy the above. The conditions can not be satisfied at all radii since u and v are both functions of r ; hence the conditions are satisfied at a particular radius r_s ,

thus at $\theta = 0 , \quad r = r_s$

$$u = C_3 = \frac{-A r_m^2}{E(b^2 - r_m^2)} \left[(1-\nu) r_s + \frac{b^2}{r_s} (1+\nu) \right]$$

$$v = 0 = -\frac{C_0}{E} + \frac{D(1+\nu)}{E} + C_2 + C_1 r_s$$

where $C_0 = A(5+\nu) r_s^2 + B(1+\nu) r_s^2 - D(1-\nu) \log r_s$

at $\theta = \frac{\alpha}{2}$, $r = r_s$

$$v = 0 = -\frac{C_0 \cos\frac{\alpha}{2}}{E} + \frac{D\alpha \sin\frac{\alpha}{2}}{E} + \frac{D(1+\nu)}{E}\cos\frac{\alpha}{2} + C_2\cos\tfrac{\alpha}{2} - C_3 \sin\tfrac{\alpha}{2} + C_1 r_s$$

$$= \frac{D\alpha \sin\frac{\alpha}{2}}{E} - C_3 \sin\tfrac{\alpha}{2} + C_1 r_s\left(1-\cos\tfrac{\alpha}{2}\right)$$

$$\therefore \quad C_1 = \frac{\sin\frac{\alpha}{2}}{r_s(1-\cos\frac{\alpha}{2})}\left[C_3 - \frac{D\alpha}{E}\right]$$

and $$C_2 = \frac{C_0}{E} - \frac{D(1+\nu)}{E} - \frac{\sin\frac{\alpha}{2}}{(1-\cos\frac{\alpha}{2})}\left[C_3 - \frac{D\alpha}{E}\right]$$

The final condition, $\frac{\partial u}{\partial \theta} = 0$ at $\theta = \frac{\alpha}{2}$, $r = r_s$ is used to determine H_0 in terms of p and gives,

$$\frac{H_0}{h_0} = \frac{N p\, r_m^2 \left[(1-\nu) r_s + \frac{b^2}{r_s}(1+\nu)\right]\sin\frac{\alpha}{2}}{(1-\cos\frac{\alpha}{2})(b^2-r_m^2)\left[\alpha(r_m^2+b^2)\sin\frac{\alpha}{2} - \cos\frac{\alpha}{2}\left(r_s^2(3-\nu) - \frac{r_m^2 b^2}{r_s^2}(1+\nu) + (r_m^2+b^2)\left(3+\nu - \frac{\alpha \sin\frac{\alpha}{2}}{1-\cos\frac{\alpha}{2}}\right)\right)\right]}$$

hence:

$$u_\theta = \frac{p r_m^2}{E(b^2-r_m^2)}\left[(1-\nu)r + \frac{b^2}{r}(1+\nu)\right] - \frac{p r_m^2}{E(b^2-r_m^2)}\left[(1-\nu) r_s + \frac{b^2}{r_s}(1+\nu)\right]\left(\cos\theta - \frac{\sin\frac{\alpha}{2}\sin\theta}{1-\cos\frac{\alpha}{2}}\right)$$

$$+ \frac{H_0 \sin\theta}{h_0 N E}\left[\frac{r^2}{2}(1-3\nu) - \frac{r_m^2 b^2}{2r^2}(1+\nu) - (r_m^2+b^2)\left(\frac{\alpha \sin\frac{\alpha}{2}}{1-\cos\frac{\alpha}{2}} - (1+\nu) + (1-\nu)\log r\right)\right]$$

$$+ \frac{C_0 \sin\theta}{E} + \frac{2 H_0}{h_0 N E}(r_m^2+b^2)\theta\cos\theta$$

where all constants may be determined from E, ν, r_m, b and the pressure p.

In order to relate this solution to the meniscus, the meniscus was again assumed to be a triangular wedge as in Diagram 4.13. The value of $\frac{H_0}{h_0}$ is approximately 0.1 for a variety of ν, r_m and b, so that the assumption was made that the pressure is resisted by the circumferential tension, and the criterion that the cross-sectional areas of the two sections must be the same was used. Hence $b - r_m = c/2$, and $u_\theta = F_\theta \frac{p}{E}$ where F_θ may

be calculated from the relationship above.

p acts on the area $\alpha h_o r_m$ of the rectangular section and hence for the meniscus, the total vertical load P is determined from $P = \frac{\alpha h_o r_m p}{\tan\beta} = \frac{\alpha E_c r_m u_{(r,h)}}{F_\theta}$

Method 4:

Table 4.2 shows the percentages obtained from methods 1,2 & 3 for 200 Kgf load. The three systems considered are elastic so the expansion values taken from the graphs are the expansions from 0 to 200 Kgf along a line tangential to the curves at high loads. E is taken to be 150 N/mm^2 and the dimensions for each specimen are as measured.

For Method 1, the average of the anterior/posterior and central deflections is used and for Methods 2 and 3 the expansions at the crown are related to the deflections there. In Method 3, if the specific radius of the boundary conditions is taken to be $(a-b)/2$ then contraction occurs near the pin giving negative deflections there. It is not known if negative deflections occur in practice, but such deflections may be eliminated by taking $r_s = b$. The difference in the percentages calculated for these conditions is not great, the latter being slightly less than the former. The values quoted in Table 4.2 are for $r_s = b$. The computer programs for numerical solution of methods 1, 2 and 3 are at the end of Appendix 4.

Consideration of Table 4.2 shows that none of the three methods described above simulates the real system. Further estimates may be made from the solution for the wedge shaped

Spec. No.	Slope Method	Deflection Method	R.E.M. 1(a) & (b)	R.E.M. 2	R.E.M. 3	R.E.M. 4
Human 7	0	93	291 (147)	79	115	42.8
8	2	45	449 (245)	101	141	71
9	-13.5	55.5	422 (216)	98.5	132	60
10	11	45	581 (312)	137.5	134	66
11	0	33	335 (172)	113	206	72.5
12	N/A	N/A	576 (277)	110	134	75
13	5	36.5	490 (262)	80	108	53
14	-1	33.5	505 (270)	103	139	41
15	-6	28	390 (213)	70.5	95	39
16	9	43	570 (295)	94	70	47
17	0	30	244 (130)	62	114	33
Pig 27	5	48	567 (212)	238	534	96
28	21	85	1115 (505)	457	957	194
29	10	69	950 (405)	420	1010	177
30	5	87	579 (268)	204	321	127
31	3	57	470 (191)	241	615	104
32	22	87	416 (170)	288	790	127
33	19.5	55	493 (208)	227	483	85.5
34	5	58	399 (167)	169.5	325	92
35	9	66	561 (218)	259	633	89
36	23	77.5	511 (238)	215	400	134
37	18.5	76	745 (312)	330	731	150
38	20.5	83	544 (229)	244	496	127
39	13	63	404 (170)	164	310	84.5
40	26	65	560 (234)	229	475	110
41	22	75	580 (231)	275	644	115
42	36.5	76	394 (154)	191	461	80
43	8	56	511 (213)	290	726	148.5
44	15	76	665 (281)	228	468	91.5
45	16	58	511 (206)	209	410	99.5

Table 4.2

Compression of Estimates of % load carried by menisci using various methods for which comparison may be made. Radial Expansion Method 1(b) is for $\frac{E\theta}{E_z} = 10.0$ (isotropic case $\frac{E\theta}{E_z} = 1.0$ is R.E.M. 1(a)). Estimates calculated from the radial expansion measurements assume linear elasticity whereas the menisci have non-linear viscoelastic properties (see page A65). There are also idealizations regarding geometry and modes of fixation. It is clear that the most reasonable estimate is obtained from the deflection method.

ring by finite element method analysis as described in Appendix 2(b). Two different geometries are considered. The one used for the human specimens is as in Diagram 2.b.; that is 7mm height, 12mm width and an inner radius of 10mm in the undeformed state. For the pig specimens the width and height remain the same, but the inner radius is reduced to 4mm. The isotropic elastic modulus is changed to 150 N/mm^2. The assumed geometry is considered reasonable. The average values of the specimens considered are for humans: C, 10.9 mm., r_m, 9.5 mm., h_o, 7.2 mm.; and pigs: C, 13.0 mm., r_m, 4.0 mm., h_o, 8.0 mm.

The expansion measurements were taken near the centre of the exposed surface. If the expansion of node 32 is taken as the measured expansion, then for the human case, a pressure of 1 N/mm^2 on a surface area of 384π mm^2 causes a radial expansion of 0.69 mm.. For the pigs, the area is $240\pi mm^2$ the pressure the same and the expansion 0.34 mm. Taking the average of the four expansions for each joint, and assuming the menisci combine to form one ring as for the analysis, a simple calculation gives the load carried by the menisci in each joint. The estimates using this method are also presented in Table 4.2.

There are obvious deficiencies in all of the methods 1 to 4 in terms of the geometry simulation, the modes of fixation, the assumptions concerning loading and the assumptions regarding the stress-strain behaviour of the menisci. All estimates are consistently high and are calculated from equations of the type,

$$P = F\ E\ d$$

where P is the load carried by the menisci, F is a factor calculated for each method, E is the Young's Modulus in the cir-

cumferential direction and d is the measured deflection as described in 4.

A major cause of the overestimations is probably the assumption for the menisci of isotropic, homogeneous elastic behaviour. The menisci are anisotropic, the modulus of elasticity in the circumferential direction being much greater than the modulus of elasticity in the orthogonal directions. Hence the assumption of isotropy with the modulus of elasticity being that in the circumferential direction means that the menisci are stiffer in the orthogonal directions than in reality. Therefore radial expansions calculated under the isotropic conditions assumed will be smaller than would occur in reality. The factor, F, is therefore an overestimate, directly affecting the value of P.

The effect may be seen from consideration of the results of Method 1. If $\frac{E_\theta}{E_z}$ is set to 10 (rather than 1 for the isotropic case) then the values in brackets in Table 4.2 are obtained. Unfortunately, it has not been possible to obtain an anisotropic solution using the finite element method, although the results from the finite element calculation seem to be the most realistic.

4.5 Conclusions

The results of the experiments performed indicate that the menisci bear a significant proportion of the load in the tibio-femoral joint. The evidence is that:-

(1) in compressive load/deflection tests on complete joints there was an increase in deflection for a given load after a meniscus had been excised in all 62 tests

performed:

(2) The menisci were loose under light load but became stiff and immovable when loads greater than 10-30 Kgf were applied to the joint:

(3) Dye did not penetrate the menisci-articular cartilage contact areas:

(4) Use of a pressure transducer indicated a significant change in the pressure distribution in the joint occurred after meniscectomy.

Quantitative estimates of the meniscal load were made from the load/deflection tests and the radial expansion tests. The two values obtained from the load/deflection tests are underestimates because of the change in initial contact area and rate of increase in contact area with load after meniscectomy. The deflection method gave the more reasonable estimate and indicated that the menisci carry between at least 15 and 90% (majority near 45%) of the total load through old human joints subjected to 100 Kgf. For pig specimens the range was 50 to 100% (majority near 75%).

The four estimates obtained from the radial expansion measurements were subject to errors in assumed geometry, modes of fixation and material properties of the menisci. The Finite Element Method gave the most reasonable estimate with the majority of values within an acceptable range. Generally values of P menisci were unrealistically high. The estimates from the six methods used are shown in Table 4.2 and indicate that of the six, the deflection method using the load/deflection curves is the most

reasonable.

At the British Orthopaedic Research Society meeting on October 31st, 1973, (Abstracts in J.B.J.S. 56-B p.381), the paper following that read by myself was based on the same topic. The conclusion drawn by B. B. Seedhom from two experiments similar to the load/deflection tests described in this thesis, was that the menisci carry between 60 and 70% of the load transmitted through the knee. The estimate was based on the 'deflection' method and the confirmation of the findings submitted in this thesis was very gratifying.

A second point indicated by the load/deflection tests was that there is a gap between the femoral and tibial condyles at low loads. The existence of the gap was indicated by the final load/deflection test on each joint. Also in the dye tests, whereas dye would not penetrate the menisci-articular cartilage contact areas, it was possible to inject dye on to the articular cartilage of the tibial condyles enclosed by the menisci. If the menisci were removed, both femoral and tibial condyles could be completely stained with dye. The significance of the conclusions drawn from the experimental results with regard to published work and physiological observations concerning the tibio-femoral joint will be discussed in the next chapter. In the next section a few ideas for further work are discussed.

4.6 Further work

There are two basic questions which are not fully answered by the work described in this thesis:-

(1) Do synovial joints transmit loads by the development of uniform pressure distributions?

(2) What proportion of the load in the tibio-femoral joint is carried by the meniscus?

As will be shown in the next chapter it is possible for a uniform pressure distribution to develop in the knee with the menisci as load-bearers. To determine if such a pressure distribution does occur it would seem best to use a pressure transducer. A method for maintaining the transducer in a fixed known position in the joint whilst load was being applied would have to be determined. Measurement of the pressure distribution over the contact area for a given load would then be possible. Conversion of the transducer readings to actual pressures would involve knowledge of the total cartilage thickness at each joint where the transducer was placed, because different errors in the measured pressure would occur with different cartilage thickness. Hence it would be possible to determine the actual pressure distribution in the joint.

Furthermore if the actual pressure was known, it would be relatively simple to determine the meniscal load.

Estimations of the meniscal load from load/deflection curves will always involve the change in the mode of contact between the femur and tibia after meniscectomy and hence the different areas of direct tibio-femoral articular cartilage contact. It would seem reasonable that the

most accurate estimate of the meniscal load should be obtained from a study of the menisci 'in situ', either by use of a pressure transducer or use of radial expansion readings.

To use the radial expansion readings it would be essential to eliminate any rigid body motion from the measured expansions. Complete knowledge of the relevant mechanical properties of the meniscus, and a solution by the finite element method of a three dimensional model of the meniscus would give the radial expansion for known pressure distributions. Problems would remain concerning ignorance of the centre of the arc of the meniscus and the necessity to assume a pressure distribution. The use of a pressure transducer would therefore seem most appropriate. The estimate of the load carried by the menisci using a pressure transducer would probably be more accurate than the estimates obtained by the methods discussed in this thesis, and would also increase knowledge concerning the pressure distribution within the joint.

CHAPTER 5

SIGNIFICANCE OF LOAD BEARING ROLE

5.1 Introduction

The conclusion drawn from chapters 2 and 4 is that the menisci bear a significant proportion of the total load transmitted through the tibio-femoral joint. Before summarizing this conclusion its significance with respect to (a) the age dependent degeneration of the cartilage in the knee, (b) the effects of meniscectomy and (c) the occurrence of meniscal tears will be discussed. Furthermore, during the work, observations were made of the effects of cutting various ligaments. A short review is therefore given of the roles of the ligaments and menisci with regard to stability of the knee.

5.1.1. Stability of the knee

In the light of the new knowledge concerning various structures of the knee, the stability of the knee joint may be examined.

During the experiments it was observed that cutting the cruciate ligaments produced a marked effect on the load/deflection curve (see 4.2.5). The effect was always greater than the effect produced by the cutting of the collateral ligaments although various fibres of the latter are

taut throughout flexion and extension[55]. In the position of hyperextension, the cruciate ligaments are subject to considerable tension and appear to play an important role in limiting the position. Due to their weight-bearing role, the menisci also limit the position because the anterior portions of the menisci become trapped between the femur and the tibia and transmit load between them.

In flexion, dislocation of the femur on the tibia often occurred both anteriorly and posteriorly after the cruciate ligaments had been cut. In all positions of flexion, the patellar tendon is taut and hence the patella exerts a force posteriorly on the patellar surface of the femur. Therefore arterior/posterior movement of the femur on the tibia is controlled by the cruciate ligaments and the forces exerted by the patella on the femur. The menisci will only limit extreme anterior/posterior movement because initially they will pivot on their tibial attachments.

Abduction will be limited by the medial collateral ligament and the weight-bearing lateral meniscus and adduction by the lateral collateral ligament and the weight-bearing medial meniscus.

As shown in diagram 1.3 the tibial condyles are inclined at small angles to the horizontal. Side motion of the femur on the tibia will cause the condyle of the femur approaching the tibial eminence to slide up the tibial condyle and the other femoral condyle to slide down its opposing tibial condyle. Thus ab- or ad-duction will occur during the process of side motion and will be resisted as such.

Furthermore, any rotation of the femur on the tibia will cause both femoral condyles to slide up their opposing tibial condyles, and hence the axial distance between the shafts of the femur and tibia will increase. All axial ligaments between the femur and the tibia will automati-

cally resist such movement and hence the cruciate and collateral ligaments will all restrict rotation of the femur on the tibia. Also when load is applied to the joint, the femoral condyles will naturally align themselves (as low as possible) on the tibial condyles ensuring maximum contact occurs with the weight-bearing menisci.

It will be recalled that the divergence of the femoral condyles posteriorly causes the menisci to remain flush with the condyles throughout flexion. Thus it is evident that, as for other joints, the geometry of the tibio-femoral joint is closely linked with its function.

5.2 Degeneration Pattern of Articular Cartilage

The load/deflection test performed after the cruciate ligaments had been cut indicated that there was a gap between the femoral and tibial condyles when no load was transmitted through the joint. The results of some of the dye tests confirmed the existence of a gap between the condyles.

Therefore, to presuppose that direct tibio-femoral contact occurs when no load is being transmitted through the joint is incorrect. Deane[58] observed that under 4 Kgf load, the contact area after meniscectomy lay within the area of articular cartilage enclosed by the meniscus: it is probable that there was no direct tibio-femoral contact under the applied load, but after meniscectomy tibio-femoral contact must occur if load is to be transmitted between the two bones. Under light load the contact area would not be large. Deane's conclusion that the menisci do not transmit load under static conditions, therefore, takes no account of the fact that there is a gap between the tibial and femoral condyles at low loads. Kettelkamp and Jacobs[63] and Walker and Hajeks'[64] results are similar to those of Deane and are sub-

ject to the same error. Deane's work does show that the articular cartilage-meniscal contact is impenetrable by dye under light loads. Although the dye technique does have its limitations, Deane's results confirm that the menisci lie flush with both femoral and tibial condyles under light load during flexion.

It is therefore apparent that the areas of articular cartilage in contact with the menisci are areas of habitual contact. Some load is required to cause contact on the areas of articular cartilage on the tibial plateau enclosed by the menisci. Suppose that the gap, d_g , between the condyles is taken to be the gap designated by the flat zone on the final test of a load/deflection series; and further suppose that the load on the curve for the complete joint at the deflection, d_g is the load required for tibio-femoral condylar contact. This contact load may be determined for the 16 human joints successfully tested and is found to be body weight or more in six cases and over half body weight in nine cases. Morrison[49] shows that the knee transmits a load of more than half body weight for 60% of the walking cycle. Bullough et al[(37)] note that 85% of the population take no more than 750 steps per hour. Assuming that 16 hours are spent actively each day, that one step takes one second and that half body weight is required for full tibio-femoral contact in the healthy joint, then full tibio-femoral contact occurs for only 2 hours each day. Hence, the areas of cartilage enclosed by the menisci on the tibial condyles are areas of non-habitual contact.

The areas of cartilage enclosed by the menisci are the areas which first show signs of degeneration[66]. There is, therefore, a direct relationship between the non-habitual contact areas of the healthy joint and the areas of cartilage

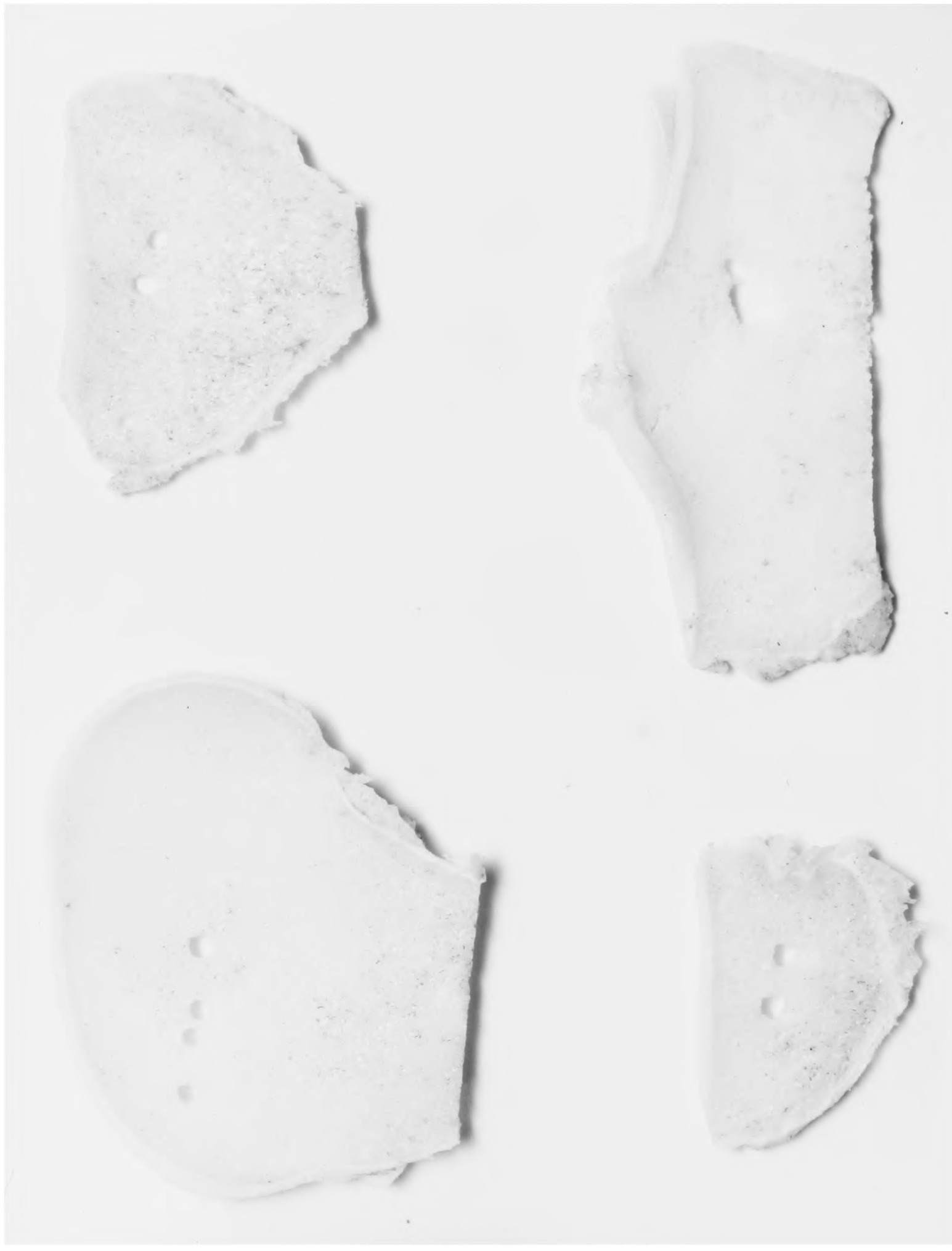

Sections Showing Articular Cartilage Thickness Distribution

Top left: Saggital plane
Medial tibial condyle

Top right: Coronal plane
Tibial condyles with part of lateral meniscus still attached.

Bottom left: Saggital plane
Lateral femoral condyle

Bottom right: Saggital plane
Medial tibial condyle

which first show degenerative changes. The same direct relationship has been observed in the hip[34, 39], the elbow[3], and the patellar-femoral joints[42], and hence the degeneration pattern of the articular cartilage of the tibio-femoral joint is consistent with other joints.

5.3 Stress distributions

As load is applied to the tibio-femoral joint and the bones approach each other, the menisci carry load as they slide out prior to and after becoming taut. The areas of articular cartilage with which the menisci are in contact, therefore, are stressed before direct tibio-femoral contact occurs. Continuation of load application after direct tibio-femoral contact has occurred will cause the addition of a stress distribution similar to that shown in Appendix 2.f.9 (with meniscus) to the distribution which already exists in the joint. Hence the stress distribution will probably be more uniform than that shown in Appendix 2.f.9 (with meniscus). Also, sections through the tibia and femur show that the articular cartilage thickness distribution is such that the thickness is uniform in the centre of the condyles becoming thinner towards the outer edges of the condyles, where the menisci lie. Hence, for a given deformation as in the analysis in Chapter 2, the stresses in the cartilage under the meniscus will be higher than calculated. The cartilage thickness distribution, therefore, will also tend to produce a uniform stress distribution.

Articular cartilage is 65-85% liquid. Hence development of uniform hydrostatic pressure would be an excellent method for transmitting load between the bone components of a joint. Highly non-uniform stress distributions will cause large pressure gradients in the liquid in the cartilage and hence a gross loss of fluid from the high pressure zones. This loss would have a detrimental effect on the cartilage and its capability of transmitting load.

The removal of a meniscus from a compartment of the knee will cause the contact area to alter and the stress distribution across this new contact area will be of the type shown in Appendix 2.f.8 (no meniscus). This type of distribution will not be conducive to efficient load transmission. Also the new contact area, previously an area of non-habitual contact, will be required to carry load regularly and at higher stress levels than before.

The increase in stresses and the greater frequency of the occurrence of these stresses is likely to reduce the fatigue life of the material and increase the wear-rate. The regularity with which articular cartilage degenerates after meniscectomy[67] is not surprising. Also, if the underlying bone structure adapts itself to the stresses it is required to carry[1], the post-meniscectomy changes observed by Fairbank[61] could be due to an attempt to increase the overall contact area and hence reduce the applied stresses.

As mentioned in section 1.4, the development of uniform pressure in the cartilage in heavily loaded joints must have an effect on the mode of lubrication within synovial joints.

Therefore, on loading, lubrication regimes of the types proposed by Wiggins and Malkin[31] and Linn[32] would seem most likely to exist, although a different mode of lubrication probably occurs on unloading because fluid flows into rather than out of the articular cartilage.

5.4 Meniscal Tears

The surgical procedure of meniscectomy is usually performed as a result of damage to the meniscus causing instability or incapacity of motion of the knee joint. The reason for the vulnerability of the menisci to injury probably lies in their weight-bearing role.

In the period 1940-1968 Smillie[60] performed 8000 menisectomies. He noted two major types of tear (see diagram 5.1). The horizontal tear is usually of degenerative origin and is most common in the middle-aged and elderly. The injury of youth is the longitudinal (or circumferential) tear and this type of tear has become more prevalent in recent years. It is the circumferential tear which produces incapacity and requires more urgent surgical treatment than the horizontal tear.

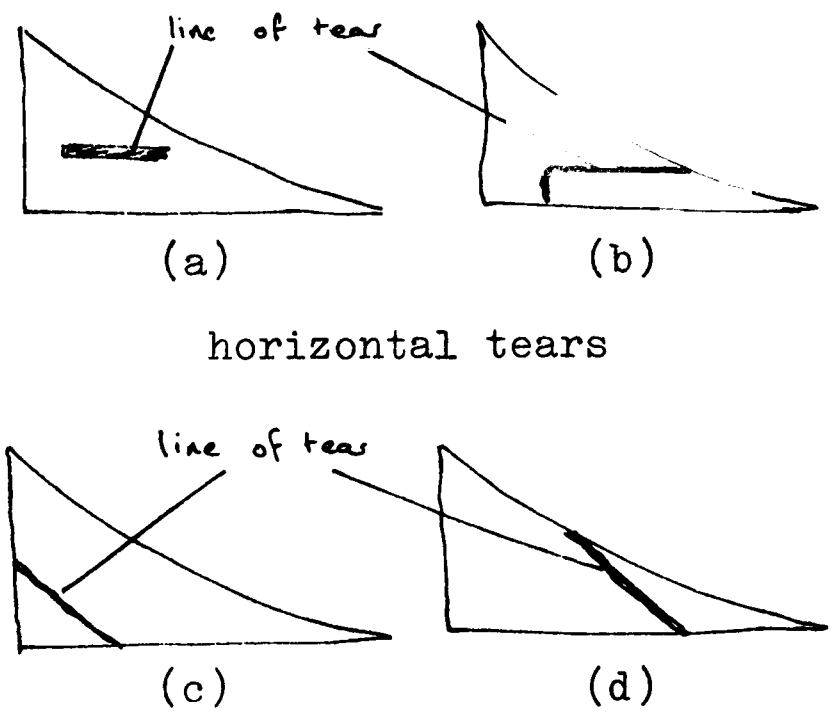

Diagram 5.1 Meniscal tears seen on cross-section

The analyses in Chapter 2 and Appendix 2b indicate that two major components of stress are developed when the menisci are loaded. These stress components are a large circumferential tensile stress and a smaller compressive 'vertical' stress. The radial stress is generally an order of magnitude lower than the 'vertical' stress. The Mohr's circle for stress for such a system is shown in Diagram 5.2.

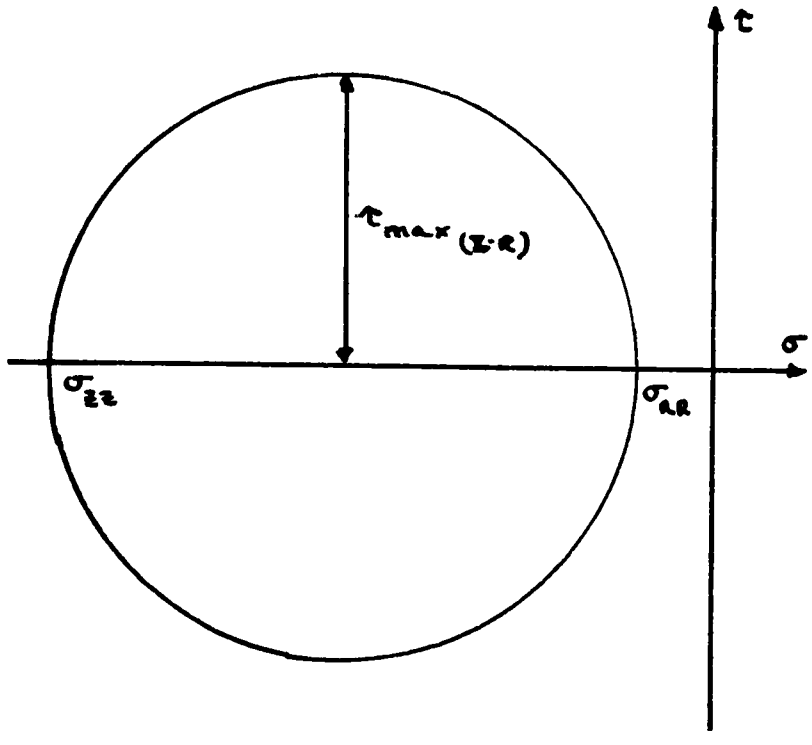

Diagram 5.2

Mohr's circle for stress in the meniscus (Z-R SYSTEM)

The menisci are **anisotropic** and stiffest and strongest in the circumferential direction[62]. The weakest directions are perpendicular to the fibre (circumferential) direction. Hence interfibre failure is likely to occur, and failure will probably be caused by shear or tensile stresses on the weak interfibre planes. Hence the longitudinal failure of youth is probably caused by the maximum shear stress of the Z-R plane system, τ max(ZR) at approximately 45^{o} to the radial direction. High, impact loading from playing 'physical' sports, such as rugby football or soccer is likely to create the necessary shear stress to initiate failure. In his 8000 cases, Smillie points out that over 7000 patients were male. Only recently have females begun to play 'physical' sports, and again in middle-age, females tend to lead a more sedate life than males.

The cause of the horizontal tear is less clear. The existence

of a tensile σ_{zz} seems unlikely, so failure is probably caused by the shear stress, τ_{zR} . Under the conditions applied to the analysis in Appendix 2b, although τ_{zR} does exist its magnitude is small. Certainly increasing age leads to the deterioration of the structure and elasticity of the menisci[66]. During the process of deterioration, the horizontal interfibre matrix would appear to become very susceptible to failure. Stresses causing tears in the weaker meniscus may now occur in running or climbing up or down stairs - activities which produce high loads through the knee joint[50].

5.5 Regenerated Menisci

In some instances the menisci heal or regrow after meniscectomy. If the firm attachment to the tibia is maintained, then the healed or new meniscus will continue to function as a load-bearer. However, if there is no firm attachment to the tibia, then the healed or new meniscus will be unable to bear weight and hence load-bearing will not be a major functional role of the regenerated meniscus.

5.6 General Summary

A major role of the menisci is to bear weight. The function is performed by the development of circumferential tension as the menisci are forced to expand radially as the femur approaches the tibia when the knee joint is subjected to load.

The conclusion that the menisci have a weight-bearing role is drawn from a simple model of the joint and experi-

mental results. The experimental evidence consists of:-

(1) The compressive load/deflection curve of the joint is altered by meniscectomy, invariably with an increase in deflection for a given load;

(2) The menisci are usually loose under light load but become stiff and immovable when loads greater than 10-30 Kgf are applied to the joint;

(3) Dye does not penetrate the menisci-articular cartilage contact areas;

(4) After meniscectomy, a load smaller than the load when the meniscus is present, is required to produce a particular reading on a pressure transducer.

Six estimates of the load carried by the menisci were made from the experimental results. Four estimates from the radial expansion measurements were inaccurate because of simplifications and assumptions regarding the mode of fixation, geometry and material properties of the menisci. The most reasonable estimate, an underestimate, was calculated using the difference in load between the load/deflection curves of the joint with and without the menisci at a given deflection. The estimates using this method showed that in old human knees at least 45% of the load is carried by the menisci when the tibio-femoral joint is subjected to a load of 100 Kgf.

The weight-bearing role of the menisci can be shown to explain a large number of physiological observations concerning the knee joint.

APPENDIX 1a. BIBLIOGRAPHY

1 WOLFF J. Das Gesetz der Transformation der Knochen. Quarto, Berlin (1892).

2 TORIDIS T.G. Stress analysis of the femur. J. Biomech. Vol. 2 163-174, (1969).

3 GOODFELLOW J.W., BULLOUGH P.G. The pattern of ageing of the articular cartilage of the elbow joint. J Bone Jt. Surg. 49-B 175-181, (1967).

4 KEMPSON G.E., MUIR H., POLLARD C., TUKE M., The tensile properties of the cartilage of human femoral condyles related to the content of collagen and glycos-amino-glycans. Biochimica et Biophysica Acta 297 456-472, (1973).

5 SIMON W.H., Scale effects in Animal Joints I. Articular cartilage thickness and compressive stress. Arthritis & Rheumatism 13 244-255, (1970).

6 SIMON W.H., Scale effects in Animal Joints II. Thickness and elasticity in the deformability of Articular Cartilage. Arthritis & Rheumatism 14 493-503 (1971).

7 STOCKWELL R.A., The cell density of human articular and costal cartilage. Journal of Anatomy 101 753, (1967).

8 EDWARDS J., Physical Characteristics of Articular Cartilage. Proc. Inst. Mech. Eng. 181 (3J) 16-24 (1967).

9 BULLOUCH P.G., GOODFELLOW J.W., The Significance of the fine structure of Articular Cartilage. J.B.J.S. 50-B 852-857 (1968).

10 CLARKE I.C., Articular Cartilage: A review and scanning electron microscope study I. Interterritorial Fibrillar Architecture J.B.J.S. 53-B 732-750 (1971).

11 MUIR H., BULLOUGH P.G., MAROUDAS A., The Distribution of collagen in human articular cartilage with some of its physiological implications. J.B.J.S. 52-B 554 (1970).

12 MEACHIM G., ROY S., Surface Ultrastructure of Mature adult Human articular cartilage. J.B.J.S. 51-B 529 (1969).

13 KEMPSON G.E., FREEMAN M.A.R., SWANSON S.A.V., Tensile properties of Articular Cartilage. Nature 220 1127, (1968).

14 HONNER R., THOMPSON R.C., The Nutritional Pathways of Articular Cartilage. J.B.J.S. 53-A 742-748 (1971).

15 GREENWALD A.S., HAYNES D.W., A Pathway for Nutrients from the Medullary Cavity to the articular cartilage of the human femoral head. J.B.J.S. 51-B 747-753 (1969).

16 BASSETT, C.A.L., PAWLUK, R.J., Electric Behaviour of Cartilage during Loading. Science 178 982-983 (1972).

17 ZAREK J.M., EDWARDS J., The stress-structure relationship in articular cartilage. Med. Electron Biol. Eng. 1 497-507 (1963).

18 LITTLE K., PIMM L.H., TRUETA J., Osteoarthritis of the hip - an electron microscope study. J.B.J.S. 40-B 123-131 (1958).

19 McCUTCHEN C.W., The frictional properties of animal joints. Wear 5 (1962).

20 WALKER P.S., DOWSON D., LONGFIELD M.D., WRIGHT V., Boosted lubrication in synovial joints by fluid entrapment and enrichment. Ann. Rheum. Dis. 27 512, (1968).

21 SIMON W.H., Wear Properties of articular cartilage in vitro. J. Biomech. 4 379-389 (1971).

22 MacCONNAIL M.A., The function of intra-articular fibrocartilage with special reference to the knee and the inferior radio ulnarjoints. J. Anat. (London) 66 210 (1932).

23 CHARNLEY J., The lubrication of animal joints. Proc. Symp. Biomech. Inst. Mech. Eng. 12 (1959).

24 DINTENFASS L., Lubrication in synovial joints - a theoretical analysis. J.B.J.S. 45-A 1241-1256 (1963).

25 McCUTCHEN, C.W., Physiological lubrication Paper 1. Symposium on lubrication and wear in living and artificial joints. Inst. Mech. Eng. (1967).

26 DOWSON D., LONGFIELD M.D., WALKER P.S., WRIGHT V., An investigation of the friction and lubrication in human joints. Proc. Mech. Eng. 182 (3N) 68-76 (1968).

27 DOWSON D., UNSWORTH U., WRIGHT V., Analysis of 'boosted lubrication' in human joints. J. Mech. Eng. Sc. 12 364-369 (1970).

28 FEIN R.S., Are Synovial joints squeeze film lubricated? Proc. Inst. Mech. Eng. 181 (35) 125 (1967).

29 RADIN E.L., PAUL I.L., A consolidated concept of Joint lubrication. J.B.J.S. 54-A 607 (1972)

30 WILSON R., PASTERNAK H.S., The Biomechanics of Joint lubrication. Hartford Hospital Bulletin 27 93-99 (1972).

31 WIGGINS K.L., MALKIN S., Bearing Pressure distribution in Joints. Wear 19 (1972).

32 LINN F.C., Lubrication in animal joints II. The mechanism J. Biomech. 1 193-205 (1968).

33 GREENWALD A.S., O'CONNOR J.J. The transmission of load through the human hip joint. J. Biomech. 4 507-528 (1971).

34 HARRISON M.H.M., SHAJOWICZ F., TRUETA J., Osteoarthritis of the hip: a study of the nature and evolution of the disease. J.B.J.S. 35-B 598 (1953)

35 KEMPSON G.E., SPIVEY C.J., FREEMAN M.A.R., SWANSON S.A.V., Patterns of cartilage stiffness on normal and degenerate human femoral heads. J. Biomech 4 597-609 (1971).

36 BULLOUGH P.G., GOODFELLOW J.W., GREENWALD A.S., O'CONNOR J.J., Incongruent surfaces in the human hip joint. Nature 217 (1968).

37 BULLOUGH P.G., GOODFELLOW J.W., O'CONNOR J.J., The relationship between degenerative changes and load bearing in the human hip. J.B.J.S. 55-B 746-758 (1973)

38 GREENWALD A.S., D. Phil. Thesis, Oxford (1970).

39 BULLOUGH P.G., GOODFELLOW J.W., Studies on age changes in the human hip. J.B.J.S. 50-B 222 (1968).

40 BYERS P.D., CONTEPOMI, C.A., FARKAS T.A., A post mortem study of the hip joint. Ann. Rheum. Dis. 29 15 (1970)

41 KEMPSON G.E., FREEMAN M.A.R., SWANSON S.A.V., The determination of a creep modulus for articular cartilage from indentation tests on the human femoral head. J. Biomech 4 239 (1971).

42 GOODFELLOW J.W., HUNGERFORD D., ZINDEL M., Chondromalacia Patellae Orthopaedics: Oxford 4 111 (1971).

43 WEIGHTMAN B.O., FREEMAN M.A.R., SWANSON S.A.V., Fatigue in Articular Cartilage. Nature 244 (1973).

44 RADIN E.L., PAUL I.L., Does cartilage compliance reduce skeletal impact loading? Arth. Rheum. 13 139-145 (1970).

45 SIMON S.R., RADIN E.L., PAUL I.L, ROSE R.M., The response of joints to impact loading II - In vivo behaviour of subchrondral bone. J. Biomech. 5 267-272 (1972).

46 RADIN E.L., PARKER H.G., PUGH J.W., STEINBERG R.S., PAUL I.L., ROSE R.M., Response of Joints to impact loading III. J. Biomech. 6 51-57 (1973).

47 PAUL J.P., Forces transmitted by joints in the human body. Proc. Inst. Mech. Eng. 181 (3J) (1967).

48 RYDELL N., Forces acting on the femoral head prosthesis Trycheri A.B. Litotyp, Goteburg, Sweden (1966).

49 MORRISON J.B., The mechanics of the knee joint in relation to normal walking. J. Biomech. 3 51-61 (1970).

50 POULSON J., D. Phil. Thesis. Univ. Strathclyde 1973.

51 MORRIS J.R.W., D. Phil. Thesis. Oxford 1973.

52 GRAY'S Anatomy 34th Edn. Longmans 1967.

53 Anatomy Regional and Applied 5th Edn. Churchill Livingstone (Edinburgh) (1972).

54 KIMBER-GRAY-STACKPOLE'S, Anatomy and Physiology 16th Edn. Macmillan Company, New York (1972).

55 BRANTIGAN O.C., VOSHELL A.F., The mechanics of the ligaments and menisci of the knee joint. J.B.J.S. 23 (1941).

56 KENNEDY J.C., FOWLER P.J., Medial and Anterior instability of the knee. J.B.J.S. 53-A 1257-1270 (1971).

57 KING D., The function of semi lunar cartilages. J.B.J.S. 18 1069 (1936).

58 DEANE G., M.Sc. Thesis, Univ. Surrey (1970).

59 MacCONNAIL M.A., Movements of Bones and Joints - III The synovial fluid and its assistants. J.B.J.S. 32-B 244 (1950).

60 SMILLIE I.S., Injuries of the Knee Joint. 4th Edn. E.& S. Livingstone (1970).

61 FAIRBANK T.J., Knee Joint changes after meniscectomy. J.B.J.S. 30-B 664 (1948).

62 BULLOUGH P.G., MUNUERA L., MURPHY J., WEINSTEIN A.M., The strength of the menisci as it relates to their fine structure. J.B.J.S. 52-B (1970).

63 KETTELKAMP D.B., JACOBS A.W., Tibio-femoral contact area- Determination and Implications J.B.J.S. 54-A 349 (1972)

64 WALKER P.S., HAJEK J.V., The load bearing area in the knee joint. J. Biomech. 5 581-589 (1972).

65 WALKER P.S., Trends in Knee Prosthesis Development. Engineering in Medicine 2 76-82 (1973).

66 BENNETT G.A., WAINE H., BAUER W., Changes in the knee joint at various ages with particular reference to the nature and development of degenerative joint disease. New York, The Commonwealth Fund, 1942.

67 WOODYARD J., Meniscectomy: Long term survey after meniscectomy. Orthopaedics: Oxford 1 29 (1968).

68 KEMPSON G.E., Ph.D. Thesis. Univ. London (1969).

69 TIMOSHENKO S.,GOODIER J.N,Theory of Elasticity 3rd Ed. McGraw-Hill (1970).

70 BELYTSCHKO T., KULAK R.F., SCHULTZ A.B., GALANTE J.O., Numerical Stress Analysis of Intervertebral Disk. Winter Annual Meeting. A.S.M.E. 72-WA/BMF-12 (1972).

71 KOBAYASHI, A.S., WOO S. L-Y., LAWRENCE C., SCHLEGEL W.A., Analysis of the corneo-scleral shell by the method of direct stiffness. J. Biomech. 4 323-330 (1971).

72 WIEDERHIELM C.A., KOBAYASHI A.S., STROMBERG D.D., WOO S.L-Y., Structural response of relaxed and constricted arterioles. J. Biomech. 1 259-270 (1968).

73 WRIGHT G.P., D..Phil. Thesis. Oxford (1970).

74 LAU M.G., D. Phil. Thesis, Oxford (1972).

75 BRAMHALL R., D. Phil. Thesis, Oxford (1973).

76 TU, YIH-O, GAZIS D.C., The contact problem of a plate pressed between two spheres. Journal of Applied Mechanics 31 Trans. A.S.M.E. 86 Series E 659-666 (1964).

77 O'CONNOR J.J., Compliance under a small torsional couple of an elastic plate pressed between two identical elastic spheres. Journal of Applied Mechanics 33. Trans. A.S.M.E. 88 Series E 377-383 (1966).

78 O'CONNOR J.J., Personal Communication (1974).

79 HAYES W.C., KEER L.M., HERRMANN G., MOCKROS L.F., A mathematical analysis for indentation tests of articular cartilage. J. Biomech. 5 541 (1972).

80 COX J.A., DAVIDSON J.M.F., 3rd Year Project, O.U.Eng. Lab., Oxford (1970).

81 NIRANJAN V., Dynamic Properties of bone and some engineering considerations in the design of internal orthopaedic prostheses. Univ. Toronto. Inst. Aerospace Studies Report 190 (1973).

82 KEER L.M., Personal Communication (1974).

83 PAFEC 70+ Department of Mechanical Engineering, Nottingham University (1972).

84 IRONS B.M., A frontal solution finite element program for finite element analysis. Int.. J. Num. Meth. Eng. 2 5 (1970).

85 ZIENKIEWICZ O.C., (in collaboration with CHEUNG Y.K.) The finite element method in structural and continuum mechanics. McGraw-Hill (1967).

APPENDIX 1b. GLOSSARY OF CERTAIN TERMS

Articular cartilage	-	hyaline cartilage covering the articulating surfaces of synovial joints.
collagen fibre	-	a white inelastic fibre of connective tissues.
condyle	-	a smooth protruberance at the end of a bone for articulation with the adjacent bone.
epiphysis	-	a separate terminal ossification of some bones which only becomes united with the main bone with the attainment of full maturity.
extension	-	straightening out of a limb.
femur	-	the long bone of the thigh.
fibula	-	the thin bone of the lower part of the leg to which many muscles are attached.
flexion	-	the act of bending a joint so that the parts which it connects approach one another.
glucos-amino-glycans	-	one of a group of organic compounds which can be resolved by hydrolysis into sugar and other organic substances.
lateral	-	descriptive of the outer side of the body or limbs.
ligament	-	a bundle of fibrous tissue joining two or more bones or cartilages.
medial	-	descriptive of the middle side of an organ or limb.
meniscus	-	a semi-lunar wedge-shaped fibrocartilage in the knee joint attached to the tibia.
mucopolysaccharide	-	a polysaccharide composed of alternate units of uronic acids and amino sugars: mucopolysaccharides act as structural supports for connective tissue.
osteophyte	-	a bony outgrowth from the margin of an osteoarthritic joint or from diseased bone.
patella	-	the knee cap.

popliteus - a weak flexor and medial rotator of the knee. It rises on the lateral aspect of the lateral condyle and inserts into the back of the tibia.

proteoglycans - complex long chain polymers of proteins and sugars. Proteins are the basic component of connective tissues.

quadriceps femoris - a group of four muscles in the front of the thigh which extend the knee through the patellar tendon.

subchondral - any structure situated beneath a joint cartilage.

synovial fluid - fluid produced by synovial membranes which nourishes and lubricates articular cartilage.

synovial joint - an articulation in which the opposed surfaces are separated by a space containing fluid.

synovial membrane- the soft tissue limiting a joint space, attached to the margins of the articulating skeletal structures.

tendon - a sheet or band of fibrous tissue by which a muscle is attached to the skeleton or to another muscle.

tibia - the major weight-bearing bone of the lower part of the leg.

vasti - a group of three muscles in the quadriceps group. The fourth muscle in the quadriceps group is rectus femoris.

APPENDIX 2a

Solution of problems of rigid indentors pressing into thin layers of cartilage using Thin Layer approximation.

(a) Spherically ended indentor, radius R.

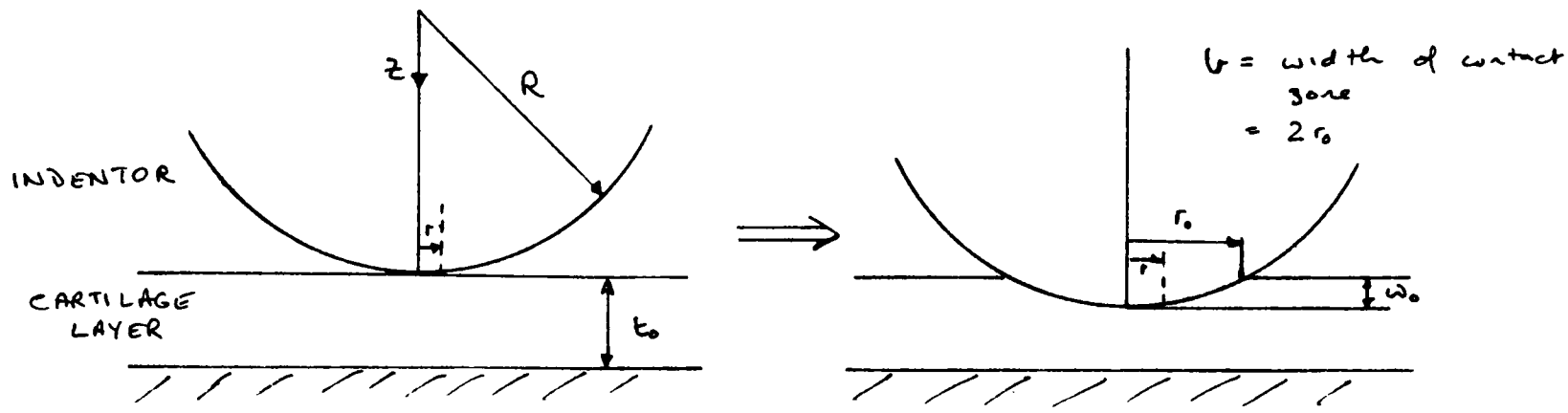

Bone layer (rigid)

at any radius r, the original gap between the indentor surface and the upper surface of the thin layer is t_o

$$t_o = \frac{r^2}{2R} \qquad \text{if } t_o << R$$

If the indentor approaches the bone layer by a distance ω_o then the deformation in the z-direction of the surface of the thin layer is $\omega = \omega_o - t_o \ (r \leq r_o)$ and $\omega_o = \frac{r_o^2}{2R}$

hence using Tu and Gazis' relationship

$$\sigma_{zz}(r) = \frac{E\,(r_o^2 - r^2)}{2(1-\nu^2)\,2R\,t_o} \qquad \text{for} \quad r \leq r_o$$

$$= \frac{G\,(1+\nu)(r_o^2 - r^2)}{2(1-\nu^2)\,R\,t_o}$$

where G is the shear modulus,

hence P = Total vertical load = $2\pi \int_o^{r_o} \sigma_{zz}(r)\, r\, dr$

$$P = \pi G \frac{(1+\nu)}{(1-\nu^2)} \left(\frac{t_o}{R}\right)\left(\frac{r_o}{t}\right)^2 \int_o^{r_o} \left(1 - \left(\frac{r}{r_o}\right)^2\right) r\, dr$$

$$= \pi G \frac{(1+\nu)}{(1-\nu^2)} \left(\frac{t_o}{R}\right)\left(\frac{r_o}{t}\right)^2 \frac{r_o^2}{4}$$

now $\omega_o = \frac{r_o^2}{2R}$

hence $P = \pi G \left(\frac{1+\nu}{1-\nu^2}\right)\left(\frac{t_o}{R}\right)\frac{2R\omega_o}{t^2}\,\frac{2R\omega_o}{4}$ and $\frac{P}{GR^2} = \pi \frac{(1+\nu)}{(1-\nu^2)}\left(\frac{t_o}{R}\right)\left(\frac{\omega_o}{t}\right)^2$

The values of $\frac{P}{GR^2}$ so obtained are compared to Hayes et al[79] numerical solution in Table 2.a.1.

$\frac{\omega_o}{t_o}$ →	0.01		0.02		0.03		0.04		0.05	
$\frac{R}{t_o}$ ↓	A	B	A	B	A	B	A	B	A	B
5	5.43	1.14	17.9	4.57	41	10.3		18.3		28.6
10	2.42	0.57	7.7	2.28	16.3	5.14	29	9.14		14.3
20	0.905	0.286	3.62	1.14	8.15	2.57	14.9	4.57	24	7.14
40	0.423	0.143	1.81	0.57	3.8	1.29	8	2.28	13	3.57

Table 2.a.1.

Values of $\left(\frac{P}{GR^2}\right) \times 10^4$ compared for Numerical solution (A)

Thin layer approximation (B)

(b) Cylindrical Indentor.

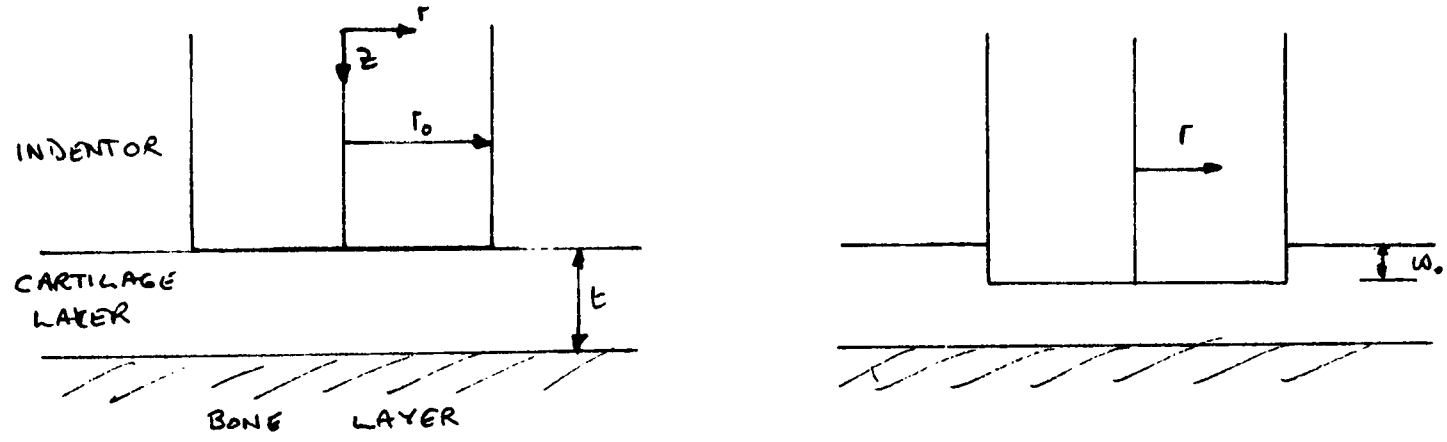

In this case the surface displacement in the z-direction at any radius, r, within the contact zone is ω_o.

Using Tu and Gazis relationship gives

$$\sigma_{zz} = \frac{E}{2(1-\nu^2)} \frac{\omega_o}{t} = \frac{G(1+\nu)}{(1-\nu^2)} \frac{\omega_o}{t}$$

hence $$P = \pi r_o^2 G \frac{(1+\nu)}{(1-\nu^2)} \frac{\omega_o}{t}$$

and the indentation factor $$\frac{\frac{\omega_o}{t}}{\left(\frac{P}{GR^2}\right)} = \frac{1-\nu^2}{\pi(1+\nu)}$$

This is constant for all area-aspect ratios and is compared to the values obtained by Hayes et al in Table 2.a.2.

0.35		0.4		0.45	
A	B	A	B	A	B
0.075	0.207	0.058	0.191	0.036	0.175

Table 2.a.2 Value of

A, B as for Table 2.a.1.

In both Tables 2.a.1 and 2.a.2. there should be reasonable agreement at high area-aspect ratios. In Table 2.a.1, the values for the numerical solution are obtained from the graph of load factor $\left(\frac{P}{GR^3}\right)$ v. relative approach $\left(\frac{\omega_0}{t_0}\right)$ in the article by Hayes et al.

For the cylindrical indentor, the numerical solution tends to a constant value of indentation factor when plotted against area-aspect ratio for various values of Poisson's ratio. Comparison in Table 2.a.2. again shows a difference between the two solutions, the difference being approximately a factor of π (load factor might be $\frac{P}{\pi G r_0^3}$ not $\frac{P}{G r_0^3}$)

L.M. Keer[82] indicates that the results presented by Hayes et al are correct. For $\frac{R}{t_0} = 20$ and $\frac{\omega_0}{t} = 0.4$ Keer gives $\frac{b}{t} = 1.265$[82]. Using the approximate theory $\frac{b}{t} = 8$ is obtained. The approximate theory is invalid for $\frac{b}{t} = 1.265$ and hence the discrepancy in Table 2.a.1. may be due to the approximate theory being invalid for the indentation range considered by Hayes et al, although with $\frac{R}{t} = 40$ and $\frac{\omega_0}{t} = 0.06$, $\frac{b}{t} = 4.4$ using the approximate theory. The discrepancy for the cylindrical

indentor results can not similarly be explained since high area-aspect ratios are quoted by Hayes et al.

APPENDIX 2b.

Comparison of approximate method used for meniscus with finite element stress analysis solution.

1. Solution of problem of meniscus subject to uniform pressure on femoral surface using approximate method.

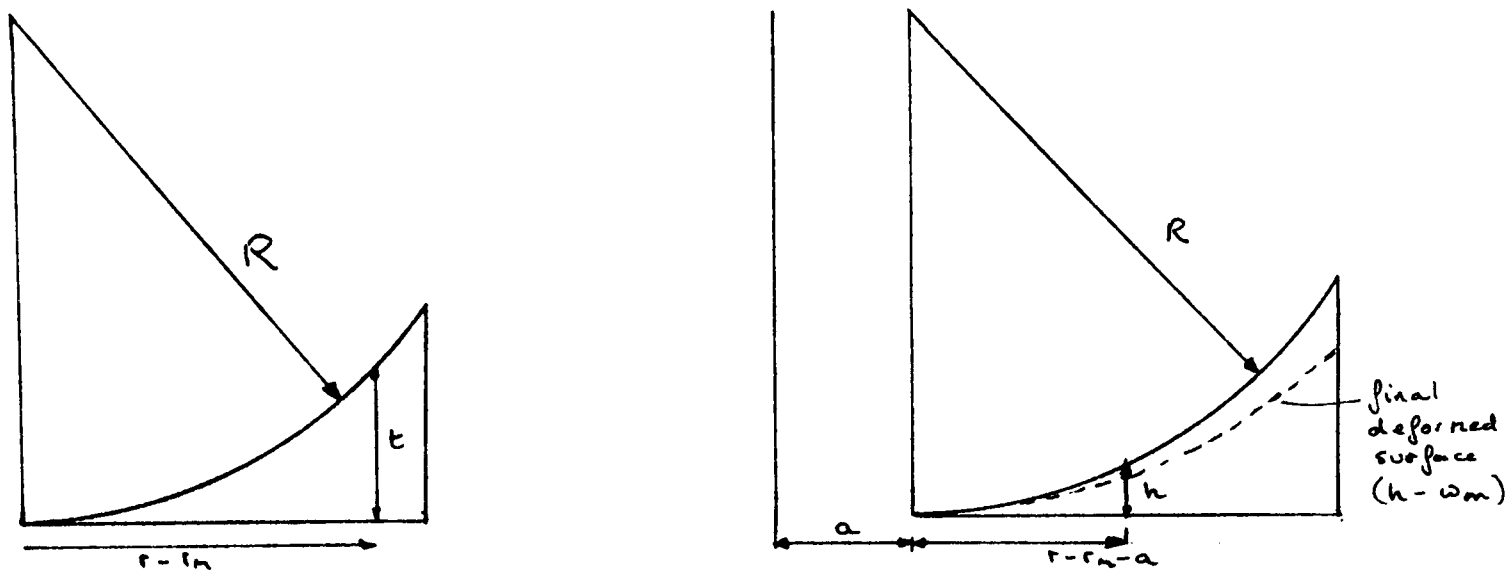

The original height of themeniscus at radius r is t where

$$t = R - \sqrt{R^2-(r-r_m)^2} \qquad \text{....b.1.}$$

The meniscus slides out a distance, a, and if there is no deformation the undeformed height will be

$$h = R - \sqrt{R^2-(r-r_m-a)^2} \qquad \text{.....b.2.}$$

A deformation ω_m occurs, and using the relationship between stress and strain as in equation 2.12.

$$\omega_m = \sigma_{zz}\,\frac{h}{k_1} \qquad \text{....b.3.}$$

where the applied pressure is σ_{zz} . The approximate theory used in the analysis assumes that the stress on the femoral surface of the meniscus has components in the z and r-directions and that these act totally independently,

hence, the deformed height of the meniscus

$$t' = h - \omega_m = h\left(1 - \frac{\sigma_{zz}}{k_1}\right) \qquad \text{.....b.4.}$$

At radius r the strain of the circumferential fibre is, from equation 2.21

$$\epsilon_{\theta\theta} = \frac{a}{r-a} \qquad \text{.....b.5.}$$

The finite element method used assumes the material to be isotropic and homogeneous, hence $k_3 = k_1$

$$\text{and} \qquad \sigma_{\theta\theta} = k_1 \frac{a}{r-a} \qquad \text{.....b.6}$$

hence the circumferential force F is

$$F = \int_{r_m+a}^{r_m+a+c} k_1 \frac{a}{r-a}\, t'\, dr = k_1\left(1 - \frac{\sigma_{zz}}{k_1}\right)\int_{r_m+a}^{r_m+a+c} \frac{a\,h}{r-a}\, dr \qquad \text{.....b.7.}$$

From equilibrium considerations as in equation 2.20

$$F\,\delta\theta = \left(\int_{r_m+a}^{r_m+a+c} \sigma_{zz} \tan\alpha'\, r\, \delta_1\right)\delta\theta$$

$$\text{hence } F = \sigma_{zz}\left(1 - \frac{\sigma_{zz}}{k_1}\right)\int_{r_m+a}^{r_m+a+c} \frac{\partial h}{\partial r} r\, dr = \sigma_{zz}\left(1 - \frac{\sigma_{zz}}{k_1}\right)\int_{r_m+a}^{r_m+a+c} \frac{(r - r_m - a)\,r}{\sqrt{R^2 - (r-r_m-a)^2}}\, dr \qquad \text{..b.8}$$

$$\text{hence } k_1 \int_{r_m+a}^{r_m+a+c} \frac{a\,h}{r-a}\, dr = \sigma_{zz} \int_{r_m+a}^{r_m+a+c} \frac{(r-r_m-a)\,r}{\sqrt{R^2 - (r-r_m-a)^2}}\, dr \qquad \text{....b.9}$$

The Integrals of equation b.9 may be numerically calculated as functions of a. When the two integrals have the same numerical

value, the correct value of the expansion, a, will have been obtained.

Substituting the value of a so obtained into b.2 and thence into b.4 gives the final deformation curve.

2. Finite element method.

The finite element program used was the Program for Automatic Finite Element Calculations developed at Nottingham University[83]. The program used the frontal method of solution[84]. The Axi-symmetric Finite Element Theory used is standard[85].

The input mesh is shown in Diagram 2.b.1. For the comparison of the results of this method with the approximate theory, nodes on the face 1-133 are set on the arc of a circle of radius 24 with the inner radius at 10 and the width 12 (nodes 133 (10,0); 139 (22,0) - co-ordinates (r, z). The diagram shown is the size used for the 'human case' in Chapter 4 with the corner nodes (133 (10,0); 139, (22,0); 1 (22,7)). For the 'pig case' the radial values are reduced by 6 units, the units in the latter two cases being millimeters. The Young's modulus of the material is taken to be 150 N/mm^2 for the latter two cases with a pressure of 1 N/mm^2 and the comparison case has the same pressure but a Young's modulus of 25 N/mm^2. Poisson's ratio is taken to be 0.4 [79] in all cases.

The mesh is loaded with uniform pressure applied to the femoral surface (nodes 1 - 133). No vertical movement is allowed on the tibial surface (nodes 133-139). Vertical stresses will be developed therefore on the tibial face, but as radial movement is allowed, there will be no shear stresses.

The deformation due to a uniform pressure on the femoral

GRID FOR FINITE ELEMENT ANALYSIS
CERTAIN NODES INDICATED
ALL ELEMENTS NUMBERED

ELEMENT IS 6 NODE ISOPARAMETRIC TRIANGLE

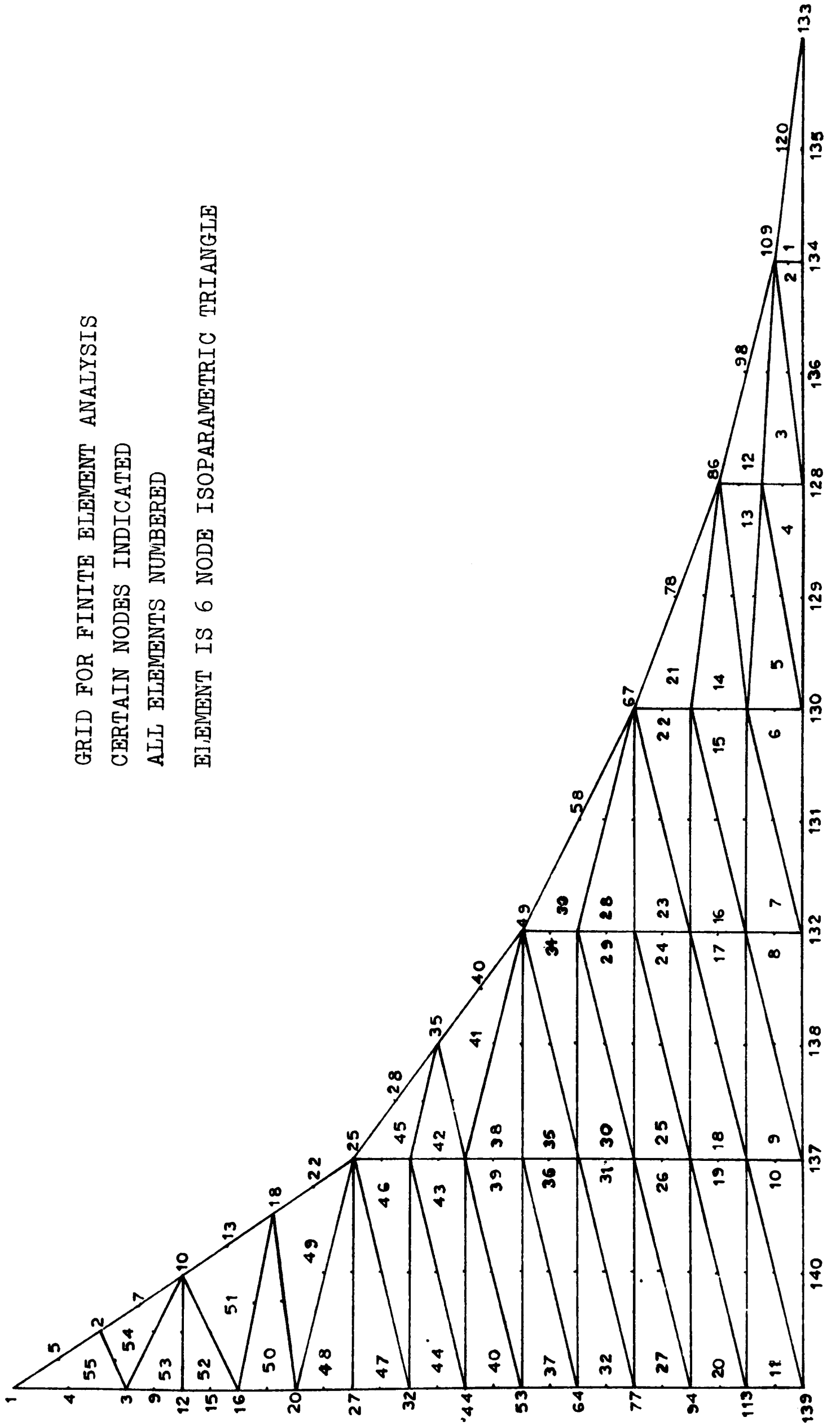

Fig. 2.b.1

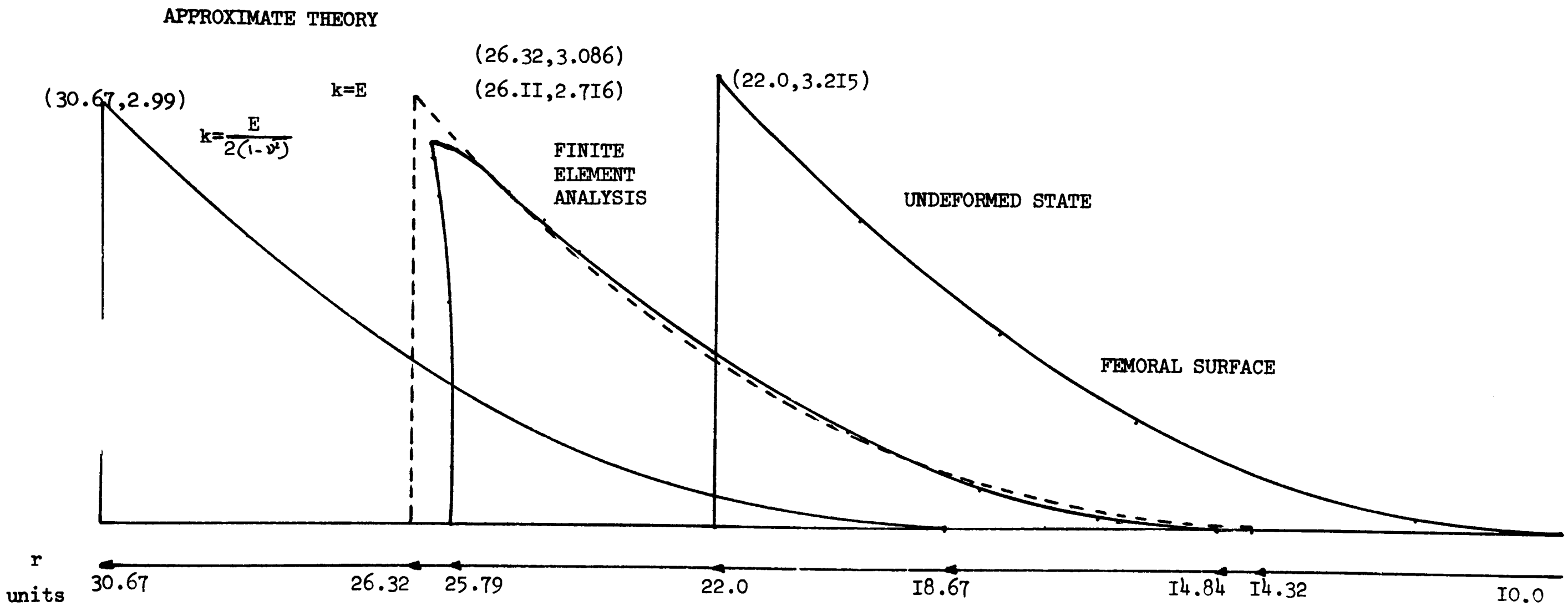

COMPARISON OF MENISCUS DEFORMATION DUE TO UNIFORM PRESSURE ON FEMORAL SURFACE USING APPROXIMATE THEORY AND FINITE ELEMENT ANALYSIS

Diagram 2.b.2.

surface calculated by both methods is shown on diagram 2.b.2. With $k_1 = \frac{E}{2(1-\nu^2)}$, that is, Tu and Gazis' relationship, the approximate theory gives a much larger expansion and hence for a given deformation will underestimate the applied load. With $k_1 = E$ the expansions are very similar; the approximate theory gives a slightly smaller expansion and thus the estimate of load for a given deformation will be slightly high. Since the approximate theory is an extension of Tu and Gazis' thin layer approximation, k_1 should be $\frac{E}{2(1-\nu^2)}$ and hence the estimate of load carried by the meniscus will be lower than an estimate using the finite element method.

Stresses:

The PAFEC program uses the displacement method of analysis. The primary unknowns in the calculation are the displacements of the nodes when point or distributed loading is applied. If stresses are to be calculated then they are determined after the displacements. The displacement function used ensures compatability of displacement and the first derivative of displacement at the nodes. Since the stresses are given by displacement differentials, the accuracy of stresses from a given finite element mesh is inevitably poorer than the accuracy of displacements.

The stresses obtained for the centre point of certain elements are given in Table 2.b.1. τ_{zr} is consistently low near the tibial surface of the meniscus, but increases with height. $\sigma_{\theta\theta}$ is always tensile and decreases with increasing radius. Except for elements 2, 4, 6 and 10, σ_{zz} is compressive as expected from the applied loading, and σ_{rr} is small by comparison. In

STRESSES FOR SELECTED ELEMENTS - FINITE ELEMENT ANALYSIS.

Element No.	I	2	3	4	5	6	7	8	9	I0	II
$\sigma_{\theta\theta}$	9.79	8.64	7.82	6.97	6.5	5.82	5.5I	4.97	4.7I	4.II	3.72
σ_{zz}	-I.I9	0.3	-I.08	0.II	-0.98	0.05	-0.97	-0.83	-0.79	-0.I6	-I.72
σ_{rr}	-0.03	-0.86	-0.07	-0.9	0.04	-0.9I5	0.I	-0.05	-0.I3	-I.I7	-0.I3
τ_{rz}	0.0	0.0	0.06	0.0	0.08	0.0	0.05	0.03	0.06	0.0	0.0

POSITIVE : TENSION NEGATIVE : COMPRESSION UNITS : MN/m^2 (N/mm^2)

Element No.	I7	24	29	34
$\sigma_{\theta\theta}$	4.97	4.99	5.02	5.06
σ_{zz}	-0.83	-0.79	-0.78	-0.77
σ_{rr}	-0.05	-0.06	0.0	0.07
τ_{rz}	0.I2	0.I8	0.28	0.35

Element No.	20	27	37	47	53
$\sigma_{\theta\theta}$	3.74	3.75	3.78	3.98	4.05
σ_{zz}	-I.7I	-I.70	-I.66	-I.48	-I.6
σ_{rr}	-0.I2	-0.I	-0.08	0.06	0.3
τ_{rz}	0.0	0.05	0.07	0.22	0.33

Table 2.b.1

elements 2, 4, 6 and 10, a 90^{o} rotation of the maximum principal stress in the r-z plane has occurred, thus σ_{zz} and σ_{rr} are alternated from the values determined in other elements. At other positions in elements 2, 4, 6 and 10, stresses are similar to those determined for the centre of other elements. The precise reason for the rotation is not known.

The stresses determined by the finite element calculation show that the simplifying assumptions made in the model analysis are not too unreasonable near the inner radius of the meniscus.

APPENDIX 2(c)

Determination of Articular Cartilage layer deformation.

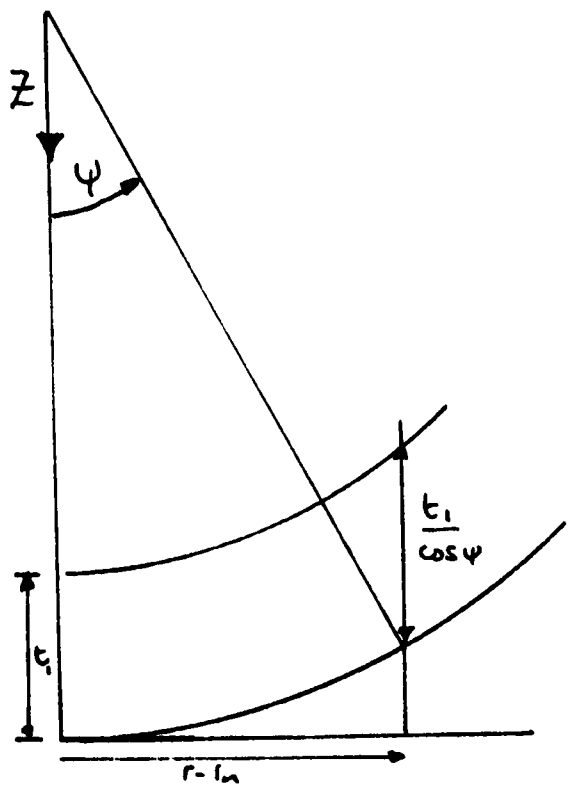

The thickness of the cartilage in the z-direction is $t_1/\cos\psi$

where $$\cos\psi = \sqrt{1 - \frac{(r - r_m)^2}{R^2}}$$

The assumption is made that there are no surface shear stresses, hence all stresses are applied normal to the cartilage surface. The stress at radius r, should therefore be applied in the radial, R, direction, causing radial, R, deformation. From equation 2.19a the radial, R, stress on the femoral articular cartilage layer is $\sigma_{zz}(r)$ at radius r. Hence, the radial, R, deformation.

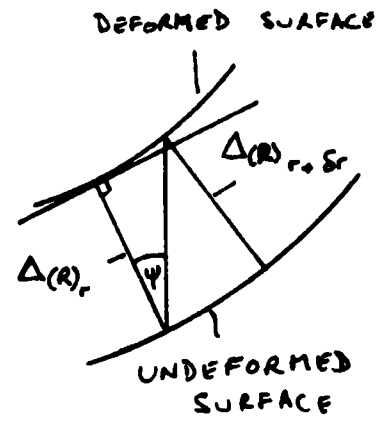

$$\Delta_{(R)_r} = \frac{t_1}{k_2}\,\sigma_{zz}(r)$$

The component of this deformation in the z-direction is approximately

$$\omega_1 \approx \frac{\Delta_{(R)_r}}{\cos\psi} = \frac{\sigma_{zz}(r)}{k_2}\left(\frac{t_1}{\cos\psi}\right)$$

Hence for determining the total deformation of both articular cartilage layers in the z direction, $\omega_1 + \omega_2$, for use in equation 2.12, the total articular cartilage thickness may be defined as $t_o = t_2 + \frac{t_1}{\cos\psi}$

$$\left(\text{hence, } \omega_1 + \omega_2 = \frac{\sigma_{zz}(r)}{k_2}\left(\frac{t_1}{\cos\psi} + t_2\right)\right)$$

APPENDIX 2(d) Derivation of Quadratic Equation for d.

Equation 2.22 gives the relationship which allows a solution of a specified, d for a given value of a. It is:-

$$F = \int_{r_m+a}^{r_m+a+c} k_3 \frac{a}{r-a} t' \, dr = \int_{r_m+a}^{r_m+a+c} \sigma_{zz}(r)\, r \tan\alpha' \, dr \qquad \ldots\ldots d.1$$

where $t' = h - \omega_m = h - \frac{\sigma_{zz}(r)\, h}{k_1} = h\left(1 - \frac{\sigma_{zz}(r)}{k_1}\right)$ ...d.2.

In the region considered, $\sigma_{zz}(r)$ was shown to be

$$\sigma_{zz}(r) = k_1 \frac{d - R\left[\left(1 - \left(\frac{r-r_m-a}{R}\right)^2\right)^{\frac{1}{2}} - \left(1 - \left(\frac{r-r_m}{R}\right)^2\right)^{\frac{1}{2}}\right]}{\left(R\left[1 - \left(1 - \left(\frac{r-r_m-a}{R}\right)^2\right)^{\frac{1}{2}}\right] + t_o \frac{k_1}{k_2}\right)} \qquad \ldots\ldots d.3$$

h is defined as $R\left[1 - \left(1 - \left(\frac{r-r_m-a}{R}\right)^2\right)^{\frac{1}{2}}\right]$ d.4

These relationships were shown in Chapter 2 equations 2.9 and 18. $\tan\alpha'$ is the slope of the femoral surface of the meniscus at radius, r, and is therefore:-

$$\frac{\partial t'}{\partial r} = \frac{\partial}{\partial r}\left(h\left(1 - \frac{\sigma_{zz}(r)}{k_1}\right)\right) = \frac{\partial h}{\partial r}\left(1 - \frac{\sigma_{zz}(r)}{k_1}\right) - \frac{h}{k_1}\frac{\partial\, \sigma_{zz}(r)}{\partial r} \qquad \ldots\ldots d.5$$

Let $\sigma_{zz}(r)$ be defined as $k_1 \frac{u}{v}$ where u and v are respectively the numerator and denominator of the equation d.3, above.

Hence,

$$h' = \frac{(r - r_m - a)}{(R^2 - (r - r_m - a)^2)^{\frac{1}{2}}}$$

$$\text{and} \quad \frac{1}{h_1} \sigma_{zt}(r)' = \frac{u'v - v'u}{v^2} \qquad \text{...d.6}$$

where the prime indicates differentiation with respect to r.

and

$$u' = \frac{r - r_m - a}{(R^2 - (r - r_m - a)^2)^{\frac{1}{2}}} - \frac{r - r_m}{(R^2 - (r - r_m)^2)^{\frac{1}{2}}}$$

$$v' = \frac{r - r_m - a}{(R^2 - (r - r_m - a)^2)^{\frac{1}{2}}} + \frac{h_1}{h_2} \frac{t_1 (r - r_m)}{R^2 \left(1 - \left(\frac{r - r_m}{R}\right)^2\right)^{\frac{1}{2}}} \qquad \text{...d.7}$$

Hence $$\frac{\partial t'}{\partial r} = \tan \alpha' = h' \left(1 - \frac{\sigma_{zz}(r)}{h_1}\right) + \frac{h (v'u - u'v)}{v^2} \qquad \text{...d.8}$$

If d is considered a constant for a given a then it may be separated from the above equation to give:-

$$\tan \alpha' = d \left(\frac{h v'}{v^2} - \frac{(r - r_m - a)}{v (R^2 - (r - r_m - a)^2)^{\frac{1}{2}}} \right) + \frac{h v' b_1}{v^2} - \frac{h u'}{v}$$

$$+ \frac{(r - r_m - a) \left(R + \frac{h_1}{h_2} t_0 - (R^2 - (r - r_m)^2)^{\frac{1}{2}}\right)}{v (R^2 - (r - r_m - a)^2)^{\frac{1}{2}}} \qquad \text{....d.9}$$

where $$b_1 = (R^2 - (r - r_m)^2)^{\frac{1}{2}} - (R^2 - (r - r_m - a)^2)^{\frac{1}{2}}$$

This value of tanα' may now be substituted into equation d.1.. d, still being considered as a constant, may be extracted

to develop a quadratic equation in d of the form:-

$$X\,d^2 + Y\,d + Z = 0$$

where

$$X = k_1 \int_{r_m+a}^{r_m+a+c} \frac{1}{V}\left(\frac{h\,V'}{V^2} - \frac{r-r_m-a}{r\left(R^2-(r-r_m-a)^2\right)^{\frac{1}{2}}}\right) r\,dr$$

$$Y = k_1 \int_{r_m+a}^{r_m+a+c} \left[\frac{k_3}{k_1}\frac{a\,h}{r-a} + \frac{r\,b_2}{V} + \frac{r\,b_1}{V}\left(\frac{h\,V'}{V^2} - \frac{r-r_m-a}{r\left(R^2-(r-r_m-a)^2\right)^{\frac{1}{2}}}\right)\right] dr$$

$$Z = k_1 \int_{r_m+a}^{r_m+a+c} \left[\frac{k_3}{k_1}\frac{a\,h}{r(r-a)}\left(\left(R^2-(r-r_m-a)^2\right)^{\frac{1}{2}} - R - \frac{k_1}{k_2}t_0\right) + \frac{r\,b_1\,b_2}{V}\right] dr$$

where $h_2 = \dfrac{\partial t'}{\partial r} - d\left(\dfrac{h\,V'}{V^2} - \dfrac{(r-r_m-a)}{r\left(R^2-(r-r_m-a)^2\right)^{\frac{1}{2}}}\right)$ (see equ^{n}. d.9)

APPENDIX 2(e) Computer program.

The contact problem is finally solved by numerical analysis using a computer. The program is listed on pages A25, A26 and A27 and is written in Fortran. Lines 0 to 4 indicate that the program is written in fortran and selects input and output channels. Arrays of the input data are then dimensioned and functions external to the main program are indicated, as are the variables common to these functions and the main program.

Input and Output format statements are followed by the reading of the data. Do loops are created to vary the parameters in turn. T_1 and T_2 and E_1 and E_2 are varied together. When specified values of R, r_m, C, $t_{1,2}$ and $E_{1,\,2}$ have been selected they are printed and a is then selected. A library subroutine D01ACF is called to perform the integrations of the functions X, Y and Z between the limits A+RM and A+RM+C. The functions

X, Y, and Z for the specified value of a are called XC, YC, and ZC on return from the subroutine. A check is then made to ensure that no attempt to find the square root of a negative number will be made. Two values of the deflection d are then found. The smaller of the two values is considered, the larger one often being of greater magnitude than the total thickness of the cartilage layers and arising from the negative square root.

Having determined d, P may be found using the appropriate values of $\sigma_{zz}(r)$ for the regions for which the values are valid. The percentage of the total load carried by the meniscus is then determined followed by a return to select a new value of a.

The program was checked by hand calculation of values of X(r), Y(r) and Z(r). These three functions were then plotted against r and the enclosed area used to calculate values of X, Y, and Z. d was then calculated and checked against the value obtained from the program. The load functions were similarly checked.

If $\sigma_{zz}(r)$ becomes tensile, that is, separation occurs, then $\sigma_{zz}(r)$ may be set to zero. A check on the sign of $\sigma_{zz}(r)$ is made at the end of the calculation of $\sigma_{zz}(r)$ (function $P_3(s)$). A compressive stress is positive, hence negative or zero values of $\sigma_{zz}(r)$ are set to zero. This has been done for all the graphs shown in 2f. The effect of separation is not great as shown in 2.e.1.

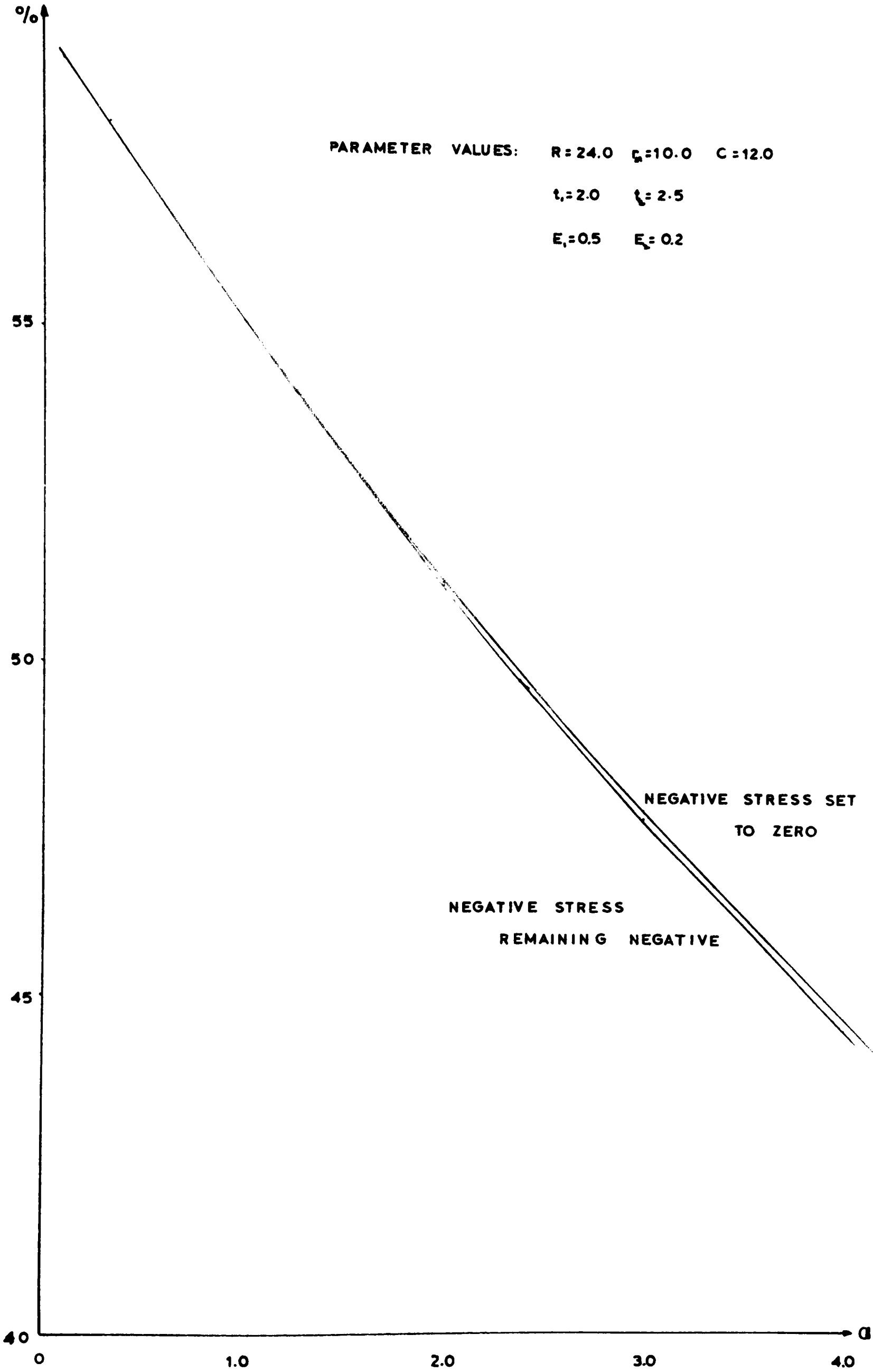
%
55
50
45
40
0
1.0
2.0
3.0
4.0
α
PARAMETER VALUES: R = 24.0 t_0 = 10.0 C = 12.0
t_1 = 2.0 t_2 = 2.5
E_1 = 0.5 E_2 = 0.2
NEGATIVE STRESS SET TO ZERO
NEGATIVE STRESS REMAINING NEGATIVE

Figure 2.e.1

Computer Program for numerically solving Model Analysis.

```
CUMENT     MODEL

    0        LIST
    1        PROGRAM(FORT)
    2        INPUT 5=CR0
    3        OUTPUT 6=LP0
    4        END
    5        MASTER MODEL
    6        DIMENSION RA(10),RMA(10),CA(10),T1A(10),T2A(10),E1A(10),E2A(10),AA
    7       1(10)
    8        EXTERNAL X,Y,Z,P2,P3
    9        COMMON R,RM,T1,T2,E1,E2,A,D
   10       1 FORMAT(6I4)
   11       2 FORMAT(10F4.1)
   12       3 FORMAT(10F6.4)
   13       4 FORMAT(1H ,5X,12HD IS COMPLEX)
   14       5 FORMAT(1H0,5X,4HDATA)
   15       6 FORMAT(1H0,3X,3HR =,F5.1,5X,4HRM =,F5.1,5X,3HC =,F5.1,5X,4HT1 =,F5
   16        1.1,5X,4HT2 =,F5.1,5X,4HE1 =,F6.4,5X,4HE2 =,F6.4)
   17       7 FORMAT(1H0,5X,3HA =,F6.4)
   18       8 FORMAT(1H ,10X,3HD =,F10.7,10X,3HP =,F10.5,10X,5HPCM =,F5.2)
   19        READ(5,1)NR,NRM,NC,NT,NE,NA
   20        READ(5,2)(RA(I),I=1,NR)
   21        READ(5,2)(RMA(J),J=1,NRM)
   22        READ(5,2)(CA(K),K=1,NC)
   23        READ(5,2)(T1A(L),L=1,NT)
   24        READ(5,2)(T2A(L),L=1,NT)
   25        READ(5,3)(E1A(M),M=1,NE)
   26        READ(5,3)(E2A(M),M=1,NE)
   27        READ(5,3)(AA(N),N=1,NA)
   28        DO 100 I=1,NR
   29        DO 100 J=1,NRM
   30        DO 100 K=1,NC
   31        DO 100 L=1,NT
   32        DO 100 M=1,NE
   33        R=RA(I)
   34        RM=RMA(J)
   35        C=CA(K)
   36        T1=T1A(L)
   37        T2=T2A(L)
   38        E1=E1A(M)
   39        E2=E2A(M)
   40        WRITE(6,5)
   41        WRITE(6,6)R,RM,C,T1,T2,E1,E2
   42        DO 100 N=1,NA
   43        A=AA(N)
   44        WRITE(6,7)A
   45        CALL D01ACF((A+RM),(A+RM+C),X,0.0001,0.0001,ACC1,XC,NPTS1,IFAIL)
   46        CALL D01ACF((A+RM),(A+RM+C),Y,0.0001,0.0001,ACC2,YC,NPTS2,IFAIL)
   47        CALL D01ACF((A+RM),(A+RM+C),Z,0.0001,0.0001,ACC3,ZC,NPTS3,IFAIL)
   48        IF((4.*XC*ZC).GT.(YC*YC))GO TO 99
   49        D1=(-YC-SQRT(YC*YC-4.*XC*ZC))/(2.*XC)
   50        D2=(-YC+SQRT(YC*YC-4.*XC*ZC))/(2.*XC)
   51        DO 98 NB=1,2
   52        IF(NB.EQ.1)D=D1
   53        IF(NB.EQ.2)D=D2
   54        P1=(D*RM**2)/(2.*(T1+T2))
   55        CALL D01ACF(RM,(A+RM),P2,0.0001,0.0001,ACC4,P2C,NPTS4,IFAIL)
   56        CALL D01ACF((A+RM),(A+RM+C),P3,0.0001,0.0001,ACC5,P3C,NPTS5,IFAIL)
```

```
      P=(P1+P2C+P3C)*2.
      PCM=((P3C*2.)/P)*100.
      WRITE(6,8)D,P,PCM
   98 CONTINUE
      GO TO 100
   99 WRITE(6,4)
  100 CONTINUE
      STOP
      END
      FUNCTION X(S)
      COMMON R,RM,T1,T2,E1,E2,A,D
      Q=1.0E-12
      IF(S.LT.(A+RM+Q).AND.S.GT.(A+RM-Q))GO TO 101
      V1=SQRT(R**2-(S-RM-A)**2)
      H=R-V1
      T0=T2+(T1/(1.-(((S-RM)**2)/(R**2))))
      V=H+(E1*T0)
      F=((S-RM-A)/V1)+(E1*T1*(S-RM)/(R**2*((1.-(((S-RM)/R)**2))**(3./2.)
     1)))
      X1=(H*F/(V**2))-((S-RM-A)/(V*V1))
      X=X1*S/V
      RETURN
  101 X=0.0
      RETURN
      END
      FUNCTION Y(S)
      COMMON R,RM,T1,T2,E1,E2,A,D
      Q=1.0E-12
      IF(S.LT.(A+RM+Q).AND.S.GT.(A+RM-Q))GO TO 102
      V1=SQRT(R**2-(S-RM-A)**2)
      H=R-V1
      T0=T2+(T1/(1.-(((S-RM)**2)/(R**2))))
      V=H+(E1*T0)
      F=((S-RM-A)/V1)+(F1*T1*(S-RM)/(R**2*((1.-(((S-RM)/R)**2))**(3./2.)
     1)))
      V2=R+(E1*T0)-SQRT(R**2-(S-RM)**2)
      V3=(S-RM-A)*V2/(V*V1)
      V4=H*F*(SQRT(R**2-(S-RM)**2)-V1)/(V**2)
      V5=H*(((S-RM)/(SQRT(R**2-(S-RM)**2)))-((S-RM-A)/V1))/V
      Y1=A*H/(E2*V*(S-A))
      Y2=S*(V3+V4+V5)/V
      V6=(H*F/(V**2))-((S-RM-A)/(V*V1))
      V7=SQRT(R**2-(S-RM)**2)-V1
      Y3=S*V6*V7/V
      Y=Y1+Y2+Y3
      RETURN
  102 Y=0.0
      RETURN
      END
      FUNCTION Z(S)
      COMMON R,RM,T1,T2,E1,E2,A,D
      Q=1.0E-12
      IF(S.LT.(A+RM+Q).AND.S.GT.(A+RM-Q))GO TO 103
      V1=SQRT(R**2-(S-RM-A)**2)
      H=R-V1
      T0=T2+(T1/(1.-(((S-RM)**2)/(R**2))))
      V=H+(E1*T0)
      F=((S-RM-A)/V1)+(F1*T1*(S-RM)/(R**2*((1.-(((S-RM)/R)**2))**(3./2.)
     1)))
      V2=R+(E1*T0)-SQRT(R**2-(S-RM)**2)
      V3=(S-RM-A)*V2/(V*V1)
      V4=H*F*(SQRT(R**2-(S-RM)**2)-V1)/(V**2)
      V5=H*(((S-RM)/(SQRT(R**2-(S-RM)**2)))-((S-RM-A)/V1))/V
      V6=SQRT(R**2-(S-RM)**2)-V1
      V7=SQRT(R**2-(S-RM)**2)-R-(E1*T0)
      Z1=(V3+V4+V5)*V6*S/V
```

```
      Z2=A*H*V7/(V*E2*(S-1))
      Z=Z1+Z2
      RETURN
  103 Z=0.0
      RETURN
      END
      FUNCTION P2(S)
      COMMON R,RM,T1,T2,E1,E2,A,D
      P21=SQRT(1.-((S-RM-1)**2/(R**2)))
      P22=SQRT(1.-((S-RM)**2/(R**2)))
      P23=T2+(T1/P22)
      P2=(S*(D-(R*(1.-P22))))/P23
      RETURN
      END
      FUNCTION P3(S)
      COMMON R,RM,T1,T2,E1,E2,A,D
      P31=SQRT(1.-((S-RM-A)**2/(R**2)))
      P32=SQRT(1.-((S-RM)**2/(R**2)))
      P33=R*(1.-P31)
      P34=R*(P31-P32)
      P35=T2+(T1/P32)
      P36=(R*(1.-P31))+(E1*P35)
      P3=(S*E1*(D-P34))/P36
      IF(P3)104,104,105
  104 P3=0.0
      GO TO 106
  105 P3=P3
  106 CONTINUE
      RETURN
      END
      FINISH
****
```

APPENDIX 2.f Model Analysis Results, Graphical Presentation.

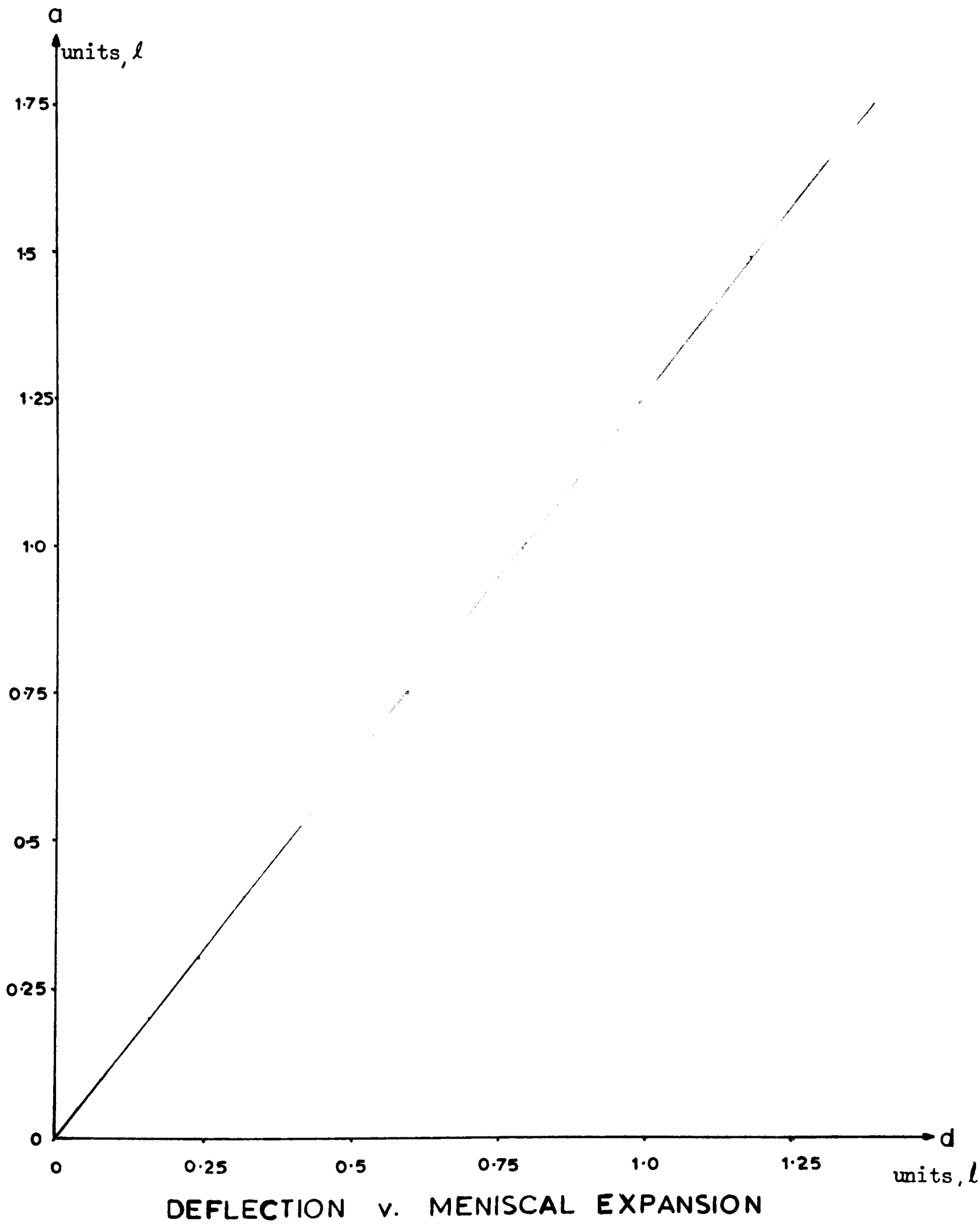

Figure 2.f.1

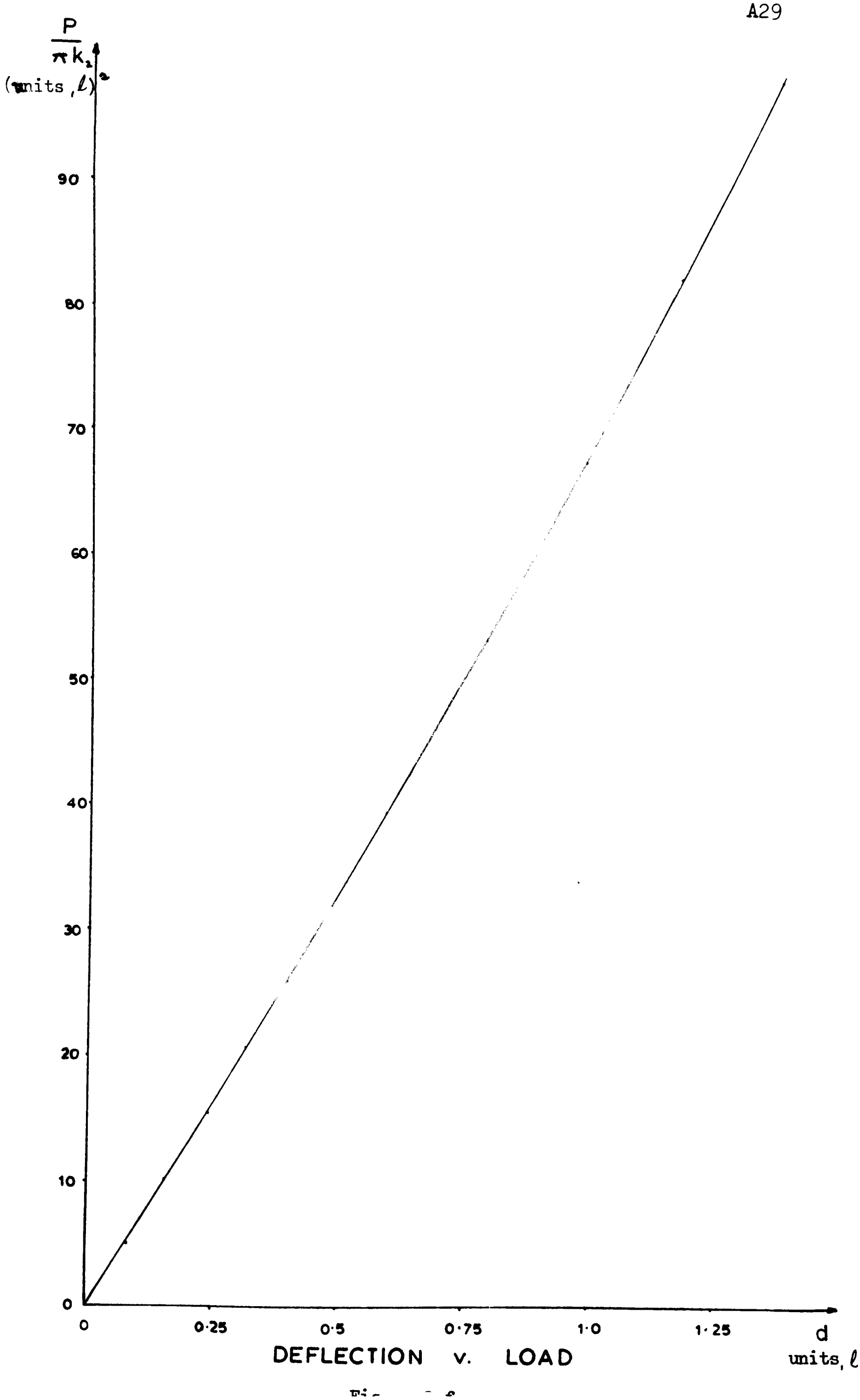
P / πk₂ (units, ℓ)²
90
80
70
60
50
40
30
20
10
0
0
0·25
0·5
0·75
1·0
1·25
d units, ℓ
DEFLECTION v. LOAD

Fig. - -

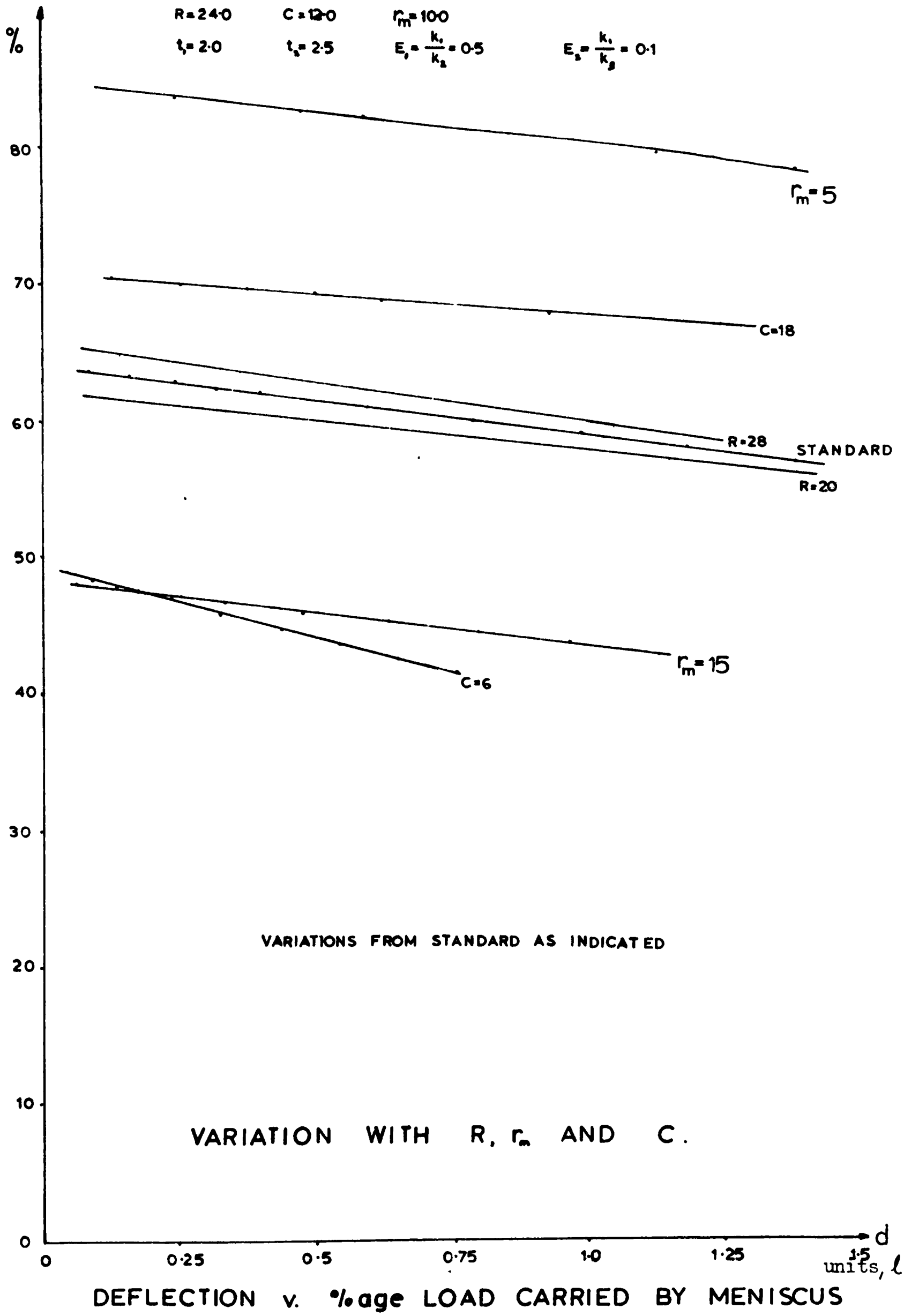
PARAMETER VALUES OF STANDARD CASE
R = 24·0
C = 12·0
r_m = 100
t_1 = 2·0
t_2 = 2·5
$E_1 = \frac{k_1}{k_2}$ = 0·5
$E_2 = \frac{k_1}{k_3}$ = 0·1
%
80
70
60
50
40
30
20
10
0
r_m = 5
C=18
R=28
STANDARD
R=20
r_m = 15
C=6
VARIATIONS FROM STANDARD AS INDICATED
VARIATION WITH R, r_m AND C.
0
0·25
0·5
0·75
1·0
1·25
1·5
d
units, ℓ
DEFLECTION v. %age LOAD CARRIED BY MENISCUS

Figure 2.f.3

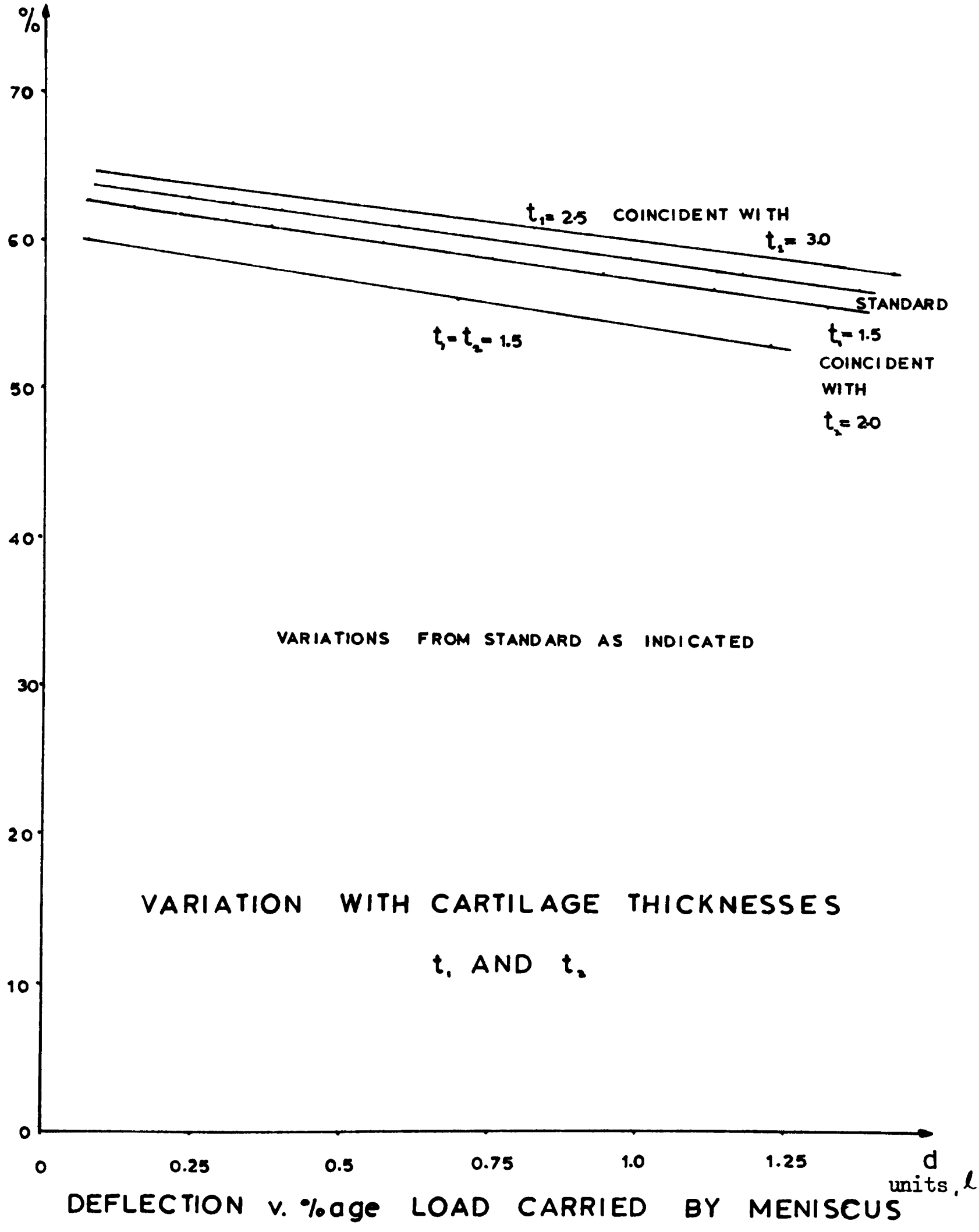
%
70
60
50
40
30
20
10
0
t_1= 2.5 COINCIDENT WITH t_1= 3.0
STANDARD t_1= 1.5
COINCIDENT WITH t_2= 2.0
$t_1 = t_2$ = 1.5
VARIATIONS FROM STANDARD AS INDICATED
VARIATION WITH CARTILAGE THICKNESSES
t_1 AND t_2
0
0.25
0.5
0.75
1.0
1.25
d units, l
DEFLECTION v. %age LOAD CARRIED BY MENISCUS

Figure 2.f.4

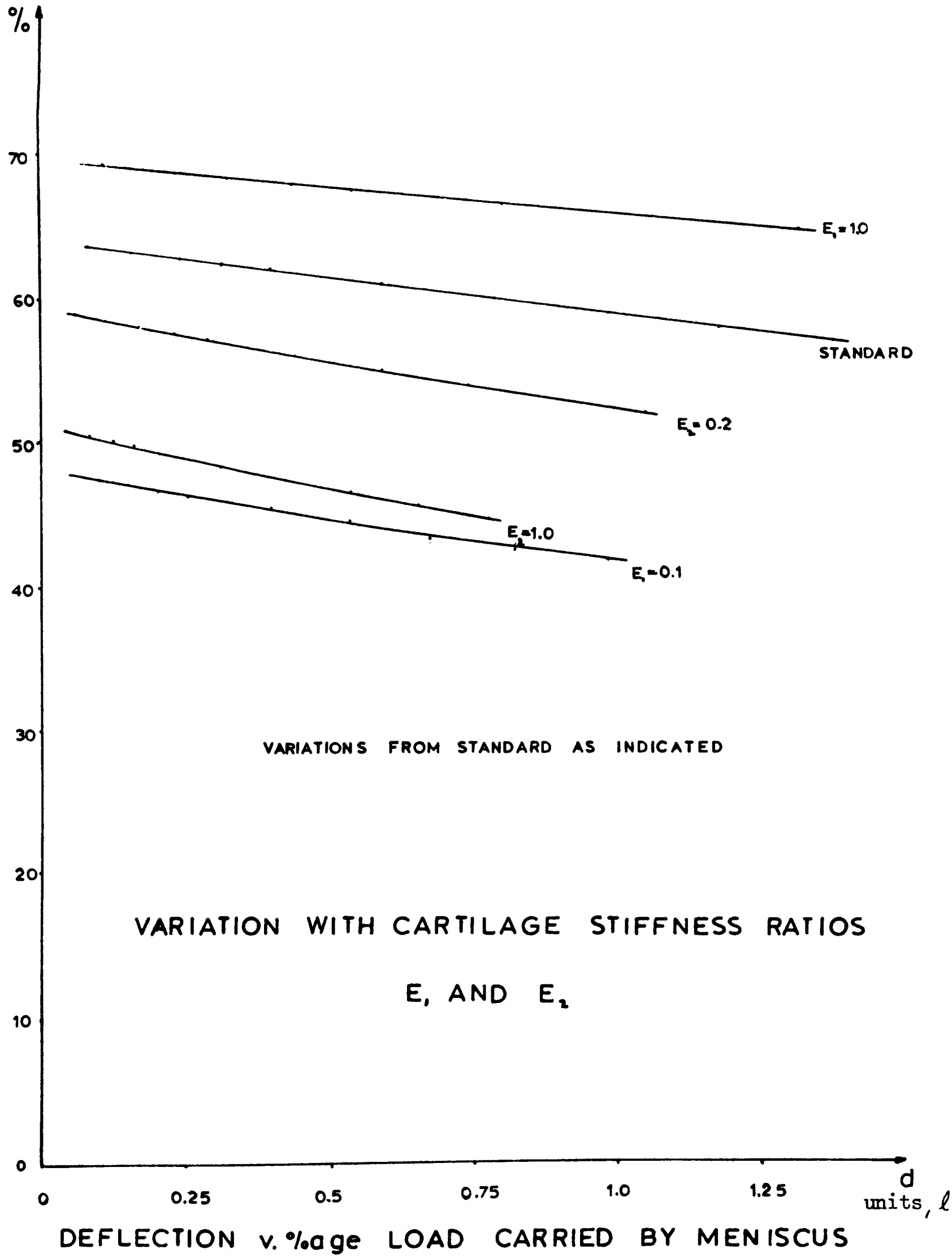
%
70
60
50
40
30
20
10
0
$E_1 = 1.0$
STANDARD
$E_2 = 0.2$
$E_2 = 1.0$
$E_1 = 0.1$
VARIATIONS FROM STANDARD AS INDICATED
VARIATION WITH CARTILAGE STIFFNESS RATIOS
E_1 AND E_2
0
0.25
0.5
0.75
1.0
1.25
d
units, ℓ
DEFLECTION v. %age LOAD CARRIED BY MENISCUS

Figure 2.f.5

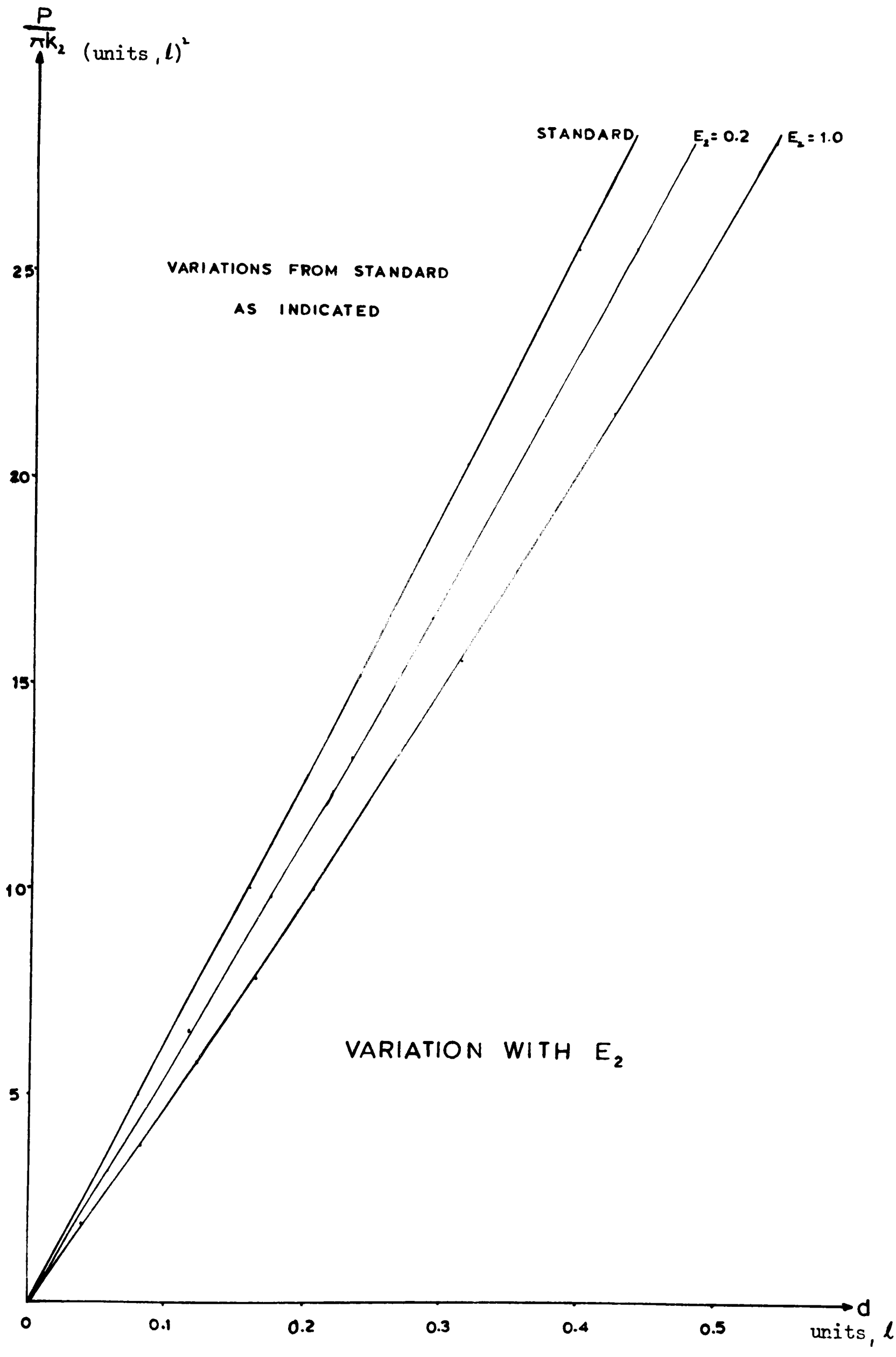
P/πk₂ (units, l)²
STANDARD
E₂ = 0.2
E₂ = 1.0
VARIATIONS FROM STANDARD
AS INDICATED
25
20
15
10
5
0
0.1
0.2
0.3
0.4
0.5
d
units, l
VARIATION WITH E₂
DEFLECTION v. LOAD

Figure 2.f.6

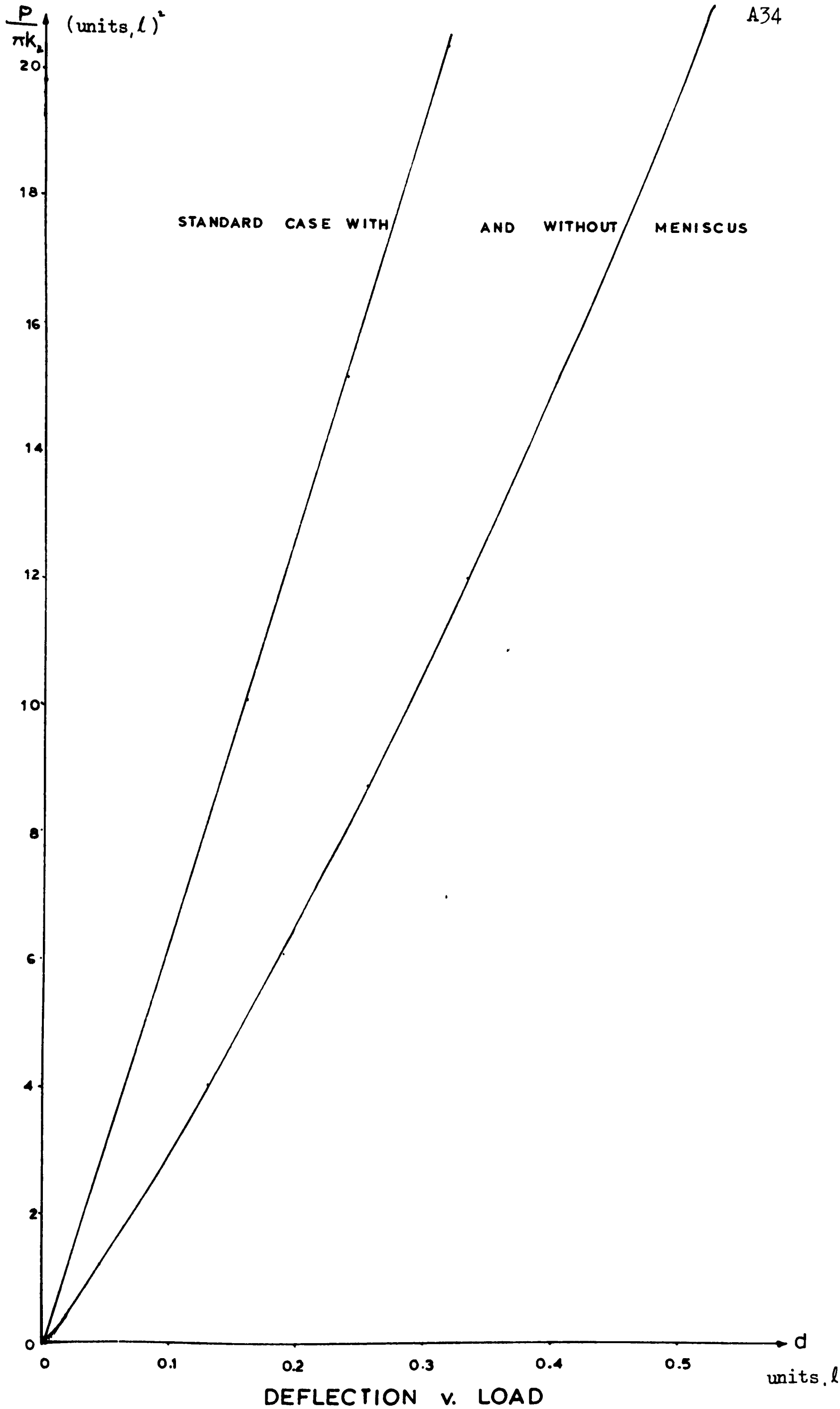

DEFLECTION v. LOAD

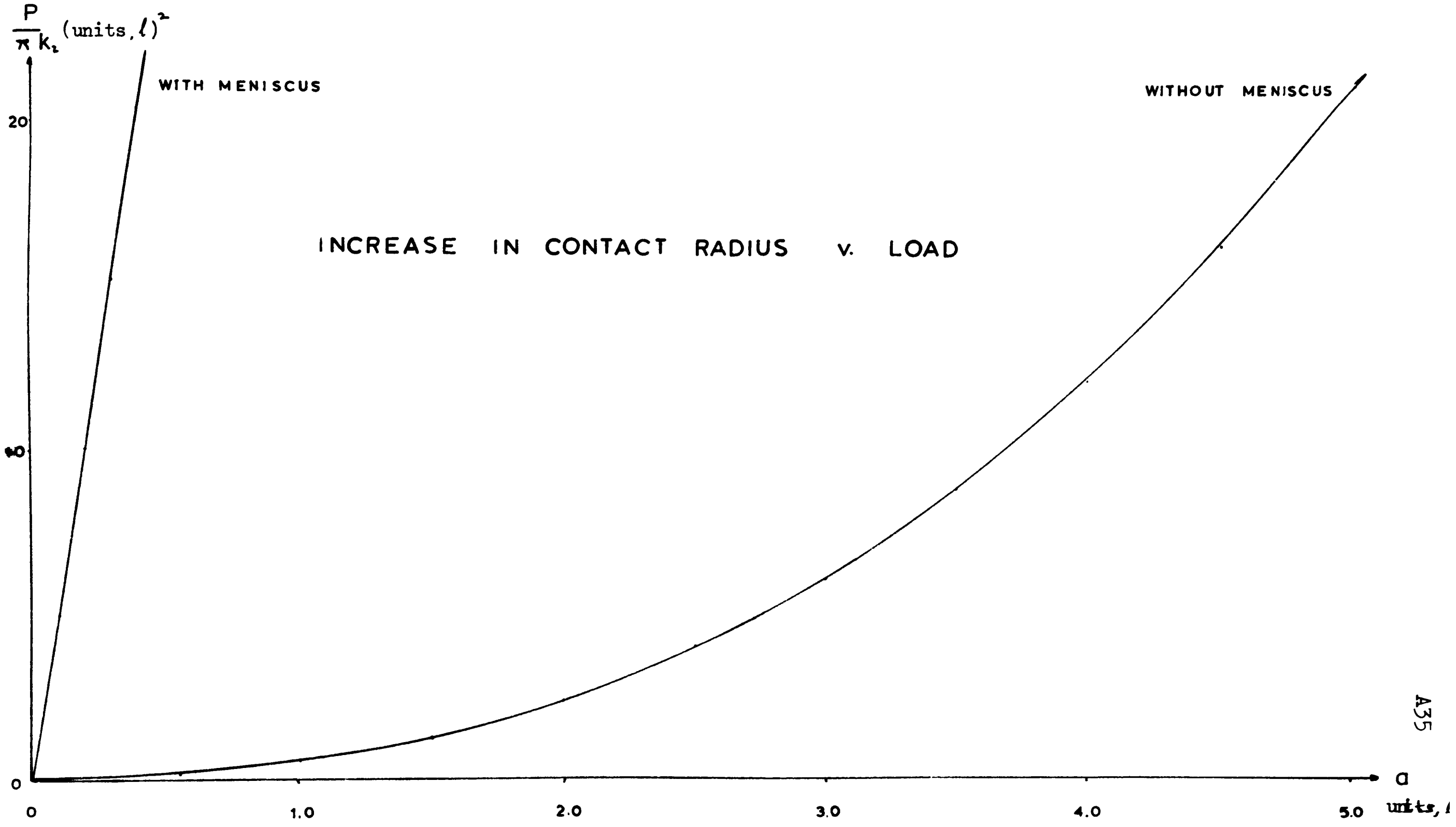

INCREASE IN CONTACT RADIUS v. LOAD

A35

Figure 2.f.8

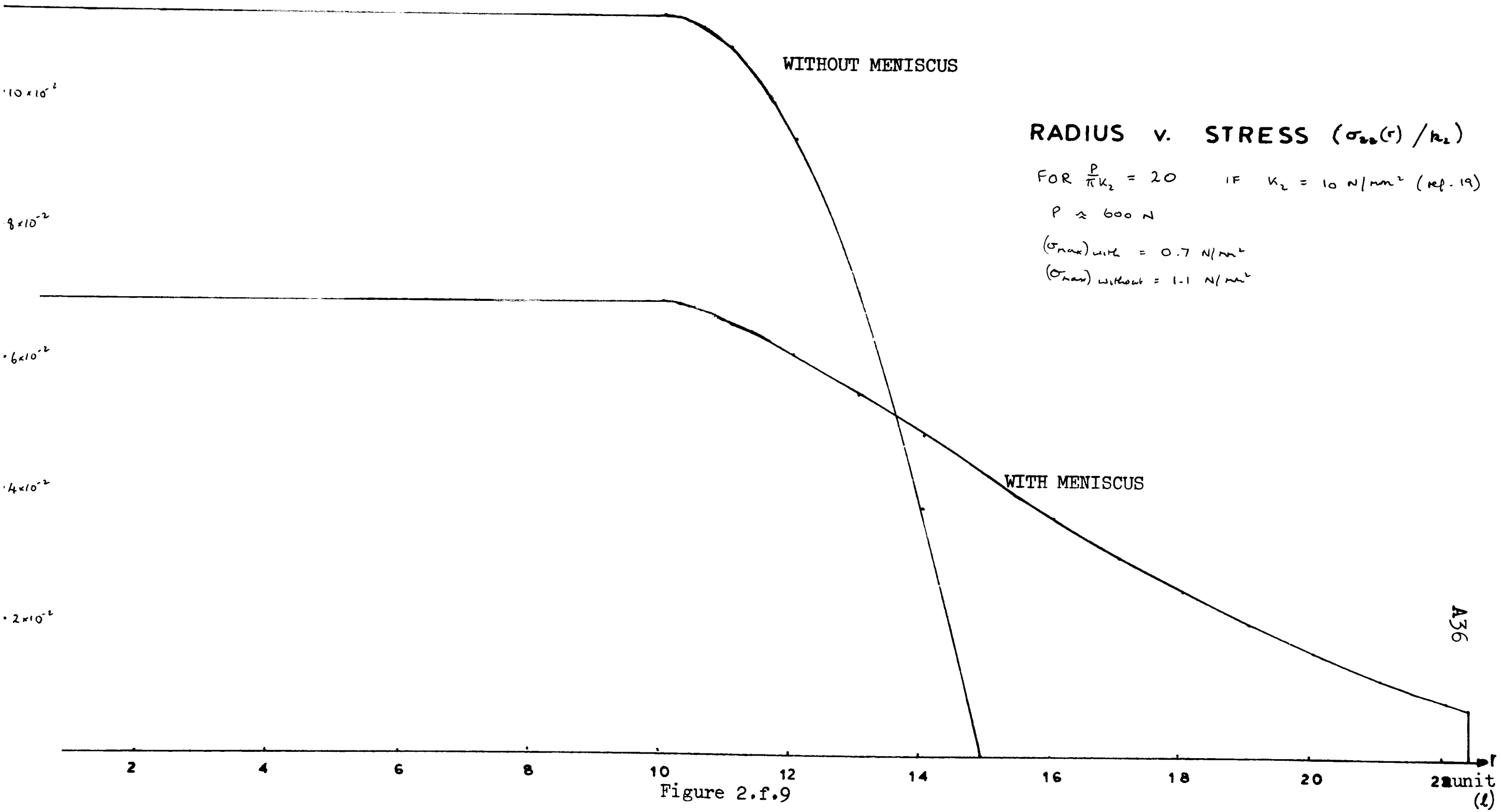

RADIUS v. STRESS ($\sigma_{\theta\theta}(r)/k_2$)

FOR $\frac{P}{\pi k_2} = 20$ IF $k_2 = 10\ N/mm^2$ (ref. 19)

$P \approx 600\ N$

$(\sigma_{max})_{with} = 0.7\ N/mm^2$

$(\sigma_{max})_{without} = 1.1\ N/mm^2$

A36

Figure 2.f.9

APPENDIX 4

This Appendix contains the experimental results, in the following order.

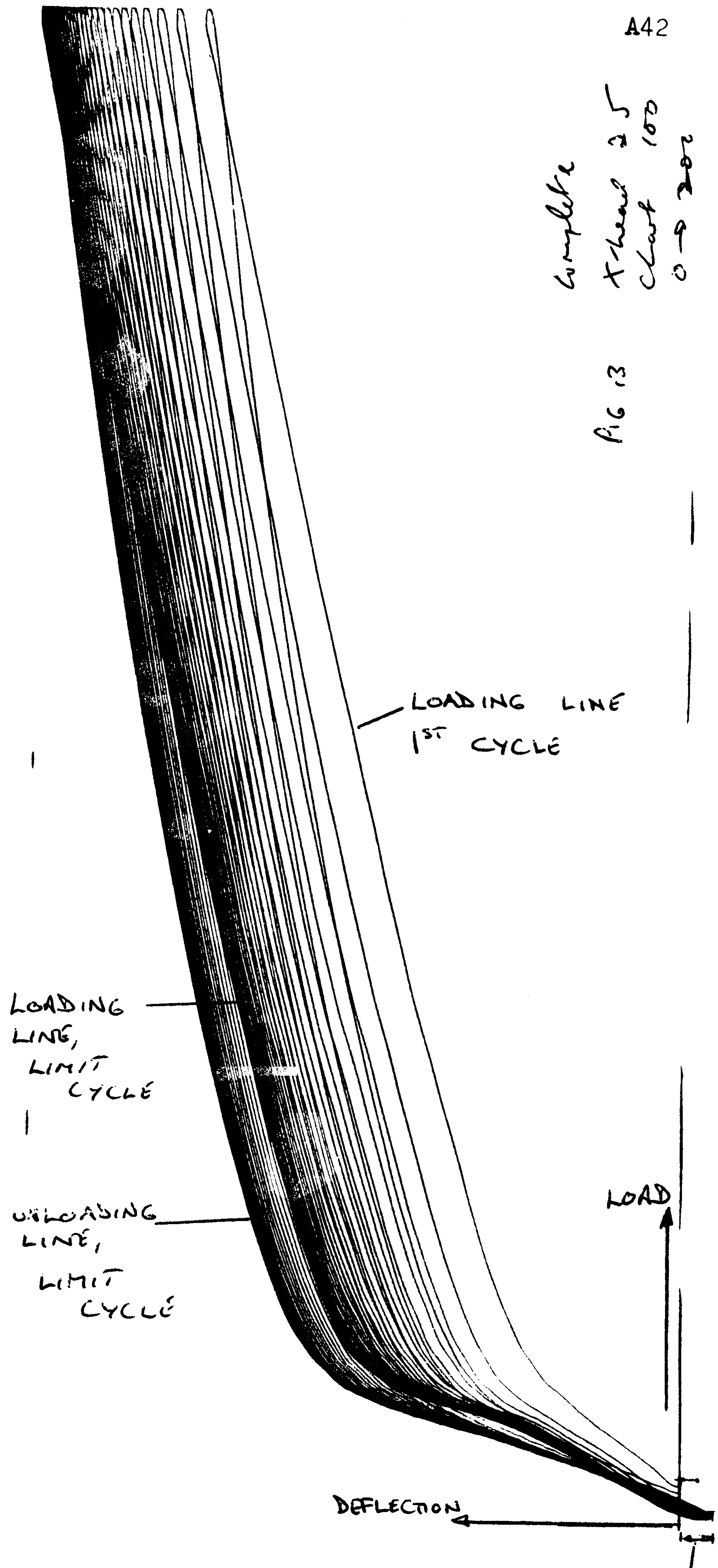

Example of achieval of Limit Cycle.

Specimen No.	Joint Position when tested	Specimen No.	Sex	Age (yrs)	Weight (kg.)	Height (cms)	Joint Position when tested
Pig I	hyperextension	Human I	M	65	63.5	I72	hyperextension
2	"	2	M	60	46.3	I65	"
3	"	3	M	60	69.8	I55	"
4	"	4	F	75	57.I	I62.5	"
5	"	5	F	52	70.0	I69	slight extension
6	"	6	F	73	83.0	I66	"
7	slight extension	7	M	79	63.5	I69	20° flexion
8	"	8	M	73	63.5	I65	30° flexion
9	hyperextension	9	M	76	79.5	I72.5	I5° flexion
I0	"	I0	M	64	67.0	I68	I5° flexion
II	"	II	F	65	38.0	I57	25° flexion
I2	"	I2	M	68	63.5	I68	30° flexion
I3	"	I3	M	42	82.5	I78	5° flexion
I4	"	I4	F	37	5I.0	I6I	neutral
I5	"	I5	M	60	57.0	I66	5° flexion
I6	"	I6	M	73	63.5	I62	I0° flexion
I7	"	I7	M	55	57.0	I64	neutral

Specimen	Test Position	Specimen	Test Position
I8	"		
I9	"	Pig 28	20° flexion	Pig 37	5° flexion
20	"	29	"	38	I0° flexion
2I	"	30	neutral	39	7° flexion
22	"	3I	I5° flexion	40	I0° flexion
23	"	32	neutral	4I	5° flexion
24	"	33	slight extension	42	5° flexion
25	"	34	"	43	20° flexion
26	"	35	I5° flexion	44	5° flexion
27	I0° flexion	36	neutral	45	neutral

SPECIMEN DATA

All pig specimens were from young adult animals approximately 2 yrs. old and weighing between I00 and II0 Kgs..

For human specimens, weight and height are judged at P.M..

(F : Female; M : Male)

Table 4.a.I

Specimen 6 F/73yrs./83.0 kg./166 cms. slight extension

A44

Chart Speed: 100cms./min.
X-head Speed: 2.5cms./min.

(a)complete
(b)patella removed
(c)collaterals cut, soft tissue removed
(d)lateral cut
(e)medial cut
(f)both excised
(g)cruciates cut

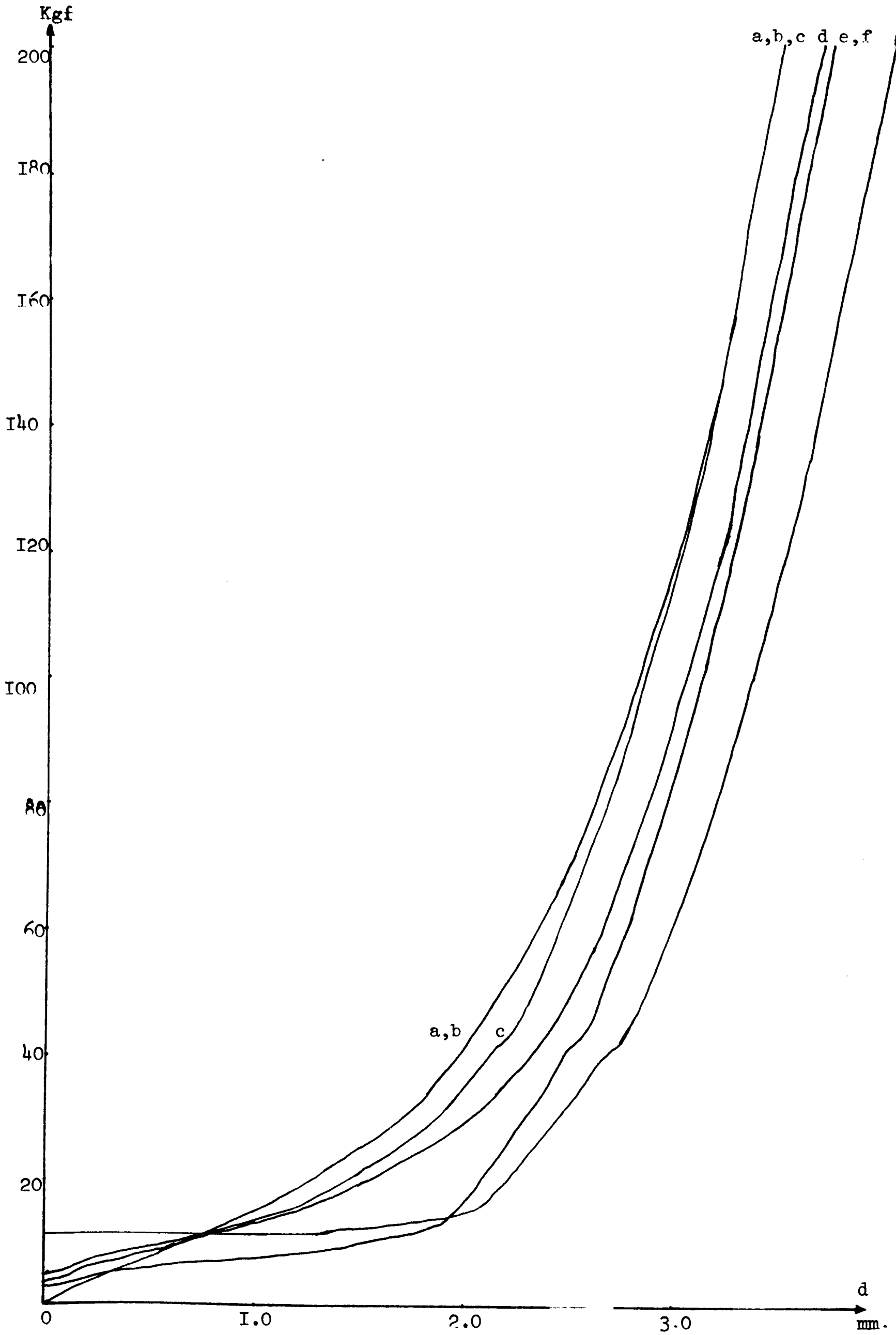

Specimen 7 M/79yrs./63.5 kg./I69 cms. 20° flexion

A45

(a)complete
(b)patella removed
(c)collaterals cut
soft tissue removed
(d)medial cut
(e)lateral cut
(f)both excised
(g)cruciates cut

Chart Speed: I00cms./min.
X-head Speed: 2.5cms./min.

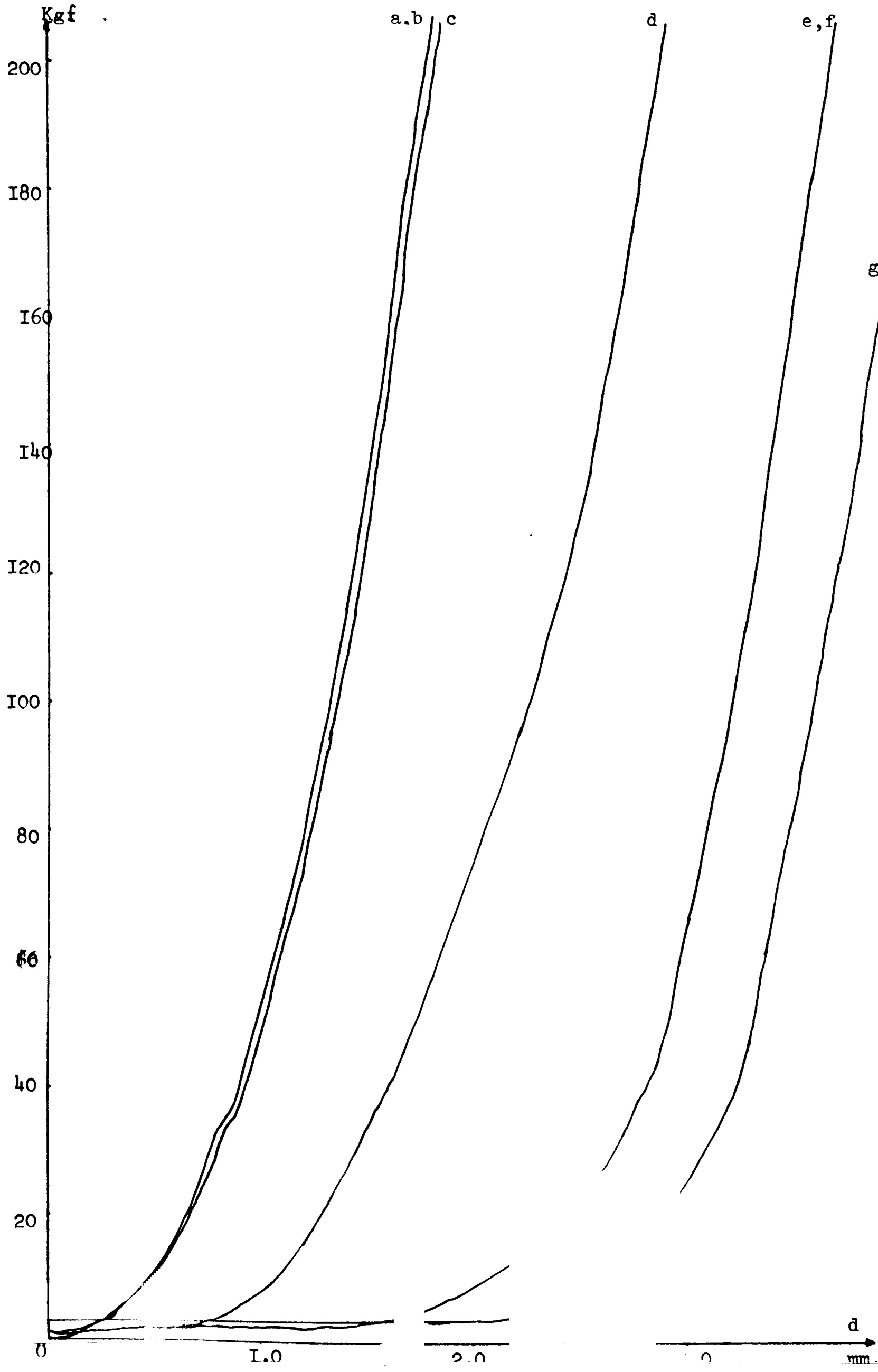

Specimen IO M/64yrs./67.0 kg./I68 cms. I5° flexion

(a)complete
(b)patella removed
(c)collaterals cut
soft tissue removed
(d)lateral cut
(e)medial cut
(f)both excised
(g)cruciates cut

Chart Speed: I00cms /min.
X-head Speed: 2.5cms./min.

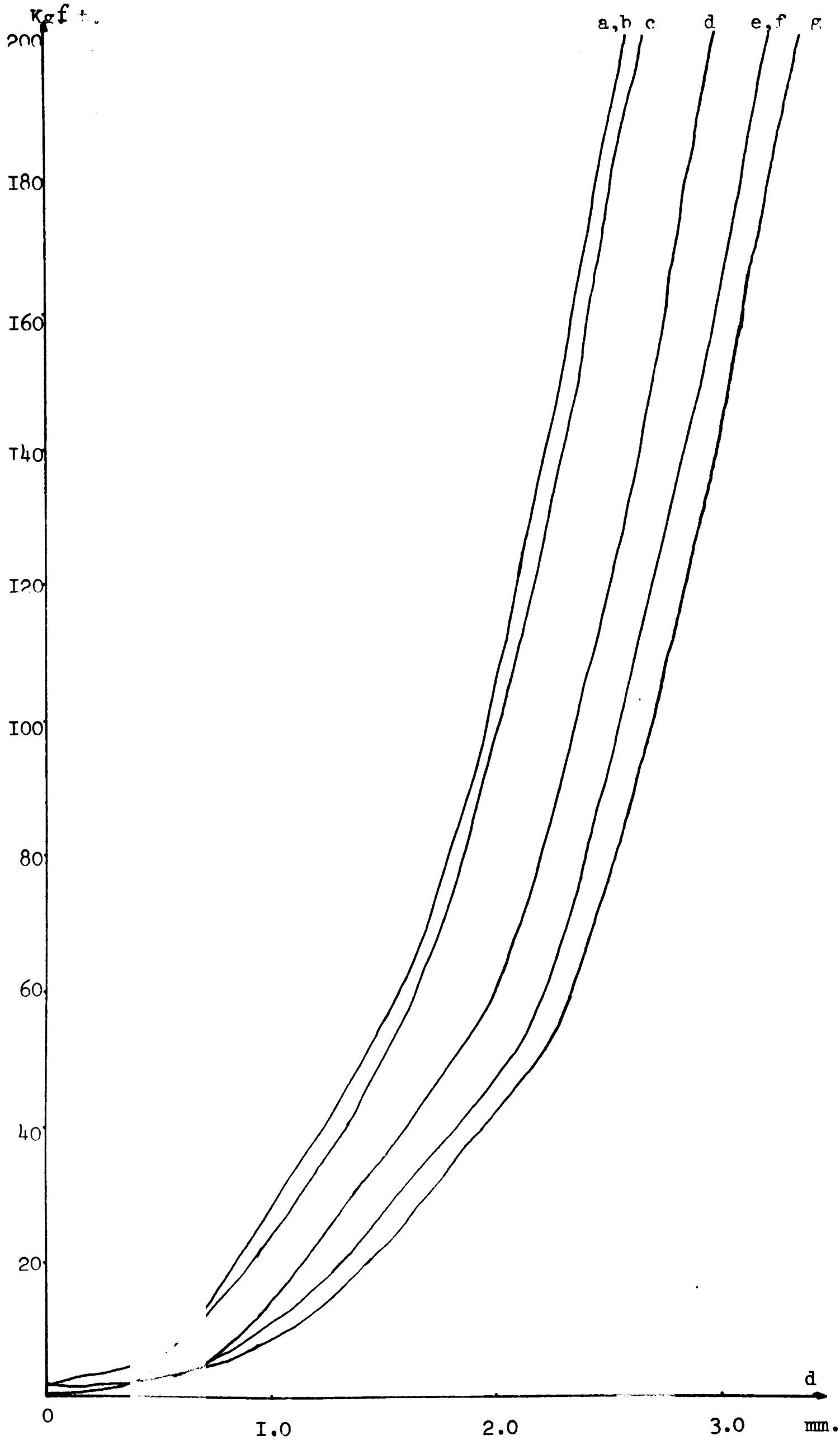

Pig Specimen 2

hyperextension

(a)complete
(b)patella removed
(c)collaterals cut
(d)anterior horns both menisci cut
(e)both excised

Chart Speed: I^0cms./min.
X-head Speed: 2.5cms./min.

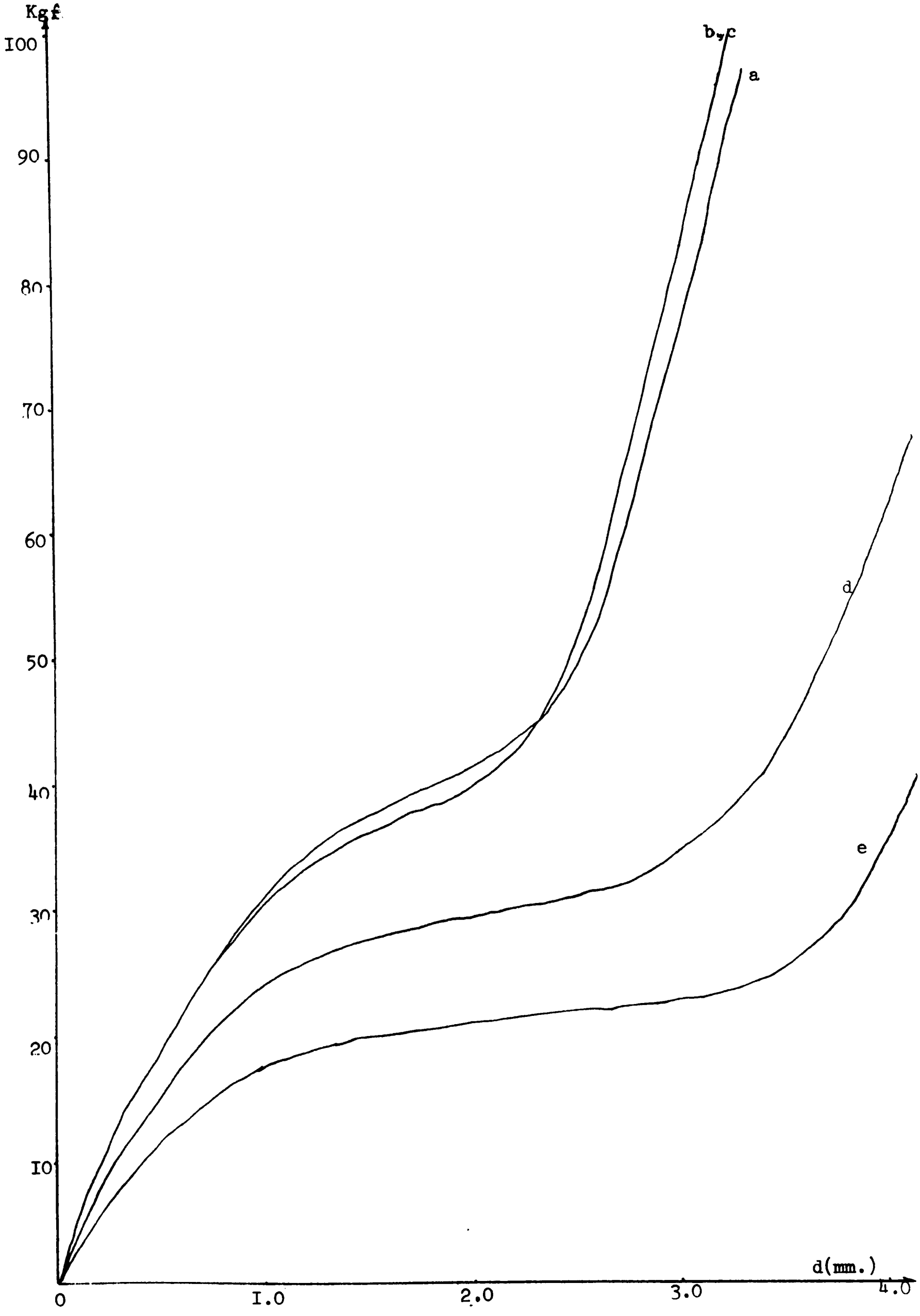

Pig Specimen TO A48 hyperextension

(a) complete
(b) patella removed
(c) collaterals cut soft tissue removed
(d) lateral cut
(e) medial cut
(f) both excised
(g) cruciates cut

Chart Speed: I00cms./min.
X-head Speed: 2.5cms./min.

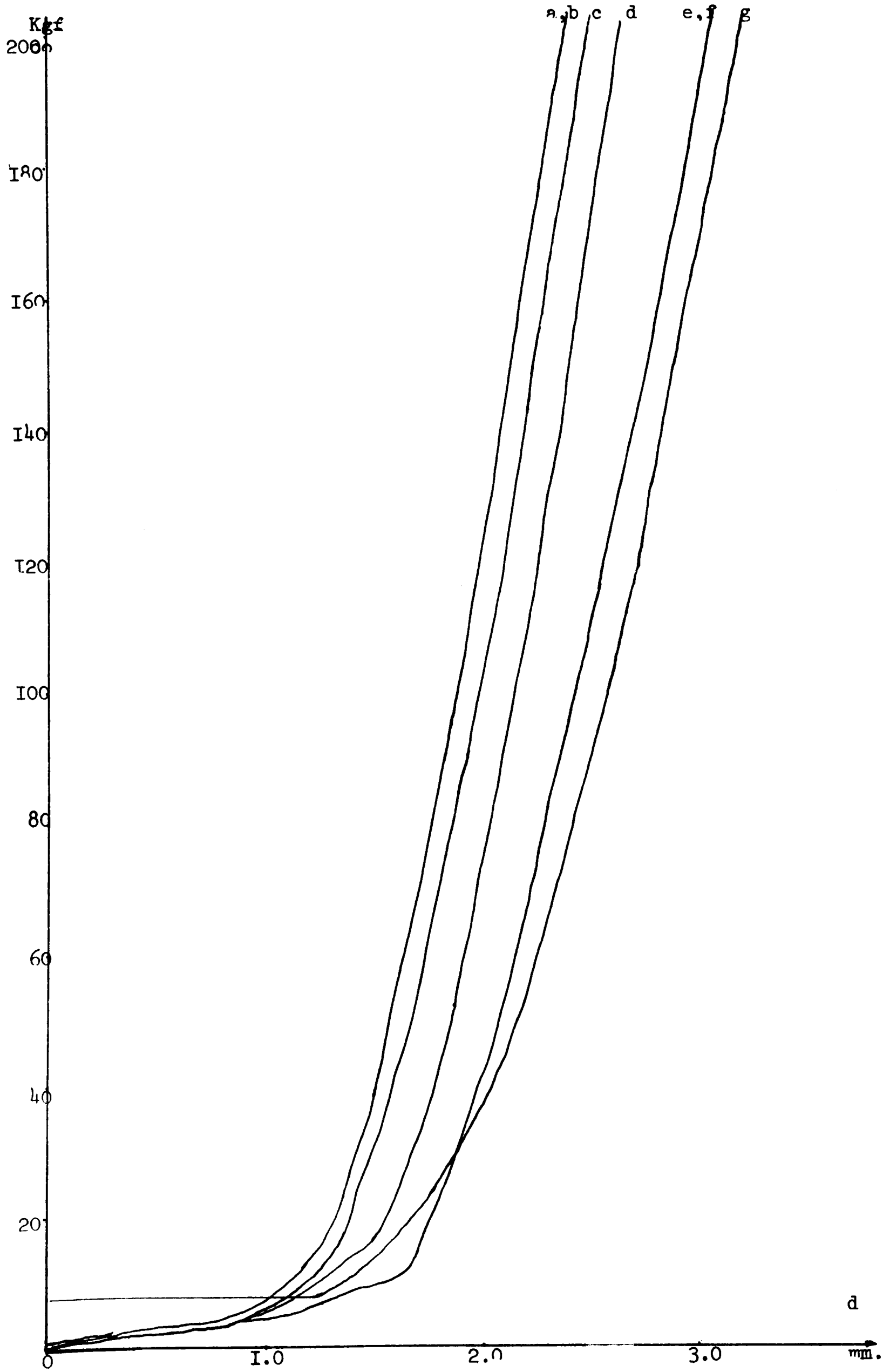

Pig Specimen I5

hyperextension

(a)complete
(b)patella removed
(c)collaterals cut
soft tissue removed
(d)lateral cut
(e)medial cut
(f)both excised
(g)cruciates cut

Chart Speed: I00cms./min.
Y-head Speed: 2.5cms./min.

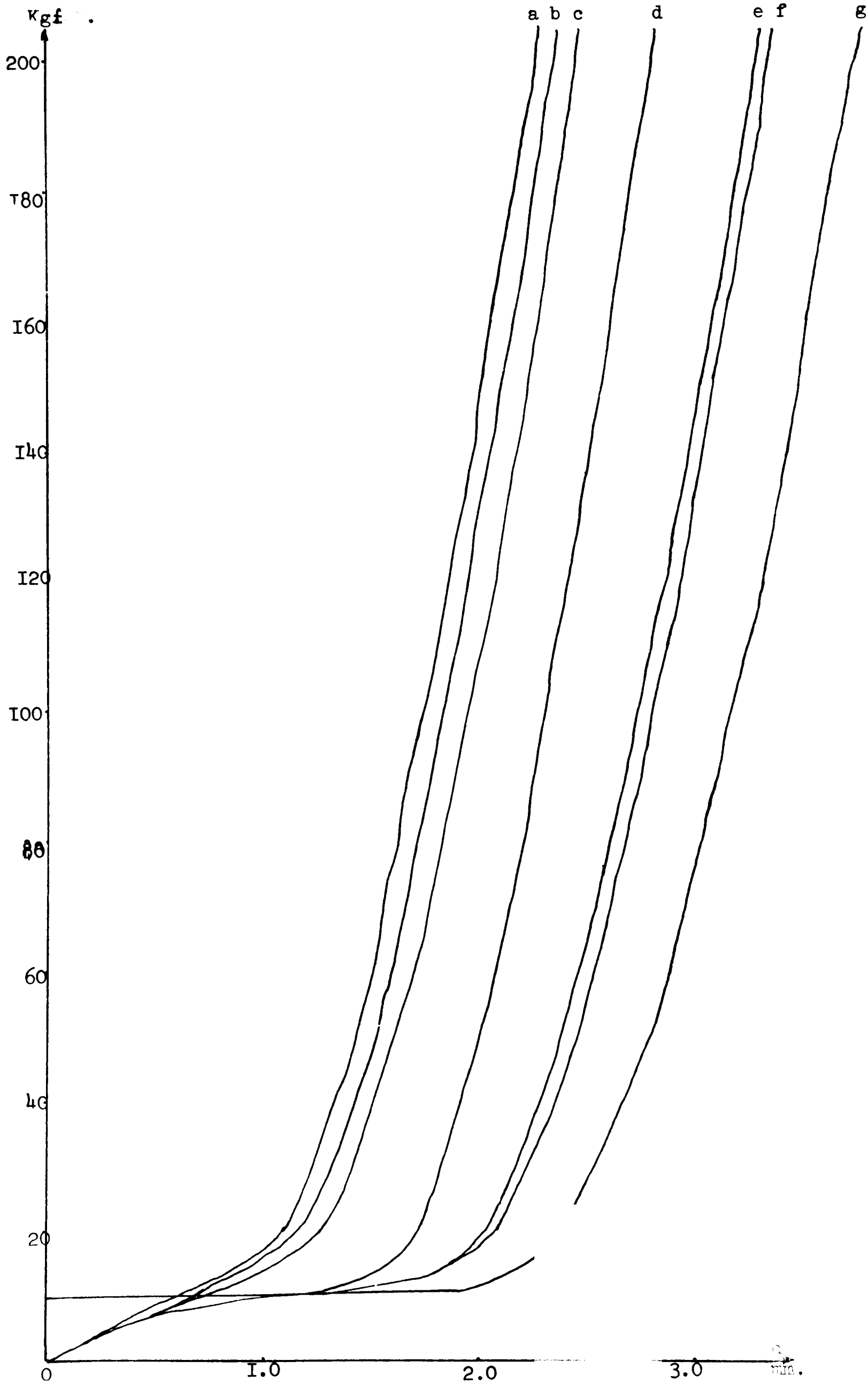

Pig Specimen 3I

A50

I5° flexion

(a)complete
(b)patella removed
(c)collaterals cut
soft tissue removed

(d)medial cut
(e)lateral cut
(f)both excised
anterior dislocation of
femur on tibia after
cutting of cruciates

Chart Speed: I00cms./min.
X-head Speed: 2.5cms./min

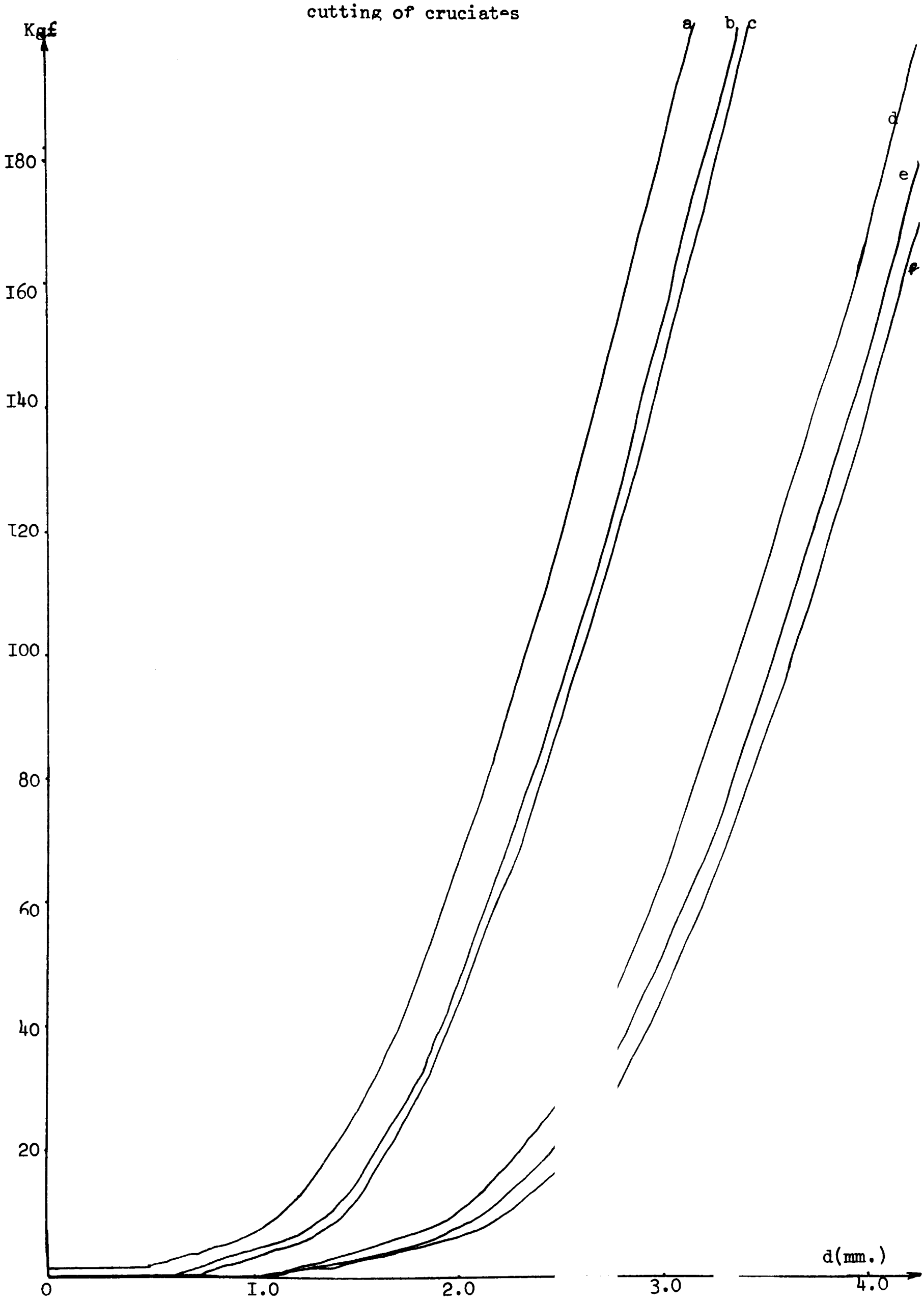

Pig Specimen 44

A51

5° flexion

(a)complete
(b)patella removed
(c)collaterals cut
soft tissue removed
(d)medial cut
(e)lateral cut
(f)both excised
(g)cruciates cut

Chart Speed: 100cms./min.
X-head Speed: 2.5cms./min.

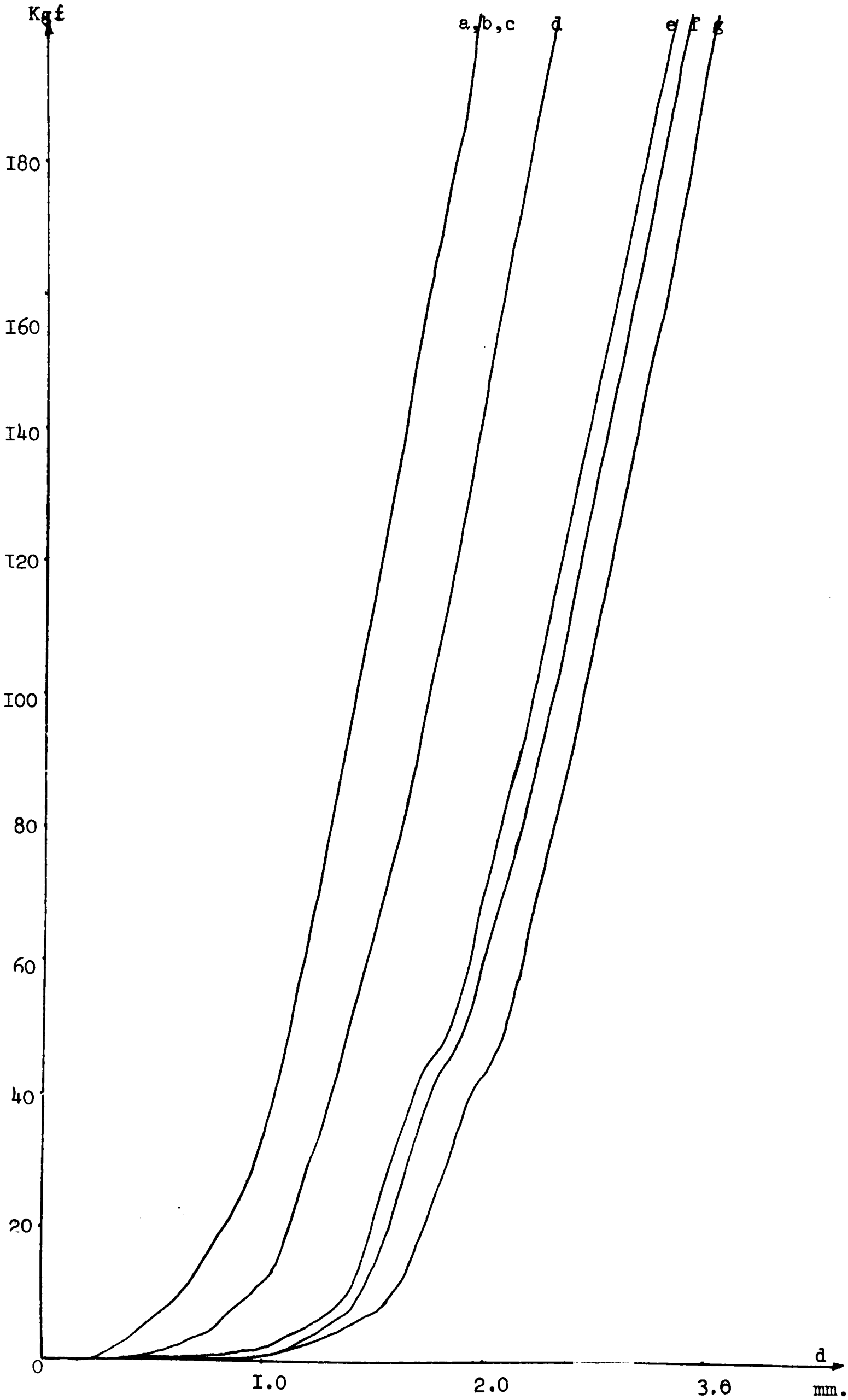

Specimen	P_{col}	$P_{menisci}$	% -age	Specimen	P_{col}	$P_{menisci}$	% -age
Human I	200	I38.5	30.75	I6	200	22.5	88.75
2	I96	I77.5	9.25	I7	I96	48.0	74.0
3	200	I40.0	3000	I8	I62	9.0	76.5
4	I39	65.5	36.75	I9	200	28.0	86.0
5	I69	I30.5	I9.25	2I	I78.5	I4.5	82.0
6	200	I59.0	20.25	22	200.	32.0	84.0
7	I92	6.0	93.0	23	200	7.0	96.5
8	I75	85.0	45.0	24	200	7.5	96.25
9	I93	82.0	55.5	25	I84	47.5	68.25
I0	200	II0.0	45.0	26	200	56.0	72.0
II	I8I.5	II6.0	32.75	27	I89	93.0	48.0
I3	200	I27.0	36.5	28	2000	29.5	85.25
I4	200	I33.0	33.5	29	I92	54.0	69.0
I5	I84	I28.0	28.0	30	200	25.5	87.25
I6	200	II4.5	42.75	3I	I70	56.5	56.75
I7	I66.5	I07.0	29.75	32	I82.5	9.0	86.75
Pig 3	I96.5	47.0	74.75	33	I3I	20.5	55.25
4	I89	42.5	73.25	34	200	84.0	58.0
5	200	20.0	90.0	35	I66	33.0	66.5
6	I88	I2.5	87.75	36	I67	I2.0	77.5
7	200	29.0	85.5	37	I74	22.0	76.0
8	200	38.0	8I.0	38	I87	2I.0	83.0
9	200	43.0	78.5	39	I76	50.0	63.0
I0	I65.5	72.5	46.5	40	I64.5	34.0	65.25
II	I89	37.0	76.0	4I	I70	20.5	74.75
I2	200	27.0	86.5	42	I67	I5.0	76.0
I3	I89	26.0	8I.5	43	I58	46.0	56.0
I4	I84	20.0	82.0	44	200	48.5	75.75
I5	I52	28.0	62.0	45	I65	49.0	58.0

LOADS AT DEFLECTION FOR COMPLETE JOINT UNDER 200 Kgf LOAD.

Table 4.a.2

Specimen	P_{col}	$P_{menisci}$	% -age	Specimen	P_{col}	$P_{menisci}$	% -age
Human I	I50	95.2	36.5	Pig I6	I50	I8.65	87.6
2	I43.5	II9.0	I6.3	I7	I44	3I.0	75.3
3	I50	93.0	38.0	I8	II6.8	8.3	72.3
4	I00	5I.0	32.7	I9	I50	I9.8	86.8
5	I22	94.0	I8.7	2I	I30.5	I3.0	78.3
6	I48	I09.0	26.0	22	I50.0	24.8	83.5
7	I42	5.I	9I.3	23	I50	3.5	97.7
8	I30	59.0	47.3	24	I50	6.0	96.0
9	I43.5	48.0	63.7	25	I36	29.0	7I.4
I0	I42	75.5	44.3	26	I50	4I.5	72.3
II	I29	76.7	34.9	27	I4I.5	56.8	56.5
I3	I50	85.6	42.9	28	I50	II.2	92.5
I4	I50	88.5	4I.0	29	I37.5	28.0	73.0
I5	I35	89.5	30.3	30	I50	I7.7	88.2
I6	I50	82.0	45.3	3I	II8.5	30.6	58.6
I7	I20	74.0	30.65	32	I38	6.6	87.6
Pig 3	I44.5	36.6	75.6	33	90	I2.8	5I.5
4	I42	26.6	77.0	34	T50	53.5	64.3
5	I50	I2.0	92.0	35	I2I	I4.I	7I.2
6	I40.4	9.8	87.0	36	I30	I0.0	80.0
7	I50	I7.0	88.7	37	I23	I0.8	74.7
8	I50	23.0	84.7	38	I39	IT.25	85.T5
9	T50	35.2	76.5	39	I3T.5	24.0	7I.6
IB	I23	47.2	50.I	40	II7.5	I8.0	66.3
II	I39	29.4	73.I	4I	I28.5	8.9	79.7
I2	I50	27.8	8I.7	42	I22	I0.I	74.6
I3	I42	24.0	78.7	43	II2	23.5	59.0
I4	T43	I0.I	88.6	44	I50	3I.5	79.0
I5	I05.5	I4.0	6I.0	45	TI3	24.0	59.4

LOADS AT DEFLECTION FOR COMPLETE JOINT UNDER I50 Kgf LOAD

Table 4.a.3

Specimen	P_{col}	$P_{menisci}$	%- age	Specimen	P_{col}	$P_{menisci}$	% -age
Human I	I00	59.6	40.4	Pig I6	I00	I5.5	84.5
2	97.7	73.0	24.7	I7	97	22.8	74.2
3	I00	49.3	50.7	I8	74.5	7.3	67.2
4	68.4	35.0	33.4	I9	I00	I4.0	86.0
5	82	64.5	I7.5	2I	92.5	T0.75	8I.75
6	93	6I.3	3I.7	22	I00	I5.0	85.0
7	93	3.7	89.3	23	I00	3.I	96.9
8	87	37.3	49.7	24	T00	4.0	96.0
9	95	I3.3	8I.7	25	86	I6.5	69.5
I0	94.7	48.2	46.5	26	T00	29.25	70.75
II	84.5	38.0	46.5	27	93.5	23.4	70.I
I3	T00	46.5	53.5	28	I00	3.8	96.2
I4	I00	48.0	52.0	29	90	7.2	82.8
I5	88.5	60.0	28.5	30	I00	I4.3	85.7
I6	I00	49.0	5I.0	3I	74	I2.85	6I.I5
I7	77.5	43.7	33.8	32	88.5	5.8	82.7
Pig 3	93.6	27.35	66.25	33	53.0	9.5	43.5
4	94	I9.5	74.5	34	I00	28.4	7I.6
5	I00	6.6	93.4	35	76.5	6.9	69.6
6	93.5	8.6	84.9	36	79.5	8.0	7I.5
7	I00	I0.0	90.0	37	78.5	7.9	70.6
8	I00	II.8	88.2	38	89.5	4.8	85.7
9	I00	26.0	74.0	39	84.0	I0.6	73.4
I0	75.2	23.5	5I.7	40	72.0	9.0	63.0
II	90.7	20.0	70.7	4I	8I.4	5.4	76.0
I2	I00	I4.9	85.I	42	72.5	7.0	65.5
I3	97.5	I8.I	79.4	43	67.4	I2.85	54.5
I4	93	I8.0	75.0	44	I00	9.0	9I.0
I5	64.6	9.8	54.8	45	73.	II.75	6I.25

LOADS AT DEFLECTION FOR COMPLETE JOINT UNDER I00 Kg£ LOAD

Table 4.a.4

Specimen	P_{col}	$P_{menisci}$	% -age	Specimen	P_{col}	$P_{menisci}$	% -age
HumanI	50	28.0	44.0	Pig I6	50	II.75	76.5
2	46.7	32.6	28.2	I7	48	I6.2	63.6
3	50	I9.5	6I.0	I8	35.6	6.8	57.6
4	32.5	I6.I5	32.7	I9	50	9.8	80.4
5	4I	32.3	I7.4	2I	45.5	7.9	75.2
6	37.5	20.7	33.6	22	50	7.9	84.2
7	42.3	3.0	78.6	23	50	2.5	95.0
8	42.6	I2.0	6I.2	24	50	I.9	96.2
9	46.5	3.7	85.6	25	4I.2	I3.5	55.4
I0	45	25.0	40.0	26	50	I8.6	62.8
II	43	9.I	67.8	27	45.3	9.0	72.6
I3	50	I4.9	70.2	28	50	0.9	98.2
I4	50	I8.0	64.0	29	4I.5	2.I5	78.7
I5	4o	I8.2	43.6	30	50	I2.9	74.2
I6	50	22.6	54.8	3I	30.5	5.0	5I?0
I7	34.4	I6.5	35.8	32	40.75	2.9	75.7
Pig 3	48	22.4	5I.2	33	25.3	II.5	77.6
4	47	I2.8	68.4	34	50	9.75	80.5
5	50	5.2	89.6	35	33.5	2.5	62.0
6	50	8.6	82.8	36	38.5	5.8	65.4
7	50	7.2	85.6	37	34.8	2.5	64.6
8	50	6.4	87.2	38	42	3.3	77.4
9	50	9.2	8I.6	39	39	7.5	63.0
I0	33.5	8.25	50.5	40	3I.6	2.3	58.6
II	44.4	II.2	66.4	4I	39	3.75	67.2
I2	50	3.8	92.4	42	30.2	4.I5	52.I
I3	50	I5.3	69.4	43	33.5	8.35	50.3
I4	46.4	I6.5	59.8	44	50	3.0	94.0
I5	26.2	9.I	34.2	45	29	8.0	42.0

LOADS AT DEFLECTION FOR COMPLETE JOINT UNDER 50 Kgf LOAD

Table 4.a.5

Specimen	40 kgf	60 kgf	80 kgf	I00 kgf	I20 kgf	I40 kgf	I60 kgf	I80 kgf	200 kgf
Human I	I.23	I.I8	I.07	I.05	I.03	0.98	0.96	0.95	0.97
2	0.96	I.03	I.05	I.07	I.03	I.02	I.09	I.09	I.09
3	0.96	0.87	0.89	0.84	0.86	0.87	0.95	I.0	I.0
4	I.34	I.24	I.08	0.92	0.78	0.82	0.85	0.87	0.88
5	I.09	0.85	0.87	0.95	0.97	0.96	I.04	I.04	I.05
6	0.83	0.6	0.72	0.76	0.77	0.86	0.85	0.97	0.95
7	I.02	0.89	0.9	0.98	I.0I	I.0	0.99	0.97	I.0
8	0.63	0.59	0.6I	0.74	0.92	I.06	I.I	I.06	I.02
9	0.37	0.47	0.63	0.76	0.87	0.88	0.9	0.89	0.88
I0	I.37	0.79	0.93	I.0I	I.02	I.0	I.04	I.I4	I.I2
II	I.0I	I.I	I.I3	I.I3	I.I3	I.02	I.0I	I.03	I.0
I2	0.9I	I.I	I.04	I.06	I.05	I.02	I.03	I.05	I.05
I4	I.II	I.I7	I.I	I.08	I.07	I.02	I.0I	I.0I	0.99
I5	I.I9	I.07	0.82	0.66	0.92	0.97	0.97	0.96	0.94
I6	I.03	0.97	I.I	I.03	I.I5	I.I5	I.I6	I.II	I.I
I7	I.I9	I.I	I.I	I.04	I.07	I.06	I.09	I.06	I.0

HUMAN SPECIMENS : SLOPE RATIOS AT VARIOUS LOADS

$$\text{Slope ratio} = \frac{\text{Joint Stiffness with menisci}}{\text{Joint Stiffness without menisci}} = \frac{\left(P/d\right) \text{ with}}{\left(P/d\right) \text{ without}}$$

Table 4.a.6

Specimen	60	80	I00	I20	I40	I60	I80	200
Pig 3	I.44	I.44	I.I5	I.02	I.0	I.02	I.0	I.08
4	I.69	I.55	I.42	I.4I	I.3	I.25	I.25	I.27
5	2.04	I.25	I.52	I.3I	I.27	I.28	I.28	I.25
6	I.42	I.27	I.22	I.23	I.I8	I.I9	I.2	I.26
7	I.9I	I.57	I.49	I.5	I.5	I.39	I.35	I.35
8	I.57	I.27	I.22	I.I7	I.I8	I.2I	I.2I	I.22
9	0.65	0.65	0.99	I.06	I.I2	I.I	I.09	I.06
I0	I.26	I.26	I.27	I.27	I.2	I.I7	I.I	I.09
II	I.56	I.6	I.6I	I.67	I.49	I.48	I.39	I.35
I2	I.22	I.24	I.22	I.2	I.I8	I.I8	I.I8	I.I8
I3	2.0	I.55	I.42	I.39	I.36	I.38	I.38	I.39
I4	I.28	I.38	I.39	I.24	I.35	I.33	I.3I	I.38
I5	I.24	I.I7	I.I7	I.II	I.I	I.07	I.0	I.0
I6	2.04	I.8I	I.54	I.46	I.4I	I.37	I.34	I.37
I7	0.86	I.07	I.08	I.I	I.I2	I.I3	I.07	I.0
I8	0.8	0.87	I.05	I.07	I.09	I.0	I.07	I.I4
I9	I.65	I.44	I.32	I.30	I.26	I.2I	I.22	I.26
2I	I.59	I.36	I.38	I.36	I.24	I.28	I.30	I.35
22	I.54	I.48	I.33	I.3I	I.22	I.II	I.II	I.II
23	I.29	I.3	I.25	I.25	I.24	I.I6	I.I5	I.I5
24	I.35	I.38	I.35	I.43	I.44	I.32	I.23	I.I8
25	I.49	I.I9	I.08	I.0I	I.0	I.I	I.0	I.08
26	I.63	I.04	I.33	I.I8	I.I6	I.0	0.98	I.09
27	I.09	I.05	I.05	I.I5	I.II	I.09	I.05	I.05
28	I.08	I.2I	I.I6	I.2	I.I7	I.I8	I.I6	I.27
29	I.0I	I.I	I.08	I.I8	I.I4	I.I0	I.I4	I.II
30	I.I6	I.04	I.02	I.02	I.20	I.26	I.04	I.05
3I	I.I9	I.I2	I.0I	I.03	I.04	0.98	0.97	I.03
32	I.5	I.45	I.39	I.36	I.33	I.29	I.29	I.29
33	I.89	I.8I	I.64	I.48	I.42	I.27	I.23	I.24
34	I.04	0.98	I.05	I.07	I.05	I.05	I.05	I.05
35	I.I5	I.08	I.0	I.0I	I.03	I.08	I.08	I.I
36	I.35	I.26	I.3I	I.3I	I.33	I.23	I.3I	I.3
37	I.23	I.I6	I.I7	I.22	I.I9	I.23	I.22	I.23
38	I.57	I.64	I.55	I.48	I.38	I.36	I.33	I.26
39	I.I9	I.27	I.24	I.25	I.23	I.I7	I.I3	I.I5
40	I.47	I.3	I.22	I.2I	I.22	I.22	I.3I	I.35
4I	I.67	I.47	I.35	I.26	I.35	I.42	I.32	I.28
42	I.63	I.58	I.6	I.52	I.6	I.59	I.59	I.57
43	I.08	I.I7	I.2	I.I6	I.I4	I.I5	I.I2	I.09
44	I.I7	I.26	I.27	I.28	I.3I	I.29	I.23	I.I8
45	I.2	I.I8	I.I6	I.I9	I.I9	I.I9	I.I9	I.I9

PIG SPECIMENS : SLOPE RATIOS AT VARIOUS LOADS (Kg£)

Specimen II Load Relaxation Tests 25° flexion

(a)complete

(b)post meniscectomy

Time Scales: 20cms. : I min. for 30secs.

½ cm. : I min. for remainder

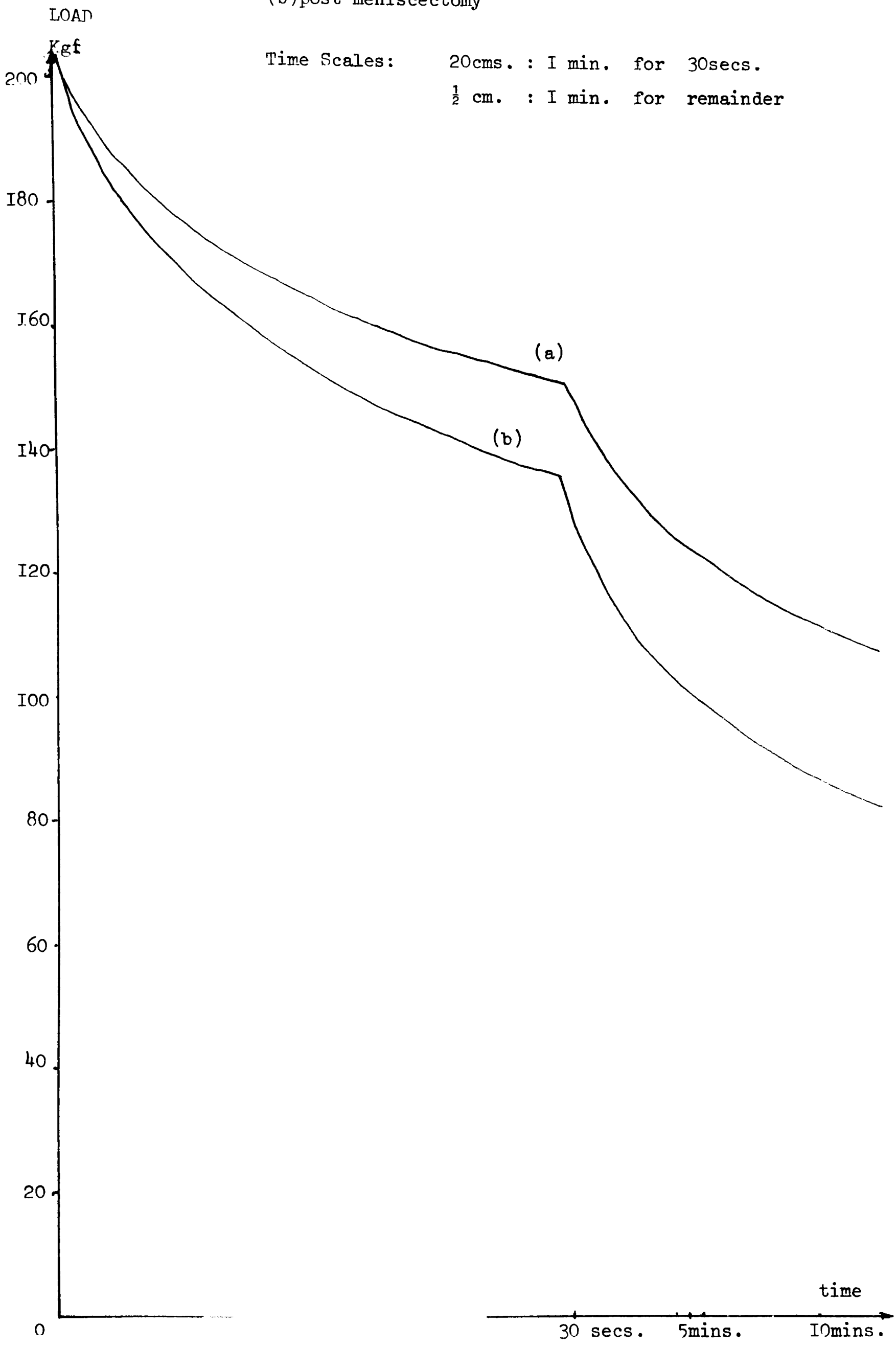

Pig Specimen 33 Load Relaxation Tests slight extension

A59

(a)complete

(b)post meniscectomy

Time Scales: 20cms. : I min. for 30secs.
2cms. : I min. for remainder

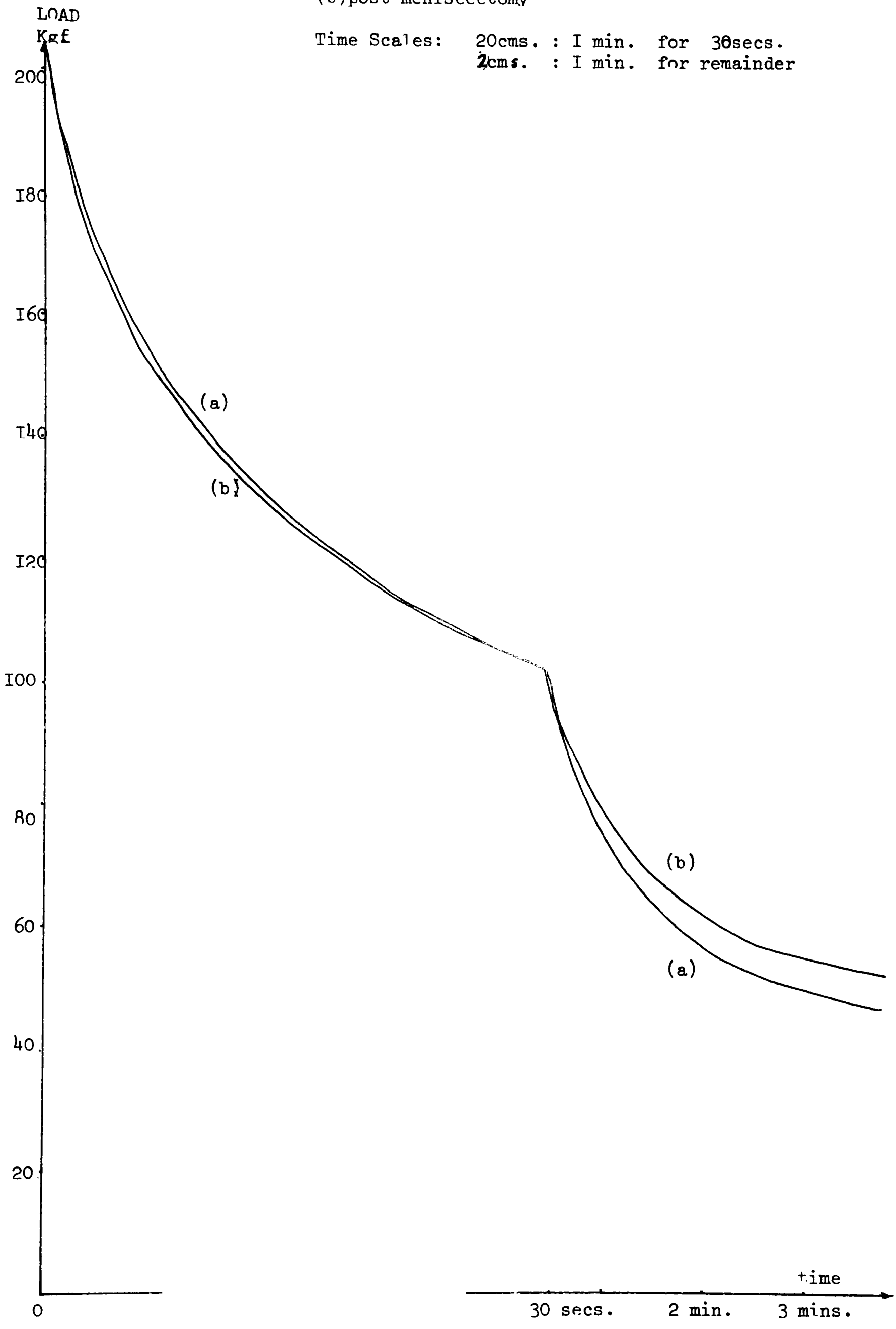

Pig Specimen 45 Load Relaxation Tests neutral

A60

(a) complete

(b) post meniscectomy

Time Scales: 20cms. : I min. for 30secs.
$\frac{1}{3}$cm. : I min. for remainder

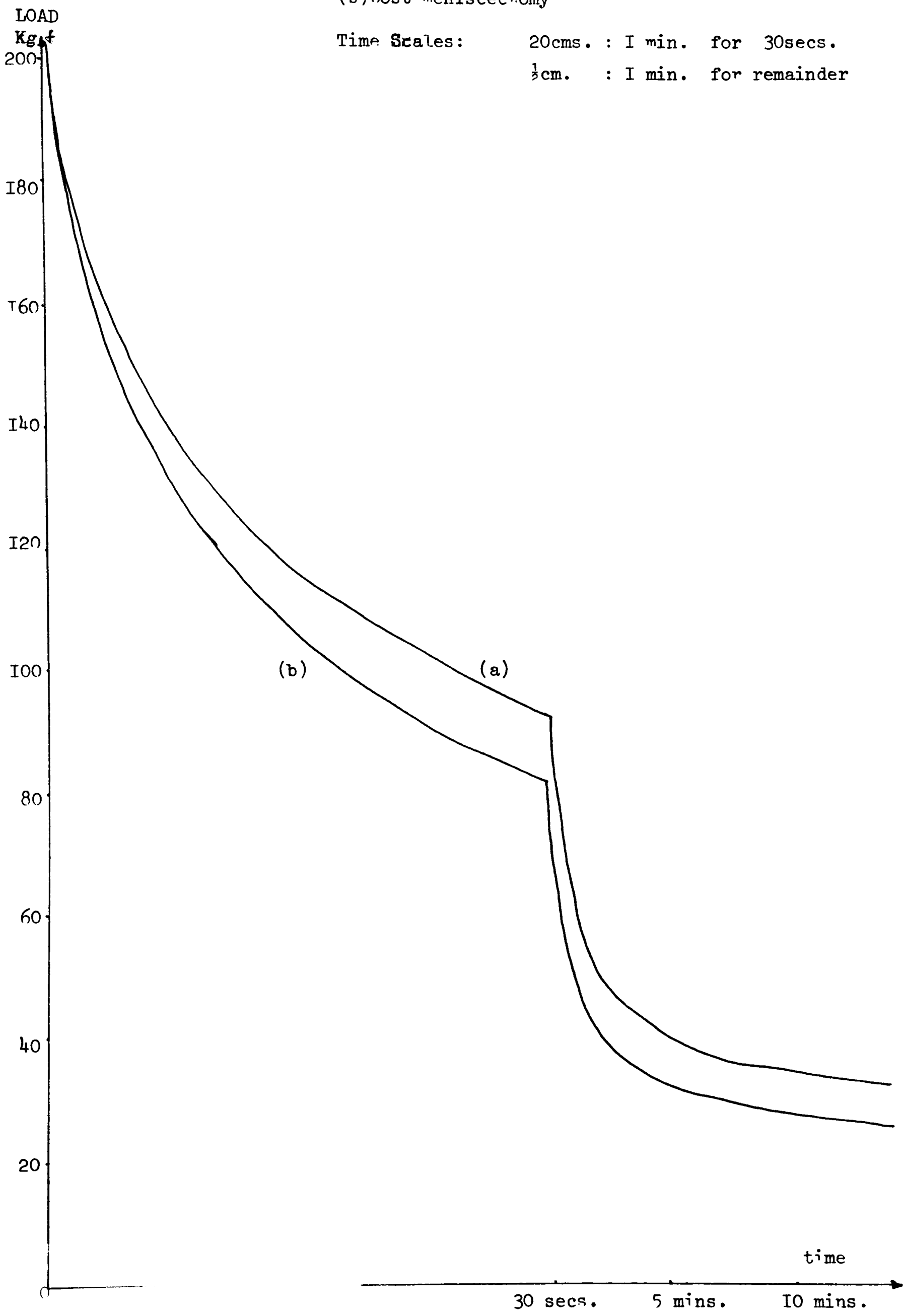

Specimen 7 Meniscal radial expansion v. Load

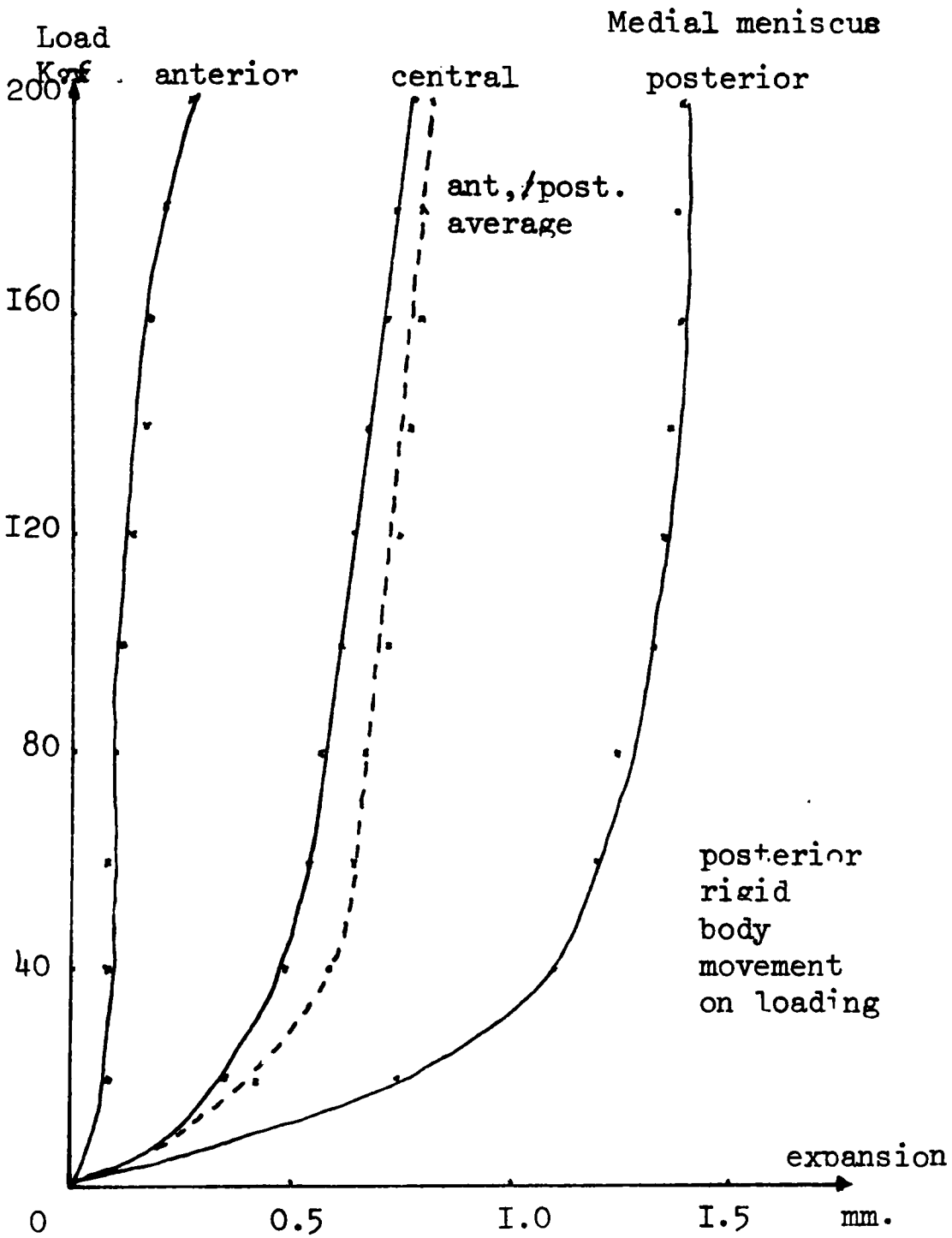

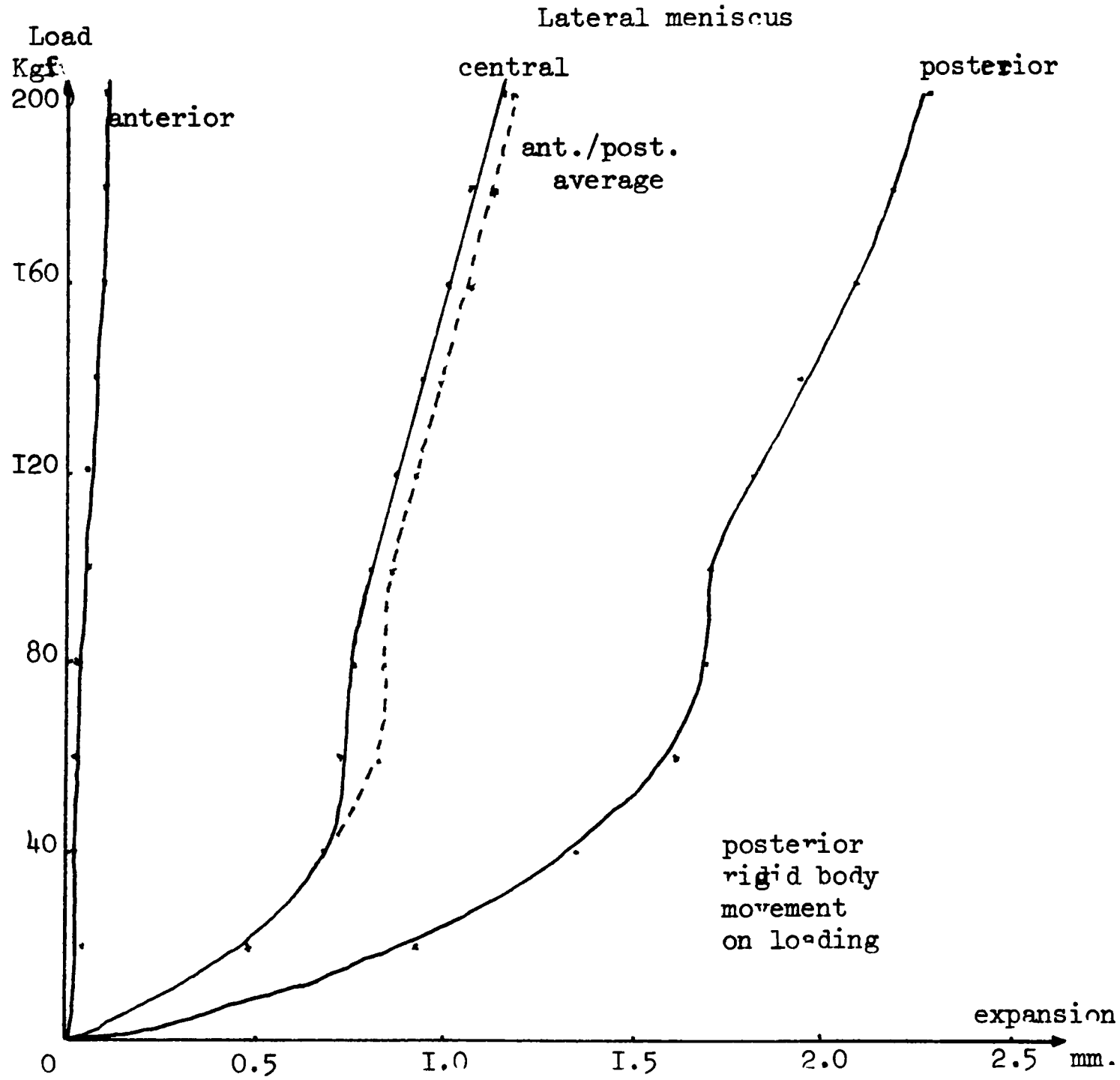

Pig Specimen 35 Meniscal radial expansion v.Load

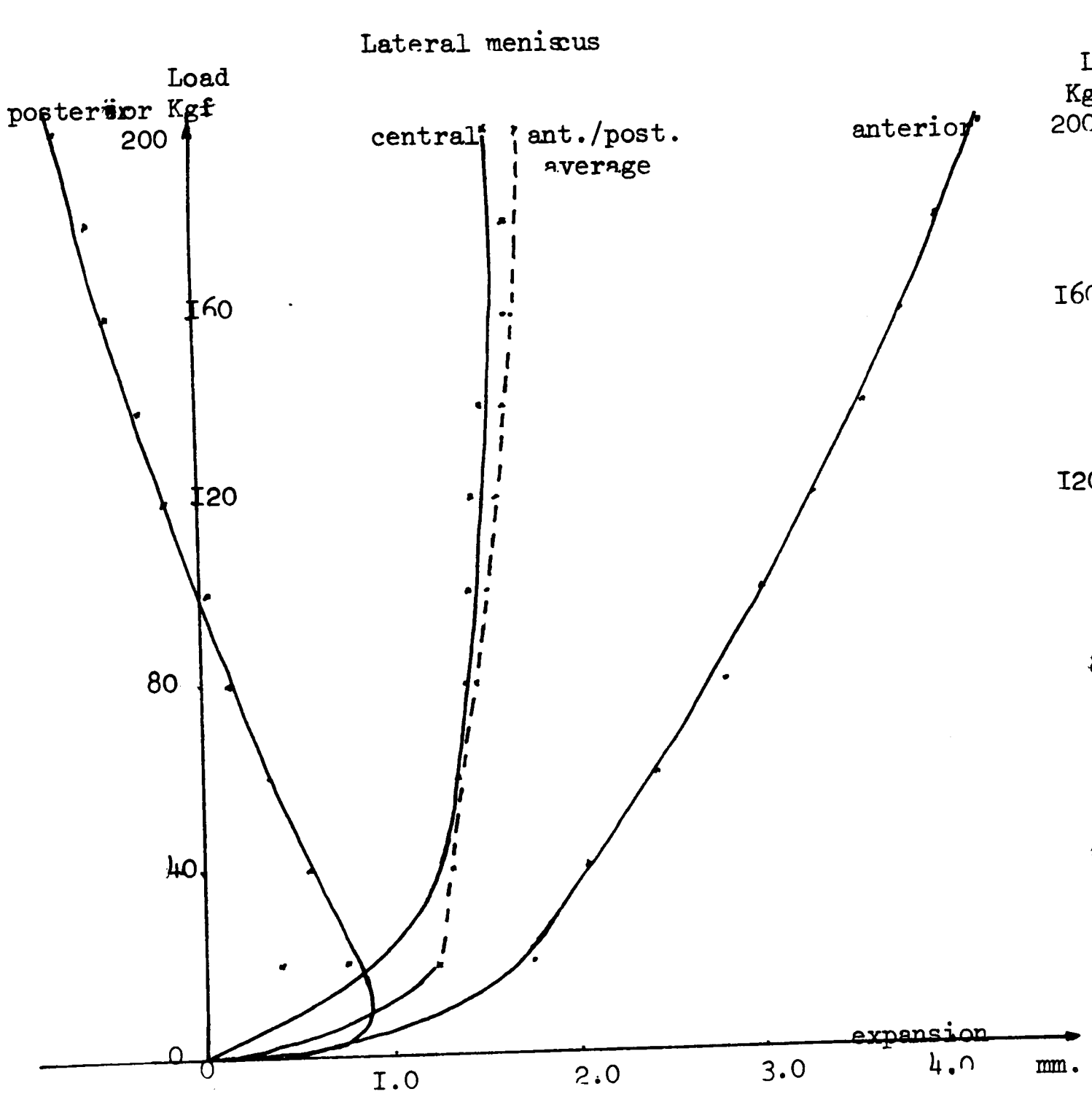

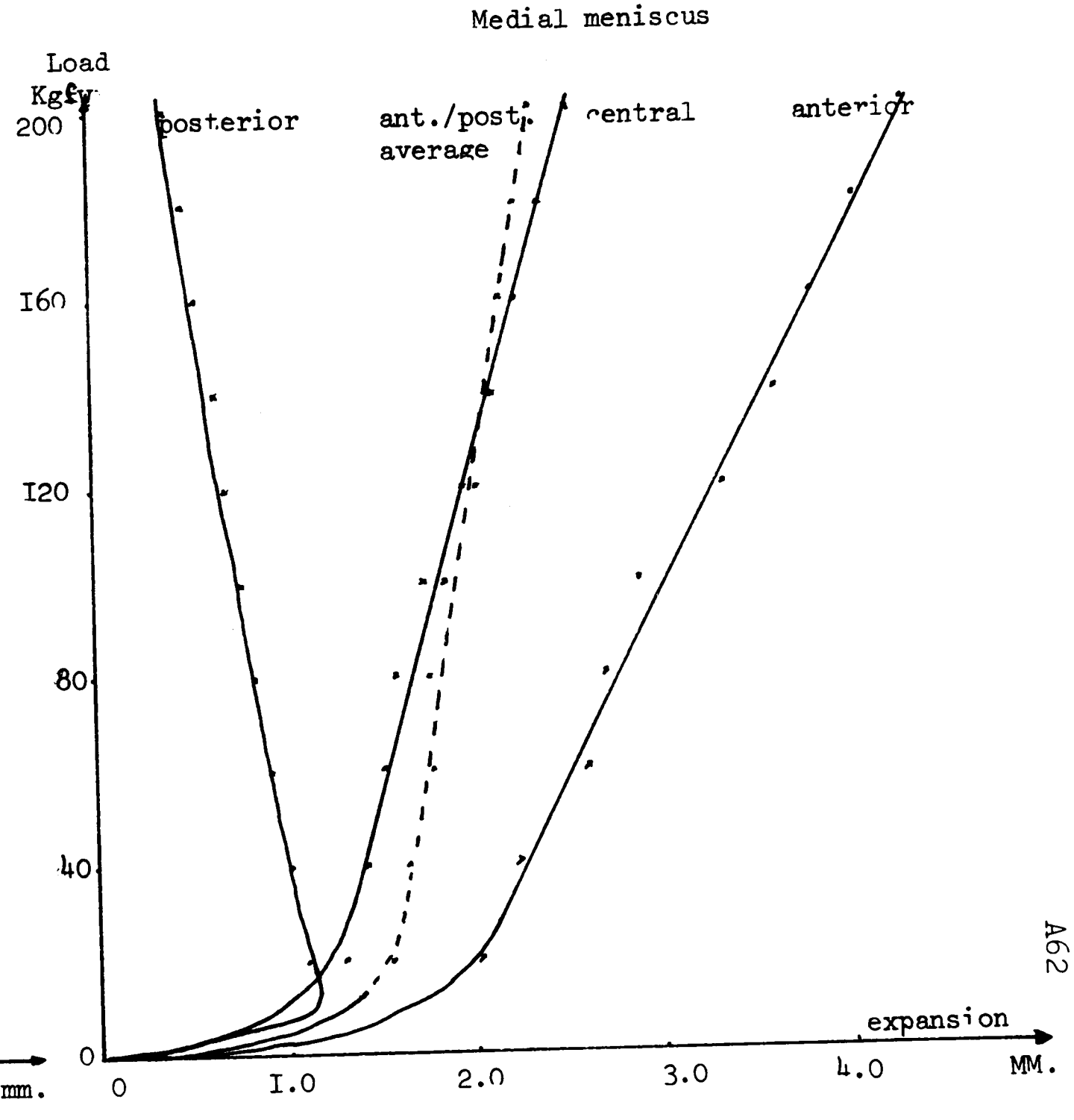

A62

Pig Specimen 39 Meniscal radial expansion v. Load

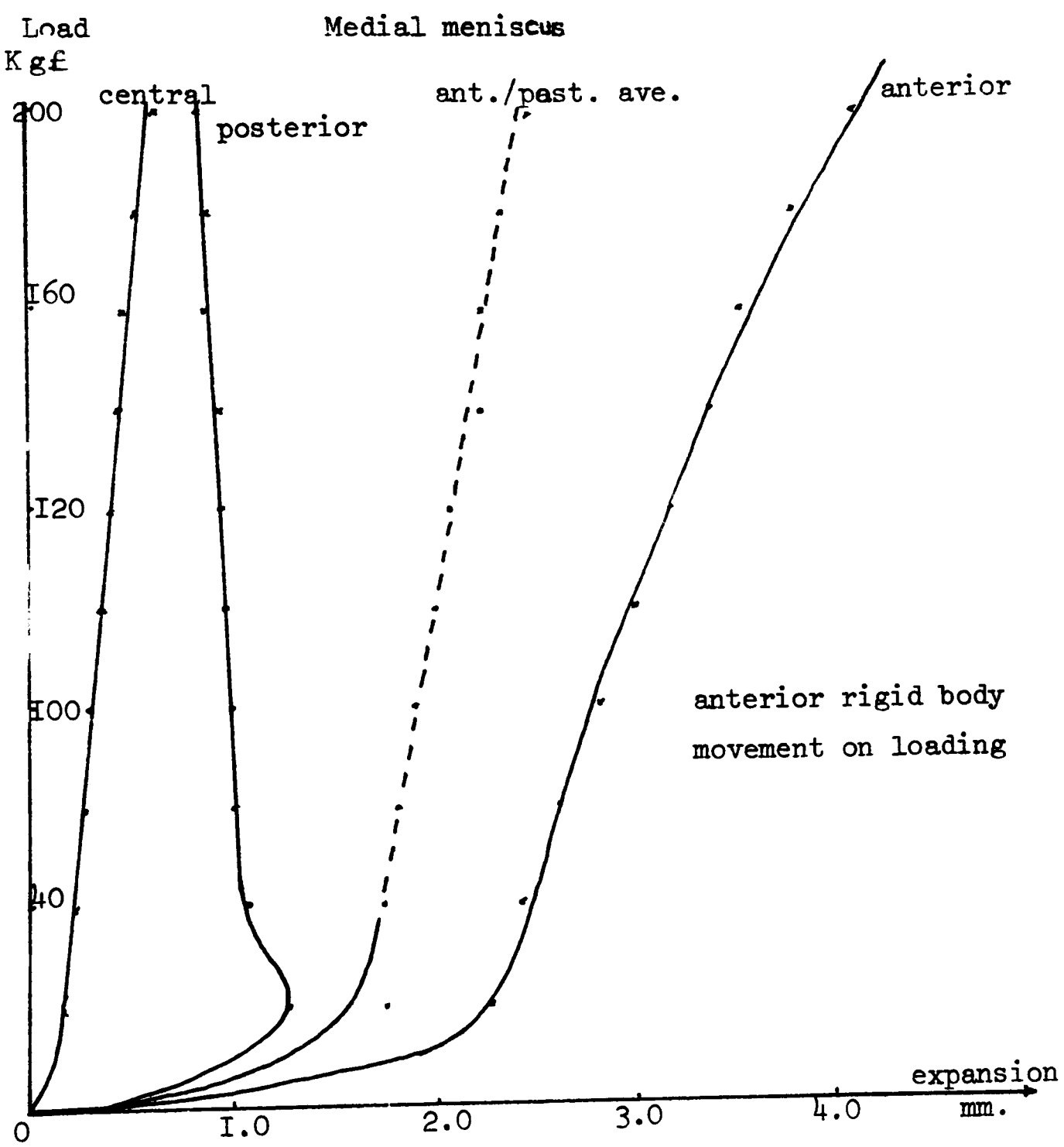

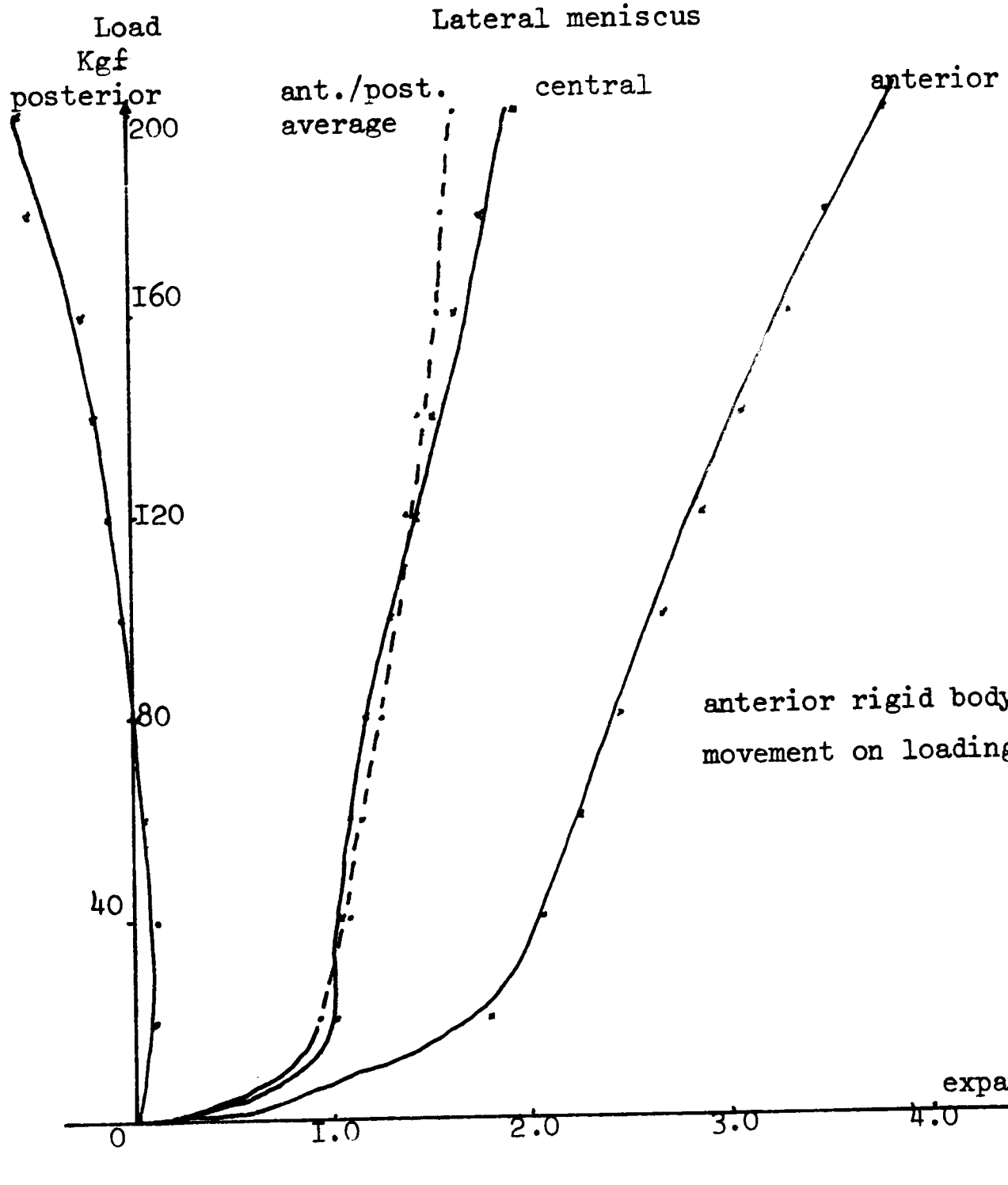

Spec. No.	Side	∝ (deg)	C (mm)	r_m (mm)	h_o (mm)	$\delta_{central}$ (mm)	$\delta_{a/p\,av}$ (mm)	Spec. No.	Side	∝ (deg)	C (mm)	r_m (mm)	h_o (mm)	$\delta_{central}$ (mm)	$\delta_{a/p\,av}$ (mm)
HUMAN 7	M	210	12.9	11.5	8.0	0.35	0.25	PIG 31	M	270	12.7	4.0	6.2	1.15	0.4
7	L	210	13.7	9.0	9.1	0.68	0.65	31	L	270	11.5	3.2	8.9	1.1	1.0
8	M	210	8.9	9.8	6.0	0.25	0.6	32	M	210	14.2	4.0	5.6	2.1	0.65
8	L	270	10.0	7.9	6.8	1.25	1.1	32	L	240	14.6	5.5	7.8	1.15	0.55
9	M	210	10.8	10.0	8.2	1.45	0.35	33	L	240	11.7	4.8	8.8	1.25	0.5
9	L	315	12.5	8.5	12.3	0.15	0.75	33	M	240	11.1	3.1	5.8	0.0	1.25
10	L	270	10.3	8.0	7.0	0.0	1.05	34	L	210	12.5	4.4	9.0	1.52	0.45
10	M	240	10.0	9.0	5.5	0.9	1.0	34	M	210	12.3	3.9	7.0	0.25	1.0
11	M	210	10.5	10.5	5.9	1.3	0.55	35	L	240	16.2	3.6	9.25	0.4	0.5
11	L	270	10.8	6.4	6.8	0.85	0.6	35	M	240	16.5	4.5	6.75	1.35	0.85
12	M	210	10.5	8.2	6.3	0.9	0.9	36	L	210	11.2	4.8	9.5	2.0	2.0
12	L	270	10.5	9.1	6.8	0.6	0.95	36	M	210	12.7	4.0	7.0	0.6	0.15
13	M	240	15.2	12.0	10.8	0.05	0.35	37	L	240	12.3	4.0	8.5	1.9	1.0
13	L	270	10.3	7.0	7.1	0.85	1.15	37	M	240	14.0	4.2	7.5	1.1	1.25
14	L	315	9.6	6.4	7.0	0.0	0.53	38	M	210	12.3	4.0	7.5	1.25	1.05
14	M	240	12.1	11.5	6.5	0.7	1.0	38	L	210	13.3	4.3	9.0	1.25	0.88
15	M	180	6.5	16.0	4.6	0.55	0.0	39	M	210	11.7	3.8	8.0	0.45	0.9
15	L	315	11.8	7.4	6.25	0.5	0.7	39	L	210	13.5	3.9	10.1	1.0	0.6
16	M	270	11.3	11.0	6.0	0.13	.33	40	L	210	13.0	4.4	9.0	0.45	1.0
16	L	270	12.4	8.4	7.5	0.4	1.25	40	M	240	12.7	3.8	6.5	1.55	0.85
17	L	315	11.5	8.4	8.1	0.0	0.48	41	L	210	13.5	3.4	10.0	1.15	0.8
17	M	210	9.2	14.4	5.9	0.8	0.2	41	M	240	13.7	3.7	7.0	1.2	1.0
PIG 27	M	210	13.5	2.5	7.1	0.8	1.1	42	L	210	14.0	3.4	9.0	1.1	0.2
27	L	240	13.5	2.5	7.0	0.7	0.75	42	M	240	13.4	3.1	6.7	0.5	1.0
28	M	240	11.5	4.5	6.6	1.35	2.0	43	L	210	13.7	4.0	9.1	0.7	0.65
28	L	270	13.6	5.0	8.5	2.75	1.5	43	M	240	11.4	3.8	7.3	2.75	1.1
29	M	240	12.0	4.75	7.1	1.0	1.6	44	L	240	11.9	3.5	9.3	0.0	0.7
29	L	240	15.0	3.5	9.35	2.3	1.3	44	M	210	13.6	4.4	6.6	0.95	1.55
30	M	210	13.8	4.6	8.5	0.25	0.34	45	M	210	13.2	4.2	5.7	0.63	0.9
30	L	210	11.7	5.4	8.9	1.95	1.9	45	L	210	13.3	3.3	8.6	1.1	0.85

RADIAL EXPANSION DATA

∝ is angle of arc of meniscus; C is width of meniscus; r_m is inner radius of meniscus; h_o is outer height of meniscus; $\delta_{central}$ is central expansion over 200 Kgf load on line tangential to curve at 180-200 Kgf ; $\delta_{a/p\,av}$ is the expansion on the anterior/posterior average curve.

Table 4.2.9

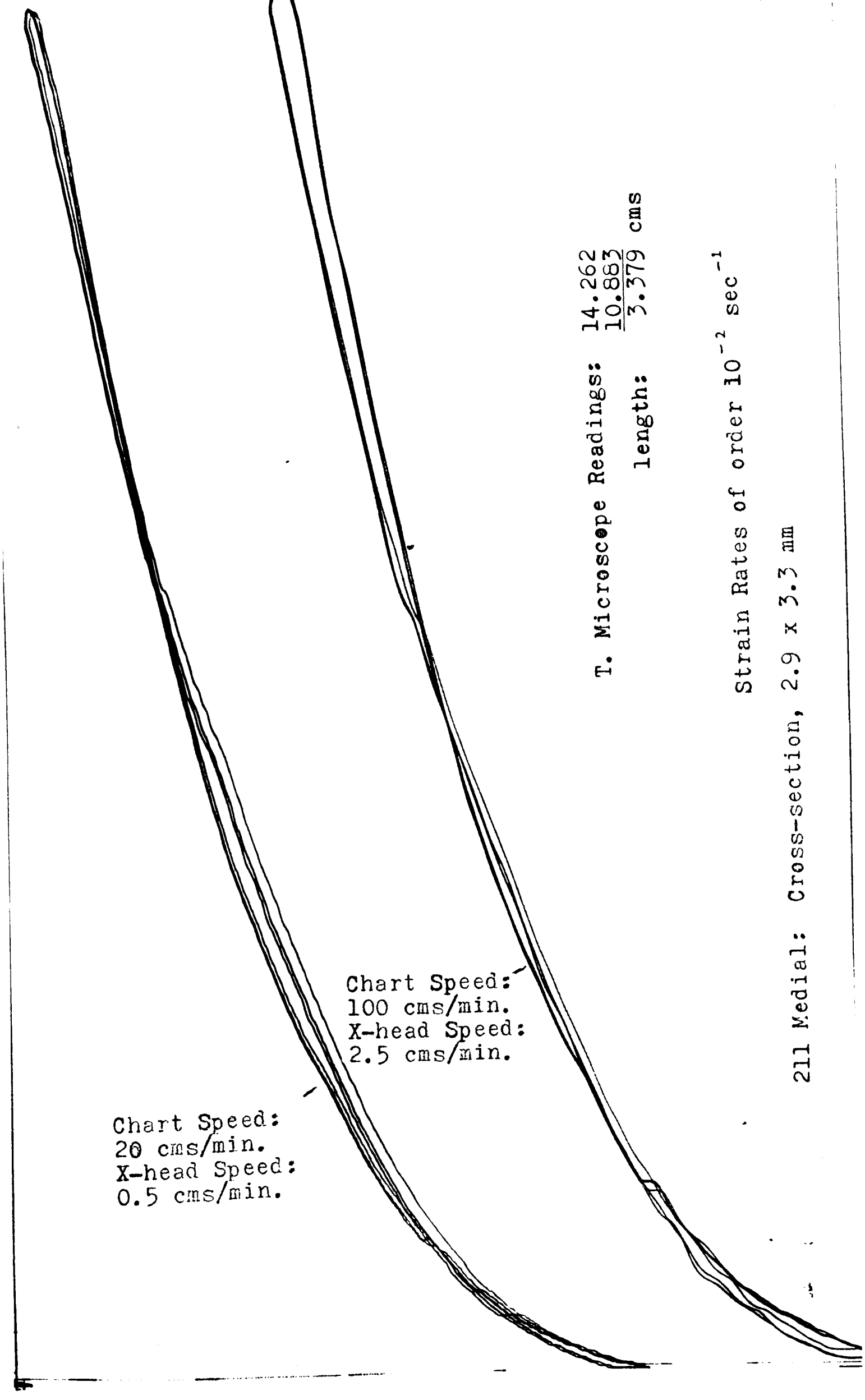

Typical Meniscus specimen extension test results at different strain rates. Cross-head and Chart speeds as indicated.

Computer Program for calculating Load Factors for Methods 1 and 2. (see 4.4.3)

Language: Fortran.

```
      MASTER VFORCE
      DIMENSION AA(60),CA(60),RMA(60),ALA(60)
    1 FORMAT(1I4)
    2 FORMAT(10F8.4)
    3 FORMAT(//10X,16HPARAMETER VALUES)
    4 FORMAT(/15X,4H A =,1PE13.6,10X,4HRM =,1PE13.6,10X,4H C =,1PE13.6,1
     10X,4HAL =,1PE13.6)
    5 FORMAT(/10X,15HREACTION VALUES)
    6 FORMAT(/15X,4H H =,1PE13.6,10X,4H M =,1PE13.6,10X,4HHO =,1PE13.6,1
     10X,4HVO =,1PE13.6)
    7 FORMAT(/10X,18HDEFLECTION FACTORS)
    8 FORMAT(15X,4HPHI=,1PE13.6,10X,4HFM =,1PE13.6,10X,4HFA =,1PE13.6,10
     1X,4HPF =,1PE13.6)
    9 FORMAT(/10X,11HLOAD FACTOR,21X,4HLF =,1PE13.6)
   10 FORMAT(10F8.6)
      REAL M,LF
      READ(5,1)N
      READ(5,10)(ALA(I),I=1,N)
      READ(5,2)(CA(I),I=1,N)
      READ(5,2)(RMA(I),I=1,N)
      READ(5,2)(AA(I),I=1,N)
      PI=4.*ATAN(1.000000)
      ER=1.0
      U=0.4
      DO 20 I=1,N
      A=AA(I)
      C=CA(I)
      RM=RMA(I)
      AL=PI*ALA(I)
      R=RM*(2.*C/3.)
      WRITE(6,3)
      WRITE(6,4)A,RM,C,AL
      F1=C*(3.*(RM*A))
      F2=(C*(1.*(ER*U)))*(3.*(RM*A))
      F3=F1/F2
      F4=C-(RM*ALOG((RM*A)/RM))
      LF=AL*A*F4*F3
      WRITE(6,9)LF
      V1=(AL/4.)*((AL/2.)*(COS(AL/2.))**2)-(0.75*SIN(AL))
      V2=(AL/4.)*(0.25*SIN(AL))
      V3=V2-SIN(AL/2.)
      V4=((18.*R**2*V1)/(C**2))*V2
      V5=((18.*R**2*V1)/(C**2))*V3
      H=V5/V4
      HO=(1.-H)*SIN(AL/2.)
      VO=1.-((1.-H)*COS(AL/2.))
      M=(1.-H)*(1.-COS(AL/2.))
      WRITE(6,5)
      WRITE(6,6)H,M,HO,VO
      WRITE(6,7)
      PHI=0.0

      GO TO 19
   18 PHI=PHI+(AL/20.)
   19 IF(PHI.GE.(AL/2.))GO TO 20
      V6=COS(AL/2.)-(0.25*COS(PHI))-(0.75*COS(AL-PHI))
      V7=(AL/4.)*(SIN(PHI)-SIN(AL-PHI))
      V8=((AL/4.)-(PHI/2.))*SIN(PHI)
      V9=V6+V7+V8
      V10=(0.25*(COS(AL-PHI)-COS(PHI)))+V8
      V11=((18.*R**2*V9)/(C**2))*V10
      A2=V11/V4
      V12=(V9-(A2*V1))*(1.-H)
      V13=((V10-(A2*V2))*(1.-H))+1.+(A2*SIN(AL/2.))-COS((AL/2.)-PHI)
      FM=(56.*R**3*V12)/(C**3)
      FA=(2.*R*V13)/C
      PF=(A*AL*C)/(FM+FA)
      WRITE(6,8)PHI,FM,FA,PF
      GO TO 18
   20 CONTINUE
      STOP
      END
```

LINE

Language: Fortran.

RUN BY
DATE :

```
      MASTER TCYLF
      DIMENSION ALA(60),CA(60),RMA(60),AA(60),SN(60),HA(60)
      INTEGER SP,SN
    1 FORMAT(1HO,10X,17HDEFLECTION VALUES)
    2 FORMAT(1H ,15X,4HDC =,1F7.4,10X,4HDH =,1F8.4,10X,4HDT =,1F7.4,10X,
     14HPF =,F11.4,10X,6HPERC =,F6.2)
    3 FORMAT(1HO,10X,14HREACTION VALUE,15X,3HH =,1F8.5)
    4 FORMAT(1I4)
    5 FORMAT(10F8.4)
    6 FORMAT(10F8.6)
    7 FORMAT(1HO,16HPARAMETER VALUES)
    8 FORMAT(1HO,11HSPECIMEN NO,I16,10X,4HAL =,1F5.3,10X,3HC =,1F5.2,10X
     1,4HRM =,1F4.1,10X,4HHO =,1F5.2,10X,3HD =,1F6.3)
    9 FORMAT(20I4)
      READ(5,4)N
      READ(5,9)(SN(I),I=1,N)
      READ(5,6)(ALA(I),I=1,N)
      READ(5,5)(CA(I),I=1,N)
      READ(5,5)(RMA(I),I=1,N)
      READ(5,5)(HA(I),I=1,N)
      READ(5,5)(AA(I),I=1,N)
      DO 20 I=1,N
      SP=SN(I)
      HO=HA(I)
      RM=RMA(I)
      A=RM
      C=CA(I)
      B=A+(C/2.)
      RS=B
      S=B
      U=0.4
      PI=4.*ATAN(1.000000)
      AL=PI*ALA(I)
      D=AA(I)
      WRITE(6,7)
      WRITE(6,8)SP,AL,C,RM,HO,D
      Q=A**2-B**2+((A**2+B**2)*ALOG(B/A))
      H1=((1.-U)*RS+((1.+U)*B**2)/RS)*Q*A**2*SIN(AL/2.)
      H2=((3.-U)*RS**2)-((A*B/RS)**2)*(1.+U)
      H3=(A**2+B**2)*(3.+U-((AL*SIN(AL/2.))/(1.-COS(AL/2.))))
      H4=((A**2+B**2)*AL*SIN(AL/2.))-((H2+H3)*COS(AL/2.))
      H5=(1.-COS(AL/2.))*(B**2-A**2)*H4
      H=H1/H5
      WRITE(6,3)H
      WRITE(6,1)
      PHI=0.0
      GO TO 19
   18 PHI=PHI+(AL/20.)
   19 IF(PHI.GT.(AL/2.))GO TO 20
      TH=(AL/2.)-PHI
      D1=A**2/(B**2-A**2)
      D2=((1.-U)*S)+(B**2*(1.+U)/S)

      DC=D1*D2
      K=1
      V1=(((K-(3.*U))*S**2)/2.)-((A*B/S)**2)*(K+U)/2.
      V2=-(A**2+B**2)*(K-U)*ALOG(S)
      F1=(H*SIN(TH)*(V1+V2))/Q
      F2=(2.*H*(A**2+B**2)*TH*COS(TH))/Q
      V3=1.+U-((AL*SIN(AL/2.))/(1.-COS(AL/2.)))
      F3=(H*SIN(TH)*(A**2+B**2)*V3)/Q
      V4=H*RS**2*(6.-K+U)/(2.*Q)
      V5=-(H*((A*B/RS)**2)*(K+U))/(2.*Q)
      V6=(H*(A**2+B**2)*(K-U)*ALOG(RS))/Q
      F4=(V4+V5+V6)*SIN(TH)
      V7=(RS*(1.-U))+(B**2*(1.+U)/RS)
      V8=COS(TH)-((SIN(AL/2.)*SIN(TH))/(1.-COS(AL/2.)))
      F5=-(A**2/(B**2-A**2))*V7*V8
      DH=F1+F2+F3+F4+F5
      DT=DC*DH
      PF=AL*D/DT
      PERC=(PF*150.*C*RM)/19.62
      WRITE(6,2)DC,DH,DT,PF,PERC
      GO TO 18
   20 CONTINUE
      STOP
      END
```